

UC Riverside

UC Riverside Electronic Theses and Dissertations

Title

Salinity, Redox and Oligotrophy: What Environmental Factors Contributed to the Late Ediacaran “Kotlin Crisis”?

Permalink

<https://escholarship.org/uc/item/631283p6>

Author

Hoffmann, Adam

Publication Date

2024

Copyright Information

This work is made available under the terms of a Creative Commons Attribution-NoDerivatives License, available at <https://creativecommons.org/licenses/by-nd/4.0/>

Peer reviewed|Thesis/dissertation

UNIVERSITY OF CALIFORNIA
RIVERSIDE

Salinity, Redox and Oligotrophy: What Environmental Factors
Contributed to the Late Ediacaran “Kotlin Crisis”?

A Dissertation submitted in partial satisfaction
of the requirements for the degree of

Doctor of Philosophy

in

Earth and Planetary Sciences

by

Adam Hoffmann

September 2024

Dissertation Committee:

Dr. Gordon Love, Chairperson

Dr. Andrey Bekker

Dr. Mary Droser

Copyright by
Adam Hoffmann
2024

The Dissertation of Adam Hoffmann is approved:

Committee Chairperson

University of California, Riverside

ACKNOWLEDGEMENTS

This research was made possible by funding from the UCR Graduate Research Mentorship Program. Conference travel funding was provided by UCR GSA.

I am very grateful to my advisor, Gordon Love. Without your support and belief in me, this dissertation would not have been possible. The countless hours in the lab working on the Autospec were critical in helping me understand GC-MS, making me a competent analyst in the process. I relish the conversations we have had over after work beers after long days in the lab, and I cannot thank you enough. I would like to thank my qualifying and defense committee members as follow: Andrey Bekker for giving me the initial opportunity to being my career as a geochemist at UCR and the many insightful conversations over the years; Mary Droser for accepting me as an honorary member of the Droser lab and having wonderful conversations about Australian hops; Tim Lyons for the insightful and thought provoking questions; and Sam Ying for asking the grounded questions.

To my lab mates and friends, Alex Kovalick, Nick Mammone, Logan Magad-Weiss, Kelden Pehr, Aaron Martinez, Alex Zumburge, Nathan Marshall, Adriana Rizzo, Ginny Winters, and Charlie Diamond. Thank you for all for the wonderful conversations and help over the years, your friendship has been crucial in my success at UCR.

None of this research would have been possible without the help from fantastic collaborators. Special thanks go to Leonid Shumlyansky for being an invaluable field guide during fieldwork in Estonia and Ukraine during our 2018 field trip. Alvar Soesoo, and Tetyana Sokur provided the samples this dissertation is based on. Simon Poulton performed the major element, trace metal, and Fe- and P-mineral speciation experiments. The text of this dissertation is a partial reprint as it appears in the following: Pehr, K., Baczynski, A. A., Bekker, A., Hoffmann, A., Freeman, K. H., Poulton, S. W., & Love, G. D. (2023). Compound-specific carbon isotope measurements of individual lipid biomarkers from immature Ediacaran rocks of Baltica. *Organic Geochemistry*, 182, 104641 and Francovschi, I., Shumlyansky, L., Soesoo, A., Tarasko, I., Melnychuk, V., Hoffmann, A., ... & Bekker, A. (2023). U–Pb geochronology of detrital zircon from the Ediacaran and Cambrian sedimentary successions of NE Estonia and Volyn region of Ukraine: Implications for the provenance and comparison with other areas within Baltica. *Precambrian Research*, 392, 107087.

Thank you to my family, mom, dad and Christopher, for always supporting me through this period in my life. RIP mom, I did it! You and dad were one of the key influences in ensuring my success and I cannot thank the both of you enough for maintaining support even when I didn't seem like I would get my head stuck out of the sand.

And finally, to the love of my life, and future wife Amanda. I would not have completed this amazing accomplishment had it not been for your persistent encouragement. You

never doubted me even when my doubt was the strongest. You were there every step of the way, and my success is in large part to you. Thank you for never leaving my side and making sure that I achieved the goal I set out to do 7 years ago.

ABSTRACT OF THE DISSERTATION

Salinity, Redox and Oligotrophy: What Environmental Factors
Contributed to the Late Ediacaran “Kotlin Crisis”?

by

Adam Hoffmann

Doctor of Philosophy, Graduate Program in Earth and Planetary Sciences
University of California, Riverside, September 2024
Dr. Gordon Love, Chairperson

The Ediacaran (635 – 539 Ma) on Baltica is marked by oligotrophic conditions concurrent with the emergence of the Ediacaran Biota. This study analyzes rocks collected from various localities around Baltica with the intent of understanding the extent of oligotrophic conditions, the nutrient limitation that allowed these conditions to persist for millions of years. To answer these questions, samples from across Baltica were measured for Fe-speciation and P-phase partitioning, lipid biomarkers, C- and N-isotopes, major and trace elements analyses, and detrital zircon age dating. C_{26}/C_{25} tricyclic terpane ratios, S contents and Fe-speciation indicate two salinity and redox states on Baltica with the Redkino being deposited under predominantly ferruginous, normal-

marine conditions and the Kotlin horizon being deposited under dominantly oxic, low salinity coastal brackish conditions. Further evidence for these distinct environments can be observed in the relative abundance of hopanes and steranes which indicate strong bacterial contributions to primary productivity in the Redkino horizon. Conversely, lower hopane/sterane ratios in the Kotlin suggest increased algal contributions.

Compound specific C-isotope measurements were made to determine the composition of individual extracted lipids from rocks across Baltica. Samples from the Utkina Zavod drillcore have bulk $\delta^{13}\text{C}_{\text{TOC}}$ that are heavier by $\sim 10\text{‰}$ compared to other localities across Baltica. $\delta^{13}\text{C}$ from individual hopanes and C_{29} steranes from all sites are within 2‰ of each other, suggesting that Bacteria were likely utilizing the RubisCO-CBB pathway. ^{13}C enrichment in these lipids in Utkina Zavod samples shows that either C-isotope fractionation was muted, or it was reflecting composition of the DIC pool. During Kotlin time, significant environmental heterogeneity existed on Baltica.

U–Pb geochronology of detrital zircons from successions in northeast Estonia and the Volyn region of Ukraine was studied to understand sediment provenance and compare it with that for other areas on Baltica. These analyses provide insights into sediment transport and deposition processes, as well as the tectonic settings that influenced Baltica's sedimentary record during the late Ediacaran to early Cambrian. The sedimentary basins across Baltica show a transition during the Late Ediacaran – Cambrian interval from a passive continental margin to a collisional setting.

TABLE OF CONTENTS

Chapter One: Introduction

1.1. The Late Ediacaran	1
1.2. Geochemical analyses	3
1.3. Summary of dissertation chapters	4
1.4. References	7

Chapter Two: Environmental salinity severely impacted the late Ediacaran marine communities across Baltica prior to the Cambrian Period

Abstract	9
1.0. Introduction	10
2.0. Geologic Setting and Stratigraphy	14
2.1. Volyn'-Podillya Basin (Ukraine)	17
2.2. Baltic Monocline (Estonia)	17
3.0. Materials and Methods	19
3.1. Total organic carbon $\delta^{13}\text{C}_{\text{org}}$ and $\delta^{15}\text{N}$	20
3.2. Fe-mineral speciation	21
3.3. P-phase partitioning	22
3.4. Major elements and trace metals	22
3.5. Total and pyrite sulfur	23
3.6. Solvent extraction and silica gel chromatography of rock bitumen	23

3.7. Gas chromatography–mass spectrometry (GC–MS)	24
3.8. Metastable reaction monitoring GC–MRM-MS	24
4.0. Results	27
4.1. Total organic carbon (TOC) content and $\delta^{13}\text{C}_{\text{org}}$ values	27
4.1.1. $\delta^{13}\text{C}_{\text{org}}$ results for drillcore 3628 (Ukraine)	28
4.1.2. $\delta^{13}\text{C}_{\text{org}}$ results for drillcore F-169 (Estonia)	29
4.2. $\delta^{15}\text{N}$ results for F-169 (Estonia)	30
4.3. Iron Speciation	31
4.4. Major and Trace Element signals for intermittent ferruginous conditions	33
4.4.1. Vanadium	33
4.4.2. Manganese as a tracer for intermittent oxic conditions	35
4.5. P-phase partitioning	35
4.6. Total and pyrite sulfur	37
4.7. lipid biomarker assemblage patterns	39
4.7.1. Thermal Maturity	39
4.7.2. $\text{C}_{26}/\text{C}_{25}$ Tricyclic terpenoids	40
4.7.3. Hopane/Sterane	42
5.0. Discussion	43
5.1. Nutrient limitation	43
5.1.1. N as a limiting nutrient	44
5.1.2. Fe as a limiting nutrient	44
5.1.3 P as a limiting nutrient	45

5.2. Environmental heterogeneity across Baltica	46
5.3. Environmental transition	49
6.0. Conclusions	51
References	52

Chapter Three: Compound-specific carbon isotope measurements of individual lipid biomarkers from immature Ediacaran rock of Baltica

ABSTRACT	64
1. INTRODUCTION	65
2. MATERIALS AND METHODS	70
2.1. Geologic setting and samples	70
2.2. Lipid biomarker analysis	73
2.3. Bulk isotope analysis	75
2.4. Pico-compound specific carbon isotope analysis	76
2.5. Iron Speciation	77
3. RESULTS	79
3.1. $\delta^{13}\text{C}_{\text{TOC}}$ and Compound-Specific Carbon Isotope Values	79
3.2. Tricyclic terpane ratios	83
3.3. Iron Speciation	85
4. DISCUSSION	85
4.1. $\delta^{13}\text{C}$ values of Lipid Biomarkers	85
4.2. Local Environmental Effects on $\delta^{13}\text{C}_{\text{TOC}}$	90

4.3. Investigating Evidence for Inverse Isotopic Ordering	96
5. CONCLUSIONS	100
REFERENCES	103

Chapter Five: U–Pb geochronology of detrital zircon from the Ediacaran and Cambrian sedimentary successions of NE Estonia and Volyn region of Ukraine: implications for the provenance and comparison with other areas within Baltica

Abstract

1. INTRODUCTION	119
2. GEOLOGIC SETTING AND STRATIGRAPHIC DATA	122
2.1 Geology of Estonia	122
2.2 Geology of the Volyn Region	137
3. SAMPLING AND METHODOLOGY	145
4. RESULTS	147
4.1 Estonia	147
4.2 Volyn Region of Ukraine	151
5. Discussion	153
5.1 Possible sources for detrital zircons	153
5.1.1 Estonia	153
5.1.2 Volyn Region	161
5.2 Comparison with other areas within Baltica	164

5.3 General patterns in the Ediacaran - Cambrian evolution of Baltica sedimentary basins	170
5.4 Inconsistencies in the late Ediacaran – Early Cambrian detrital zircon age distribution patterns for the sedimentary basins of Baltica	174
6. CONCLUSIONS	178
REFERENCES	180
Chapter 5: Conclusions	201

LIST OF FIGURES

Figure 2.1. Paleogeography and known Ediacaran body fossil occurrences across Baltica.	12
Figure 2.2. Generalized stratigraphy for drillcore the Podillya region of Ukraine and F-169 drillcore from northeastern Estonia.	17
Figure 2.3. TOC (wt%), $\delta^{13}\text{C}_{\text{org}}$ and selected inorganic geochemical proxies for drillcore 3628 from the Podillya region of Ukraine.	26
Figure 2.4. $\delta^{13}\text{C}_{\text{org}}$ and $\delta^{15}\text{N}$ for drillcore F-169 from Estonia.	29
Figure 2.5. Crossplot of $\text{Fe}_{\text{HR}}/\text{Fe}_{\text{Tot}}$ vs $\text{Fe}_{\text{py}}/\text{Fe}_{\text{HR}}$ for all samples excluding drillcore F-169.	30
Figure 2.6. Crossplots of C_{org} vs P_{reac} and C_{org} vs P_{org} .	34
Figure 2.7. Total ion chromatogram for sample F-169 126.51.	37
Figure 2.8. Down core C_{32} and C_{31} hopane isomer trends for drillcores 3628 and F-169 respectively.	38
Figure 2.9. Crossplot of $\delta^{13}\text{C}_{\text{org}}$ vs $\text{C}_{26}/\text{C}_{25}$ tricyclic terpane ratio	40
Figure 2.10. H/St vs depth for drillcore 3628	42
Figure 2.11. Schematic of hypothesized salinity, redox and sea level conditions during the Redkino and Kotlin.	48
Figure 2.12. Updated map reflecting geographic salinity conditions across Baltica after the Kotlin Crisis.	49
Figure 3.1. Paleogeography and known Ediacaran body fossil occurrences and sampling locations across Baltica.	72
Figure 3.2. Selected TIC's from and zoomed chromatograms to highlight the biomarker region.	78
Figure 3.3. Compound specific C-isotope data for C_{27-31} hopanes, pristane, phytane, and $\text{C}_{29\text{aaa}}$ steranes.	82
Figure 3.4. Box plot of CSIA hopanes, short and long n- alkanes.	84

Figure 3.5. Crossplot of $\delta^{13}\text{C}_{\text{TOC}}$ vs $\text{C}_{26}/\text{C}_{25}$ tricyclic terpane (TT).	86
Figure 3.6. Stratigraphic trends for inorganic and organic geochemical parameters of the Utkina Zavod and Lugovoe drill cores.	89
Figure 4.1. Schematic tectonic map of Baltica.	125
Figure 4.2. Generalized geological map showing the Distribution of the Ediacaran – Lower Paleozoic sedimentary cover in Estonia.	126
Figure 4.3. Ediacaran – Lower Cambrian stratigraphic columns for the central, western, and southwestern parts of Baltica.	129
Figure 4.4. Ediacaran - Cambrian lithostratigraphic column of the F-169 drill-core in Estonia.	135
Figure 4.5. Lithostratigraphic column of the N61 and N66 drill-cores (Ukraine).	144
Figure 4.6. Plot of Th/U ratio versus age for zircons from Estonia and the Volyn Region of Ukraine, respectively.	150
Figure 4.7. Paleogeographic map of western Baltica during (A) the late Ediacaran – Early Cambrian (Kotlin – Lontova regional stages) time and (B) Early Cambrian (Dominopol Regional Stage).	157
Figure 4.8. Comparison of detrital zircon age spectra (KDE plots) of the late Ediacaran - Early Cambrian sedimentary rocks.	159
Figure 4.9. Location of studied samples across Baltica.	165
Figure 4.10. Schematic diagram highlighting timing of changes in the provenance in the western, southwestern, and central parts of Baltica.	179

LIST OF TABLES

Table 2.1. Selected biomarker ratios and isotopic data.	59-61
Table 2.2. Selected concentrations for various major and trace elements, Fe- and P-mineral speciation for context on redox conditions during deposition.	61-62
Table 3.1. Selected-biomarker abundance ratios, bulk organic carbon isotope values and iron speciation redox proxies.	112
Table 3.2. Mean carbon isotope compositions for individual extractable hopanes and hopenes measured by pico-CSIA.	113-114
Table 3.3. Mean carbon isotope ratios ($\delta^{13}\text{C}$) for individual extractable <i>n</i> -alkanes measured by pico-CSIA.	115-116
Table 3.4. Mean carbon isotope compositions for extracted pristane (Pr), phytane (Ph), and C_{29} $\alpha\alpha\alpha\text{R}$ sterane, measured by pico-CSIA.	117

CHAPTER ONE

Introduction

1.1. The Late Ediacaran

The Ediacaran Period (~635 – 539 Ma) was a time of innovation and environmental expansion for early multicellular organisms, often linked with a purported rise of atmospheric and oceanic oxygen. In particular, the Middle-to-Late Ediacaran (575 – 539 Ma) captures the first appearance of macroscopic multicellular organisms known as the *Ediacaran biota*, and their appearance has been linked to a post-Gaskiers secondary rise in atmospheric oxygen at approximately 580 Ma (Fike et al., 2006; Canfield et al., 2008; Shields-Zhou and Och, 2011; Johnston et al., 2012). Following two distinct Snowball Earth glaciation events, progressive oxygenation of marine surface waters within the Ediacaran ocean system paved the way for subsequent oxygenation of deep waters becoming more prevalent following the termination of the Gaskiers glaciation at ca. 580 Ma (Fike et al., 2006; Canfield et al., 2008; Wood et al., 2015). Sedimentary strata from Baltica (comprising modern day Ukraine, Western Russia, Belorussia, Moldova, and Fennoscandia) preserved geochemical signals and fossils, which provide a unique perspective on environmental and biological community structure within largely shallow, epeiric seaways. Lipid biomarker analysis of immature Ediacaran sedimentary rocks suggests nutrient-limited marine ecosystems were sustained across Baltica (Duda et al., 2016; Goryl et al., 2018; Pehr et al., 2018, 2023), with biomarker assemblages

dominated by bacterial inputs and with distinct sedimentary intervals in the Redkino regional stage (ca. 560-550 Ma) occasionally containing abundant Ediacaran Biota fossils (Grazhdankin, 2014a; Ivantsov et al., 2015a). Previous lipid biomarker and carbon isotope studies were performed on contemporaneous organic matter-rich Ediacaran strata from the Huqf Supergroup in the South Oman Salt basin (Grosjean et al., 2009; Love et al., 2009; Lee et al., 2013). Overall, the variations in lipid biomarker distributions suggest that significant regional ocean heterogeneity existed in the late Ediacaran ocean system from location to location (Pehr et al., 2018), in terms of the amount and composition of primary productivity available for heterotrophy. The sedimentary rocks and oils sourced from South Oman are rich in C₂₇-C₃₀ sterane biomarkers, indicating high eukaryotic source contributions with certain sterane compounds interpreted to be sourced by green algae and early demosponges (Love et al., 2009; Zumberge et al., 2018). Yet, the sedimentary rocks from age-equivalent rocks sampled in outcrops in northern Oman have not revealed any significant fossil occurrences of Ediacaran Biota. With the preservation of abundant soft-bodied macro-fauna in certain intervals, combined with low thermal maturity of sedimentary units, and preservation of bentonite deposits, the ancient rocks from Baltica allow us the unique opportunity to combine results from organic and inorganic geochemistry, isotope chemostratigraphy, paleontology, and radiometric dating.

1.2. Geochemical analyses

Various types of geochemical analyses can help answer important questions about ancient sedimentary settings. In this dissertation, we used a variety of these techniques such as lipid biomarkers, stable C and N isotopes, P- and Fe-mineral speciations, major and trace elements, and U-Pb geochronology to investigate the environmental, tectonic, and geographic settings that were critical to the survival and evolution of the Ediacara biota on Baltica.

Some of these analyses require suitable samples to produce reliable data. As deep-time organic geochemists, we consider thermal maturity and organic contamination to be important factors when analyzing samples from over 500 million years ago. To produce reliable data, we screen samples to ensure they contain significant source biota information and have not been thermally cracked through catagenesis when buried. Our screening process includes, but is not limited to: systematic drill core sampling to establish downcore authentic maturity trends, rock eval pyrolysis to determine the extent of thermal maturity of a given sample and in some cases, catalytic hydrolysis to free kerogen bound biomarkers that are insulated from external contamination. In chapters one and two of this dissertation, screening measures showed that these samples are some of the most immature biomarker analyzed from the late Ediacaran along with those previously published by Pehr et al., (2018, 2023). This low thermal maturity suggests our

samples have not exceeded a temperature above 60° C and are suitable for various types of geochemical analyses that are sensitive to thermal alteration.

1.3. Summary of dissertation chapters

Chapter Two of this dissertation investigates the influence of environmental salinity on late Ediacaran marine communities on Baltica, focusing on the decline in faunal diversity observed between the Redkino and Kotlin stages. The late Ediacaran period, approximately 575 to 540 million years ago, was a crucial time for the evolution of complex life, marked by the appearance of the Ediacara biota. A significant decline in the diversity and abundance of the Ediacara biota was observed across the transition from the Redkino Stage (ca. 560-550 Ma) to the Kotlin Stage (ca. 550-540 Ma). Detailed chemo-stratigraphic records, including lipid biomarkers, isotope trend ($\delta^{13}\text{C}_{\text{org}}$ and $\delta^{15}\text{N}$), Fe- and P-mineral speciation, and trace metal analyses from drill cores in Russia, Ukraine, and Estonia, revealed an environmental changes that coincided with this decline.

The shift between the Redkino and Kotlin stages was characterized by fundamental changes in aquatic salinity, with evidence of the development of coastal deltaic conditions. These environmental changes imposed significant selection pressures on marine communities, likely influencing the structure and extinction dynamics of the Ediacara biota. This suggests that the reduction in salinity and the persistence of

oligotrophic conditions (nutrient-poor waters) played a crucial role in the observed decline in biological diversity.

Chapter Three focuses on the compound-specific carbon isotope analyses (CSIA) of individual lipid biomarkers extracted from immature Ediacaran rocks in the Baltica region. Using a newly developed picomolar-scale CSIA (pico-CSIA) method, we measured the carbon isotope compositions of various compounds, including n-alkanes, hopanes, C₂₉ sterane, pristane, and phytane. These data revealed that the total organic carbon (TOC) from the Kotlin Regional Horizon, particularly in low-salinity deltaic environments from the Utkina Zavod drill core, are ¹³C-enriched by up to 10‰ compared to marine rocks from other locations during on Baltica. This significant ¹³C-enrichment is also reflected in the n-alkanes, hopanes, phytane, and C₂₉ steranes. In every location all $\delta^{13}\text{C}$ for C₂₉ steranes are within 2‰ of $\delta^{13}\text{C}_{\text{org}}$ bacterial hopanes. The lack of variation between the carbon isotopic composition of bacterially derived hopanes and green algal derived C₂₉ steranes also suggests that the abundant hopanes within these sediments may derive from bacteria utilizing the RuBisCO-CBB pathway.

Chapter Four addresses the U–Pb geochronology of detrital zircons from the Ediacaran and Cambrian sedimentary successions in Northeast Estonia and the Volyn region of Ukraine. The chapter aims to understand the provenance of these sedimentary successions and to compare them with other regions previously studied around Baltica. This involved comprehensive U–Pb dating of detrital zircon grains to determine their ages and source regions. This geochronological analysis helped reconstruct the

depositional history and the tectonic and geographic evolution of Baltica during the late Ediacaran to early Cambrian periods.

Chapter Five is a synthesis of the dissertation and sums up concluding thoughts presented in the previous three chapters.

1.4 References

- Canfield, D.E., Poulton, S.W., Knoll, A.H., Narbonne, G.M., Ross, G., Goldberg, T., and Strauss, H., 2008, Ferruginous Conditions Dominated Later Neoproterozoic Deep-Water Chemistry: *Science*, v. 321, p. 949–952, doi:10.1126/science.1154499.
- Duda, J.-P., Thiel, V., Reitner, J., and Grazhdankin, D., 2016, Opening up a window into ecosystems with Ediacara-type organisms: preservation of molecular fossils in the Khatyspyt Lagerstätte (Arctic Siberia): *PalZ*, v. 90, p. 659–671, doi:10.1007/s12542-016-0317-5.
- Fike, D.A., Grotzinger, J.P., Pratt, L.M., and Summons, R.E., 2006, Oxidation of the Ediacaran Ocean: *Nature*, v. 444, p. 744–747, doi:10.1038/nature05345.
- Goryl, M., Marynowski, L., Brocks, J.J., Bobrovskiy, I., and Derkowski, A., 2018, Exceptional preservation of hopanoid and steroid biomarkers in Ediacaran sedimentary rocks of the East European Craton: *Precambrian Research*, v. 316, p. 38–47, doi:10.1016/j.precamres.2018.07.026.
- Grazhdankin, D., 2014, Patterns of Evolution of the Ediacaran Soft-Bodied Biota: *Journal of Paleontology*, v. 88, p. 269–283, doi:10.1666/13-072.
- Grosjean, E., Love, G.D., Stalvies, C., Fike, D.A., and Summons, R.E., 2009, Origin of petroleum in the Neoproterozoic–Cambrian South Oman Salt Basin: *Organic Geochemistry*, v. 40, p. 87–110, doi:10.1016/j.orggeochem.2008.09.011.
- Ivantsov, A.Yu., Grytsenko, V., Fedonkin, M.A., Zakrevskaya, M.A., Paliy, V.M., Velikanov, V.A., Konstantinenko, L.I., Menasova, A.Sh., and Serezhnikova, E.A., 2015, Upper Vendian macrofossils of Eastern Europe. Middle Dniester area and Volhynia.: Mosco PIN RAS.
- Johnston, D.T., Poulton, S.W., Goldberg, T., Sergeev, V.N., Podkovyrov, V., Vorob'eva, N.G., Bekker, A., and Knoll, A.H., 2012, Late Ediacaran redox stability and metazoan evolution: *Earth and Planetary Science Letters*, v. 335–336, p. 25–35, doi:10.1016/j.epsl.2012.05.010.
- Lee, C., Fike, D.A., Love, G.D., Sessions, A.L., Grotzinger, J.P., Summons, R.E., and Fischer, W.W., 2013, Carbon isotopes and lipid biomarkers from organic-rich facies of the Shuram Formation, Sultanate of Oman: *Geobiology*, v. 11, p. 406–419, doi:10.1111/gbi.12045.
- Love, G.D. et al., 2009, Fossil steroids record the appearance of Demospongiae during the Cryogenian period: *Nature*, v. 457, p. 718–721, doi:10.1038/nature07673.

- Pehr, K., Baczynski, A.A., Bekker, A., Hoffmann, A., Freeman, K.H., Poulton, S.W., and Love, G.D., 2023, Compound-specific carbon isotope measurements of individual lipid biomarkers from immature Ediacaran rocks of Baltica: *Organic Geochemistry*, v. 182, p. 104641, doi:10.1016/j.orggeochem.2023.104641.
- Pehr, K., Love, G.D., Kuznetsov, A., Podkovyrov, V., Junium, C.K., Shumlyansky, L., Sokur, T., and Bekker, A., 2018, Ediacara biota flourished in oligotrophic and bacterially dominated marine environments across Baltica: *Nature Communications*, v. 9, doi:10.1038/s41467-018-04195-8.
- Shields-Zhou, G., and Och, L., 2011, The case for a Neoproterozoic Oxygenation Event: Geochemical evidence and biological consequences: *GSA Today*, v. 21, p. 4–11, doi:10.1130/GSATG102A.1.
- Wood, R.A. et al., 2015, Dynamic redox conditions control late Ediacaran metazoan ecosystems in the Nama Group, Namibia: *Precambrian Research*, v. 261, p. 252–271, doi:10.1016/j.precamres.2015.02.004.
- Zumberge, J.A., Love, G.D., Cárdenas, P., Sperling, E.A., Gunasekera, S., Rohrssen, M., Grosjean, E., Grotzinger, J.P., and Summons, R.E., 2018, Demosponge steroid biomarker 26-methylstigmastane provides evidence for Neoproterozoic animals: *Nature Ecology & Evolution*, v. 2, p. 1709–1714, doi:10.1038/s41559-018-0676-2.

CHAPTER TWO

Environmental salinity severely impacted late Ediacaran marine communities across Baltica prior to the Cambrian Period

Adam Hoffmann¹, Kelden Pehr¹, Leonid Shumlyansky², Tetyana Sokur³, Alvar Soesoo^{4,5}, Andrey Bekker¹, and Gordon Love¹

¹Department of Earth and Planetary Sciences, University of California, Riverside, 900 University Avenue, Riverside CA 92521, USA. ²Institute of Geological Sciences, Polish Academy of Sciences (ING PAN), Research Centre in Kraków, Senacka 1, PL–31002 Kraków, Poland. ³Institute of Geological Sciences, National Academy of Sciences of Ukraine, Olesya Honchara Str., 55-b, Kiev 01054, Ukraine. ⁴Institute of Geology, Tallinn University of Technology, Tallinn, 19086, Estonia. ⁵Geological Survey of Estonia, Rakvere, 44314, Estonia

Abstract

The late Ediacaran sedimentary successions preserve fossils of the earliest known macroscopic multicellular organisms, known as the Ediacara biota, during an important transitional period in the evolution of complex life prior to the Precambrian-Cambrian boundary. The late Ediacaran interval preserved on Baltica is divided into two regional stages, comprising the older Redkino Stage (ca. 560-550 Ma) and the younger Kotlin Stage (ca. 550-540 Ma). Although nutrient limitation gave rise to widespread marine oligotrophic conditions across Baltica, which persisted through both stages and into the Early Cambrian, a sharp decline in diversity and abundance of the Ediacara biota has

been observed across the boundary between the Redkino and Kotlin horizons. This boundary, which has been considered the first major mass extinction event on Earth, marks the disappearance of both the Avalon and White Sea assemblages with only Nama-type organisms persisting through to the Kotlin Stage on Baltica. Using a combination of organic and stable isotope geochemistry, we have compiled detailed chemo-stratigraphic records using lipid biomarkers, stable isotopes ($\delta^{13}\text{C}_{\text{org}}$ and $\delta^{15}\text{N}$), Fe- and P-phase partitioning, and major and trace metals from multiple drill cores located in Russia, Ukraine, and Estonia. These records strongly suggest that an abrupt environmental shift between the Redkino and Kotlin stages coincided with the decrease in faunal diversity. This ecological perturbation beginning near the Redkino-Kotlin boundary and persisting through the Kotlin Stage was associated with fundamental changes in the aquatic salinity recorded for shallow shelf waters of epicontinental basins across the breadth of Baltica. The development of coastal brackish waters in multiple locations was likely a response to decreasing sea level from tectonic and/or climatic changes during the late Ediacaran. We propose that environmental selection pressure may have played a major role in influencing the community structure and extinction dynamics of macroscopic Ediacara biota.

1.0 Introduction

The Ediacaran Period (~635 – 539 Ma (Knoll et al., 2004; Linnemann et al., 2018) is widely regarded as a key interval in Earth history with the appearance of early

macroscopic multicellular organisms known as the *Ediacara biota*. The Ediacara biota characterize the second half of the Ediacaran Period and their radiation has been linked to environmental factors, such as a post-Gaskiers rise in atmospheric and marine oxygen concentrations at ~580 Ma (Zhang et al., 2019). The Ediacara biota are divided into three temporally distinct assemblages known as the Avalon (ca. 575–560 Ma), White Sea (ca. 560–550 Ma), and Nama (550–539 Ma), with a noticeable decline in diversity globally from the White Sea to Nama assemblages. There is currently no apparent consensus for the cause(s) of the decline in diversity of the Ediacara biota although changes in environmental conditions, seawater chemistry, food sources, and increased competition from evolving predators have all been implicated (Johnston et al., 2012; Grazhdankin, 2014b; Pehr et al., 2018). A major challenge in understanding the decline in the Ediacara biota is the limited number of well-preserved sedimentary rocks containing sufficient and thermally well-preserved organic matter and fossils of Ediacara biota (Duda et al., 2014). Thus, the stability and nature of the environmental settings that the Ediacara biota inhabited is currently poorly constrained by biogeochemical proxies.

Thermally immature sedimentary rocks deposited in multiple locations offshore of Baltica provide a unique opportunity to explore how both environmental aquatic conditions and biological communities changed during the late Ediacaran. For Baltica, the late Ediacaran is divided into two distinct biostratigraphic horizons, the *Redkino* and the younger *Kotlin*. The Redkino horizon is typically associated with containing more diverse faunal assemblages, as gauged from body fossil contents, as compared to the

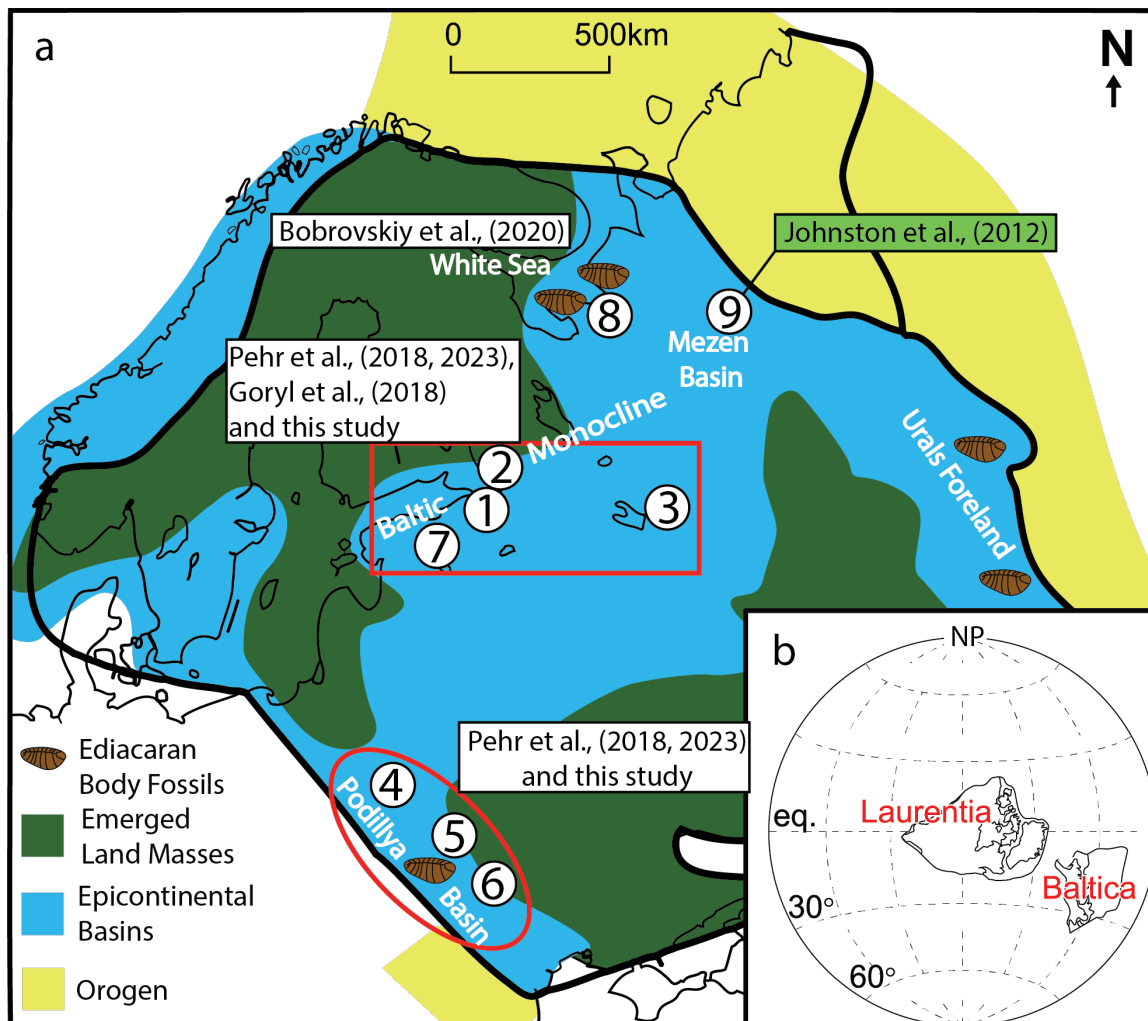


Figure 2.1. Paleogeography with known Ediacaran Biota fossils. **a.** Map Numbered regions correspond to drillcores and outcrop samples used in this study (1 - Utkina Zavod, 2 - Lugovoe, 3 - Gavrilov-Yam, 4 – Volyn Basin (4504, 4529, and 4592 drill cores), 5 - 3628 drill core from the Podoliya Basin, 6 - Outcrops 16 -PL, Ty-16, Ber, and Qua from the Podoliya Basin, 7 – F-169 drill core from Eastern Estonia, 8 – White Sea outcrop samples with abundant Ediacaran Biota fossils studied by Bobrovskiy et al. (2020) 9 – F-169 drillcore from Narva, Estonia., 9 – Kelt’ma drill core studied by Johnston et al. (2012) from Western Russia in the Mezen Basin. **b.** Reconstruction of Laurentia and Baltica during the late Ediacaran from Merdith et al. (2017). White boxes are sites of previous lipid biomarker studies, the green box is the site of a previous Fe mineral speciation study.

Kotlin horizon. The Redkino sedimentary strata has been described as having hosted Avalon-, White Sea-, and Nama-type Ediacaran biofacies contemporaneously (Grazhdankin, 2004; Duda et al., 2014; Ivantsov et al., 2015a, 2015b). Conversely, the Kotlin horizon is a period that reflects a significant reduction in biodiversity with predominantly Nama-type biofacies persisting (Grazhdankin et al., 2011; Kolesnikov et al., 2015). This dramatic decrease in faunal diversity, referred to as the “Kotlin Crisis”, is found in Podillya and Volyn, Ukraine, and White Sea and the South Urals, Russia (Grazhdankin, 2003, 2014b; Grazhdankin et al., 2011; Kolesnikov et al., 2015). This change coincides with the onset of a proposed global-scale extinction of the Ediacara biota suggested Evans et al., 2022.

In addition to the sites in Baltica preserving diverse and abundant Ediacaran body fossils, these sedimentary rocks are generally thermally immature, which makes Baltica an excellent target to perform organic geochemistry of lipid biomarkers that have not been extensively modified from burial. Biomarkers, molecular fossils, can yield valuable information pertaining to biological origins, the thermal maturity of the host rocks, and the paleoenvironmental conditions (redox, salinity, etc.), which prevailed in the water column and at the sediment surface during deposition.

Previous organic geochemical analysis of Ediacaran rocks from the Redkino and Kotlin horizons on Baltica has demonstrated that the basins surrounding Baltica were typically low-productivity marine settings that were oligotrophic (nutrient-depleted) and,

as a consequence, bacterially dominated (Goryl et al., 2018; Pehr et al., 2018, 2023; Bobrovskiy et al., 2020). The decrease in diversity of Ediacara biota across Baltica between the Redkino and Kotlin regional stages has been attributed to a shift to higher energy environmental conditions (deltas and distributary channels) where Nama-type organisms survived compared to White Sea-type and Avalon-type organisms due in part to their burrowing abilities (Grazhdankin, 2014b).

In this study we examined well preserved thermally immature sedimentary rocks, from mainly well preserved drillcores, collected in Estonia, Ukraine and Russia. Samples were collected from the Volyn'-Podillya basin and the Baltic Monocline where abundant Ediacara biota have been characterized (Grazhdankin, 2003; Ivantsov et al., 2015b, 2015a). This is one of the first studies to perform organic geochemistry on a comprehensive set of Ediacaran rocks (following Goryl et al., 2018; Pehr et al., 2018, 2023), but with the added benefit of having parallel geochemical data from iron mineral speciation and stable isotopic (C, N) analyses for the same samples. Here, we aim to better understand the ancient oceanic conditions and environmental fluctuations that drove the decrease in Ediacara biota across Baltica.

2.0 Geologic Setting and Stratigraphy

Ediacaran strata of Baltica were deposited on top of the accreted Archean and Paleoproterozoic basement rocks and portions of the Volyn' Large Igneous Province (Grazhdankin et al., 2011). These Ediacaran strata are composed of fine-grained

siliciclastic rocks including argillites, mudstones, and shales as well as fine-grained sandstones and minor amounts of diagenetic carbonate nodules. Outcrop sampling sites containing Ediacara biota were also included, along with samples from multiple drillcores, to investigate the local environmental conditions directly related to these fossils. Specific Redkino regional horizon sites in Moldova and southwestern Ukraine contain various Ediacaran body fossils including *Charniodiscus*, *Beltanella*, and *Dickinsonia* (Grazhdankin et al., 2011; Ivantsov et al., 2014, 2015a; Grazhdankin and Maslov, 2015).

This study examines rocks from both drillcore, and outcrop collected in Estonia, Ukraine, Russia, and Moldova (Fig. 2.1). Samples were collected from stratigraphic units on Baltica encompassing a wide spatial and temporal scale (Grazhdankin, 2014a; Ivantsov et al., 2015a). Stratigraphic units on Baltica are divided into two regional stages based on Ediacaran fossil assemblages: the Redkino regional horizon and the Kotlin regional horizon. The older Redkino strata are interpreted to be deposited under normal to elevated salinity, oligotrophic conditions. Redkino strata contain abundant and diverse Nama-type, White Sea-type and Avalon-type Ediacaran fossil assemblages (Ivantsov et al., 2015a; Merdith et al., 2017; Bobrovskiy et al., 2020). The younger Kotlin strata in western Russia (site 1 in Fig. 2.1) are interpreted to be deposited under mainly lower salinity, oxic, oligotrophic conditions (Pehr et al., 2018). The Kotlin crisis is the onset of the Kotlin regional stage and is described by a stark decrease in diversity of the Ediacara biota with only Nama-type fossils being preserved. This sudden drop in diversity has been speculated as the first extinction event marking the eventual demise of the Ediacara

biota leading to the Cambrian (Grazhdankin et al., 2011; Evans et al., 2022). Lack of suitable environments for ensuring good taphonomic preservation, changes in environmental conditions, as well as increased competition and evolution of predators have been proposed as causes for the disappearance of many types of the biota of the White Sea and Nama Assemblages (Laflamme et al., 2013; Kolesnikov et al., 2015).

Although the rocks in this study have undergone sedimentary diagenesis and very early catagenesis, most have not exceeded 60° C as their maximum burial temperature making them highly immature rocks which are good targets to perform organic geochemistry since primary structural features of lipid biomarkers are well preserved. Additionally, the limited exposure to high temperature burial regimes greatly decreases the chance that $\delta^{13}\text{C}_{\text{org}}$ and $\delta^{15}\text{N}_{\text{total}}$ have been significantly altered through thermal cracking and loss of volatiles. Here, we aim to understand chemical and biological heterogeneity in the ancient ocean that drove the decrease in Ediacara biota across Baltica.

The sedimentary rock samples used are younger than ca. 560 Ma, based on established correlations with the well-dated (U=Pb volcanic zircon) strata of White Sea and Ural Mountains, Russia and Podillya, Ukraine (Grazhdankin, 2014a; Grazhdankin and Maslov, 2015) and thus were deposited during the time interval when shallow-marine waters were redox-stabilized with oxic conditions commonly found on Baltica (Johnston et al., 2012).

2.1. Volyn'-Podillya basin (Ukraine)

The Volyn'-Podillya basin is located on the southwestern margin of Baltica covering modern day Western Ukraine and North-Eastern Moldova (region of Sites 4-6 in Figure 2.1). Outcrop samples collected are Ediacaran strata that are exposed in the basin carved by the Dniester River and some of its larger tributaries with additional sampling localities exposed by mining operations for the Dnestrovskaya Hydroelectric Power Station at the Novodnistrovsky quarry. Figure 2.2a shows the stratigraphy of drillcore 3628 which records the Redkino and Kotlin horizons from the Podillya basin. A disconformity is present between

the Nagoryany and Danilovka formations, marking the end of the Redkino regional stage and the beginning of the Kotlin regional stage.

2.2. Baltic Monocline (Estonia)

The Baltic Monocline is located on the northern margin of Baltica covering modern-day northwestern Russia and Estonia.

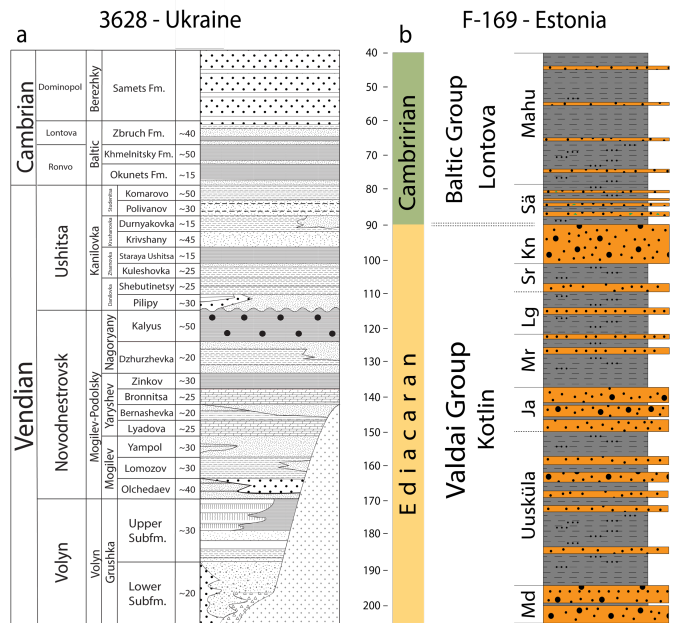


Figure 2.2. a. Generalized stratigraphic column for the Podillya Region of Ukraine (modified from Ivantsov et al., 2015). b. Generalized stratigraphic column for F-169 drill core from Narva, Estonia (modified from Francovschi et al.,

Drillcore F-169 (Baltic Monocline, Estonia) records the latest portion of the Ediacaran and the early portion the Cambrian. An unconformity exists between the Kaanuka Member of the upper Kotlin regional stage and the Sämi Member of the lower Cambrian. The F-169 drillcore (Site 9 in Figure 2.1), collected near Narva, Estonia, contains siltstones and very fine-grained sandstones interbedded with green-grey mudstones. Samples collected are from the upper portion of the Kotlin Regional Stage and extend through to the lowermost portion of the Cambrian.

Rocks from the Kotlin Regional Stage in drillcore F-169 are siltstones and argillites interbedded with fine-grained sandstones. Rocks from the Cambrian section are siltstones and argillites interbedded with fine- to very-fine-grained sandstones. Our sampling priority was focused on fine-grained rocks with the best potential for biomarker preservation. Figure 2.2b shows the detailed stratigraphy of drillcore F-169.

The exceptionally low thermal maturity of these sedimentary rocks is highlighted by the excellent preservation of structural and stereochemical features of biomarkers. Thus, the F-169 rocks are ideal targets for lipid biomarker and stable isotope analysis (C, N), despite most intervals being lean in organic matter content, since the rocks have not experienced maximum burial temperatures exceeding $\sim 60^{\circ}\text{C}$. F-169 samples allow an interesting comparison with lipid biomarker assemblages reported from Utkina Zavod (Site 1 in Figure 2.1) and Lugovoe (Site 2 in Figure 2.1) cores from northwestern Russia (Pehr et al., 2018) using the same instrumentation and methodologies optimized for deep-

time lipid biomarker analysis used routinely in the organic geochemical laboratories in the Love Research Group at UCR.

3.0. Materials and Methods

Samples were collected from various localities across Baltica including Estonia, Western Russia, West and Southwestern Ukraine and Eastern Moldova (Fig. 2.1). Samples collected represent both proximal and distal marine facies. Distal samples included shales containing diagenetic phosphorite nodules, mudstones, and argillites that represent deepest water facies in this sample set. Proximal samples were represented by fine-grained-crossbedded sandstones and very-fine-to-fine-grained, fossiliferous sandstones with impressions of *Beltanelliformis*.

Samples were prepared by cutting away the outer portion leaving the clean interior of the sample for analyses. Interiors were sonicated for 2 minutes each in deionized (DI) water, hexanes, dichloromethane (DCM), and methanol. Once dried, samples were crushed using a SPEX 8515 shatterbox using a zirconia puck mill. Between samples, the dish was fully cleaned with multiple rounds of combusted quartz sand (800°C overnight) followed by rinsing with hexane, DCM, and methanol. A full procedural blank of combusted quartz sand was then crushed and collected prior to the sample being crushed. Samples were collected into cleaned, combusted scintillation vials and capped with combusted aluminum foil for storage.

3.1. Total organic carbon $\delta^{13}\text{C}_{\text{org}}$ and $\delta^{15}\text{N}$ analyses

Total organic carbon isotope and total nitrogen isotope analyses ($\delta^{13}\text{C}_{\text{org}}$ and $\delta^{15}\text{N}$) were performed using a Costech ECS 4010 Elemental Analyzer coupled to a Thermo Scientific Delta V Advantage isotope-ratio mass-spectrometer via a Thermo Scientific Conflo IV open-split gas interface system at the SAFIR at UCR. 50-100 mg sample powders were acidified overnight for at least 12 hours using 6 N HCl in 50 mL centrifuge tubes; tubes were periodically vortexed. The tubes were then centrifuged at 3000 rpm for two minutes; acid was decanted and powders were washed with deionized water. The process was repeated four times per sample, until pH strips registered neutral to ensure complete removal of residual acid. Decarbonated and dried insoluble residues of ~5-10 mg were weighed into 9 x 10 mm tin weight boats for organic carbon isotope analysis. Combustion was achieved using a pulse of O_2 set for 60s. The combustion and reduction columns were set to 1100°C and 650°C, respectively, with helium as the carrier gas at a flow rate of 100 ml/min. Carbon isotope ratios are reported in standard (δ) delta notation relative to Vienna Pee Dee Belemnite where $\delta^{13}\text{C}_{\text{org}} = [((^{13}\text{C}/^{12}\text{C})_{\text{sample}} / (^{13}\text{C}/^{12}\text{C})_{\text{VPDB}}) - 1] * 1000$. Nitrogen isotope ratios are also reported in standard (δ) delta notation relative to Air where $\delta^{15}\text{N}_{\text{org}} = [((^{15}\text{N}/^{14}\text{N})_{\text{sample}} / (^{15}\text{N}/^{14}\text{N})_{\text{Air}}) - 1] * 1000$. Average Analytical precision of standard laboratory reference materials (Acetanilide, Hawaii glycine, and USGS SDO-1) used during analytical sessions was better than $\pm 0.10\text{‰}$ for $\delta^{13}\text{C}_{\text{org}}$ (1s) and $\pm 0.2\text{‰}$ for $\delta^{15}\text{N}$ (1s).

3.2. Major and Trace Metal Analyses and Fe-mineral speciation

As a complement organic and stable isotope geochemical data, samples were powdered for whole rock trace metal analysis. Approximately 400 mg of powdered sample were ashed at 850 °C for 12 h and then dissolved using standard procedures through a three acid (HNO₃, HF, HCl) total digestion. Samples were analyzed using a quadrupole ICP-MS (Varian 820MS) by Simon Poulton at the University of Leeds. Quantitative data for Ti, V, Cr, Mn, Fe, Ni, Cu, Zn, Mo, Ba, Re, Pb, and U were acquired, and mean reproducibility of sample solution analyses (repeat measurement of the same solution) over the full range of concentration encountered was ± 11%.

Highly reactive iron (Fe_{HR}) was calculated as the sum of Fe as pyrite, carbonate, and oxides—Fe_{py}, Fe_{carb}, and Fe_{ox}, respectively. Pyrite sulfur concentrations from standard chromium reduction methods (Canfield et al., 1986) were used to calculate Fe_{py} assuming a stoichiometry of FeS₂. Fe_{carb} and Fe_{ox} were extracted sequentially as described by Poulton and Canfield (2005). Specifically, approximately 100 mg from 64 samples were extracted sequentially: 1 M sodium acetate extraction adjusted to pH= 4.5 for 48 h with constant shaking (Fe_{carb}) followed by extraction of the sample residue for its iron oxide content (Fe_{ox}) using 50 g/L sodium dithionite buffered to pH =4.8 for 2 h while shaking. All extracts were diluted 100-fold in 2% HNO₃ and analyzed for Fe concentrations using ICP-MS at the University of Leeds.

3.3. P-phase partitioning

P-phase partitioning was performed at the University of Leeds. Selected samples were subjected to a separate sequential P extraction following the modified SEDEX methodology after Ruttenberg, 1992, adjusted for use on ancient sediments (Thompson et al., 2019). This method isolates operationally-defined P pools including P bound to Fe(oxyhydr)oxide minerals (P_{Fe}), organic matter (P_{org}), authigenic carbonate fluorapatite, biogenic apatite and CaCO_3 (P_{auth}), and detrital apatite (P_{cryst}). Reactive P (P_{reac}) equates to the sum of P_{Fe} , P_{auth} and P_{org} (Ingall et al., 1994). The concentrations of P in P_{org} , P_{auth} and P_{cryst} leachates were measured spectrophotometrically using the molybdate-blue method on a Spectronic GENESYS 6 at a wavelength of 880 nm, whereas P concentrations in the P_{Fe} leachates (including P_{Fe} and P_{mag}) were measured by ICP-OES (Thompson et al., 2019). A mean P recovery of 89% of P_{Tot} (as measured by ICP-OES after total digestion) was achieved by the sequential extraction protocol. Replicate analyses of the Fe speciation standard (WHIT, n=9) gave a relative standard deviation of <7% for all extraction steps.

3.4. Major elements and trace metals

Major element and trace metal analyses were performed at the University of Leeds. Samples were prepared for major element and trace metal analyses via total digestion, which comprised ashing at 550°C for 8h, followed by dissolution using a combination of concentrated HNO_3 , HF, and HClO_4 , with boric acid used to prevent the

formation of Al complexes. Major elements were quantified via inductively coupled plasma (ICP-OES) – optical emission spectroscopy and trace metals via inductively coupled plasma – mass spectrometry (ICP-MS). All data were within 10% of verified values.

3.5. Total and pyrite sulfur

Total sulfur (TS) for all samples from drillcore F-169 were measured using an ELTRA carbon and sulfur analyzer at UCR. Total S was determined through combustion of samples at 1350°C, with quantification of evolved gasses by infrared absorption. Pyrite Sulfur was determined by calculating the stoichiometric ratio from extracted pyrite resulting from (Canfield et al., 1986).

3.6. Solvent extraction and silica gel chromatography of rock bitumens

Typically, 5–20 g of rock powder per sample was extracted in organic solvent-cleaned Teflon vessels on a CEM microwave accelerated reaction system (MARS5) in 30 ml of 9:1 (v/v) DCM/MeOH. Samples were heated to 100°C for 15 mins with constant magnetic bar stirring. Procedural blanks were performed with combusted silica. Rock bitumens were recovered from vacuum filtration and elemental sulfur was removed with solvent-cleaned and HCl-activated copper granules. Saturated hydrocarbon, aromatic hydrocarbon, and polar (N, S, O) fractions were obtained through separation of rock bitumen on dry packed silica gel (Fisher, 60 grit) microcolumns. The silica gel was

combusted in a muffle furnace at 450°C for at least 9 h to remove any moisture and trace organic residue prior to adsorption of whole rock extracts and use in column chromatography. The saturated hydrocarbon fraction was eluted with n-hexane, aromatic hydrocarbons with 1:1 (v/v) n-hexane:DCM, and the polar hydrocarbons with 3:1 (v/v) DCM:MeOH, respectively.

3.7. Gas chromatography–mass spectrometry (GC–MS)

The saturated fractions were run in full scan mode (m/z 50–800 Dalton) on an Agilent 7890A gas chromatograph (GC) system coupled to an Agilent 5975C inert MSD mass spectrometer. Samples were injected as hexane solutions in splitless injection mode with a programmable temperature vaporizing (PTV) inlet and using He as the carrier gas. The GC was equipped with a DB1-MS capillary column (60 m \times 0.32 mm, 0.25 μ m film thickness). The GC temperature program used for full scan analysis was 60°C (held for 2 min), heated to 150°C at 20°C/min, then to 325°C at 2°C/min, and held at 325°C for 20 mins.

3.8. Metastable reaction monitoring GC–MRM-MS

The polycyclic alkane constituents of saturated hydrocarbon fractions were analyzed in detail by metastable reaction monitoring GC–MRM-MS using a Waters AutoSpec Premier mass spectrometer equipped with an Agilent 7890A GC. The GC was

equipped with a DB1- MS capillary column (60 m ×0.25 mm, 0.25 μm film thickness) with He used as the carrier gas. The samples were injected as hexane solutions in splitless mode using an inlet temperature of 320°C. The GC temperature program used for compound separation consisted of an initial hold at 60°C for 2 min, then heated to 150 °C at 10 °C/min, then to 320°C at 3°C/min and finally held isothermally for 22 mins. Analyses were performed in electron impact mode with 70 eV ionization energy and 8 kV accelerating voltage. MRM transitions for C27–C35 hopanes, C31–C36 methylhopanes, C21–C22 and C26–C30 steranes, C30 methylsteranes and C19–C26 tricyclics were selectively monitored in the method used. Procedural blanks with pre-combusted sand yielded <0.1 ng of individual hopane and sterane isomers per gram of combusted sand. Polycyclic biomarker alkanes (tricyclic terpanes, hopanes, steranes, etc.) were quantified by addition of 50 ng of deuterated C29 sterane standard [d4- ααα-24-ethylcholestane (20R), Chiron Laboratories] to saturated hydrocarbon fractions and by comparison of relative peak areas. GC–MRM- MS was used to determine accurate biomarker abundance ratios for all the polycyclic biomarkers plotted in Figs. 2.2, 2.4, and 2.5. Analytical error for individual hopane and sterane concentrations are estimated to be ±30%. Average uncertainties in hopane and sterane biomarker ratios are ±8% as

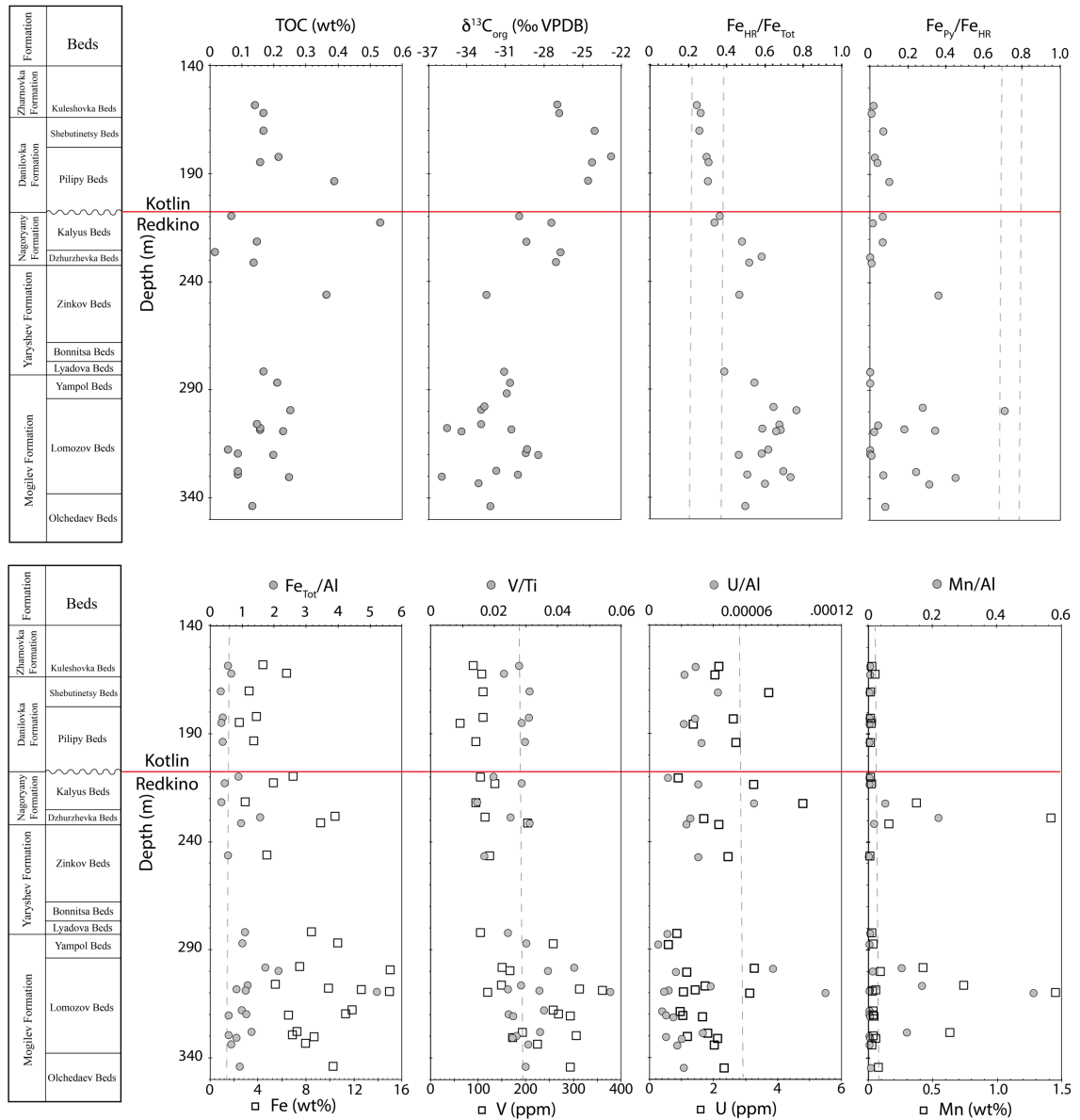


Figure 2.3. Geochemical plots vs depth for drillcore 3628. **a.** TOC (wt%), **b.** $\delta^{13}C_{org}$ reported in standard delta notation (‰ VPDB) **c.** Fe_{Tot}/Fe_{HR} , area between dashed lines represents the anoxic equivocal zone (0.22 – 0.38). **d.** Fe_{Py}/Fe_{HR} , area between dashed lines represents euxinic equivocal zone (0.7 – 0.8). **e.** Fe_{Tot}/Al and Fe concentration, dashed line represents average shale ratio and concentration (0.60/4.7 wt %). **f.** V/Ti and V concentration, dashed line represents average shale ratio and concentration (0.0028/130 ppm). **g.** U/Al and U concentration, dashed line represents average shale ratio and concentration (0.00005/3.7 ppm). **h.** Mn/Al and Mn concentration, dashed line represents average shale ratio and concentration (0.01/850 ppm). For e - h, boxes represent concentration and grey circles represent normalized values. Red horizontal line indicates the transition from the Redkino horizon to the Kotlin horizon.

calculated from multiple analyses of saturated hydrocarbon fractions from in-house oil standards.

4.0 Results

4.1. Total organic carbon (TOC) content and $\delta^{13}\text{C}_{\text{org}}$ values

As has been previously reported by several groups, TOC content in samples from across Baltica are typically low (Goryl et al., 2018; Pehr et al., 2023), especially compared with petroleum source rocks deposited in eutrophic basins from other Ediacaran locales including South Oman, Siberia, and India (Johnston et al., 2012; Dutta et al., 2013; Lee et al., 2013; Duda et al., 2016). All data for total organic carbon are reported in Table 2.1. TOC content for the Redkino Horizon ranges from 0.01 – 0.62 wt% with an average of 0.19 wt% (n=42). TOC content for the Kotlin Horizon ranges from 0.02 – 0.9 wt% with an average of 0.28% (n=50). $\delta^{13}\text{C}_{\text{org}}$ measurements from Baltica have been reported previously by Pehr et al. 2018 and Johnston et al. 2012. Their data for the Redkino horizon show lighter $\delta^{13}\text{C}_{\text{org}}$ values compared to the younger Kotlin horizon.

Redkino Horizon $\delta^{13}\text{C}_{\text{org}}$ values have a range of -36.4‰ to -24.4‰ with an average $\delta^{13}\text{C}_{\text{org}} = -30.2‰$ (n=42). Redkino Horizon samples have the lightest values in the Lomozov and Yampol beds of the Mogilev Formation, with $\delta^{13}\text{C}_{\text{org}}$ values

progressively increasing toward the boundary with the Kotlin Horizon. Kotlin Horizon $\delta^{13}\text{C}_{\text{org}}$ values have a range of -33.9‰ to -22.6‰ with an average $\delta^{13}\text{C}_{\text{org}} = -26.9\text{‰}$ (n=50). $\delta^{13}\text{C}_{\text{org}}$ values for all samples are reported in Table 2.1 and values for drillcore 3628 are plotted in Figure 2.3.

4.1.1. $\delta^{13}\text{C}_{\text{org}}$ results for drillcore 3628 (Ukraine)

Total organic carbon isotope ratios for the 3628 drillcore are shown in Figure 2.3. This sample set shows a positive carbon isotope excursion of ~10‰ that occurs at the boundary of the Redkino and Kotlin horizons. Samples from the lower part of the Redkino Horizon of the 3628 drillcore are depleted in ^{13}C ($\delta^{13}\text{C}_{\text{org}} = -36\text{‰}$ to -28‰ , mean = -31.2‰) relative to other basins of Baltica (Johnston et al., 2012; Pehr et al., 2018), but are similar to the range of values for marine sedimentary organic matter for source rocks from South Oman (Grosjean et al., 2009; Lee et al., 2011). Previously reported C isotope compositions for the Redkino Horizon for the samples closer to the Redkino-Kotlin Horizon boundary in the 3628 drillcore shift towards more ^{13}C -enriched values (-30‰ to -24‰), in agreement with those previously reported by Johnston et al., (2012). The Kotlin Horizon samples show substantial ^{13}C -enrichment compared to the underlying Redkino Horizon samples ($\delta^{13}\text{C}_{\text{org}} = -27\text{‰}$ to -23‰ , mean = -24.9‰).

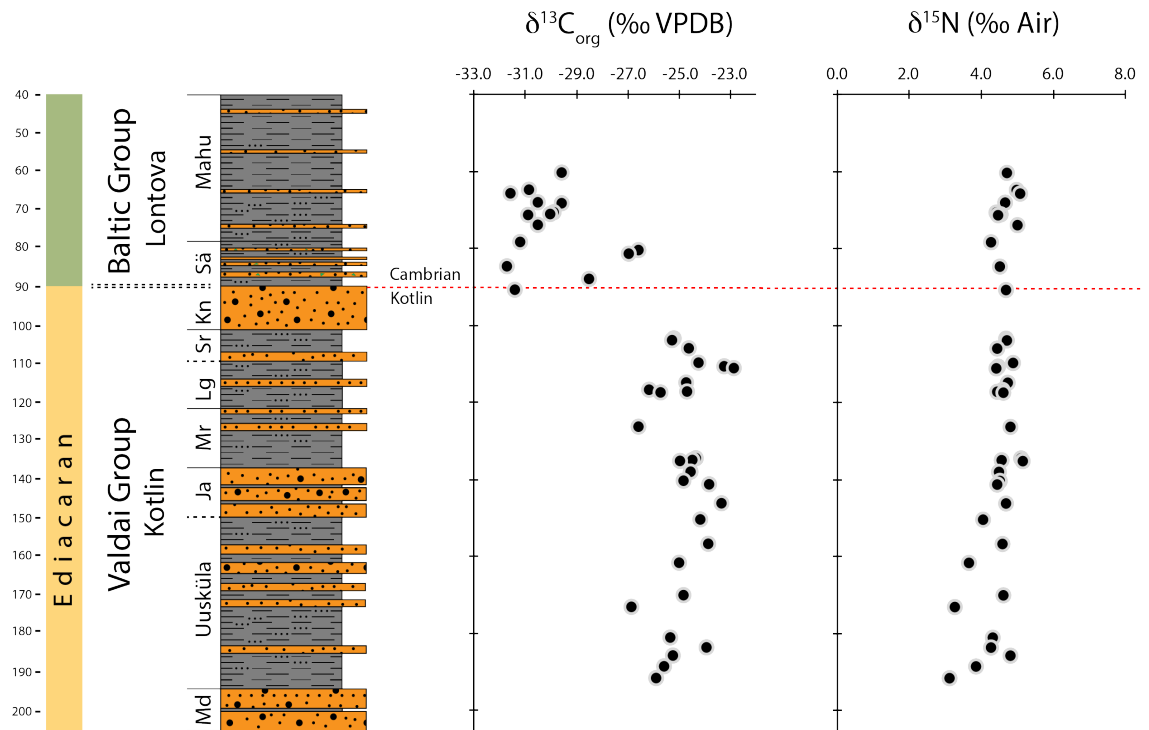


Figure 2.4. a. $\delta^{13}C_{org}$ reported in standard delta notation (‰ VPDB) b. $\delta^{15}N$ reported in standard delta notation (‰ Air)

4.1.2. $\delta^{13}C_{org}$ results for drillcore F-169 (Estonia)

Total organic carbon isotope ratios for the F-169 drillcore are shown in Figure 2.4. These samples are stratigraphically above the drillcore 3628 and show consistent enrichment in ^{13}C and have similar values to the Kotlin portion of 3628. Across an unconformity in drillcore F-169, Cambrian samples show an approximate $\sim\sim 6\%$ shift, consistent with the negative carbon isotope excursion observed at the Precambrian/Cambrian boundary (Margaritz et al., 1991; Kouchinsky et al., 2007; Wang et al., 2014). Samples from the Kotlin section of drillcore are enriched in ^{13}C ($\delta^{13}C_{org} = -26.8\%$ to -

22.9‰, mean = -24.7‰) compared to Redkino values and consistent with other basins of Baltica (Johnston et al., 2012; Pehr et al., 2018). Cambrian samples are ¹³C-depleted ($\delta^{13}\text{C}_{\text{org}} = -26.6\text{‰}$ to -31.7‰ , mean = -30.0‰) compared to the underlying Kotlin rocks and are on average of 6‰ lighter

4.2. $\delta^{15}\text{N}$ results for F-169 (Estonia)

$\delta^{15}\text{N}$ was measured on samples from drillcore F-169 and are reported in Table 2.1 and plotted in Figure 2.4. $\delta^{15}\text{N}$ from both the Kotlin and Cambrian portions of this core exhibit a small positive range ($\delta^{15}\text{N}$

= $+3.3\text{‰}$ to $+5.2\text{‰}$, mean = $+4.6\text{‰}$). These values are consistent with N-isotope values published by Pehr et al., (2018). In the lower Kotlin portion of the F-169

drillcore, $\delta^{15}\text{N}$ is relatively lighter ($\delta^{15}\text{N} = +3.3\text{‰}$ to $+4.6\text{‰}$, average = $+4.1\text{‰}$). The

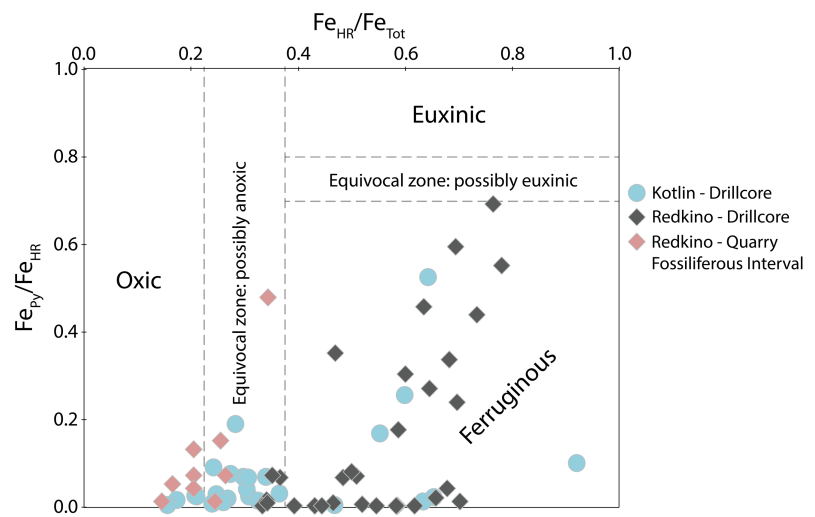


Figure 2.5. Crossplot of $\text{Fe}_{\text{Py}}/\text{Fe}_{\text{HR}}$ vs $\text{Fe}_{\text{Tot}}/\text{Fe}_{\text{HR}}$ with sectioned regions indicating Oxidic, Ferruginous, and Euxinic conditions with equivocal zones separating each region. Red diamonds represent Redkino outcrop samples with fossils of the Ediacaran Biota from the Podoliya region of Ukraine; Black diamonds represent Redkino drillcore and outcrop samples without fossils from Ukraine and Russia; and Blue circles represent Kotlin drillcore samples without fossils from Ukraine and Russia. The anoxic equivocal zone is between $\text{Fe}_{\text{HR}}/\text{Fe}_{\text{Tot}} - 0.22 - 0.38$, The Euxinic equivocal zone is between $\text{Fe}_{\text{Py}}/\text{Fe}_{\text{HR}} - 0.7 - 0.8$.

upper portion of the Kotlin and the Cambrian do not vary as widely ($\delta^{15}\text{N} = +4.7\%$ to $+5.2\%$, average = $+4.7\%$).

4.3. Iron Speciation

Fe speciation analyses were performed on 65 powdered rock samples from various locations, which represent the majority of the stratigraphical range of the Ediacaran preserved on Baltica. Fe speciation values are reported in Table 2.2 and the drillcore 3628 geochemistry is shown in Figure 2.3. The Mogilev Formation in the drillcore 3628 contains $\text{Fe}_{\text{HR}}/\text{Fe}_{\text{T}} > 0.4$ and up to 0.76, indicating anoxic/ferruginous depositional conditions. There is a trend to decreasing $\text{Fe}_{\text{HR}}/\text{Fe}_{\text{T}}$ values moving stratigraphically up towards the Nagoryany Formation that has values as low as 0.33 immediately below the boundary between the Kotlin and Redkino Horizons. $\text{Fe}_{\text{HR}}/\text{Fe}_{\text{T}}$ values further decrease in the Kotlin Horizon with a limited range between 0.24-0.30, most likely indicating oxic depositional conditions.

$\text{Fe}_{\text{HR}}/\text{Fe}_{\text{T}}$ values for the Redkino Horizon range from 0.16 to 0.74. The majority of Redkino Horizon samples are either ferruginous or equivocal. In contrast, the nine samples from the Dniester hydroelectric are oxic with values between 0.14 and 0.34. All samples from the Lugovoe drill core have relatively high $\text{Fe}_{\text{HR}}/\text{Fe}_{\text{T}}$ values of 0.55-0.92 compared to the rest of the Kotlin Horizon samples, which plot either in the oxic or equivocal zones.

Fe_{py}/Fe_{HR} values for the Kotlin Horizon range from 0.00 to 0.53. All samples are below 0.20 except for one outlier of 0.53. Fe_{py}/Fe_{HR} values for the Redkino Horizon range from 0.00 to 0.70. The 3628 drillcore ranges between 0.00 and 0.70 and the Lugovoe drill core has a range between 0.46 and 0.60. Fe speciation cross plots are shown in Figure 2.5.

Elevated Fe_T/Al values suggest Fe enrichment in our samples when compared to average (oxic) Phanerozoic shale. Redkino Horizon samples yield values between 0.39 and 2.1 with a single outlier of 5.01. The mean Fe_T/Al value for the Redkino Horizon samples, excluding the outlier, is 0.93 ± 0.43 . All but three Redkino Horizon samples have elevated Fe_T/Al relative to the average continental crust (0.5; Taylor and McLennan, 1985). Kotlin Horizon samples range between 0.32 and 0.98 with a single outlier of 8.78. The mean Fe_T/Al value for the Kotlin Horizon samples, excluding the single outlier, is 0.53 ± 0.19 . Of the 22 samples included in the Kotlin Horizon mean, 14 are lower than average continental crust composition, indicating deposition in an oxic water column.

Mn/Al ratios are reported in Table 2.2 and are plotted in Figure 2.3. Mn/Al ratios for most of the Redkino Horizon samples are at or below the that of average continental crust (0.008) with enrichments being observed in the lower part of the Redkino Horizon. Three samples from the Lomozov beds are enriched in Mn with Mn/Al values of 0.5, 0.16, and 0.12; one sample from the Lyadova beds has a value of 0.1, and the two Kalyus samples have values of 0.22 and 0.05.

4.4. Major and Trace Element signals of intermittent ferruginous conditions

Major and trace element concentrations were analyzed to constrain redox conditions across Baltica. Trace elements (e.g, V, Mo, Cr, U) have proven to be valuable markers for anoxic and euxinic conditions in the water column (Krishnaswami, 1976; Emerson and Huested, 1991; Calvert and Pedersen, 1996; Clarkson et al., 2014, 2021; Haddad et al., 2016; Han et al., 2018). Mo requires the presence of free H₂S to be deposited within the sediment while U and V are sensitive to anoxia and can be used as a tracer for dysoxic and anoxic settings (Bennett and Canfield, 2020; Dahl et al., 2021). Our samples show no enrichment in Mo or U and thus suggests that the water column in the epicontinental seas surrounding Baltica did not have significant sulfide (Scott and Lyons, 2012). Average shale ratios were calculated using data from Turekian and Wedepohl, (1961) All major and trace element data are reported in Table 2.2.

4.4.1. Vanadium

Across our sample set, vanadium concentrations in Redkino samples are highly variable with slight enrichments compared to average shale (V/Ti = 0.28) with values ranging from 0.015 to 0.57 (V/Ti average = 0.31). Kotlin samples also exhibit slight enrichment in some samples with most other samples being near crustal levels with values ranging from 0.22 to 0.45 (V/Ti average = 0.28). Drillcore 3638 shows enrichment

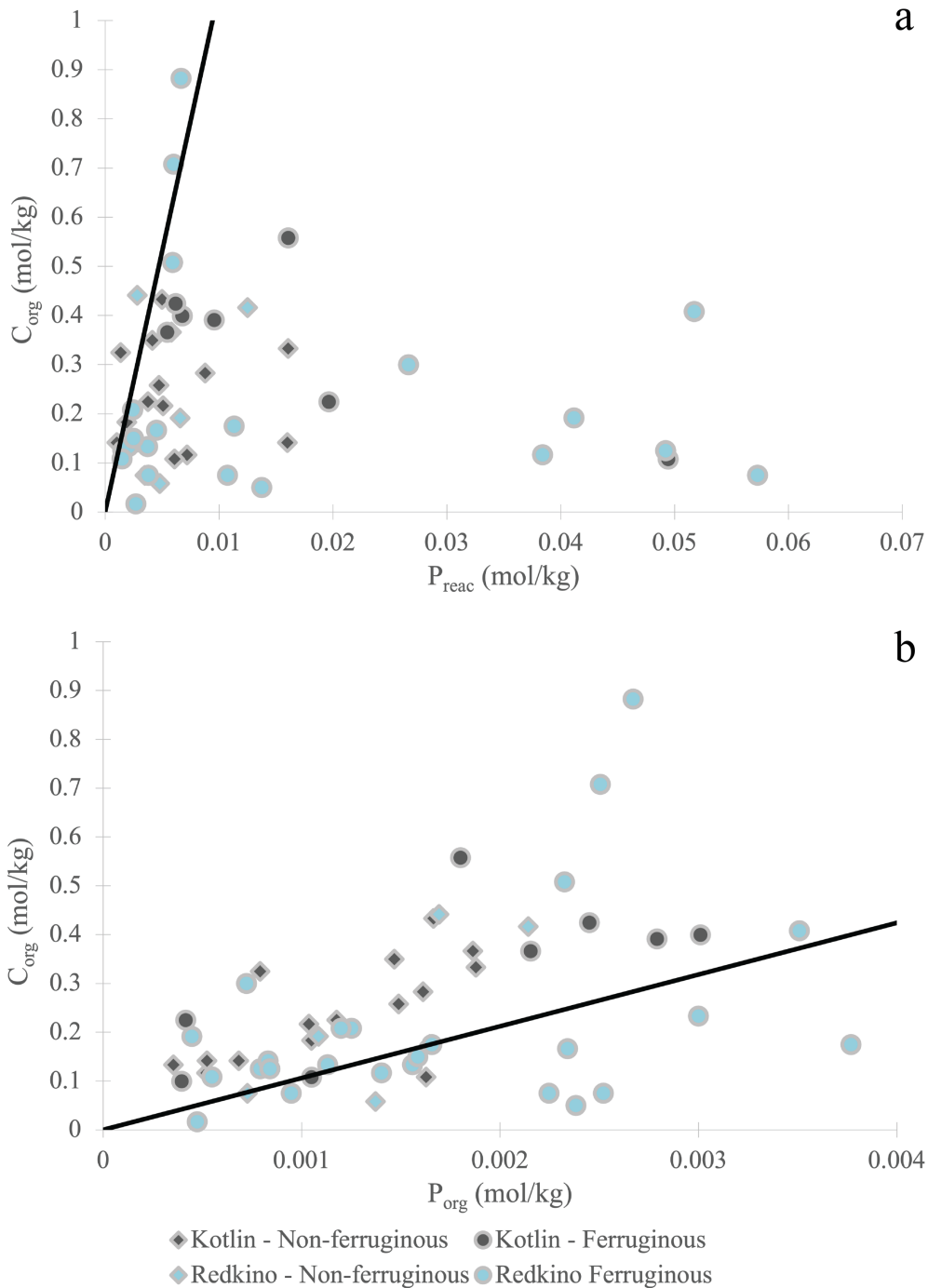


Figure 2.6. Crossplots of molar concentrations of (a.) P_{reac} vs C_{org} and (b.) P_{org} vs C_{org} . Diamonds represent oxitic conditions, circles represent ferruginous conditions. Diamonds represent non-ferruginous conditions, circles represent ferruginous conditions. Blue points are samples from the Redkino horizon, black points are samples from the Kotlin Horizon. The black line in each plot represents the Redfield ratio (106:1 C:P).

in the

lower portion of the Redkino with values returning to near or below crustal levels just below the Redkino-Kotlin boundary (Fig 2.3). For the 16 samples below 281 m V/Ti ratios range from 0.0024-0.0056 (V/Ti average = 0.32). For the 6 Redkino samples above 281 m, V/Ti ratios range from 0.015 to 0.056 (V/Ti average = 0.23). For the six Kotlin samples values range from 0.23 to 0.31 with an average that is at crustal levels (V/Ti average = 0.28).

4.4.2. Manganese as a tracer for intermittent oxic conditions

Manganese can play an important role in understanding the presence of oxygen during deposition of sediment. In particular, enrichments in manganese can help determine that oxygen was present at the time of deposition (Schaller and Wehrli, 1997; Sundby' et al.). Mn/Al ratios in our Redkino samples range from 0.0 to 0.74 (Mn/Al average = 0.05). Of the 42 Redkino samples measured, 31 are below average shale (Mn/Al = 0.01). The ten samples that are above crustal level have a range from 0.05 to 0.74 (Mn/Al average = 0.20). Mn/Al ratios in our Kotlin samples range from 0 to 0.15 (Mn/Al average = 0.004). Of the 20 Kotlin samples measured, 16 are below average shale. The four samples that are above average crustal level range from 0.4 to 0.15 (Mn/Al average = 0.06). The sporadic enrichment of Mn in both the Redkino and Kotlin suggests intermittent oxygenation.

4.5. P-phase partitioning

To evaluate P limitation, we assessed variations in molar $C_{\text{org}}/P_{\text{org}}$ and $C_{\text{org}}/P_{\text{reac}}$ ratios (Fig 2.6). $C_{\text{org}}/P_{\text{reac}}$ ratios (where P_{reac} represents potentially mobile P during deposition and early diagenesis; calculated as $P_{\text{org}} + P_{\text{auth}} + P_{\text{Fe}}$) also provide useful insight into controls on P cycling (Thompson et al., 2019; Guilbaud et al., 2020). In Redkino samples, $C_{\text{org}}/P_{\text{reac}}$ values generally plot below the Redfield ratio. Although they plot below the Redfield ratio, most samples with a ferruginous signal plot further below than samples with a non-ferruginous signal indicating drawdown of phosphorus under ferruginous conditions. In Kotlin samples, $C_{\text{org}}/P_{\text{reac}}$ plot below the Redfield ration but are generally closer than Redkino samples with ferruginous samples from Lugovoe plotting the furthest below. Kotlin samples did not experience as much drawdown since ferruginous conditions were not as widespread as during deposition of Redkino samples.

Both Redkino and Kotlin samples plot close to the Redfield ration. Redkino samples have more variability, but plot at or below the Redfield ratio while Kotlin samples have a tighter grouping and also plot above the Redfield Ratio. This indicates P_{org} was likely not remineralized and released during deposition and diagenesis (Guilbaud et al., 2020).

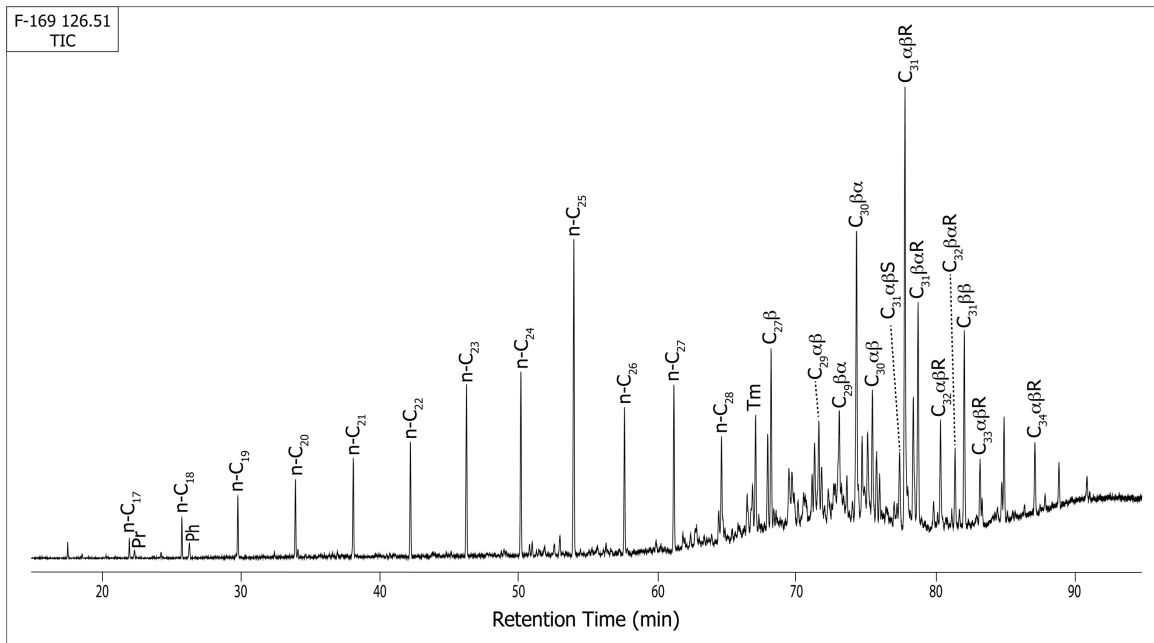


Figure 2.7. Total ion Chromatogram (TIC) for extracted aliphatic hydrocarbons for F-169 126.51 m from the Kotlin horizon. Labeled compounds include n-alkanes, pristane (pr), phytane (ph) and C₂₇(including Tm) - C₃₄ hopanes. Stereochemistry is denoted and represents the C-17, C-21, and C-22 positions (e.g., C₃₁αβR = C₃₁17α 21β 22R).

4.6. Total and pyrite sulfur

Pyrite sulfur contents was measured for 64 samples across Baltica and total S contents were measured on 28 samples from Estonia. Pyrite sulfur contents measured in rocks from both the Redkino and Kotlin portions of Lugovoe (Russia) and the Redkino portion of 3628 (Ukraine) have a wide range from 0.0 to 9.0%. Pyrite sulfur from the overlying Kotlin rocks from Utkina Zavod (Russia) and 3628 (Ukraine) range from 0.0 to 0.12%. Total sulfur contents from F-169 (Estonia) is low like for other Kotlin rocks and range from 0.0 to 0.15%. Our Kotlin Data are like that of Johnston et al., 2012 and

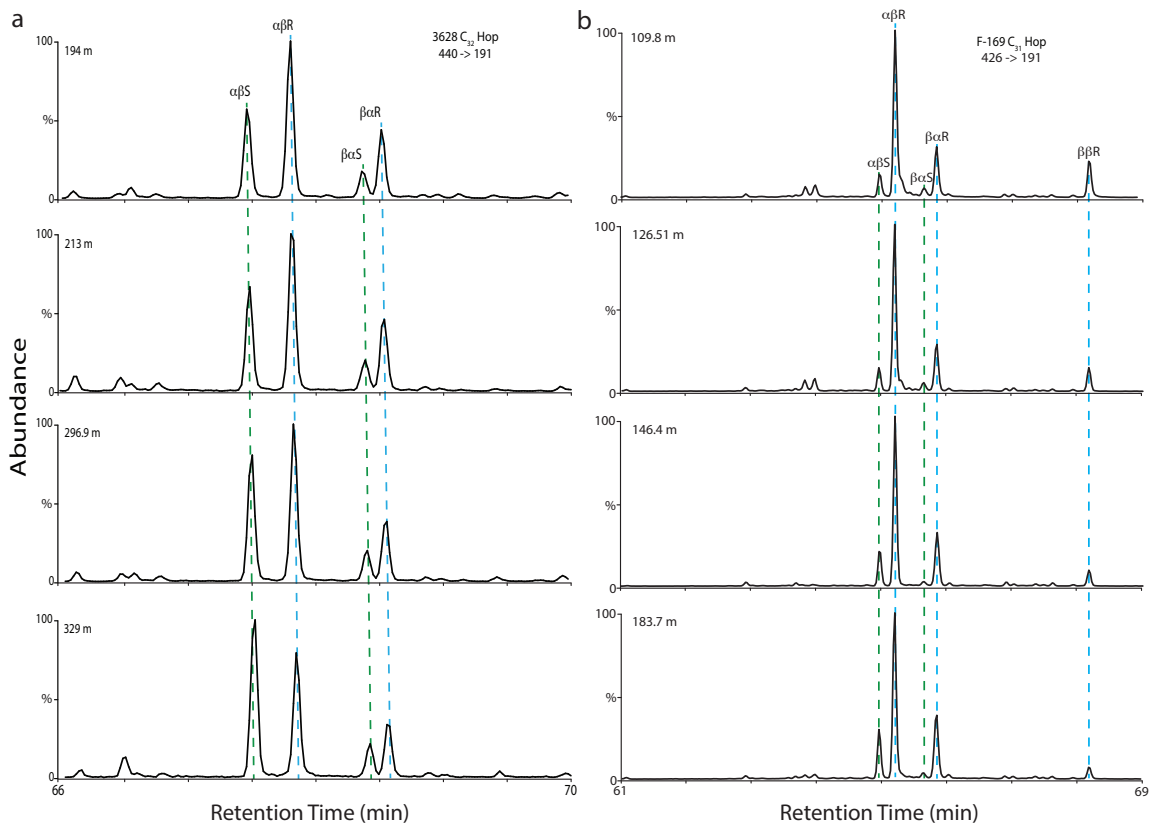


Figure 2.8. Selected Ion Chromatograms for (a.) C₃₂ hopanes at varying depths from drillcore 3628 and (b.) C₃₁ hopanes at varying depths from drillcore F-169. MRM transitions for F-169 show C₃₁αβ, βα and ββ hopane isomers. Each are labeled and aligned with green and blue dashed lines. MRM transitions for 3628 show C₃₁αβ and βα hopane isomers. Each are labeled and aligned with blue and green dashed lines.

suggest a local muted sulfate concentrations in near-shore settings. Low %S contents in these local settings suggest inputs were from brackish nearshore coastal waters.

4.7. Lipid biomarker assemblage patterns

4.7.1. Thermal Maturity

Thermal maturity is a critical component to consider when analyzing the quality of organic matter in ancient sedimentary rocks since biomarkers are susceptible to structural and stereochemical alteration with increasing burial temperatures. Rocks in this study were systematically collected from drill cores at varying depths. Multiple stereoisomer ratios using both hopanes and steranes were calculated to assess thermal maturity. These values are plotted in Table 2.1 and show a systematic increase in both the $C_{29}\alpha\alpha\alpha$ (20S/S+R), $C_{31}\alpha\beta$ (22S/S+R), and C_{27} TS/TM. The systematic increase in these ratios suggest that our samples are not contaminated by drilling fluid. The samples in this study are pre-oil window except for Kalyus and Bernashevka outcrop samples that are in the early oil window making them still suitable for biomarker analyses. Most of these

samples have likely not been exposed to burial temperatures more than 60° C. Figure 2.7 is the total ion chromatogram (TIC) for sample F-169 126.51 m depth and shows a dominance of cyclic biomarker over n-alkanes, suggesting low thermal maturity. Further evidence in Figure 2.8 confirms low thermal maturity in our samples due to the presence of resolvable 17 β , 21 β – Hopanes from major 17 β , 21 α – Hopanes and 17 α , 21 β – Hopanes.

4.7.2. C₂₆/C₂₅ Tricyclic

terpenoids

An abundance ratio between C₂₆ to C₂₅ tricyclic terpenoids is a proxy widely used in petroleum geochemistry to determine whether deposition occurred in marine or (low salinity) non-marine

conditions (Peters et al., 2005). The ratios of C₂₆/C₂₅ tricyclic terpenoids are plotted against $\delta^{13}C_{TOC}$ and are presented in Figure 2.9. When the C₂₆/C₂₅ tricyclic ratio value is above 1.2, the depositional setting

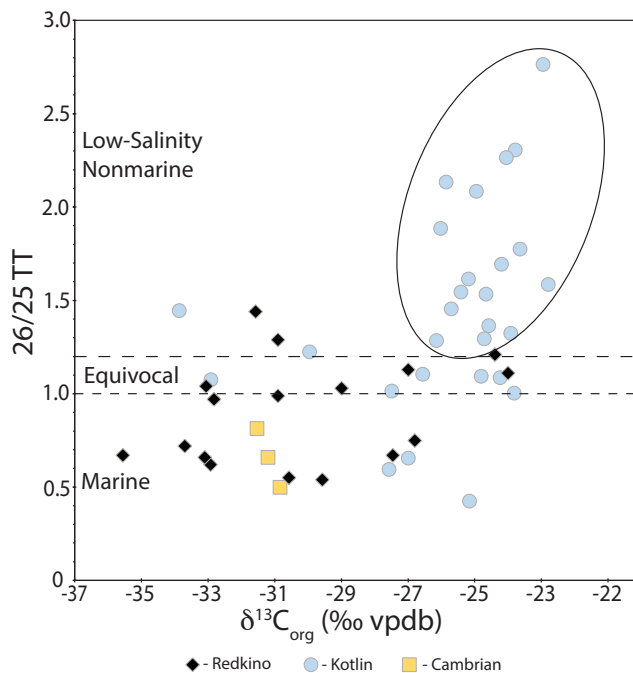


Figure 2.9. Crossplot of 26/25 Tetracyclic-Tricyclic terpane ratios vs $\delta^{13}C$. Black diamonds represent samples from the Redkino horizon, blue circles represent samples from the Kotlin horizon and yellow boxes represent Cambrian samples. The area between dashed lines (1.0 – 1.2) represents the equivocal zone between marine (below 1.0) and nonmarine settings (above 1.2). Black oval represents samples grouped together with heavy $\delta^{13}C$ and high 26/25 TT ratios.

was likely non-marine (brackish or freshwater) and if it is below 1.0, the samples are interpreted as being deposited under normal-salinity, marine conditions (Zumberge, 1987; De Grande et al., 1993). Values between 1.0 and 1.2 are equivocal for informing us about the salinity of the water column. All but two Redkino horizon samples generally plot below 1.2, averaging 0.92 (n=19), with a range of 0.55 to 1.44, indicating normal-salinity, marine conditions. Kotlin Horizon samples plot above 1.2 with an average of 1.47 (n=28), but have a much larger range of 0.44 to 2.78, indicating deposition in settings with variable salinity from brackish to normal marine. Cambrian samples plot below 1.2 and return to values similar to open-marine conditions in the Redkino horizon.

Kotlin values cluster in three distinct groups as seen in Figure 2.9. One group of 14 samples plots as non-marine with C_{26}/C_{25} signals above 1.2 threshold (with an average of 1.87). These samples also exhibit ^{13}C -enrichment (average $\delta^{13}\text{C}_{\text{org}} = -24.5\%$). The second group of five samples plots in the marine field with 25/26 TT signals below 1.2 (with an average of 0.75) combined with the ^{13}C -enrichment (average $\delta^{13}\text{C}_{\text{org}} = -26.4\%$). The third group clusters at the 1.2 threshold (with the average of 1.26) with $\delta^{13}\text{C}_{\text{org}}$ values more negative than the Kotlin Horizon average (average $\delta^{13}\text{C}_{\text{org}} = -32.24\%$).

4.7.3. Hopane/Sterane

The ratio of major (C27–C35) hopanes to major (C27–C29) steranes is often used to assess the balance of bacterial versus eukaryotic contributions to primary productivity.

Hopanes are fossil membrane lipids derived from hopanoids, which are synthesized by a wide variety of bacterial groups.

Similarly, steranes are derived from sterols, which are produced almost exclusively by eukaryotes (Summons et al., 2006). The ratio

between hopanes and steranes (H/St) for our samples ranges from 5.6 to 90.7, which covers a similar range to previous organic geochemical studies performed on late Ediacaran rocks from

Baltica (Table 2.1) (Goryl et al., 2018; Pehr et al., 2018, 2023).

For context, H/St ratios from

organic-rich Neoproterozoic rocks and oils typically fall in a narrow range from 0.5 to 2.0 (Grosjean et al., 2009; Dutta et al., 2013; Lee et al., 2013). While there is a clear difference in the values from the younger Kotlin Horizon (average H/St of 13.5) and the

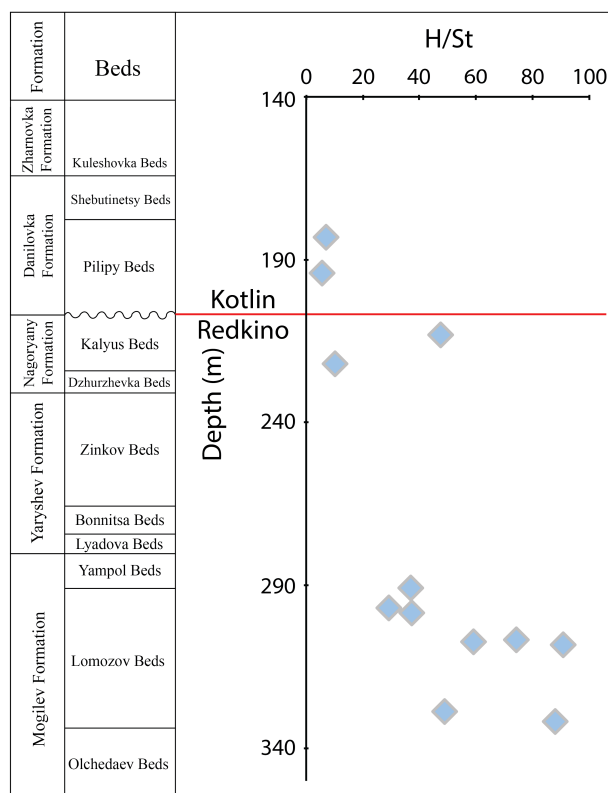


Figure 2.10. Plot hopane/sterane ratio vs depth for drill core 3628 from the Podillya basin in southwest Ukraine. Red horizontal line indicates the boundary between the Redkino and Kotlin horizons.

older Redkino Horizon (average H/St of 33.6), the values for most samples are unusually high and suggest anomalously elevated contributions of bacteria. H/St ratios are plotted vs depth for drillcore 3628 in Figure 2.10 which shows a trend of significantly higher ratios in the lower portion of the Redkino decreasing to lower H/St in the Kotlin. This suggests stronger input of eukaryotic organisms to primary production upsection.

5.0. Discussion

5.1. Nutrient limitation

Development of strongly oligotrophic conditions across Baltica has been previously reported by Goryl et al., (2018) and Pehr et al., (2018) but assessment of the nutrient limitation has not been examined fully. Additional H/St data from our study has added to the number of locations that are observed to have higher contribution of bacteria to primary productivity on Baltica. Our H/St ratios for Redkino samples have an average of 33.6 while Kotlin samples have an average of 13.6. Fe, P and N were assessed to determine their potential role as a limiting nutrient for primary producers.

5.1.1. N as a limiting nutrient

N-isotopes are a useful tool to provide insight into the balance of the nitrogen cycle. When nitrogen is fixed by nitrogen-fixing bacteria, sedimentary nitrogen isotopes cluster around 0‰ (Bauersachs et al., 2009). Previous Neoproterozoic N-isotope studies showed a positive range of +2 to +10‰ from multiple sites around the globe (Ader et al., 2008) and an average of +6‰ from south China for Late Ediacaran to Cambrian rocks (Kikumoto et al., 2014). A small range of positive N-isotope values (+3.5 to +6.5‰) reported by Pehr et al., (2018) suggested nitrate as the dominant dissolved inorganic nitrogen species in the epicontinental seas across Baltica. In our sample set, $\delta^{15}\text{N}$ values from F-169 align with previously reported values and have a small positive range from +3.3 to +5.2‰. These N-isotope data suggest that nitrogen was not limiting, thus making it unlikely to be responsible for the long-lived oligotrophic conditions across Baltica.

5.1.2. Fe as a limiting nutrient

Iron based proteins play a key role in various cellular processes such as photosynthesis and nitrogen fixation for two. Due to its importance in cellular growth in primary producers it has been observed as a biolimiting nutrient in modern oceanic settings like the Pacific and Southern Oceans (Moore et al., 2001; Tagliabue et al., 2017; Birchill et al., 2019; Paine et al., 2023). Most our samples have $\text{Fe}_T/\text{Fe}_{\text{HR}}$ above 0.22 and many are above 0.38, indicating their deposition under suboxic to dysoxic settings in both

the Redkino and Kotlin. This excess suggests that the presence of free Fe (III) in the water column eliminates it as being responsible for nutrient limitation on Baltica.

5.1.3. P as a limiting Nutrient

Phosphorus has been suggested as the primary biolimiting nutrient through much of Earth's history and has played a key role in the persistence of oligotrophic condition in many settings in both the ancient and modern oceans (Guildford and Hecky, 2000; Paytan and McLaughlin, 2007; Reinhard et al., 2017). Previous P speciation studies indicate ferruginous conditions during the early Neoproterozoic that could have led to enhanced drawdown of P, ultimately limiting its bioavailability in the water column (Guilbaud et al., 2015, 2020). Our samples from Baltica show a similar trend for the Redkino and the Kotlin section of the Lugovoe drillcore. Figure 2.6 shows that $C_{\text{org}}/P_{\text{reac}}$ values for most ferruginous samples plot significantly lower than the Redfield ratio indicating efficient drawdown by adsorption to Fe-bearing minerals. This contrasts with Kotlin samples (excluding the Lugovoe drillcore) where most samples are closer to the Redfield ratio. The combination of shallow-water ferruginous conditions and high $C_{\text{org}}/P_{\text{reac}}$ highly suggests that P limitation was responsible for the long-lived oligotrophic conditions during the late Ediacaran on Baltica.

5.2. Environmental heterogeneity across Baltica

Our dataset suggests that the Redkino Regional Stage on Baltica is characterized by a more complex redox history with marine conditions fluctuating between oxic and ferruginous, but with no evidence for euxinic conditions. In particular, Fe speciation and Mn data suggest intermittent dysoxic to ferruginous conditions in deeper-water settings along Baltica's margins concurrently with the most biodiverse time during deposition of the Redkino Horizon. Lugovoe samples from the Kotlin horizon have Fe_{HR}/Fe_T values above 0.38 and C_{26}/C_{25} tricyclic terpane ratios below 1.0, indicating deposition in an anoxic, normal marine salinity environment. Kotlin samples from Utkina Zavod have Fe_{HR}/Fe_T values below 0.38 and C_{26}/C_{25} tricyclic terpane ratios values between 1.2 and 2.8 indicating deposition in fresh to brackish water conditions.

Contemporaneous marine settings may provide insight to the mechanism allowing ferruginous bottom waters with intermittent pulses of Mn. Previous studies of the Nama Group deposited during a slightly younger (by 5-10 Ma) time period have shown that the Ediacara Biota established itself during intervals of oxic conditions (Bowyer et al., 2017). Furthermore, Bowyer et al. (2017) have shown that the Ediacara biota thrived during the last few million years of the Ediacaran when significant ocean redox heterogeneity characterized the seas of Baltica. Wave mixing in nearshore environments, provided a stable oxic ecosystem for these organisms to survive. C_{26}/C_{25} tricyclic terpane ratios and Fe speciation values show a transition from deeper marine to marginal marine

conditions where wave mixing allowed oxygen to be more abundant at the Kotlin stage horizons where. Our Fe speciation data for the two horizons in the Podillya basin show a consistently decreasing trend from ~0.50 before the transition to ~0.26. These data and the 14‰ C isotope excursion in the same samples suggests a relative drop in sea level.

Fe-mineral speciation of the Redkino samples containing Ediacara biota indicates oxic conditions at the sediment-water interface, while deeper-water facies during the same time suggest ferruginous or dysoxic redox conditions. Samples taken near the boundary with the Kotlin Horizon indicate an overall decrease in the Fe_{HR}/Fe_T ratios reflecting transition to conditions more akin to those of oxygenated waters described in previous studies of the late Ediacaran (Canfield et al., 2007; Johnston et al., 2012; Bowyer et al., 2017). Redox proxies indicate that during the late part of the Redkino Regional Stage redox conditions were similar to those inferred for the slightly younger, shallow-marine Nama Group that hosts the Ediacara biota (Bowyer et al., 2017). Importantly, deeper-water settings of the late Ediacaran Nama Group with ferruginous conditions do not host the Ediacara biota (Bowyer et al., 2017).

Fe_{HR}/Fe_T ratios from drillcore 3628 show that the depositional conditions for the Redkino Horizon sample were primarily dysoxic/anoxic and shift toward oxic conditions closer to the boundary between the Redkino and Kotlin Horizons. The Redkino Horizon samples close to the boundary are equivocal and show a trend toward oxic conditions captured in the Kotlin horizon. Kotlin samples in this core all plot as equivocal and trend

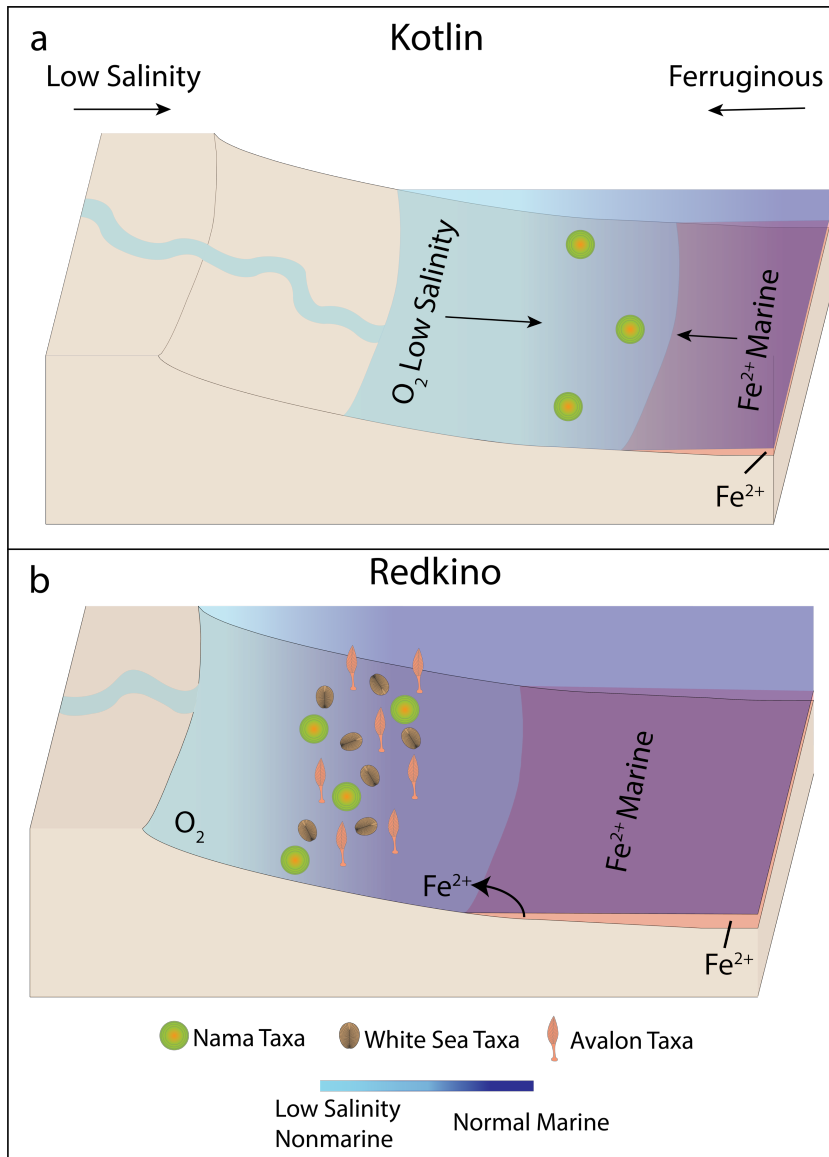


Figure 2.11. Cross section showing the change in redox, salinity and biodiversity between the Redkino (b) and Kotlin (a) Regional Horizons. Red color represent ferruginous waters and light blue to dark blue gradient represents oxic, low salinity environmental conditions to oxic, normal marine environmental conditions.

conditions during the Redkino. These data suggest that intermittently ferruginous conditions were developed close to the sediment-water interface during deposition of the

toward oxic conditions. Generally, the Redkino Horizon samples from our dataset are ferruginous aside from quarry samples containing abundant fossils of the Ediacara biota. Fig. 2.3 shows that all the Redkino Horizon quarry samples plot as oxic or equivocal. When combined with the Mn data, the drill core 3628 samples show intermittent Mn-enrichment associated with ferruginous

Redkino Horizon. The oxic nature of the quarry samples indicate that the Ediacara biota likely preferred oxic waters and likely lived in environments above the chemocline.

5.3. Environmental Transition

In addition to the transition from ferruginous to oxic conditions from the Redkino to Kotlin Horizon, $\delta^{13}\text{C}_{\text{org}}$ values increase from -36.0 to -22.8‰, which could signify a transition from open marine to brackish water (Pehr et al., 2023). The positive $\delta^{13}\text{C}_{\text{org}}$ excursion observed through the 3628 drillcore (Figure 2.3) coincides with the Fe-mineral speciation data reflecting

transition from dysoxic and ferruginous to oxic conditions potentially coinciding with a fall in regional sea-level.

Further, biomarker evidence in addition to iron-mineral speciation data and carbon isotope data add additional evidence suggesting a sea-level drop. 25/26 TT ratios combined with the associated $\delta^{13}\text{C}_{\text{org}}$ values indicate that the

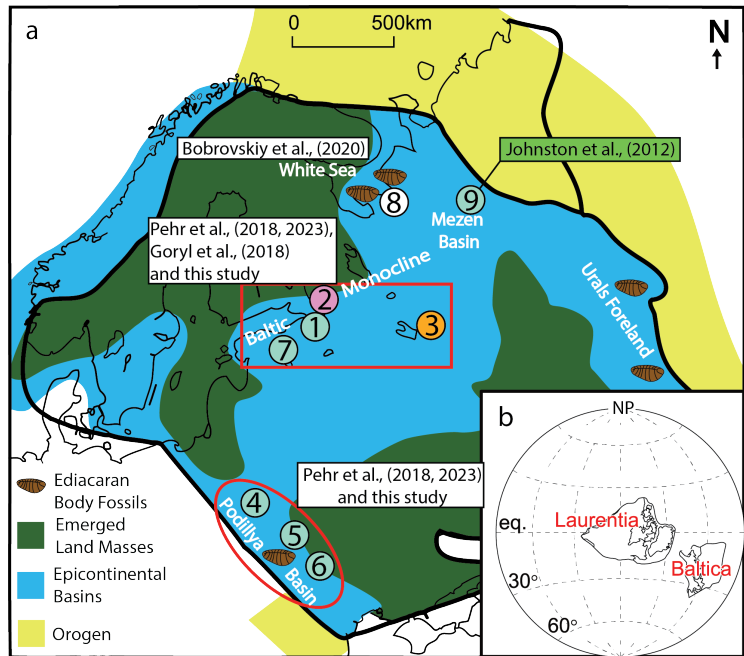


Figure 2.12. Updated paleogeographic reconstruction presented in Figure 2.1 with environmental conditions labeled for Kotlin aged samples. Teal circles exhibit oxic, low salinity conditions, the pink circle is ferruginous, normal marine during the Kotlin, and the orange circle is transitional between low salinity and normal marine.

Redkino Horizon samples are marine with light $\delta^{13}\text{C}_{\text{org}}$ values. The Redkino Horizon 25/26 TT values range from 0.44 to 1.44 and have C isotope values that range between -36.4 to -24.4‰. The Kotlin Horizon 25/26 TT values range from 0.54 to 2.78 and have C isotope values that range between -33.9 to -22.8‰. Although the ranges for each horizon are strikingly similar, the average $\delta^{13}\text{C}_{\text{org}}$ shows a difference between the two time periods. Redkino samples have an average $\delta^{13}\text{C}_{\text{org}}$ of -30.2‰ while Kotlin samples are significantly heavier on average at -26.9‰.

A significant decrease in relative sea level inferred here could be a potential mechanistic driver of the major environmental changes observed, which likely contributed to the decrease in faunal diversity across the boundary between the Redkino and Kotlin horizons (Fig 2.11). Along with the environmental change, the shallower water would have had higher water-energy conditions. This transition coincides with the advent of bioturbation in low-energy environments as well as burrowing abilities in higher energy, wave-dominated settings (Grazhdankin, 2014b). Changes in salinity and redox conditions in nearshore marine environments likely contributed to changes in ecological structure of marine communities during the Kotlin Crisis, though the nature of the major driving forces would have depended on the environmental conditions prevailing at different locations.

6.0. Conclusions

Our stratigraphic records of lipid biomarker, stable carbon/nitrogen isotope ratios, Fe and P-mineral speciation, and trace metal analyses suggest a major environmental shift occurred during deposition of sedimentary strata in the late Ediacaran across Baltica. The upper Redkino regional horizon indicates a shift from typical marine salinity to coastal brackish (such as deltaic) conditions in the younger Kotlin regional horizon. An updated map of Baltica plots the extent of lower salinity condition across Baltica based on C_{26}/C_{25} tricyclic terpane and sulfur data (Fig 2.12). Trace element geochemistry and Fe-mineral speciation further indicate that mildly reducing aquatic conditions, most likely a stratified water column with ferruginous conditions persisting at the sediment-water interface for the Redkino Regional Horizon, gave way to redox conditions that were more predominantly oxic and brackish through the Kotlin Regional Horizon. Sustained changes in aquatic environmental conditions, especially major changes in aquatic salinity and redox conditions in nearshore marine settings, provided metabolic challenges affecting the survival of benthic macroscopic organisms in nearshore marine settings during the late Ediacaran across the breadth of Baltica.

References

- Ader, M., Chaudhuri, S., Coates, J.D., and Coleman, M., 2008, Microbial perchlorate reduction: A precise laboratory determination of the chlorine isotope fractionation and its possible biochemical basis: *Earth and Planetary Science Letters*, v. 269, p. 605–613, doi:10.1016/j.epsl.2008.03.023.
- Bauersachs, T., Schouten, S., Compaoré, J., Wollenzien, U., Stal, L.J., and Sinninghe Damsté, J.S., 2009, Nitrogen isotopic fractionation associated with growth on dinitrogen gas and nitrate by cyanobacteria: *Limnology and Oceanography*, v. 54, p. 1403–1411, doi:10.4319/lo.2009.54.4.1403.
- Bennett, W.W., and Canfield, D.E., 2020, Redox-sensitive trace metals as paleoredox proxies: A review and analysis of data from modern sediments: *Earth-Science Reviews*, v. 204, p. 103175, doi:10.1016/j.earscirev.2020.103175.
- Birchill, A.J. et al., 2019, The eastern extent of seasonal iron limitation in the high latitude North Atlantic Ocean: *Scientific Reports*, v. 9, p. 1435, doi:10.1038/s41598-018-37436-3.
- Bobrovskiy, I., Hope, J.M., Golubkova, E., and Brocks, J.J., 2020, Food sources for the Ediacara biota communities: *Nature Communications*, v. 11, p. 1261, doi:10.1038/s41467-020-15063-9.
- Bowyer, F., Wood, R.A., and Poulton, S.W., 2017, Controls on the evolution of Ediacaran metazoan ecosystems: A redox perspective: *Geobiology*, v. 15, p. 516–551, doi:10.1111/gbi.12232.
- Calvert, S.E., and Pedersen, T.F., 1996, Sedimentary geochemistry of manganese; implications for the environment of formation of manganiferous black shales: *Economic Geology*, v. 91, p. 36–47, doi:10.2113/gsecongeo.91.1.36.
- Canfield, D.E., Poulton, S.W., Knoll, A.H., Narbonne, G.M., Ross, G., Goldberg, T., and Strauss, H., 2008, Ferruginous Conditions Dominated Later Neoproterozoic Deep-Water Chemistry: *Science*, v. 321, p. 949–952, doi:10.1126/science.1154499.
- Canfield, D.E., Poulton, S.W., and Narbonne, G.M., 2007, Late-Neoproterozoic Deep-Ocean Oxygenation and the Rise of Animal Life: *Science*, v. 315, p. 92–95, doi:10.1126/science.1135013.
- Clarkson, M.O., Lenton, T.M., Andersen, M.B., Bagard, M.-L., Dickson, A.J., and Vance, D., 2021, Upper limits on the extent of seafloor anoxia during the PETM

- from uranium isotopes: *Nature Communications*, v. 12, p. 399, doi:10.1038/s41467-020-20486-5.
- Clarkson, M.O., Poulton, S.W., Guilbaud, R., and Wood, R.A., 2014, Assessing the utility of Fe/Al and Fe-speciation to record water column redox conditions in carbonate-rich sediments: *Chemical Geology*, v. 382, p. 111–122, doi:10.1016/j.chemgeo.2014.05.031.
- Dahl, T.W., Hammarlund, E.U., Rasmussen, C.M.Ø., Bond, D.P.G., and Canfield, D.E., 2021, Sulfidic anoxia in the oceans during the Late Ordovician mass extinctions – insights from molybdenum and uranium isotopic global redox proxies: *Earth-Science Reviews*, v. 220, p. 103748, doi:10.1016/j.earscirev.2021.103748.
- De Grande, S.M.B., Aquino Neto, F.R., and Mello, M.R., 1993, Extended tricyclic terpanes in sediments and petroleums: *Organic Geochemistry*, v. 20, p. 1039–1047, doi:10.1016/0146-6380(93)90112-O.
- Duda, J.-P., Blumenberg, M., Thiel, V., Simon, K., Zhu, M., and Reitner, J., 2014, Geobiology of a palaeoecosystem with Ediacara-type fossils: The Shibantan Member (Dengying Formation, South China): *Precambrian Research*, v. 255, p. 48–62, doi:10.1016/j.precamres.2014.09.012.
- Duda, J.-P., Thiel, V., Reitner, J., and Grazhdankin, D., 2016, Opening up a window into ecosystems with Ediacara-type organisms: preservation of molecular fossils in the Khatyspyt Lagerstätte (Arctic Siberia): *PalZ*, v. 90, p. 659–671, doi:10.1007/s12542-016-0317-5.
- Dutta, S., Bhattacharya, S., and Raju, S.V., 2013, Biomarker signatures from Neoproterozoic–Early Cambrian oil, western India: *Organic Geochemistry*, v. 56, p. 68–80, doi:10.1016/j.orggeochem.2012.12.007.
- Emerson, S.R., and Husted, S.S., 1991, Ocean anoxia and the concentrations of molybdenum and vanadium in seawater: *Marine Chemistry*, v. 34, p. 177–196, doi:10.1016/0304-4203(91)90002-E.
- Evans, S.D., Tu, C., Rizzo, A., Suprenant, R.L., Boan, P.C., McCandless, H., Marshall, N., Xiao, S., and Droser, M.L., 2022, Environmental drivers of the first major animal extinction across the Ediacaran White Sea-Nama transition: *Proceedings of the National Academy of Sciences*, v. 119.
- Fedorova, N.M., Levashova, N.M., Bazhenov, M.L., Meert, J.G., Sergeeva, N.D., Golovanova, I.V., Danukalov, K.N., Kuznetsov, N.B., Kadyrov, A.F., and Khidiyatov, M.M., 2013, The East European Platform in the late Ediacaran: new paleomagnetic and geochronological data: *Russian Geology and Geophysics*, v. 54, p. 1392–1401, doi:10.1016/j.rgg.2013.10.003.

- Fike, D.A., Grotzinger, J.P., Pratt, L.M., and Summons, R.E., 2006, Oxidation of the Ediacaran Ocean: *Nature*, v. 444, p. 744–747, doi:10.1038/nature05345.
- Goryl, M., Marynowski, L., Brocks, J.J., Bobrovskiy, I., and Derkowski, A., 2018, Exceptional preservation of hopanoid and steroid biomarkers in Ediacaran sedimentary rocks of the East European Craton: *Precambrian Research*, v. 316, p. 38–47, doi:10.1016/j.precamres.2018.07.026.
- Grazhdankin, D.V., 2004, Patterns of Distribution in the Ediacaran Biotas: Facies versus Biogeography and Evolution: *Paleobiology*, v. 30, p. 203–221.
- Grazhdankin, D., 2014a, Patterns of Evolution of the Ediacaran Soft-Bodied Biota: *Journal of Paleontology*, v. 88, p. 269–283, doi:10.1666/13-072.
- Grazhdankin, D., 2014b, Patterns of Evolution of the Ediacaran Soft-Bodied Biota: *Journal of Paleontology*, v. 88, p. 269–283, doi:10.1666/13-072.
- Grazhdankin, D.V., 2003, Structure and Depositional Environment of the Vendian Complex in the Southeastern White Sea Area: v. 11, p. 19.
- Grazhdankin, D.V., Marusin, V.V., Meert, J., Krupenin, M.T., and Maslov, A.V., 2011, Kotlin regional stage in the South Urals: *Doklady Earth Sciences*, v. 440, p. 1222–1226, doi:10.1134/S1028334X11090170.
- Grazhdankin, D.V., and Maslov, A.V., 2015, The room for the Vendian in the International Chronostratigraphic Chart: *Russian Geology and Geophysics*, v. 56, p. 549–559, doi:10.1016/j.rgg.2015.03.007.
- Grosjean, E., Love, G.D., Stalvies, C., Fike, D.A., and Summons, R.E., 2009, Origin of petroleum in the Neoproterozoic–Cambrian South Oman Salt Basin: *Organic Geochemistry*, v. 40, p. 87–110, doi:10.1016/j.orggeochem.2008.09.011.
- Guilbaud, R., Poulton, S.W., Butterfield, N.J., Zhu, M., and Shields-Zhou, G.A., 2015, A global transition to ferruginous conditions in the early Neoproterozoic oceans: *Nature Geoscience*, v. 8, p. 466–470, doi:10.1038/ngeo2434.
- Guilbaud, R., Poulton, S.W., Thompson, J., Husband, K.F., Zhu, M., Zhou, Y., Shields, G.A., and Lenton, T.M., 2020, Phosphorus-limited conditions in the early Neoproterozoic ocean maintained low levels of atmospheric oxygen: *Nature Geoscience*, v. 13, p. 296–301, doi:10.1038/s41561-020-0548-7.
- Guildford, S.J., and Hecky, R.E., 2000, Total nitrogen, total phosphorus, and nutrient limitation in lakes and oceans: Is there a common relationship? *Limnology and Oceanography*, v. 45, p. 1213–1223, doi:10.4319/lo.2000.45.6.1213.

- Haddad, E.E., Tuite, M.L., Martinez, A.M., Williford, K., Boyer, D.L., Droser, M.L., and Love, G.D., 2016, Lipid biomarker stratigraphic records through the Late Devonian Frasnian/Famennian boundary: Comparison of high- and low-latitude epicontinental marine settings: *Organic Geochemistry*, v. 98, p. 38–53, doi:10.1016/j.orggeochem.2016.05.007.
- Han, T., Fan, H., and Wen, H., 2018, Dwindling vanadium in seawater during the early Cambrian, South China: *Chemical Geology*, v. 492, p. 20–29, doi:10.1016/j.chemgeo.2018.05.022.
- Ivantsov, A.Yu., Gritsenko, V.P., Konstantinenko, L.I., and Zakrevskaya, M.A., 2014, Revision of the problematic Vendian macrofossil *Beltanelliformis* (=Beltanelloides, Nemiana): *Paleontological Journal*, v. 48, p. 1415–1440, doi:10.1134/S0031030114130036.
- Ivantsov, A.Yu., Grytsenko, V., Fedonkin, M.A., Zakrevskaya, M.A., Paliy, V.M., Velikanov, V.A., Konstantinenko, L.I., Menasova, A.Sh., and Serezhnikova, E.A., 2015a, Upper Vendian macrofossils of Eastern Europe. Middle Dniester area and Volhynia.: Mosco PIN RAS.
- Ivantsov, A.Yu., Razumovskiy, A.A., and Zakrevskaya, M.A., 2015b, Upper Vendian macrofossils of Eastern Europe. Middle and South Urals.: Moscow: PIN RAN.
- Johnston, D.T., Poulton, S.W., Goldberg, T., Sergeev, V.N., Podkovyrov, V., Vorob'eva, N.G., Bekker, A., and Knoll, A.H., 2012, Late Ediacaran redox stability and metazoan evolution: *Earth and Planetary Science Letters*, v. 335–336, p. 25–35, doi:10.1016/j.epsl.2012.05.010.
- Kikumoto, R., Tahata, M., Nishizawa, M., Sawaki, Y., Maruyama, S., Shu, D., Han, J., Komiya, T., Takai, K., and Ueno, Y., 2014, Nitrogen isotope chemostratigraphy of the Ediacaran and Early Cambrian platform sequence at Three Gorges, South China: *Gondwana Research*, v. 25, p. 1057–1069, doi:10.1016/j.gr.2013.06.002.
- Knoll, A.H., Walter, M.R., Narbonne, G.M., and Christie-Blick, N., 2004, Three “First Places” for Ediacaran Period:., doi:10.7916/D8697DK7.
- Kolesnikov, A.V., Marusin, V.V., Nagovitsin, K.E., Maslov, A.V., and Grazhdankin, D.V., 2015, Ediacaran biota in the aftermath of the Kotlinian Crisis: Asha Group of the South Urals: *Precambrian Research*, v. 263, p. 59–78, doi:10.1016/j.precamres.2015.03.011.
- Kouchinsky, A., Bengtson, S., Pavlov, V., Runnegar, B., Torssander, P., Young, E., and Ziegler, K., 2007, Carbon isotope stratigraphy of the Precambrian–Cambrian Sukharikha River section, northwestern Siberian platform: *Geological Magazine*, v. 144, p. 609–618, doi:10.1017/S0016756807003354.

- Krishnaswami, S., 1976, Authigenic transition elements in Pacific pelagic clays: *Geochimica et Cosmochimica Acta*, v. 40, p. 425–434, doi:10.1016/0016-7037(76)90007-7.
- Laflamme, M., Darroch, S.A.F., Tweedt, S.M., Peterson, K.J., and Erwin, D.H., 2013, The end of the Ediacara biota: Extinction, biotic replacement, or Cheshire Cat? *Gondwana Research*, v. 23, p. 558–573, doi:10.1016/j.gr.2012.11.004.
- Lee, C., Fike, D.A., Love, G.D., Sessions, A.L., Grotzinger, J.P., Summons, R.E., and Fischer, W.W., 2013, Carbon isotopes and lipid biomarkers from organic-rich facies of the Shuram Formation, Sultanate of Oman: *Geobiology*, v. 11, p. 406–419, doi:10.1111/gbi.12045.
- Linnemann, U. et al., 2018, A ~565 Ma old glaciation in the Ediacaran of peri-Gondwanan West Africa: *International Journal of Earth Sciences*, v. 107, p. 885–911, doi:10.1007/s00531-017-1520-7.
- Love, G.D. et al., 2009, Fossil steroids record the appearance of Demospongiae during the Cryogenian period: *Nature*, v. 457, p. 718–721, doi:10.1038/nature07673.
- Margaritz, M., Kirshvink, J.L., Latham, A.J., Zhuravlev, A.Yu., and Rozanov, A.Yu., 1991, Precambrian/Cambrian boundary problem: Carbon isotope correlations for Vendian and Tommotian time between Siberia and Morocco: v. 19, p. 847–850.
- Merdith, A.S. et al., 2017, A full-plate global reconstruction of the Neoproterozoic: *Gondwana Research*, v. 50, p. 84–134, doi:10.1016/j.gr.2017.04.001.
- Moore, J.K., Doney, S.C., Glover, D.M., and Fung, I.Y., 2001, Iron cycling and nutrient-limitation patterns in surface waters of the World Ocean: *Deep Sea Research Part II: Topical Studies in Oceanography*, v. 49, p. 463–507, doi:10.1016/S0967-0645(01)00109-6.
- Paine, E.R., Boyd, P.W., Strzepek, R.F., Ellwood, M., Brewer, E.A., Diaz-Pulido, G., Schmid, M., and Hurd, C.L., 2023, Iron limitation of kelp growth may prevent ocean afforestation: *Communications Biology*, v. 6, p. 607, doi:10.1038/s42003-023-04962-4.
- Paytan, A., and McLaughlin, K., 2007, The Oceanic Phosphorus Cycle: *Chemical Reviews*, v. 107, p. 563–576, doi:10.1021/cr0503613.
- Pebr, K., Baczynski, A.A., Bekker, A., Hoffmann, A., Freeman, K.H., Poulton, S.W., and Love, G.D., 2023, Compound-specific carbon isotope measurements of individual lipid biomarkers from immature Ediacaran rocks of Baltica: *Organic Geochemistry*, v. 182, p. 104641, doi:10.1016/j.orggeochem.2023.104641.

- Pehr, K., Love, G.D., Kuznetsov, A., Podkovyrov, V., Junium, C.K., Shumlyansky, L., Sokur, T., and Bekker, A., 2018, Ediacara biota flourished in oligotrophic and bacterially dominated marine environments across Baltica: *Nature Communications*, v. 9, doi:10.1038/s41467-018-04195-8.
- Peters, K.E., Walters, C.C., and Moldowan, J.M., 2005, *The biomarker guide*: Cambridge, UK, Cambridge University Press.
- Reinhard, C.T., Planavsky, N.J., Gill, B.C., Ozaki, K., Robbins, L.J., Lyons, T.W., Fischer, W.W., Wang, C., Cole, D.B., and Konhauser, K.O., 2017, Evolution of the global phosphorus cycle: *Nature*, v. 541, p. 386–389, doi:10.1038/nature20772.
- Schaller, T., and Wehrli, B., 1997, Geochemical-focusing of manganese in lake sediments ? An indicator of deep-water oxygen conditions: *Aquatic Geochemistry*, v. 2, p. 359–378, doi:10.1007/BF00115977.
- Scott, C., and Lyons, T.W., 2012, Contrasting molybdenum cycling and isotopic properties in euxinic versus non-euxinic sediments and sedimentary rocks: Refining the paleoproxies: *Chemical Geology*, v. 324–325, p. 19–27, doi:10.1016/j.chemgeo.2012.05.012.
- Shields-Zhou, G., and Och, L., 2011, The case for a Neoproterozoic Oxygenation Event: Geochemical evidence and biological consequences: *GSA Today*, v. 21, p. 4–11, doi:10.1130/GSATG102A.1.
- Sundby, B., Anderson, L.G., and Hall, J. The effect of oxygen on release and uptake of cobalt, manganese, iron and phosphate at the sediment-water interface:
- Tagliabue, A., Bowie, A.R., Boyd, P.W., Buck, K.N., Johnson, K.S., and Saito, M.A., 2017, The integral role of iron in ocean biogeochemistry: *Nature*, v. 543, p. 51–59, doi:10.1038/nature21058.
- Thompson, J., Poulton, S.W., Guilbaud, R., Doyle, K.A., Reid, S., and Krom, M.D., 2019, Development of a modified SEDEX phosphorus speciation method for ancient rocks and modern iron-rich sediments: *Chemical Geology*, v. 524, p. 383–393, doi:10.1016/j.chemgeo.2019.07.003.
- Turekian, K.K., and Wedepohl, K.H., 1961, Distribution of the Elements in Some Major Units of the Earth's Crust: *Geological Society of America Bulletin*, v. 72, p. 175, doi:10.1130/0016-7606(1961)72[175:DOTEIS]2.0.CO;2.
- Wang, X., Shi, X., Jiang, G., and Tang, D., 2014, Organic carbon isotope gradient and ocean stratification across the late Ediacaran-Early Cambrian Yangtze Platform:

- Science China Earth Sciences, v. 57, p. 919–929, doi:10.1007/s11430-013-4732-0.
- Wood, R.A. et al., 2015, Dynamic redox conditions control late Ediacaran metazoan ecosystems in the Nama Group, Namibia: *Precambrian Research*, v. 261, p. 252–271, doi:10.1016/j.precamres.2015.02.004.
- Zhang, F. et al., 2019, Global marine redox changes drove the rise and fall of the Ediacara biota: *Geobiology*, v. 17, p. 594–610, doi:10.1111/gbi.12359.
- Zumberge, J.E., 1987, Prediction of source rock characteristics based on terpane biomarkers in crude oils: A multivariate statistical approach: *Geochimica et Cosmochimica Acta*, v. 51, p. 1625–1637, doi:10.1016/0016-7037(87)90343-7.
- Zumberge, J.A., Love, G.D., Cárdenas, P., Sperling, E.A., Gunasekera, S., Rohrssen, M., Grosjean, E., Grotzinger, J.P., and Summons, R.E., 2018, Demosponge steroid biomarker 26-methylstigmastane provides evidence for Neoproterozoic animals: *Nature Ecology & Evolution*, v. 2, p. 1709–1714, doi:10.1038/s41559-018-0676-2.

Table 2.1. Selected biomarker abundance ratios, bulk organic carbon and nitrogen isotope values, and total and pyrite sulfur measurements that provide environmental constraints.

Sample ID	Horizon	Outcrop/Drill Core	Region	Depth (m)	TOC (wt%)	$\delta^{13}C_{org}$ (‰ VPDB)	Hydrogen Index	Tmax (°C)	Hop/Ster ¹	26/25 TT ²	Grammacrane/C ₃₀ Hop	C ₂₇ Hop 1s/(1s+1m)	C ₃₁ ep 22S/(S+R)	C ₂₉ ster 20S/20S+20R	C ₃₁ hop $\beta\beta$ / ($\beta\beta$ + $\alpha\beta$ + $\beta\alpha$)	2MeH/3MeH	2MeH Index (%)	3MeH Index (%)
3628-159.3	Kotlin	Drill Core	Podolia Basin	159.3	0.07	-	14	-	-	-	-	-	-	-	-	-	-	-
3628-163	Kotlin	Drill Core	Podolia Basin	163	0.17	-	-	-	-	-	-	-	-	-	-	-	-	-
3628-171.1	Kotlin	Drill Core	Podolia Basin	171.1	0.17	-	-	-	-	-	-	-	-	-	-	-	-	-
3628-183	Kotlin	Drill Core	Podolia Basin	183	0.22	-	-	-	5.6	1.6	0.01	0.02	0.50	0.11	0.00	5.4	7.0	1.3
3628-185.5	Kotlin	Drill Core	Podolia Basin	185.5	0.16	-	-	-	-	-	-	-	-	-	-	-	-	-
3628-194	Kotlin	Drill Core	Podolia Basin	194	0.39	-	-	-	7.0	1.38	0.01	0.02	0.50	0.13	0.00	4.5	8.1	1.8
3628-210	Redkino	Drill Core	Podolia Basin	210	0.07	-	-	-	-	-	-	-	-	-	-	-	-	-
3628-213	Redkino	Drill Core	Podolia Basin	213	0.53	-	139	429	47.4	0.67	0.05	0.02	0.51	0.13	0.00	3.7	4.6	1.3
3628-221.7	Redkino	Drill Core	Podolia Basin	221.7	0.15	-	-	-	-	-	-	-	-	-	-	-	-	-
3628-226.5	Redkino	Drill Core	Podolia Basin	226.5	0.30	-	113	425	16.1	1.03	0.01	0.05	0.49	0.16	0.00	2.1	5.1	2.4
3628-231.2	Redkino	Drill Core	Podolia Basin	231.2	0.14	-	-	-	-	-	-	-	-	-	-	-	-	-
3628-246	Redkino	Drill Core	Podolia Basin	246	0.36	-	-	-	-	-	-	-	-	-	-	-	-	-
3628-281	Redkino	Drill Core	Podolia Basin	281	0.05	-	97	-	-	-	-	-	-	-	-	-	-	-
3628-286	Redkino	Drill Core	Podolia Basin	286	0.21	-	-	-	-	-	-	-	-	-	-	-	-	-
3628-291	Redkino	Drill Core	Podolia Basin	291	0.43	-	67	426	36.9	1.29	0.01	0.02	0.56	0.22	0.00	0.3	0.7	2.7
3628-296.9	Redkino	Drill Core	Podolia Basin	298.5	0.62	-	-	-	28.9	0.99	0.00	0.03	0.55	0.19	0.00	0.5	0.9	2.1
3628-298.5	Redkino	Drill Core	Podolia Basin	305	0.25	-	-	-	37.1	0.62	0.00	0.03	0.58	0.21	0.00	1.1	0.9	0.8
3628-305	Redkino	Drill Core	Podolia Basin	306.8	0.15	-	-	-	-	-	-	-	-	-	-	-	-	-
3628-306.8	Redkino	Drill Core	Podolia Basin	307.5	0.16	-	-	-	59.0	0.67	0.02	0.03	0.60	0.13	0.00	1.2	0.6	0.5
3628-307.5	Redkino	Drill Core	Podolia Basin	308.2	0.16	-	-	-	90.7	0.55	0.01	0.02	0.60	0.29	0.00	0.9	0.5	0.5
3628-308.2	Redkino	Drill Core	Podolia Basin	316.5	0.23	-	-	-	-	-	-	-	-	-	-	-	-	-
3628-316.5	Redkino	Drill Core	Podolia Basin	318.3	0.06	-	-	-	-	-	-	-	-	-	-	-	-	-
3628-318.3	Redkino	Drill Core	Podolia Basin	319	0.09	-	-	-	-	-	-	-	-	-	-	-	-	-
3628-319	Redkino	Drill Core	Podolia Basin	326.4	0.20	-	-	-	-	-	-	-	-	-	-	-	-	-
3628-326.4	Redkino	Drill Core	Podolia Basin	328	0.09	-	-	-	-	-	-	-	-	-	-	-	-	-
3628-328	Redkino	Drill Core	Podolia Basin	329	0.09	-	-	-	-	-	-	-	-	-	-	-	-	-
3628-329	Redkino	Drill Core	Podolia Basin	332	0.25	-	-	-	-	-	-	-	-	-	-	-	-	-
3628-332	Redkino	Drill Core	Podolia Basin	332	0.18	-	44	n/a	87.9	0.66	0.04	0.01	0.59	0.22	0.00	1.5	0.3	0.2
3628-342.3	Redkino	Drill Core	Podolia Basin	342.3	0.07	-	14	-	-	-	-	-	-	-	-	-	-	-
L-13-41	Kotlin	Drill Core	Baltic Monocline	41	0.48	-	76	424	7.2	1.24	0.03	0.09	0.20	0.10	0.04	0.7	1.5	2.1
L-13-44	Kotlin	Drill Core	Baltic Monocline	44	0.44	-	95	427	8.3	1.09	0.02	0.09	0.19	0.07	0.02	0.0	0.2	3.7
L-13-47	Kotlin	Drill Core	Baltic Monocline	47	0.51	-	80	425	2.0	1.46	0.03	0.09	0.17	0.09	0.03	0.1	0.3	3.9
L-13-71	Redkino	Drill Core	Baltic Monocline	71	1.06	-	85	417	35.3	1.04	0.01	0.08	0.17	0.12	0.04	0.1	0.1	0.9
L-13-73	Redkino	Drill Core	Baltic Monocline	73	0.85	-	112	417	73.4	0.97	0.01	0.09	0.18	0.15	0.04	0.1	0.1	0.8
L-13-75	Redkino	Drill Core	Baltic Monocline	75	0.49	-	28	n/a	29.5	0.54	0.02	0.13	0.27	0.11	0.03	0.7	0.4	0.7
UZ 1-9	Kotlin	Drill Core	Baltic Monocline	64.15	0.42	-	143	431	3.4	2.32	0.03	0.09	0.13	0.06	0.11	5.2	8.1	1.7
UZ 1-10	Kotlin	Drill Core	Baltic Monocline	71.67	0.34	-	131	428	1.6	2.15	0.03	0.14	0.15	0.06	0.11	1.7	5.1	3.1
UZ 1-14	Kotlin	Drill Core	Baltic Monocline	87	0.27	-	219	427	3.9	1.9	0.03	0.16	0.19	0.07	0.05	1.3	7.0	5.5
UZ 1-20	Kotlin	Drill Core	Baltic Monocline	111.6	0.67	-	199	419	3.2	2.78	0.05	0.15	0.16	0.06	0.10	1.8	7.3	4.1
UZ 1-21	Kotlin	Drill Core	Baltic Monocline	119.9	0.40	-	172	425	7.7	1.79	0.02	0.13	0.15	0.06	0.06	3.8	5.7	1.6
UZ 1-22 (1-22b)	Kotlin	Drill Core	Baltic Monocline	124.6	0.52	-	118	426	3.6	2.28	0.03	0.17	0.17	0.06	0.08	2.6	8.2	3.3
UZ 1-26x (1-26a)	Kotlin	Drill Core	Baltic Monocline	152.8	0.31	-	190	428	4.8	1.56	0.04	0.16	0.24	0.08	0.04	4.4	7.1	1.7
UZ 1-26 (1-26b)	Kotlin	Drill Core	Baltic Monocline	153.5	0.27	-	170	426	5.0	1.71	0.04	0.15	0.25	0.05	0.04	4.4	8.2	2.0
UZ 1-27	Kotlin	Drill Core	Baltic Monocline	162.1	0.44	-	195	427	5.0	1.63	0.04	0.11	0.21	0.06	0.05	3.3	5.9	1.9
UZ 1-28	Kotlin	Drill Core	Baltic Monocline	171.4	0.21	-	157	426	4.0	2.1	0.04	0.08	0.22	0.08	0.06	3.1	9.9	3.4

87-25	Kotlin	Drill Core	Mosco Syncline	2018	0.26	-	218	433	22.2	0.44	0.01	0.02	0.58	0.18	0.01	2.7	3.9	1.5
87-13	Cambrian	Drill Core	Mosco Syncline	1860	0.23	-	217	433	27.8	0.66	0.00	0.02	0.47	0.13	0.01	6.4	4.2	0.7
3-13 (4592-13)	Redkino	Drill Core	Volyn Basin	~166	0.47	-	57	421	119.2	1.44	0.01	0.01	0.35	0.10	0.01	1.5	0.4	0.2
4-15 (4529-15)	Kotlin	Drill Core	Volyn Basin	~195	0.12	-	83	n/a	22.8	1.03	0.02	0.07	0.16	0.04	0.14	15.8	9.9	0.7
4-24 (4504-24)	Kotlin	Drill Core	Volyn Basin	~200	0.13	-	148	n/a	22.5	0.61	0.00	0.03	0.31	0.07	0.03	9.1	7.2	0.8
4-13 (4529-13)	Kotlin	Drill Core	Volyn Basin	~207	0.09	-	114	n/a	25.9	0.67	0.00	0.05	0.18	0.05	0.11	13.0	7.3	0.6
16PL-11	Redkino	Outcrop	Podolia Basin	-	0.21	-	10	n/a	11.5	0.75	0.13	0.26	0.60	0.38	0.00	2.3	5.9	2.7
16PL-18	Redkino	Outcrop	Podolia Basin	-	0.23	-	22	n/a	11.1	1.13	0.09	0.20	0.60	0.33	0.00	2.3	5.6	2.5
16PL-22	Redkino	Outcrop	Podolia Basin	-	0.50	-	94	443	8.1	1.11	0.10	0.25	0.62	0.40	0.00	2.2	5.4	2.6
Ty-16-1/+5 p	Redkino	Outcrop	Podolia Basin	-	0.28	-	-	-	7.9	1.01	0.15	0.41	0.58	0.50	0.00	-	-	-
Ty-16-1/+5 s	Redkino	Outcrop	Podolia Basin	-	0.61	-	-	-	9.3	1.04	0.08	0.21	0.58	0.54	0.00	-	-	-
Bel001	Redkino	Outcrop	Podolia Basin	-	0.01	-	-	-	-	-	-	-	-	-	-	-	-	-
Bel002	Redkino	Outcrop	Podolia Basin	-	0.01	-	-	-	-	-	-	-	-	-	-	-	-	-
Bel003	Redkino	Outcrop	Podolia Basin	-	0.01	-	-	-	-	-	-	-	-	-	-	-	-	-
Ber003	Redkino	Outcrop	Podolia Basin	-	0.37	-	-	-	9.9	0.72	0.77	0.61	0.61	0.43	0.00	-	-	-
Qua002	Redkino	Outcrop	Podolia Basin	-	0.09	-	-	-	-	-	-	-	-	-	-	-	-	-
Qua003	Redkino	Outcrop	Podolia Basin	-	0.02	-	-	-	-	-	-	-	-	-	-	-	-	-
Qua004	Redkino	Outcrop	Podolia Basin	-	0.4	-	-	-	-	-	-	-	-	-	-	-	-	-
Qua005	Redkino	Outcrop	Podolia Basin	-	0.01	-	-	-	-	-	-	-	-	-	-	-	-	-
Qua006	Redkino	Outcrop	Podolia Basin	-	0.07	-	-	-	-	-	-	-	-	-	-	-	-	-
Tym003c	Redkino	Outcrop	Podolia Basin	-	0.28	-	18	-	11.8	1.21	0.07	0.60	0.59	0.40	0.00	-	-	-
F-169-60.54	Cambrian	Drill Core	Baltic Monocline	-29.6	0.05	-29.6	-	-	-	-	-	-	-	-	-	-	-	-
F-169-64.9	Cambrian	Drill Core	Baltic Monocline	-30.8	0.06	-30.8	-	-	-	-	-	-	-	-	-	-	-	-
F-169-65.75	Cambrian	Drill Core	Baltic Monocline	-31.5	0.06	-31.5	-	-	9.4	0.82	0.07	0.04	0.11	0.11	0.02	0.3	1.0	3.0
F-169-68.1	Cambrian	Drill Core	Baltic Monocline	-30.5	0.06	-30.5	-	-	-	-	-	-	-	-	-	-	-	-
F-169-68.5	Cambrian	Drill Core	Baltic Monocline	-29.6	0.05	-29.6	-	-	-	-	-	-	-	-	-	-	-	-
F-169-70.72	Cambrian	Drill Core	Baltic Monocline	-29.9	0.04	-29.9	-	-	-	-	-	-	-	-	-	-	-	-
F-169-71.22	Cambrian	Drill Core	Baltic Monocline	-30.0	0.03	-30.0	-	-	-	-	-	-	-	-	-	-	-	-
F-169-71.5	Cambrian	Drill Core	Baltic Monocline	-30.8	0.05	-30.8	-	-	17.9	0.50	0.05	0.03	0.23	0.15	0.03	0.2	0.6	3.4
F-169-74	Cambrian	Drill Core	Baltic Monocline	-30.5	0.05	-30.5	-	-	-	-	-	-	-	-	-	-	-	-
F-169-78.4	Cambrian	Drill Core	Baltic Monocline	-31.2	0.05	-31.2	-	-	-	-	-	-	-	-	-	-	-	-
F-169-80.6	Cambrian	Drill Core	Baltic Monocline	-26.6	0.01	-26.6	-	-	-	-	-	-	-	-	-	-	-	-
F-169-81.5	Cambrian	Drill Core	Baltic Monocline	-26.9	0.01	-26.9	-	-	-	-	-	-	-	-	-	-	-	-
F-169-84.7	Cambrian	Drill Core	Baltic Monocline	-31.7	0.09	-31.7	-	-	-	-	-	-	-	-	-	-	-	-
F-169-88.1	Cambrian	Drill Core	Baltic Monocline	-28.5	0.01	-28.5	-	-	-	-	-	-	-	-	-	-	-	-
F-169-90.9	Cambrian	Drill Core	Baltic Monocline	-31.4	0.14	-31.4	-	-	-	-	-	-	-	-	-	-	-	-
F-169-103.4	Kotlin	Drill Core	Baltic Monocline	-25.2	0.00	-25.2	-	-	-	-	-	-	-	-	-	-	-	-
F-169-104	Kotlin	Drill Core	Baltic Monocline	-25.3	0.01	-25.3	-	-	-	-	-	-	-	-	-	-	-	-
F-169-106	Kotlin	Drill Core	Baltic Monocline	-24.6	0.01	-24.6	-	-	-	-	-	-	-	-	-	-	-	-
F-169-109.8	Kotlin	Drill Core	Baltic Monocline	-24.2	0.65	-24.2	-	-	15.1	1.10	0.02	0.03	0.11	0.05	0.14	2.3	7.4	3.3
F-169-110.85	Kotlin	Drill Core	Baltic Monocline	-23.2	0.04	-23.2	-	-	-	-	-	-	-	-	-	-	-	-
F-169-111.25	Kotlin	Drill Core	Baltic Monocline	-22.9	0.18	-22.9	-	-	-	-	-	-	-	-	-	-	-	-
F-169-115	Kotlin	Drill Core	Baltic Monocline	-24.7	0.34	-24.7	-	-	13.1	1.31	0.03	0.04	0.12	0.04	0.09	2.6	10.2	3.9
F-169-116.8	Kotlin	Drill Core	Baltic Monocline	-26.1	0.53	-26.1	-	-	10.7	1.30	0.01	0.03	0.12	0.05	0.08	3.6	7.7	2.1
F-169-117.25	Kotlin	Drill Core	Baltic Monocline	-24.7	0.46	-24.7	-	-	7.7	1.55	0.02	0.03	0.13	0.06	0.03	4.2	9.2	2.2
F-169-117.5	Kotlin	Drill Core	Baltic Monocline	-25.7	0.47	-25.7	-	-	12.2	1.47	0.02	0.03	0.12	0.09	0.09	2.1	8.3	3.9
F-169-126.51	Kotlin	Drill Core	Baltic Monocline	-26.6	0.73	-26.6	-	-	13.9	1.12	0.00	0.03	0.11	0.27	0.08	2.8	8.2	3.0
F-169-134.62	Kotlin	Drill Core	Baltic Monocline	-24.3	0.25	-24.3	-	-	-	-	-	-	-	-	-	-	-	-
F-169-135.05	Kotlin	Drill Core	Baltic Monocline	-24.5	0.03	-24.5	-	-	-	-	-	-	-	-	-	-	-	-
F-169-135.25	Kotlin	Drill Core	Baltic Monocline	-24.9	0.01	-24.9	-	-	-	-	-	-	-	-	-	-	-	-
F-169-138.05	Kotlin	Drill Core	Baltic Monocline	-24.5	0.29	-24.5	-	-	27.7	-	0.00	0.03	0.32	0.28	0.04	4.3	8.8	2.0
F-169-140.55	Kotlin	Drill Core	Baltic Monocline	-24.8	0.46	-24.8	-	-	16.4	1.11	0.01	0.02	0.11	0.23	0.04	4.6	8.0	1.8

F-169 - 141.48	Kotlin	Drill Core	Baltic Monocline	-23.8	0.46	-23.8	-	-	12.9	1.02	0.01	0.01	0.15	0.06	0.04	4.7	7.6	1.6
F-169 - 146.4	Kotlin	Drill Core	Baltic Monocline	-23.3	0.02	-23.3	-	-	11.6	-	0.00	0.03	0.17	0.08	0.05	6.1	7.8	1.3
F-169 - 150.6	Kotlin	Drill Core	Baltic Monocline	-24.2	0.02	-24.2	-	-	-	-	-	-	-	-	-	-	-	-
F-169 - 156.75	Kotlin	Drill Core	Baltic Monocline	-23.8	0.02	-23.8	-	-	-	-	-	-	-	-	-	-	-	-
F-169 - 161.7	Kotlin	Drill Core	Baltic Monocline	-25.0	0.02	-25.0	-	-	-	-	-	-	-	-	-	-	-	-
F-169 - 170.28	Kotlin	Drill Core	Baltic Monocline	-24.8	0.01	-24.8	-	-	-	-	-	-	-	-	-	-	-	-
F-169 - 173.23	Kotlin	Drill Core	Baltic Monocline	-26.8	0.04	-26.8	-	-	-	-	-	-	-	-	-	-	-	-
F-169 - 181.14	Kotlin	Drill Core	Baltic Monocline	-25.3	0.25	-25.3	-	-	-	-	-	-	-	-	-	-	-	-
F-169 - 183.7	Kotlin	Drill Core	Baltic Monocline	-23.9	0.90	-23.9	-	-	21.6	1.34	0.02	0.03	0.23	0.08	0.04	4.4	10.6	2.4
F-169 - 185.85	Kotlin	Drill Core	Baltic Monocline	-25.2	0.05	-25.2	-	-	-	-	-	-	-	-	-	-	-	-
F-169 - 188.62	Kotlin	Drill Core	Baltic Monocline	-25.6	0.03	-25.6	-	-	-	-	-	-	-	-	-	-	-	-

¹Hop/Ster is the ratio of major C₂₇ - C₃₅ hopane isomers/ C₂₇ - C₃₀ diasteranes and regular steranes

²26/25 TT is the ratio of C₂₆ tricyclic terpanes/C₂₅ tricyclic terpanes

Boxes highlighted blue are data from Pehr et al., (2018) and Pehr et al., (2023)

Table 2.2. Selected concentrations for various major and trace elements, Fe- and P-mineral speciation for context on redox conditions during deposition.

	Horizon	Outcrop/Core	Region	Depth	Al (wt%)	Ti (wt%)	Mn (ppm)	V (ppm)	U (ppm)	Fe _T (wt%)	Fe _{ox}	Fe _{py}	Fe _{ox} /Fe _T	Fe _{py} /Fe _T	P _{ox} (wt%)	P _{ox} (ppm)	P _{org} (ppm)
3628-159.3	K	C	Podolia Basin	159.3	7.4	0.3	0.0	87.4	2.2	4.3	1.1	0.0	0.2	0.0	0.0	222.8	16.1
3628-163	K	C	Podolia Basin	163.0	9.1	0.5	0.1	105.7	2.1	6.2	1.7	0.0	0.3	0.0	0.1	495.7	16.2
3628-171.1	K	C	Podolia Basin	171.1	8.7	0.3	0.0	108.0	3.7	3.2	0.8	0.1	0.3	0.1	0.0	31.6	21.2
3628-183	K	C	Podolia Basin	183.0	9.1	0.4	0.0	108.5	2.6	3.8	1.1	0.0	0.3	0.0	0.0	58.8	32.5
3628-185.5	K	C	Podolia Basin	185.5	6.3	0.2	0.0	60.3	1.4	2.4	0.7	0.0	0.3	0.0	0.0	64.0	11.0
3628-194	K	C	Podolia Basin	194.0	8.3	0.3	0.0	92.8	2.7	3.6	1.1	0.1	0.3	0.1	0.0	41.8	24.5
3628-210	R	C	Podolia Basin	210.0	7.6	0.5	0.0	102.2	0.9	6.8	2.5	0.2	0.4	0.1	0.0	148.1	42.5
3628-213	R	C	Podolia Basin	213.0	10.6	0.5	0.0	132.3	3.3	5.2	1.7	0.0	0.3	0.0	0.0	87.0	52.4
3628-221.7	R	C	Podolia Basin	221.7	7.3	0.6	0.4	93.5	4.8	2.9	1.4	0.1	0.5	0.1	0.0	47.7	24.5
3628-226.5	R	C	Podolia Basin	226.5	6.6	0.4	1.4	112.4	1.7	10.2	6.0	0.0	0.6	0.0	0.1	83.5	14.7
3628-231.2	R	C	Podolia Basin	231.2	9.2	0.6	0.2	199.2	2.2	9.1	4.7	0.0	0.5	0.0	0.4	1189.4	43.4
3628-246	R	C	Podolia Basin	246.0	8.0	0.7	0.0	121.3	2.5	4.6	2.2	0.8	0.5	0.4	0.1	825.1	22.4
3628-281	R	C	Podolia Basin	281.0	7.5	0.4	0.0	102.3	0.9	8.3	3.2	0.0	0.4	0.0	0.0	80.0	25.7
3628-286	R	C	Podolia Basin	286.0	10.2	0.8	0.0	252.5	0.6	10.4	5.7	0.0	0.5	0.0	0.1	350.6	116.7
3628-296.9	R	C	Podolia Basin	298.5	4.3	0.3	0.4	147.0	3.3	7.3	4.7	1.3	0.6	0.3	3.0	1955.2	45.3
3628-298.5	R	C	Podolia Basin	305.0	7.0	0.4	0.1	163.9	1.2	14.7	11.3	7.8	0.8	0.7	0.0	74.4	38.7
3628-305	R	C	Podolia Basin	306.8	4.6	0.5	0.8	146.1	1.8	5.3	3.6	0.1	0.7	0.0	1.6	1524.2	26.0
3628-306.8	R	C	Podolia Basin	307.5	11.6	1.3	0.1	305.8	1.5	9.7	5.7	1.0	0.6	0.2	0.0	63.3	35.0
3628-307.5	R	C	Podolia Basin	308.2	11.0	1.0	0.0	352.9	1.1	12.3	8.4	2.8	0.7	0.3	0.0	115.1	48.3
3628-308.2	R	C	Podolia Basin	316.5	2.9	0.2	1.5	118.0	3.2	14.6	9.6	0.2	0.7	0.0	1.9	1274.8	13.8
3628-316.5	R	C	Podolia Basin	318.3	11.6	0.7	0.0	252.3	1.0	11.6	7.2	0.0	0.6	0.0	0.1	425.7	73.8
3628-318.3	R	C	Podolia Basin	319.0	9.7	1.1	0.0	263.0	1.1	11.1	6.5	0.0	0.6	0.0	0.1	332.3	78.1
3628-319	R	C	Podolia Basin	326.4	10.8	1.1	0.1	287.9	1.7	6.4	3.0	0.0	0.5	0.0	0.0	139.6	72.5
3628-326.4	R	C	Podolia Basin	328.0	5.4	0.6	0.6	188.2	1.8	7.1	4.9	1.2	0.7	0.2	2.1	1773.9	29.3
3628-328	R	C	Podolia Basin	329.0	11.0	1.1	0.0	299.3	1.2	6.7	3.4	0.2	0.5	0.1	0.0	117.4	69.6
3628-329	R	C	Podolia Basin	332.0	10.2	0.7	0.1	168.1	2.1	8.5	6.2	2.7	0.7	0.4	0.0	75.1	37.1
3628-332	R	C	Podolia Basin	332.0	11.3	0.7	0.0	219.4	2.0	7.8	4.7	1.4	0.6	0.3	0.0	77.2	49.1
3628-342.3	R	C	Podolia Basin	342.3	10.7	1.0	0.1	287.0	2.4	10.0	5.0	0.4	0.5	0.1	0.0	45.7	17.0
L-13-41	K	C	Baltic Monocline	41.0	11.6	0.5	0.0	124.2	3.6	4.7	4.3	2.3	0.9	0.5	0.0	106.9	93.2
L-13-44	K	C	Baltic Monocline	44.0	5.0	0.2		99.9	2.8	4.6	3.0	0.5	0.6	0.2	0.0	100.9	66.7

L-13-47	K	C	Baltic Monocline	47.0	10.7	0.5	0.1	100.0	2.9	4.7	2.6	0.5	0.6	0.2	0.0	106.7	75.9
L-13-71	R	C	Baltic Monocline	71.0	12.2	0.5	0.0	293.1	3.6	7.2	5.0	3.0	0.7	0.6	0.0	105.7	82.7
L-13-73	R	C	Baltic Monocline	73.0	12.0	0.5	0.0	186.1	4.2	6.5	5.1	2.8	0.8	0.6	0.0	94.3	77.6
L-13-75	R	C	Baltic Monocline	75.0	12.3	0.6	0.0	181.5	15.2	5.4	3.4	1.6	0.6	0.5	0.2	1739.6	108.6
UZ 1-9	K	C	Baltic Monocline	64.2	9.9	0.4	0.0	128.4	4.7	4.0	1.1	0.1	0.3	0.1	0.0	60.6	45.4
UZ 1-10	K	C	Baltic Monocline	71.7	10.0	0.4	0.0	130.7	2.5	4.7	1.4	0.1	0.3	0.1	0.0	176.9	49.9
UZ 1-14	K	C	Baltic Monocline	87.0	8.6	0.4	0.0	111.0	2.6	4.2	1.1	0.0	0.3	0.0	0.0	48.5	36.4
UZ 1-20	K	C	Baltic Monocline	111.6	9.3	0.4	0.4	134.7	2.6	8.5	3.9	0.0	0.5	0.0	0.1	167.0	55.8
UZ 1-21	K	C	Baltic Monocline	119.9	10.3	0.5		142.5	2.8	4.2	0.7	0.0	0.2	0.0	0.0	63.7	58.2
UZ 1-22	K	C	Baltic Monocline	124.6	9.6	0.4	0.0	128.3	2.6	4.0	0.9	0.0	0.2	0.0	0.0	60.3	51.5
UZ 1-26	K	C	Baltic Monocline	153.5	3.6	0.1	2.3	79.6	2.8	31.6	20.7	0.0	0.7	0.0	0.1	68.2	12.9
UZ 1-27	K	C	Baltic Monocline	162.1	9.2	0.4	0.0	115.7	3.6	3.0	0.5	0.0	0.2	0.1	0.0	66.3	57.7
UZ 1-28	K	C	Baltic Monocline	171.4	8.4	0.4	0.2	97.7	2.8	5.6	1.3	0.0	0.2	0.0	0.0	90.4	51.0
87- 25	K	C	Mosco Syncline	2018.0	9.8	0.4	0.1	126.4	2.3	4.7	1.0	0.0	0.2	0.0	0.0	177.4	32.1
3-13	R	C	Volyn Basin	~166	9.0	1.0	0.0	330.1	1.6	8.8	5.5	1.4	0.6	0.3	0.0	116.3	86.4
4-15	K	C	Volyn Basin	~195	5.0	0.3	0.8	60.3	4.8	3.2	1.9	0.0	0.6	0.0	0.4	407.5	12.2
4-24	K	C	Volyn Basin	~200	8.8	0.4	0.0	110.3	2.4	4.6	1.5	0.0	0.3	0.0	0.0	57.2	50.4
4-13	K	C	Volyn Basin	~207	7.3	0.3	0.1	84.4	2.6	3.8	1.3	0.1	0.3	0.1	0.0	33.9	22.5
16PL-11	R	OC	Podolia Basin	-	8.3	0.4	0.0	128.3	4.0	7.0	4.1	0.0	0.6	0.0	0.8	2955.3	51.3
16PL-18	R	OC	Podolia Basin	-	9.3	0.4	0.0	120.7	2.5	8.6	2.8	0.0	0.3	0.0	0.0	84.2	33.6
16PL-22	R	OC	Podolia Basin	-	10.5	0.4	0.0	69.5	1.8	7.0	2.4	0.0	0.3	0.0	0.0	200.7	66.3
Ty-16-1/+5 p	R	OC	Podolia Basin	-	0.7	0.0	0.1	9.9	0.4	1.3	0.6	0.0	0.4	0.0	15.7	7231.3	92.9
Ty-16-1/+5 s	R	OC	Podolia Basin	-	10.1	0.5	0.0	148.9	3.2	5.7	2.5	0.0	0.4	0.0	0.0	124.1	72.0
Bel001	R	OC	Podolia Basin	-	5.7	-	0.0	22.8	1.6	1.3	0.3	0.1	0.3	0.2	-	-	-
Bel002	R	OC	Podolia Basin	-	6.5	-	0.0	29.8	1.9	1.6	0.3	0.0	0.2	0.1	-	-	-
Bel003	R	OC	Podolia Basin	-	7.3	-	0.0	38.4	0.9	2.1	0.4	0.0	0.2	0.1	-	-	-
Ber003	R	OC	Podolia Basin	-	9.9	-	0.0	224.5	4.2	2.4	0.3	0.0	0.1	0.0	-	-	-
Qua002	R	OC	Podolia Basin	-	10.7	-	0.0	102.5	5.7	5.0	1.3	0.1	0.3	0.1	-	-	-
Qua003	R	OC	Podolia Basin	-	8.3	-	0.0	28.3	9.0	1.2	0.4	0.2	0.3	0.5	-	-	-
Qua004	R	OC	Podolia Basin	-	9.7	-	0.0	76.4	3.8	4.0	0.8	0.0	0.2	0.0	-	-	-
Qua005	R	OC	Podolia Basin	-	9.2	-	0.0	38.1	2.6	1.5	0.3	0.0	0.2	0.0	-	-	-
Qua006	R	OC	Podolia Basin	-	11.0	-	0.1	109.8	3.1	6.5	1.6	0.0	0.2	0.0	-	-	-
Tym003c	R	OC	Podolia Basin	-	2.5	-	1.8	42.7	0.7	1.9	1.3	0.0	0.7	0.0	-	-	-

CHAPTER THREE

Compound-specific carbon isotope measurements of individual lipid biomarkers from
immature Ediacaran rocks of Baltica

K. Pehr^{1,2*}, A. A. Baczynski³, A. Bekker^{1,4}, A. Hoffmann¹, K. H. Freeman³, S.W.
Poulton⁵, G.D. Love¹

¹Department of Earth & Planetary Sciences, University of California, Riverside, CA 92521, USA

²Present address: Department of Earth and Environmental Sciences, Lehigh University,
Bethlehem, PA 18015, USA

³Department of Geosciences, Pennsylvania State University, University Park, PA, 16802, USA

⁴Department of Geology, University of Johannesburg, Auckland Park 2006, South Africa

⁵School of Earth and Environment, University of Leeds, Leeds LS2 9JT, UK

**corresponding author: kep220@lehigh.edu*

ABSTRACT

Compound-specific carbon isotope ratios (CSIA) were measured for a suite of lipid biomarker compounds extracted from immature, late Ediacaran sedimentary rocks from drill cores sampled across Baltica. Using a newly developed picomolar-scale CSIA (pico-CSIA) method, we measured carbon isotope compositions of the abundant *n*-alkanes and hopanes, as well as C₂₉ sterane, pristane, and phytane. Total organic carbon (TOC) of the Kotlin Regional Horizon in Baltica (Saint Petersburg area, Utkina Zavod drill core), from

a low-salinity coastal environment, is consistently enriched in ^{13}C by up to 10‰, compared to that for Redkino and Kotlin marine rocks from other locations in Baltica. This ^{13}C enrichment is also recorded by the *n*-alkanes, hopanes, phytane, and C_{29} sterane. In all locations, the $\delta^{13}\text{C}$ values of the C_{29} sterane are within 2‰ of the bacterial hopane $\delta^{13}\text{C}$ values and within 0.7‰ of $\delta^{13}\text{C}_{\text{TOC}}$, suggesting that the abundant hopanes within these sediments could be derived from RuBisCO Calvin-Benson-Bassham pathway-utilizing organisms, as well as from bacterial heterotrophs. Since $\delta^{13}\text{C}_{\text{lipid}}$ signature tracks $\delta^{13}\text{C}_{\text{TOC}}$ values for the Kotlin Regional Horizon samples from Utkina Zavod location, the significant ^{13}C enrichments in this interval reflect either the $\delta^{13}\text{C}$ composition of DIC used for autotrophy or a muted magnitude of carbon isotope fractionation during lipid biosynthesis, but are not due to enhanced preservation of organic compounds and geopolymers derived from ^{13}C -enriched biochemicals. Pico-CSIA and biomarker data provide evidence for both regional environmental heterogeneity and secular changes in carbon cycling during deposition of sediments of the Kotlin and Redkino Regional Horizon intervals.

1. INTRODUCTION

The total organic carbon (TOC) isotope composition ($\delta^{13}\text{C}_{\text{TOC}}$) of ancient sedimentary rocks reflects the overall balance of the organic matter (OM) contributions from source organisms, the taphonomy of molecular preservation during diagenesis and long-term burial (e.g., selective preservation under oxic versus more reducing redox conditions), and the carbon isotope composition of the dissolved inorganic carbon (DIC) pool within

the local depositional setting (Hayes et al., 1990; Freeman, 2001). While broad changes in $\delta^{13}\text{C}_{\text{TOC}}$ over geological time can represent global perturbations to the carbon cycle, including changes to the fraction of organic carbon burial and atmospheric pCO_2 concentrations, ecological and environmental factors pertinent to the local depositional setting often have a greater influence (Pagani et al., 1999; Pancost et al., 2013; Holtvoeth et al., 2019). CSIA can help disentangle this complex web of biogenic inputs and preservation effects on bulk $\delta^{13}\text{C}_{\text{TOC}}$ by constraining OM source influences on $\delta^{13}\text{C}_{\text{TOC}}$ and informing on the pathways of carbon acquisition for different biomarker compounds and their parent biota (Hayes, 2001; Pancost and Damsté, 2003).

There is a protracted increase in the abundance and diversity of eukaryotic organisms in the marine realm throughout the end of the Neoproterozoic Era (1000-541 Ma). The oceans of the Mesoproterozoic were bacterially dominated, however, during the late Tonian-Cryogenian Period (820-635 Ma) eukaryotes increased in their ecological abundance (Brocks et al., 2017; Zumberge et al., 2020). The most common early-mid Neoproterozoic eukaryotes were likely red algae and unicellular heterotrophs, as gauged from the dominance of cholestane amongst the total detectable $\text{C}_{27}\text{-C}_{30}$ steranes (Brocks et al., 2017; Zumberge et al., 2020), with lower amounts of C_{28} steranes (ergostane and cryostane), and a dearth of C_{29} steranes (Zumberge et al., 2020). Following the Sturtian glaciation, green algae replaced red algae as the dominant eukaryotic primary producers, and these eukaryotes rivaled bacteria in terms of biomass production within the oceans (Love et al., 2009; Brocks et al., 2017; Hoshino et al., 2017). However, even by the end

of the Ediacaran, in contrast to deep-water, open-marine settings, the contemporaneous Ediacaran sedimentary strata from Baltica, deposited in shallow-marine, epicontinental basins, show bacterially dominated biomarker assemblage patterns and consistently low TOC contents (Pehr et al., 2018; Goryl et al., 2018; Bobrovskiy et al., 2020). Much higher algal productivity was sustained during petroleum source rock deposition in the South Oman Salt basin (Grosjean et al., 2009; Love et al., 2009; Lee et al., 2015) and East Siberia (Kelly et al., 2011), where eutrophic conditions persisted over extended intervals of Ediacaran time. These biomarker distribution differences strongly imply that there was significant biological and chemical heterogeneity in the oceans affecting the relative bacterial and eukaryotic contributions to microbial ecology in different marine locations. This is expected for both modern and ancient ocean systems due to geographically variable biogeochemical cycling and nutrient availability.

One enigmatic geochemical signal found in the Proterozoic sedimentary rocks and oils derived from these source rocks, that has been linked to the rise of eukaryotes, is a switch in the relative carbon isotopic ordering of *n*-alkanes versus the acyclic isoprenoids, pristane (2,6,10,14-tetramethylpentadecane; C₁₉H₄₀; Pr) and phytane (2,6,10,14-tetramethylhexadecane; C₂₀H₄₂; Ph) (Logan et al., 1995, 1997). Many Neoproterozoic samples are characterized by an ‘inverse ordering’, where δ¹³C of pristane and phytane is more negative with respect to that of *n*-alkanes and bulk OM (Logan et al., 1995, 1997; Close et al., 2011). Phanerozoic samples, as well as some of the younger Ediacaran samples, often show the opposite trend, where the sedimentary total organic carbon

(TOC) consisting largely of kerogen has more positive $\delta^{13}\text{C}$ values typically 3-8‰ relative to those of *n*-alkanes and 1-5‰ relative to pristane and phytane (Hayes, 2001; Corso et al., 2012; Jaraula et al., 2013; Fox et al., 2020). This isotopic ordering in most Phanerozoic samples reflects the isotopic pattern originating from isotope fractionations in biosynthesis with organisms commonly using the RuBisCO Calvin-Benson-Bassham (RuBisCO-CBB) metabolic pathway for autotrophic carbon acquisition (Hayes, 2001), which accounts for most of the primary productivity in modern oceans (Pearson, 2010).

Logan et al. (1997) proposed that the ^{13}C -enriched *n*-alkanes relative to pristane, phytane, and bulk OM in Proterozoic sediments may be a consequence of intense microbial heterotrophic reworking of lipids with linear chains in the water column where high dissolved organic matter (DOM) concentrations were sustained. The ecological rise of macroscopic, multicellular eukaryotes and, eventually, the packaging of OM into fecal pellets may have facilitated increased sinking rates of OM, which could have significantly muted the impact of intensive water column heterotrophy starting at the late Ediacaran to early Phanerozoic transition. However, modeling by Close et al. (2011) suggested instead that an alternative explanation for such appreciably ^{13}C -enriched *n*-alkanes might be a large difference in isotope fractionation between small-sized bacterial producers and large-sized eukaryotic primary producers (Popp et al., 1998). An important caveat to this rationale is whether source contribution from archaea, including methanogens and methanotrophs, to the acyclic isoprenoids was significant. This would complicate the interpretation of molecular isotopic ordering patterns, since pristane and

phytane may be derived from biogenic sources other than chlorophyll pigments from photoautotrophs such as cyanobacteria and/or algae, which is usually their assumed major source.

Here we report the results of the first detailed CSIA study on individual Ediacaran biomarkers from rocks that have undergone only a mild thermal history. These biomarker hydrocarbons were obtained via solvent extraction from a suite of thermally immature, organic carbon-lean siliciclastic sediments sampled from drill cores across Baltica (Russia and Ukraine). These sediments were likely deposited under widespread and protracted oligotrophic conditions that were seemingly persistent in different locations across Baltica (Pehr et al., 2018; Goryl et al., 2018) from the late Ediacaran through to the Early Cambrian. Using the newly developed picomolar-scale CSIA (Baczynski et al., 2018), we were able to measure $\delta^{13}\text{C}$ signatures for the major *n*-alkane and hopane compounds, as well as other individual biomarker alkanes, including C_{29} sterane ($\alpha\alpha\alpha\text{R}$), pristane, and phytane. Through this approach, we could assess the magnitude of the secular variations in $\delta^{13}\text{C}$ values for bulk sedimentary OM, as well as for individual lipid biomarkers in the same samples, within studied drill cores. Additionally, we could compare the organic carbon isotopic systematics for the same stratigraphic intervals from drill cores from numerous locations across Baltica, to assess the extent of regional heterogeneity, through this important interval in Earth history.

2. MATERIALS AND METHODS

2.1. Geological setting and samples

Baltica hosts the most thermally immature Ediacaran rocks reported worldwide for this time interval (Goryl et al., 2018; Pehr et al., 2018). A subset of late Ediacaran and Early Cambrian samples was selected from the suite of thermally immature samples used in a previous study for detailed biomarker analysis (Pehr et al., 2018). The sedimentary rocks were collected from the Utkina Zavod and Lugovoe drill cores located near St. Petersburg in the northeastern part of the Baltic monocline, the Gavrilov-Yam-1 drill core from the Moscow basin, the 4592 drill core from the Volyn region of Ukraine, and the 3628 drill core of the Podillya basin in southwestern Ukraine (Fig. 3.1, Table 3.1). The samples encompass strata from the Redkino, Kotlin, and Lontova Regional horizons. Detailed locations and descriptions of these samples, with geochemical screening data, have been reported previously (Pehr et al. 2018).

The age of the Redkino Regional Stage is now well-constrained by high-precision U-Pb Thermal Ionization Mass Spectrometry (TIMS) dates from White Sea, Russia and the Podillya basin in Ukraine at ca. 556 Ma (Martin et al., 2000; Soldatenko et al., 2019). By contrast, the age of the younger Kotlin Regional Horizon is not well-constrained geochronologically, but is mostly considered to represent the terminal ~10 million years of the Ediacaran Period (Grazhdankin et al., 2011; Meidla, 2017). Recently, an Early Cambrian age has been suggested for the Kotlin Regional Stage based on detrital zircon dates for sandstones from the Kanyliv Group in the Podillya basin in Ukraine

(Paszkowski et al., 2021), and the Kotlin Regional Horizon in the Saint Petersburg and Ladoga areas of Russia (Ivleva et al., 2016, 2018; Ershova et al., 2019). These data were produced by the LA-ICP-MS method and so should be further verified with the CA-ID-TIMS method to check for potential Pb loss, may result in younger dates. Importantly, *Harlaniella podolica* and *Vendotaenia antiqua Gnil.* that are common in the Kotlin Regional Horizon of Baltica are unknown in the Early Cambrian deposits. We therefore use the conventional late Ediacaran age assignment for the Kotlin Regional Horizon in this study.

Rock-Eval pyrolysis parameters (particularly low T_{max} values) and biomarker stereoisomer ratios are self-consistent in indicating that these sedimentary rocks are all thermally immature (Pehr et al., 2018). The drill-core samples from Utkina Zavod, Lugovoe, and the Volyn and Podillya basins (Table 3.1) correspond to a pre-oil window stage of maturity. Samples from the Gavrilov Yam-1 drill core and the 16PL outcrops are within the oil window, but at a maturity level prior to peak oil generation (Pehr et al., 2018). Analysis of the kerogen-bound hydrocarbons for these samples (Pehr et al., 2018) indicated that this immature biomarker profile for steranes and hopanes is also preserved

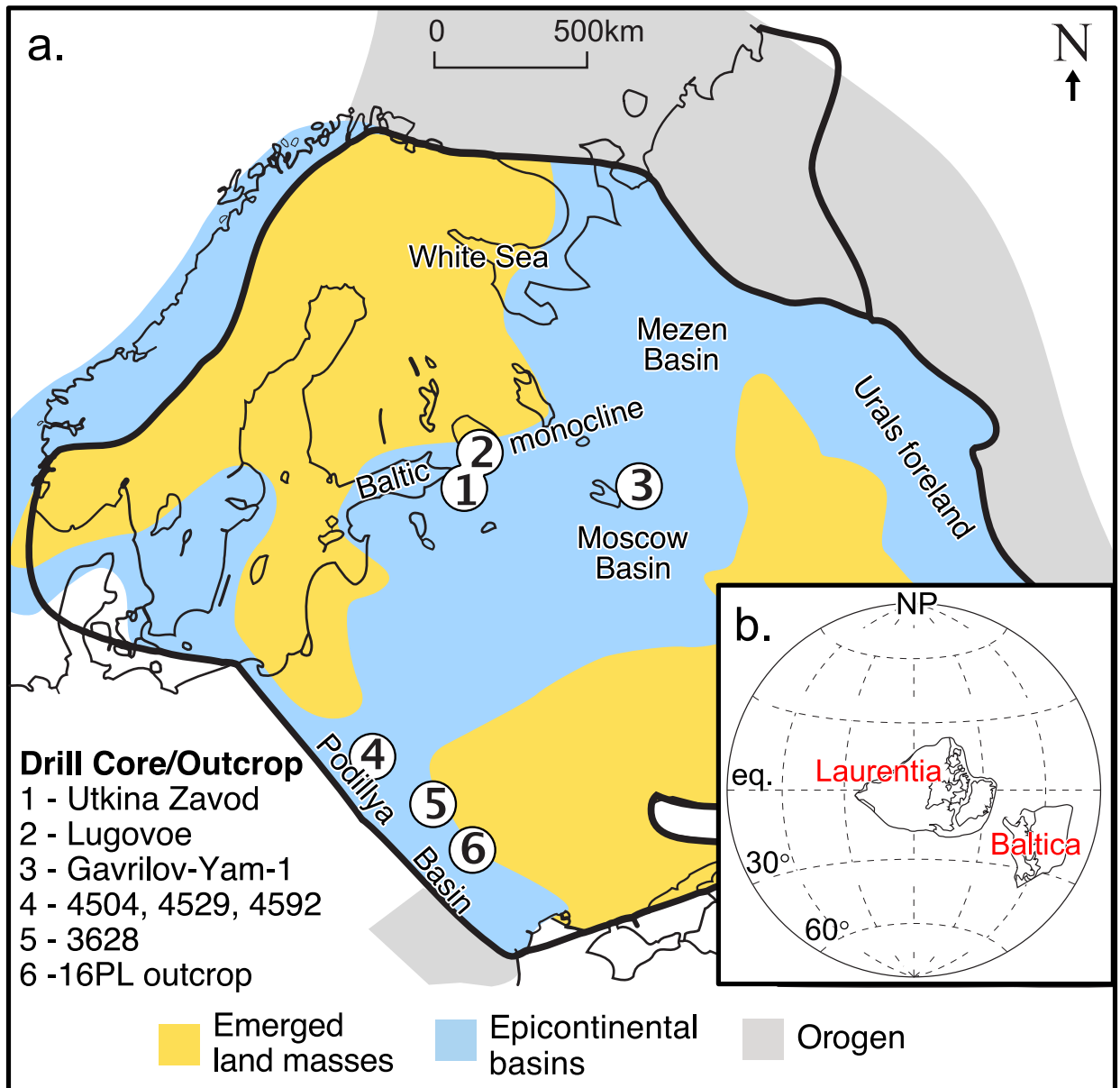


Figure 3.1. (a) Paleogeographic reconstruction of Baltica during the late Ediacaran (modified from Sliupa et al. 2006 and Pehr et al., 2018) with drill cores and outcrop locations labeled; (b) Global reconstruction of Laurentia and Baltica at ca. 550 Ma, modified from Fedorova et al. (2013).

in the kerogen phase, confirming that the exceptionally immature polycyclic alkanes found in our bitumen extracts are primary and genuine Ediacaran biomarkers. Similar biomarker distribution profiles for immature Ediacaran rocks from Baltica have also been

reported in another study and interpreted as predominantly endogenous lipid biomarker signals (Goryl et al., 2018).

2.2. Lipid biomarker analysis.

Rock samples (ranging from 5-20 g) were cut, pulverized, and solvent extracted, followed by separation of the bitumen extracts into three constituent fractions: aliphatic hydrocarbons, aromatics, and polar fractions, as previously described in detail (Pehr et al., 2018). Aliphatic and aromatic hydrocarbon fractions were analyzed using a gas chromatography–mass spectrometry (GC–MS). Aliphatic hydrocarbons were also analyzed by metastable reaction monitoring (MRM)–GC–MS on a Waters Autospec Premier mass spectrometer to look at polycyclic biomarker stereoisomer patterns in more detail. Standardized and proven analytical procedures were employed to prevent and check for contribution of contaminants to the rock bitumens. The immature downcore biomarker patterns, with the *n*-alkane, hopane, and sterane compound distributions ($C_{27\text{hopane}} \text{Ts}/(\text{Ts}+\text{Tm}) < 0.26$ and $C_{31\text{hopane}} \alpha\beta \text{ 22S}/(\text{S}+\text{R}) < 0.6$) and the polycyclic biomarker dominance, are consistent with the thermal immaturity of the rocks indicated by Rock-Eval pyrolysis parameters. The aliphatic hydrocarbon fractions were analyzed to generate total ion chromatograms (Fig. 3.2) in full-scan mode (monitoring from m/z 50 to 800) using gas chromatography–mass spectrometry (GC–MS) with an Agilent 7890A GC system coupled to an Agilent 5975C inert MSD mass spectrometer. The GC temperature program for full-scan analysis (m/z 50 to 800) was 60 °C (held for 2 min), heated to 150 °C at 20 °C /min, then to 325 °C at 2 °C /min, and held at 325 °C for 20 min. The GC

was equipped with a DB1-MS capillary column (60 m × 0.32 mm, 0.25- μ m film thickness) and helium was used as a carrier gas.

To determine accurate molecular biomarker ratios (Table 3.1), aliphatic hydrocarbons were also analyzed by metastable reaction monitoring (MRM)–GC–MS on a Waters Autospec Premier mass spectrometer equipped with an Agilent 7890A gas chromatograph and DB-1MS coated capillary column (60 m × 0.25 mm, 0.25- μ m film thickness), using He as a carrier gas to investigate polycyclic biomarker stereoisomer patterns in more detail. The GC temperature program started with an initial hold at 60 °C for 2 min, then heated to 150 °C at 10 °C /min rate, followed by 320 °C at 3 °C /min rate, and a final hold for 22 min. Analyses were performed via splitless injection in an electron-impact mode, with an ionization energy of 70 eV and an accelerating voltage of 8 kV. MRM ion-pair transitions were used for a suite of biomarker compounds (C_{27} – C_{35} hopanes, C_{31} – C_{36} methylhopanes, C_{19} – C_{26} tricyclic terpanes, C_{24} tetracyclic terpanes, C_{21} – C_{22} and C_{26} – C_{30} steranes, and C_{30} methylsteranes). Individual analyte peaks in rock extract hydrocarbon fractions were quantified and found to constitute at least a three orders of magnitude larger signal than any trace peak detected in a full-laboratory blank using combusted sand. Procedural blanks with pre-combusted sand typically yielded less than 0.1 ng of individual hopane and sterane compounds per gram of combusted sand.

2.3. Bulk isotope analysis.

Total organic carbon isotope analyses ($\delta^{13}\text{C}_{\text{TOC}}$) on samples marked with *b* in Table 3.1 were performed on samples using a Costech ECS 4010 Elemental Analyzer coupled to a Thermo Scientific Delta V Advantage isotope-ratio mass-spectrometer via a Thermo Scientific Conflo IV open-split gas interface system at UCR. 50-100 mg sample powders were acidified for at least 3 hours using 12 N HCl in 50 mL centrifuge tubes; tubes were periodically vortexed. The tubes were then centrifuged at 2500 rpm for two minutes; acid was decanted, and powders were washed with deionized water. The process was repeated four times per sample to ensure removal of residual acid. Decarbonated and dried insoluble residues of ~5-10 mg were weighed into 9 x 10 mm tin boats for organic carbon isotope analysis. Combustion was achieved using a pulse of O₂ set for 60s. The combustion and reduction columns were set to 1100 °C and 650 °C, respectively, with helium as the carrier gas at a flow rate of 100 mL/min. Isotope ratios are reported in standard (δ) delta notation relative to Vienna Pee Dee Belemnite where $\delta^{13}\text{C}_{\text{org}} = [((^{13}\text{C}/^{12}\text{C})_{\text{sample}} / (^{13}\text{C}/^{12}\text{C})_{\text{VPDB}}) - 1] * 1000$. Average analytical precision of standard laboratory reference materials (Acetanilide, Hawaii glycine, and USGS SDO-1) used during analytical sessions was better than 0.10‰ for $\delta^{13}\text{C}_{\text{org}}$ values (1 σ).

Bulk organic carbon isotope analysis on samples marked with *a* in Table 3.1 was performed on acidified rock powder residuals using an Elementar Isotope Cube elemental analyzer coupled to an Isoprime 100 isotope-mass-spectrometer as previously reported (Pehr et al., 2018). EA conditions were the following: helium purge was set for 30 s,

oxidation and reduction reactor temperatures were 1100 °C and 650 °C, respectively, helium carrier gas flow was 230 mL/min, O₂ pulse was set for 60 s, and CO₂ trap was heated to 230 °C to release trapped sample CO₂. International reference materials (ANU sucrose [−10.4‰] and NIST 1547 peach leaves [−26.0‰]) were used to develop the correction scheme for sample data as described previously (Coplen et al., 2006). Reproducibility for samples and standards was better than ±0.1‰.

2.4. Pico-compound specific carbon isotope analysis

Hydrocarbon fractions were analyzed using the pico-CSIA method for $\delta^{13}\text{C}$ measurements developed at Pennsylvania State University (Baczynski et al., 2018). The pico-CSIA method uses a Thermo Trace 1310 GC coupled to a Thermo MAT 253 IRMS via a GC Isolink (see Baczynski et al., 2018 for details). The GC was fitted with a PTV injector that was held at 300 °C and operated in splitless mode. A fused silica capillary column (Agilent J&W DB-5, 10 m, 0.10 mm I.D., 0.10 μm film thickness) was used with helium as the carrier gas. The carrier gas had a programmed pressure method to ensure a consistent flow of ~0.48 mL/min throughout the run. The oven temperature program began at a temperature of 60 °C (held for 1.5 min), ramped to 230 °C at 100 °C /min (no hold) then to a maximum temperature of 320 °C at 40 °C /min with a final hold time of 5 min. The auxiliary gas pressure to the microfluidic splitter was held at 24 psi while solvent was vented, and then reduced to 18 psi while the GC effluent was directed to the IRMS.

Isotopic abundances were determined relative to a reference gas calibrated with Mix A ($n\text{-C}_{16}$ to $n\text{-C}_{30}$; supplied by Arndt Schimmelmann, Indiana University). The $\delta^{13}\text{C}$ values were normalized to the standard Vienna Pee Dee Belemnite scale and are reported in standard delta notation. Standard errors of the mean for individual biomarker compounds range from 0.00‰ to 1.36‰ from repeat runs. Average standard errors for replicate sample analyses for individual n -alkanes were 0.22‰, 0.19‰ for phytane, and 0.28‰ for hopanes and C_{29} sterane ($\alpha\alpha\alpha\text{R}$).

2.5. Iron Speciation

Iron speciation was performed to gauge the environmental redox conditions by quantifying the total iron content of the rocks as well as contribution from iron minerals that are considered highly reactive (Fe_{HR}) to H_2S under anoxic conditions (Canfield et al., 1992; Poulton et al., 2004). Iron carbonate (Fe_{CARB} ; including siderite and ankerite), ferric iron-(oxyhydr)oxide minerals (Fe_{OX} ; including hematite and goethite), and magnetite (Fe_{MAG}), were separated following the sequential extraction technique described in Poulton and Canfield (2005). Pyrite (Fe_{PY}) was determined stoichiometrically by weight from the Ag_2S precipitate formed after HCl and chromous chloride distillation (Canfield et al., 1986). These four iron phases combined make up the pool of Fe_{HR} (Poulton and Canfield, 2011). Fe_{HR} increases in concentration with respect to total iron (Fe_{T}) under anoxic water column conditions. $\text{Fe}_{\text{HR}}/\text{Fe}_{\text{T}} < 0.22$ may indicate oxic water column conditions, while $\text{Fe}_{\text{HR}}/\text{Fe}_{\text{T}} > 0.38$ commonly corresponds to anoxic conditions (Raiswell and Canfield, 1998; Raiswell et al., 2001; Poulton and Canfield,

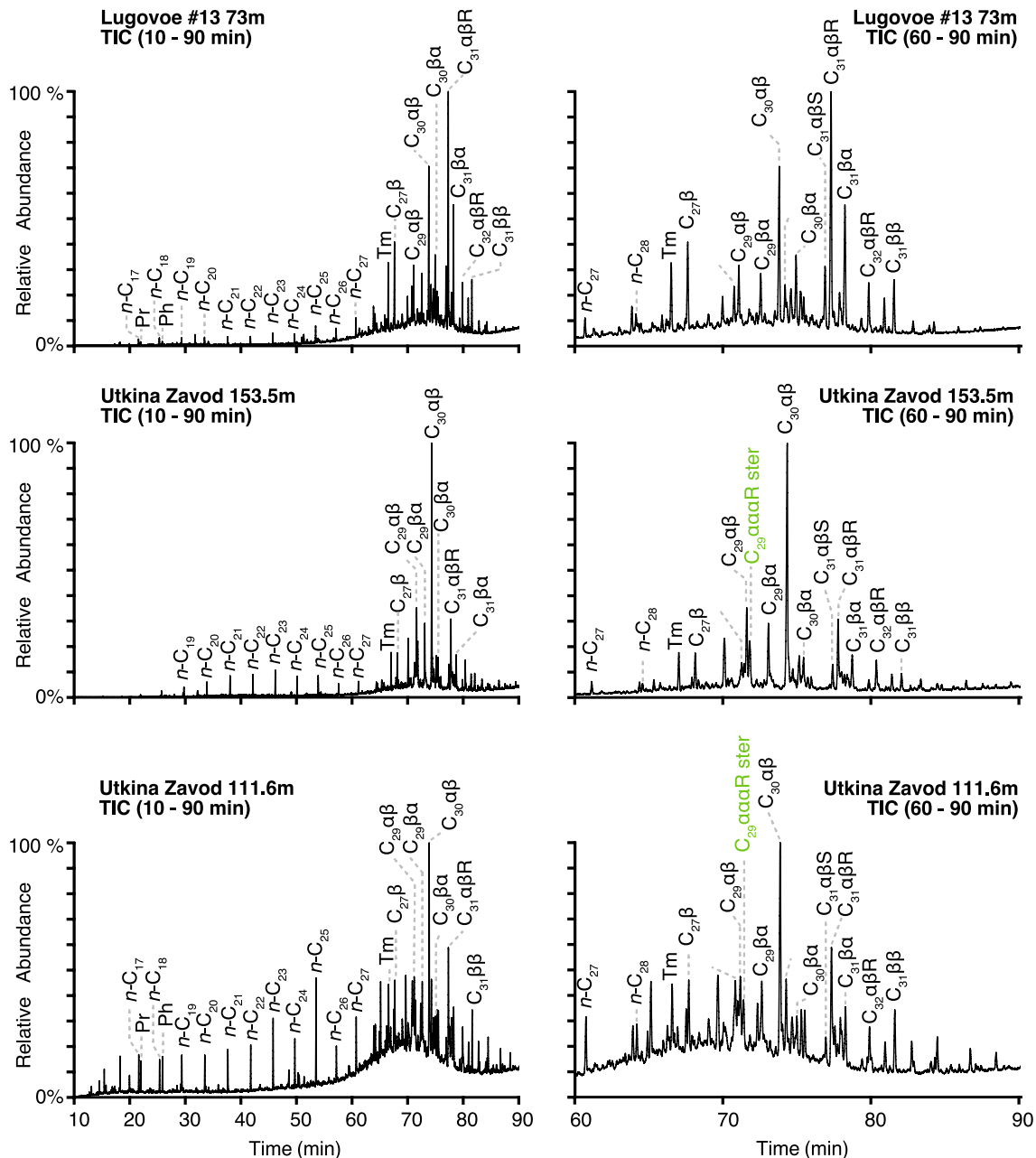


Figure 3.2. Total ion chromatograms (TIC) for the extractable aliphatic hydrocarbons for the late Ediacaran sample Lugovoe #13 73 m, and the Early Cambrian samples Utkina Zavod 153.5 m and Utkina Zavod 111.6 m. The *n*-alkane series (*n*-C₁₇ – *n*-C₂₈), pristane (Pr), phytane (Ph), C₂₉ sterane 5 α ,14 α ,17 α ,20R-stigmastane (C₂₉aaaR ster), and C₂₇–C₃₁ hopanes denoted by their total carbon number and stereochemistry at C-17, C-21, and C-22 (e.g., C₃₁ α β R), are all labeled. Hopanes are the most abundant series of biomarker alkanes in the aliphatic hydrocarbon fractions.

2011). The relative abundance of Fe_{py} is used to constrain the type of anoxia. For anoxic samples (i.e., $Fe_{HR}/Fe_T > 0.38$), $Fe_{py}/Fe_{HR} < 0.6$ suggests ferruginous (anoxic with dissolved Fe^{2+}) bottom water conditions, while euxinia (anoxic with free sulfide) is indicated when $Fe_{py}/Fe_{HR} > 0.6-0.8$ (Poulton, 2021).

3. RESULTS

3.1. $\delta^{13}C_{TOC}$ and Compound-Specific Carbon Isotope Values

Bulk organic carbon isotope values ($\delta^{13}C_{TOC}$) for sedimentary OM were previously reported in (Pehr et al., 2018) and show consistent stratigraphic trends for multiple sections across Baltica for the Redkino and Kotlin Regional horizons within single cores. Note that these bulk isotopic signatures vary markedly from location to location, which suggest they depend on prevailing environmental conditions in the ancient aquatic settings. Briefly summarized, for multiple samples from the Kotlin Regional Horizon from the Utkina Zavod drill core (Location 1 in Fig. 3.1), $\delta^{13}C_{TOC}$ values are significantly ^{13}C -enriched relative to typical Ediacaran marine OM, ranging from -26.0 to -23.0‰. Samples from the nearby Lugovoe drill core (Location 2 in Fig. 3.2) from the same Kotlin Regional Horizon are more depleted in ^{13}C , by up to 10‰, ranging from -33.9 to -30.0‰. These latter values are more typical for marine-sourced Ediacaran sedimentary organic matter, as found for Ediacaran source rocks from the South Oman Salt Basin (Grosjean et al., 2009, Lee et al., 2013).

Hopanes, *n*-alkanes and acyclic isoprenoids are the three most abundant series of resolvable biomarker compounds in the aliphatic hydrocarbon fractions (Fig. 3.2). The high relative abundance of polycyclic alkanes, such as hopanes and/or steranes, is typical for thermally immature (pre-oil window maturity) rocks of all geological ages, since dilution with abundant *n*-alkanes cleaved from kerogen and other macromolecules does not occur until a higher maturity level at the onset of catagenesis. The consistency in immature hydrocarbon patterns (Fig. 3.2) from systematic downcore sampling of the Utkina Zavod and Lugovoe drill-cores also confirms that these are genuine Ediacaran lipid biomarkers. CSIA of individual *n*-alkanes and hopane compounds reveals that $\delta^{13}\text{C}$ values of both compound classes generally closely track bulk $\delta^{13}\text{C}_{\text{TOC}}$ values. $\delta^{13}\text{C}$ values were measured for hopanes ranging in molecular mass from C_{27} to C_{32} (Table 3.2). For all hopanes reported in Table 3.2, mean $\delta^{13}\text{C}_{\text{hopane}}$ differs from $\delta^{13}\text{C}_{\text{TOC}}$ in the host rocks by an average of only $1.3 \pm 0.9\text{‰}$ (Fig. 3.3a) for each sample. By contrast, the range of $\delta^{13}\text{C}_{\text{hopane}}$ found between differing drill-core locations and stratigraphic horizons is far larger, at 10.6‰ . This holds for the two most abundant hopane constituents, $17\alpha,21\beta\text{-C}_{30}(\text{H})$ and $17\alpha,21\beta,22\text{R-C}_{31}(\text{H})$, which have an average $|\Delta\delta^{13}\text{C}_{\text{hopane} - \text{TOC}}|$ of $1.4 \pm 0.7\text{‰}$, even with a $\delta^{13}\text{C}_{\text{hopane}}$ range between samples for these compounds spanning 10.2‰ and 11.2‰ , respectively.

The $\delta^{13}\text{C}$ values of the $\text{C}_{27}\text{-C}_{32}$ hopane series are more negative with increasing hopane carbon number, although the range for individual hopanes within any particular sample is fairly small ($<4.5\text{‰}$) considering that diverse groups of bacteria can biosynthesize

hopanoids. The C₂₇ hopanes have, on average, the most positive $\delta^{13}\text{C}$ values of the hopanes, followed by the C₂₉, and then the C₃₀ hopanes. The C₃₁ and C₃₂ hopanes typically possess the most negative $\delta^{13}\text{C}$ signatures in our sample set.

The $\delta^{13}\text{C}_{\text{hopane}}$ values of the Utkina Zavod samples are close to $\delta^{13}\text{C}_{\text{TOC}}$ values but the relationship varies depending on the sample. Drill core 4592 $\delta^{13}\text{C}_{\text{hopane}}$ values are slightly more positive with respect to $\delta^{13}\text{C}_{\text{TOC}}$, while Gavrilov Yam drill core $\delta^{13}\text{C}_{\text{hopane}}$ values are all more negative with respect to $\delta^{13}\text{C}_{\text{TOC}}$. Lugovoe drill core $\delta^{13}\text{C}_{\text{hopane}}$ transitions from more negative with respect to $\delta^{13}\text{C}_{\text{TOC}}$ to more positive with respect to $\delta^{13}\text{C}_{\text{TOC}}$ moving stratigraphically upwards through the Redkino and Kotlin Regional horizons.

$\delta^{13}\text{C}$ values were measured for individual *n*-alkanes ranging from *n*-C₁₇ to *n*-C₂₉ (Table 3.3). The $\delta^{13}\text{C}_{n\text{-alkanes}}$ also closely match the $\delta^{13}\text{C}_{\text{TOC}}$ trend, although not as tightly as for the hopane compound series (Fig. 3.4). The $\Delta\delta^{13}\text{C}_{n\text{-alkane} - \text{TOC}}$ of the Lugovoe, 4592, and Gavrilov Yam drill-core samples all fall within 2.2‰ of $\delta^{13}\text{C}_{\text{TOC}}$. For the Utkina Zavod drill core, *n*-alkanes display a wider carbon isotope range, particularly among the *n*-C₂₂ to *n*-C₂₅ alkanes, which are as much as 6.6‰ more negative than $\delta^{13}\text{C}_{\text{TOC}}$. Overall, the *n*-alkanes from the Utkina Zavod drill core are on average more negative than $\delta^{13}\text{C}_{\text{TOC}}$ by 2.3‰, while the Lugovoe drill-core *n*-alkanes are on average 0.3‰ more positive than $\delta^{13}\text{C}_{\text{TOC}}$.

Despite the high hopane/sterane (Hop/Ster) abundance ratios for most samples, we were able to measure the $\delta^{13}\text{C}$ values of the $\text{C}_{29}\alpha\alpha\alpha\text{R}$ sterane (stigmastane) in aliphatic fractions that exhibited a Hop/Ster ratio below 10 (Table 3.4). These were the Kotlin Regional Horizon samples, and the $\delta^{13}\text{C}$ values of the C_{29} sterane was within 0.7‰ of $\delta^{13}\text{C}_{\text{TOC}}$ values (Fig. 3.3b).

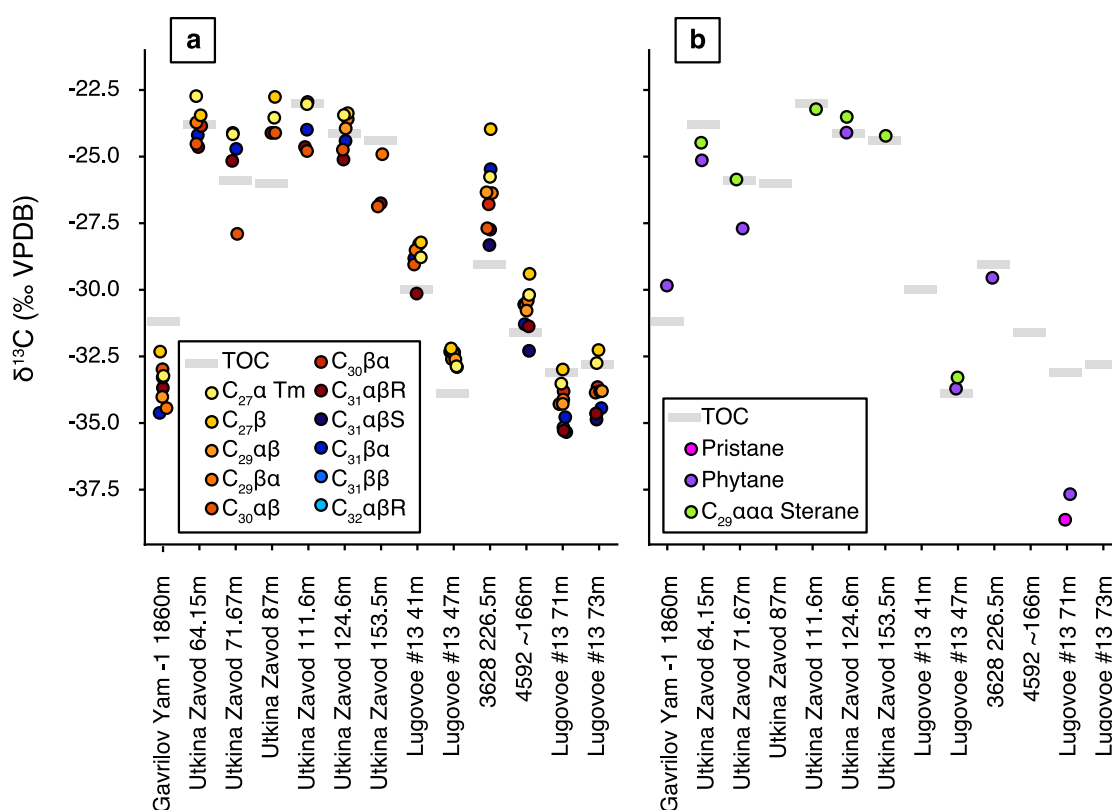


Figure 3.3. (a) CSIA of individual hopanes and $\delta^{13}\text{C}_{\text{TOC}}$ for the late Ediacaran and Early Cambrian samples. (b) CSIA of pristane, phytane, $\text{C}_{29}\alpha\alpha\alpha\text{R}$ sterane, and $\delta^{13}\text{C}_{\text{TOC}}$. The $\delta^{13}\text{C}_{\text{org}}$ values of $\text{C}_{29}\alpha\alpha\alpha\text{R}$ sterane, mainly sourced by RuBisCO-CBB-utilizing green algae, tracks closely the $\delta^{13}\text{C}_{\text{TOC}}$ values. $\delta^{13}\text{C}_{\text{org}}$ values of pristane and phytane show a large negative offset compared to $\delta^{13}\text{C}_{\text{TOC}}$ values for samples Lugovoe 13-71 and 3628 226.5m, but closely match $\delta^{13}\text{C}_{\text{TOC}}$ values for other samples.

Isotopic compositions of the acyclic isoprenoids, pristane and phytane were also measured. Phytane $\delta^{13}\text{C}$ ranges from -1.8‰ to +0.2‰ relative to the $\delta^{13}\text{C}_{\text{TOC}}$ values for the Kotlin Regional Horizon samples. In contrast, phytane and pristane in the Lugovoe drill-core sample 13-71 (Redkino Regional Horizon) are very depleted in ^{13}C , with $\delta^{13}\text{C}$ values of -37.7‰ and -38.6‰, respectively, and are more negative than $\delta^{13}\text{C}_{\text{TOC}}$ values by -4.6‰ and -5.5‰, respectively.

3.2. Tricyclic terpane ratios

The ratio of the $\text{C}_{26}/\text{C}_{25}$ tricyclic terpanes (TT), measured from relative peak areas using MRM-GC-MS analysis, was used to help distinguish marine environments from fresh water/brackish settings. This parameter can be sensitive and informative about ancient aquatic salinity and can distinguish lacustrine from marine organic facies (Zumberge, 1987). It is especially useful for Precambrian OM since most biomarker ratios for distinguishing such salinity differences (for example, the presence or absence of 24-*n*-propylcholestanes from marine pelagophyte algae; Moldowan et al., 1990) are only applicable to Phanerozoic rocks and oils. A threshold value of greater than 1.2 usually indicates fresh water/brackish conditions, and high values from 1.4 and higher have been reported previously for freshwater, lacustrine source rocks (Zumberge, 1987; Korkmaz et al., 2022). The $\text{C}_{26}/\text{C}_{25}$ TT abundance ratios for the Utkina Zavod drill-core samples are consistently elevated, ranging from 1.6 to 2.8 (Fig. 3.5, Table 3.1), whereas the remaining samples have lower values in the range of 0.4 to 1.5 (mean value = 1.0).

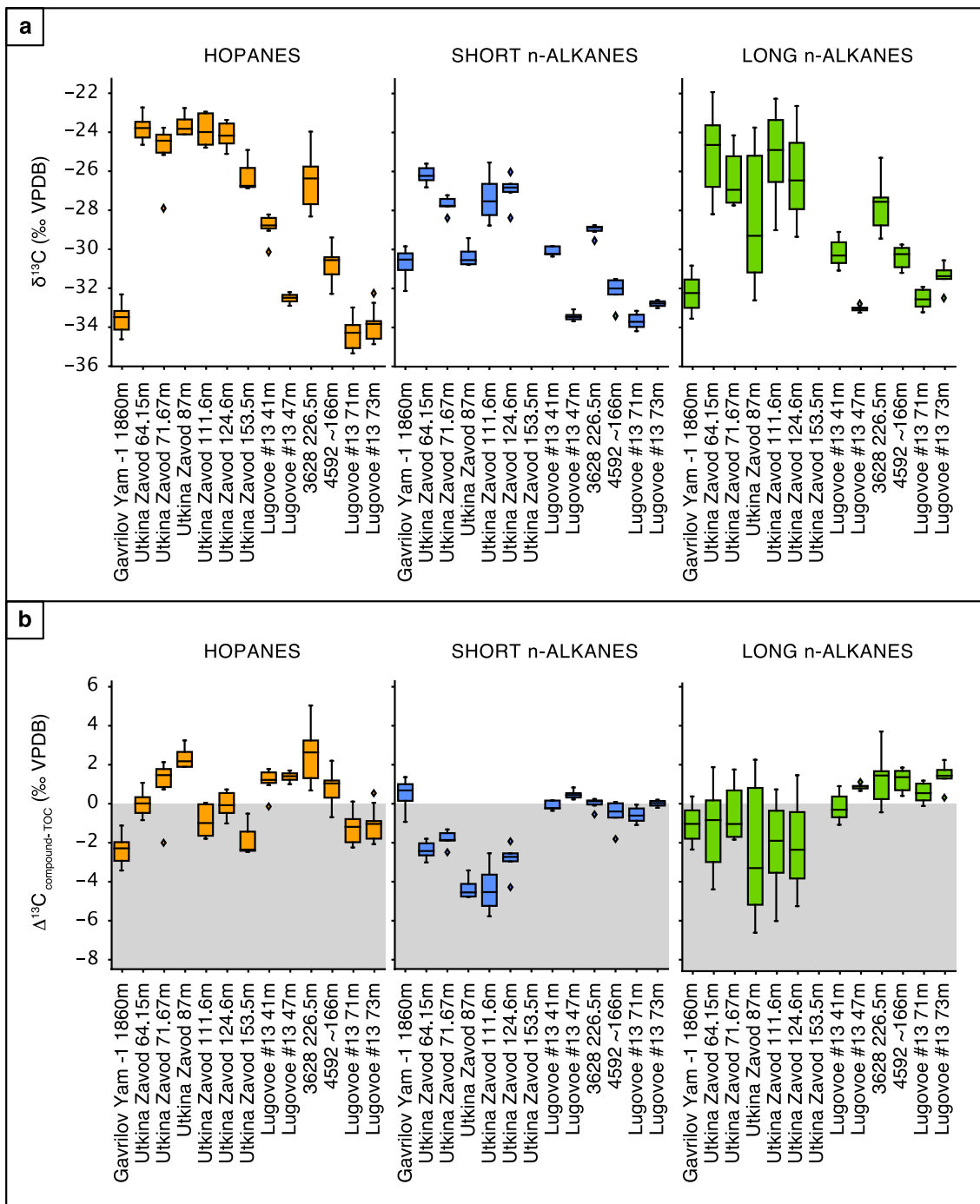


Figure 3.4. (a) Box plots of CSIA of hopanes, short-chain *n*-alkanes (range shown for *n*-C₁₇ to *n*-C₂₁), and long-chain *n*-alkanes (range shown for *n*-C₂₂ to *n*-C₂₉). Mean $\delta^{13}\text{C}_{\text{hopane}}$ values vary by 10.6‰, mean $\delta^{13}\text{C}_{\text{short } n\text{-alkanes}}$ values vary by 7.5‰, and mean $\delta^{13}\text{C}_{\text{long } n\text{-alkanes}}$ values vary by 7.7‰ from sample to sample. (b) Box plots of CSIA relative to $\delta^{13}\text{C}_{\text{TOC}}$ values for hopanes, short-chain *n*-alkanes (*n*-C₁₇ to *n*-C₂₁), and long-chain *n*-alkanes (*n*-C₂₂ to *n*-C₂₉).

3.3. Iron Speciation

The Fe_{HR}/Fe_T ratios for Kotlin Regional Horizon samples range in value from 0.15 to 0.92 (Table 3.1). The majority of the Utkina Zavod and Volyn core samples of the Kotlin Regional Horizon have lower Fe_{HR}/Fe_T ratios, with several samples below 0.22, indicative of deposition under oxic water column conditions (Fig. 3.6). The Lugovoe samples from both the Kotlin and Redkino Regional horizons are all above 0.38, indicative of deposition under anoxic conditions (Poulton and Canfield, 2005). Fe_{py}/Fe_{HR} ratios are below 0.6 for all samples indicating that ferruginous, rather than euxinic, conditions were most common in during anoxic deposition (Poulton, 2021).

4. DISCUSSION

4.1 $\delta^{13}C$ values of Lipid Biomarkers

The $\delta^{13}C$ values of individual alkane compounds and bulk sedimentary OM are controlled by the balance of a variety of biogenic inputs, as well as by local environmental conditions. Ancient epicontinental seaways were susceptible to changes in water circulation, redox, temperature, and sea level, which can all affect metabolic carbon isotopic fractionation relative to $\delta^{13}C_{DIC}$ and $\delta^{13}C_{TOC}$ (Pancost et al., 2013). As discussed in detail by Pehr et al. (2018), the sedimentary rocks from Baltica are exceptionally thermally well-preserved with multiple indicators (low T_{max} , values consistent with immature hopane and sterane stereoisomer ratios) confirming their low thermal maturity equivalent to a pre-oil window stage. Thermal maturation effects on $\delta^{13}C$ values due to cracking of biomolecules are therefore minimal. Significant overprinting from migrated

OM from petroleum fluids can also be ruled out based on the immature biomarker stereoisomer patterns found, and from the self-consistency check provided from parallel analysis of kerogen-bound hydrocarbons (Pehr et al., 2018).

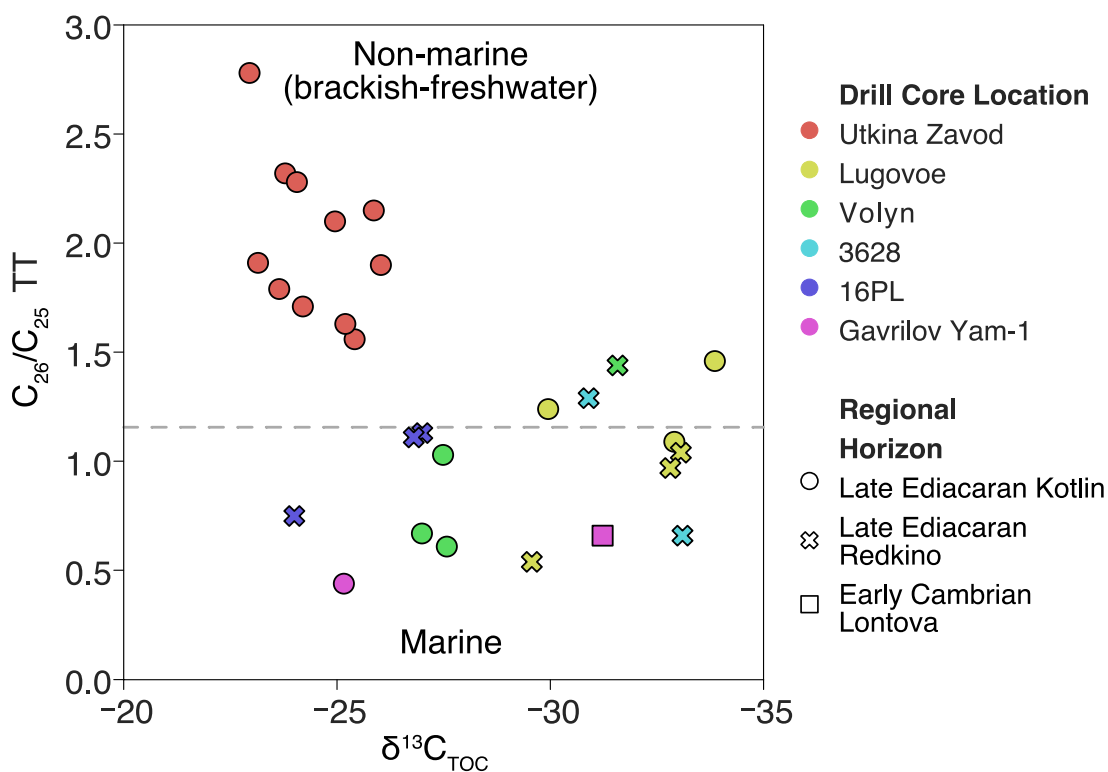


Figure 3.5. Bulk organic carbon isotope values ($\delta^{13}\text{C}_{\text{TOC}}$) versus the ratio of $\text{C}_{26}/\text{C}_{25}$ tricyclic terpanes (TT); $\text{C}_{26}/\text{C}_{25}$ TT > 1.2 usually indicates lower-salinity, aquatic environments, either freshwater or brackish; $\text{C}_{26}/\text{C}_{25}$ TT < 1.2 (dashed line) is typically indicative of normal marine conditions. Here, values > 1.2 are likely indicative of marginal marine/estuarine setting with brackish waters. Notably, the Utkina Zavod drill-core sediments from the Kotlin Regional Horizon all fall within non-marine field.

Hopanes, the most abundant compounds in the aliphatic fractions, have $\delta^{13}\text{C}$ values that closely track $\delta^{13}\text{C}_{\text{TOC}}$ values. Derived from hopanoids, these cell membrane lipids are synthesized by a wide variety of bacterial groups (Rohmer et al., 1984; Pearson et al.,

2007). Given their high abundance (Fig. 3.2), the ancient hopanes were likely derived from both bacterial primary producers and heterotrophs. Across all samples, most isotope values for hopane compounds are fairly close ($\pm 2\%$) to the $\delta^{13}\text{C}_{\text{TOC}}$ values. However, delta values for individual hopanes in any particular sample can differ from TOC by up to 4%, which likely reflects the production-weighted average from multiple bacterial lipid sources. The slightly more positive carbon isotope ratios for the lower carbon number hopanes, particularly C_{27} compounds, may be due to a greater degree of diagenetic reworking of these compounds within the water column and sediments. C_{27} hopanes are derived from complete side-chain cleavage of C_{30} and/or C_{35} biohopanoid precursors and hence are the most altered hopane compounds within the series.

Carbon isotope compositions of *n*-alkanes are either more negative (particularly for some samples from the Utkina Zavod drill core) or close to $\delta^{13}\text{C}_{\text{TOC}}$. The offset between free alkanes and bulk TOC (mainly composed of kerogen) could, in theory, reflect the isotopic differences between lipids and melanoidin-like organic geopolymers containing significant contributions from non-lipid biochemicals (carbohydrates or proteins).

Sterane distributions are more diagnostic of specific biological sources than hopanes. A dominance of C_{29} steranes, derived from C_{29} sterol precursors, represents contributions by green algae and plants (Grantham and Wakefield, 1988; Schwark and Empt, 2006; Kodner et al., 2008; Love et al., 2009). Prior to the appearance of terrestrial plants in the Paleozoic, a C_{29} sterane (stigmastane) dominance generally indicates high green algal

inputs (Grosjean et al., 2009; Love et al., 2009). Green algae are primary producers, which use RuBisCO-CBB for autotrophic carbon fixation, a pathway that yields biomass fractionated by up to ca. -29‰ from the $\delta^{13}\text{C}$ values of dissolved CO_2 (Roeske and O'Leary, 1984; Hayes, 2001; Scott et al., 2004; Pearson, 2010; Carvalho and Eyre, 2011).

For Ediacaran OM preserved in ancient sedimentary rocks, extractable alkane fractions typically have very similar bulk $\delta^{13}\text{C}$ signatures, within $\sim 1\%$ (Grosjean et al., 2009), relative to $\delta^{13}\text{C}_{\text{TOC}}$ values. The most ^{13}C -depleted ancient and modern alkane compounds produced by marine autotrophs using RuBisCO-CBB for carbon fixation are around -36‰, and is typically associated with times of high atmospheric pCO_2 (Pagani et al., 2005), which maximizes biological carbon isotope fractionations by autotrophs (Hayes, 1993). However, it is common to observe less than the maximum possible fractionation value, due to elevated growth rates associated with high nutrients or other environmental factors. The $\delta^{13}\text{C}_{\text{C}_{29}\text{sterane}}$ values for our samples range from -23.22‰ to -33.29‰ and closely align with the corresponding $\delta^{13}\text{C}_{\text{TOC}}$ and $\delta^{13}\text{C}_{\text{hopane}}$ values. The most negative $\delta^{13}\text{C}_{\text{C}_{29}\text{sterane}}$ value of -33.29‰ still falls within the predicted ^{13}C -depleted range for lipids derived from green algae. Strikingly similar $\delta^{13}\text{C}$ values for C_{29} $\alpha\alpha\alpha\text{R}$ sterane and the most abundant ($\text{C}_{27}\text{-C}_{32}$) hopanes suggest that the major bacterial source organisms included RuBisCO-CBB-utilizing photoautotrophs, such as cyanobacteria, as well as bacterial heterotrophs consuming primary biomass.

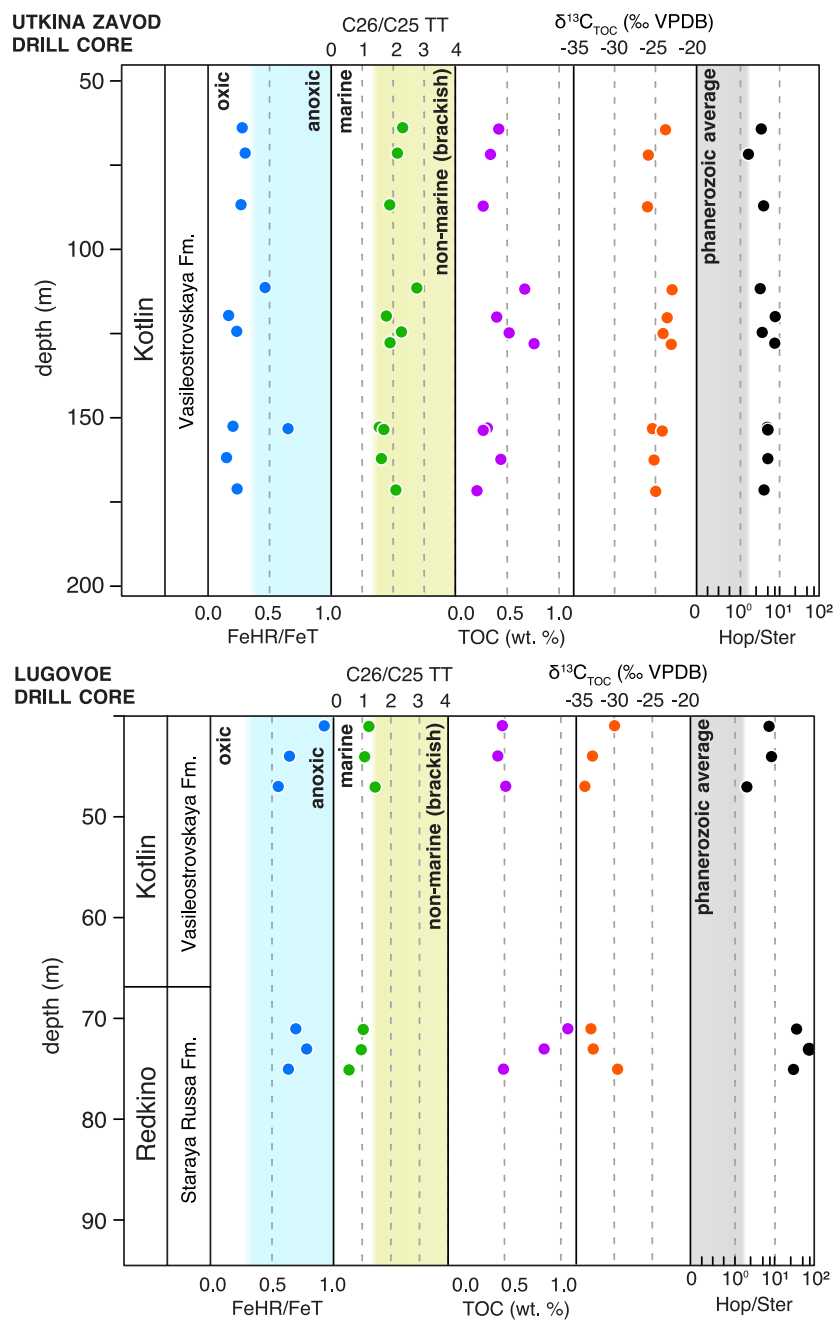


Figure 3.6. Stratigraphic trends for inorganic and organic geochemical proxies measured for sediments from the Utkina Zavod and Lugovoe drill cores. C₂₆/C₂₅ TT (tricyclic terpanes), FeHR/FeT, $\delta^{13}\text{C}_{\text{TOC}}$, TOC, and Hop/Ster values are given in Table 3.1. The threshold value for C₂₆/C₂₅ TT is ~1.2 to distinguish low-salinity lacustrine or marginal marine waters (>1.2) from marine waters (≤ 1.2).

4.2. Local Environmental Effects on $\delta^{13}\text{C}_{\text{TOC}}$

Organics in the Utkina Zavod drill-core samples are enriched by ~10‰ compared to other samples of late Ediacaran – Early Cambrian including other localities in Baltica used in this study (Table 3.1), and for sediments and oils from South Oman, Siberia, Australia, and South China (Grosjean et al., 2009; Kelly et al., 2011; Lan et al., 2012; Lee et al., 2013; Pagès et al., 2016; Wang et al., 2019; Roussel et al., 2020). This enrichment is observed in both the bulk TOC and individual compounds. CSIA data reveals the Kotlin Regional Horizon ^{13}C -enrichment is captured across a variety of major lipid compound classes, including the hopanes, *n*-alkanes, phytane, and C_{29} $\alpha\alpha\alpha\text{R}$ sterane. The large magnitude of this ^{13}C -enrichment, which is unusual for Ediacaran marine samples, points to unusual environmental conditions during deposition of the Kotlin Regional Stage strata at the Utkina Zavod drill-core location. In contrast to other depositional sites in Baltica, the data are suggestive of a non-marine and/or highly restricted aquatic setting.

The ~10‰ difference between the Utkina Zavod and Lugovoe drill cores, which are less than 100 km apart in the Saint Petersburg area of Russia, could reflect the $\delta^{13}\text{C}$ composition of the local DIC pool or metabolic fractionation potentially related to nutrient-fueled growth rates or productivity- or circulation-linked differences in dissolved CO_2 concentrations (Fogel et al., 1992; Popp et al., 1998). Notably, lipid compounds from phototrophs carry the enrichment. Thus, we can rule out other factors that influence isotope abundances in bulk sedimentary organic matter, including heterotrophic

reworking, enhanced preservation of protein and carbohydrate residues as melanoidin-like geopolymers, or shifts in the microbial communities.

Diminished fractionation by photoautotrophs can result from several mechanisms. Low $\text{CO}_{2(\text{aq})}$ concentrations limit the flux of carbon supplied across cell membranes by diffusion, which limits expression of enzymatic isotope fractionation during carbon fixation. Low concentrations and associated carbon limitation can further trigger carbon-concentration mechanisms (CCM), including active bicarbonate uptake (Badger and Price, 2003; Reinfelder, 2011). These active carbon transport mechanisms yield biomass that is significantly enriched in ^{13}C (Hayes, 1993; Smith et al., 1999). In modern marine waters, $\text{CO}_{2(\text{aq})}$ concentrations represent a balance between carbon uptake by photosynthesis with that supplied by upwelling and equilibration with the atmosphere, and potential carbonate equilibria shifts tied to pH and water temperatures (Freeman, 2001). Atmospheric CO_2 concentrations were likely high in the late Ediacaran – Early Cambrian (Kanzaki et al., 2018; Mills et al., 2019), and, more importantly, as a global feature they would not differ by locality, so this option seems unlikely. Variations in nutrient supply and ocean circulation or upwelling could have varied by locality.

Diminished fractionation can also result from increased carbon demand due to elevated phytoplankton growth rates spurred by high nutrient availability. Elevated productivity is often associated with enhanced OM burial efficiency due to decreased oxygen exposure times (Hartnett et al., 1998). Yet, craton-scale low nutrient, oligotrophic conditions have

been inferred for Baltica during the late Ediacaran to Early Cambrian (Pehr et al., 2018). This inference is based on the absence of evidence for enhanced carbon burial, including consistently low TOC content (mostly <0.5 wt%), low Hydrogen Index values for TOC, and biomarkers signifying bacterial input dominance over eukaryotes.

It is conceivable that the absence of evidence for enhanced carbon burial reflects more efficient heterotrophic respiration. If so, substantial biomass from elevated productivity was largely not preserved in the sedimentary rock record. This is possible under the mainly oxic (based on Fe speciation, Fig. 3.6) and oligotrophic conditions, which implies well ventilated conditions persisted in the coastal waters at the Utkina Zavod drill-core location during the Kotlin Regional Stage (Pehr et al., 2018). However, there is no geochemical evidence for enhanced carbon remineralization, such as accumulation of pyrite or Fe- and Mn-rich carbonates, and geochemical proxies for reducing water-column redox conditions in the sample localities. Combined, this evidence points to lower rates of primary biomass production due to limited nutrient supplies.

The C₂₆/C₂₅ tricyclic terpane (TT) ratio, which tracks environmental conditions during deposition, clearly differentiates between the Utkina Zavod and Lugovoe drill-core samples of the Kotlin Regional Horizon. The ratio of C₂₆/C₂₅ TT correlates with the salinity in the depositional setting (Zumberge, 1987). C₂₆/C₂₅ TT values at or below ~1.0 are associated with marine conditions, whereas values greater than or equal to ~1.2 are typically associated with brackish or freshwater conditions (Zumberge, 1987; Grande et

al., 1993). Intermediate values of 1.0-1.2 are equivocal. The Utkina Zavod drill-core samples (C_{26}/C_{25} TT ranges 1.6 to 2.8, mean = 2.0) all fall within the range of brackish-freshwater conditions. In contrast, the Lugovoe drill-core samples have values that range from 0.5 to 1.5 (mean = 1.1), close to normal marine conditions.

The tricyclic terpane ratios suggest that sediments from the Utkina Zavod drill-core were deposited under lower salinities, typical of a coastal setting. They also indicate the Lugovoe sediments, sitting <100 km north towards the craton margin, were deposited in a less restricted marine setting. The Lugovoe drill-core biomarker distributions also have noticeably higher ratios of C_{31}/C_{30} hopanes than those for the Utkina Zavod drill-core rocks. This difference is consistent with iron speciation data that indicate that the Lugovoe location hosted more reducing water-column conditions during the Kotlin Regional Stage (Figs. 3.1 and 3.6). A low salinity coastal setting at Utkina Zavod drill core is consistent with the environmental conditions inferred for the Kotlin Regional Stage in Estonia, located more than 150 km west-southwest of the Utkina Zavod drill core. In Estonia, a fresh-brackish aquatic setting with warm and humid climatic conditions was suggested based on a common presence of diagenetic siderite, lack of pyrite and glauconite, and low boron content in the clay fraction of fine-grained siliciclastic sediments (Pirrus, 1992; Mens and Pirrus, 1997). Freshwater conditions on the western side of the East European craton during the Ediacaran were also described based on the occurrence of pedogenic siderites (Bojanowski et al., 2019).

Shallow coastal, deltaic, and estuarine environments are the mixing zone of marine and fresh waters, and pH and temperature are more variable than in open-marine environments. Freshwater feeding into the coastal waters could have had a higher pH and higher alkalinity, that varied depending on the water provenance (Krishna et al., 2019). The proportion of $\text{CO}_{2(\text{aq})}$ versus both bicarbonate and carbonate within the DIC pool decreases with higher pH (Zhang et al., 1995), resulting in a potential $\text{CO}_{2(\text{aq})}$ limitation. We suggest alkaline riverine water input to the brackish coastal waters led to higher pH and/or alkalinity, resulting in $\text{CO}_{2(\text{aq})}$ limitation and enhanced utilization of CCMs and bicarbonate uptake by phytoplankton. These processes likely contributed to the ^{13}C -enriched composition of TOC and individual lipid biomarkers during deposition of the Kotlin Regional Horizon at the Utkina Zavod drill-core location.

In modern estuaries, the $\delta^{13}\text{C}$ values of DIC is typically more negative than marine values, due to the remineralization of organic carbon from plants and soil (Fogel et al., 1992; Boschker et al., 2005). However, terrestrial inputs of organic carbon would have been very low in the late Ediacaran to the Early Cambrian, due to the absence of land plants. It is possible that seawater input of DIC derived from carbonate weathering may have contributed more positive $\delta^{13}\text{C}_{\text{DIC}}$ values to the coastal environment (Kump and Arthur, 1999; Kump et al., 1999), although it seems unlikely that the aqueous $\delta^{13}\text{C}_{\text{DIC}}$ shifted by as much as $\sim 10\text{‰}$ to solely drive the change in the $\delta^{13}\text{C}_{\text{TOC}}$. Further, pre-late Ediacaran (Cryogenian and Tonian) sedimentary successions are predominantly

siliciclastic on Baltica and so they could not have been a significant source of inorganic carbon input.

There has been some emerging evidence for localized nearshore DIC gradients in late Ediacaran marine margins, resulting in ^{13}C -enriched sedimentary OM and carbonates. This is supported by gradients in $\delta^{13}\text{C}_{\text{carb}}$ of carbonates deposited in basinal and proximal ramp settings, for late Ediacaran marine rocks in Namibia (Wood et al., 2015). More positive values of $\delta^{13}\text{C}_{\text{carb}}$ were associated with proximal (inner ramp) depositional settings. The underlying cause of this phenomenon is not well understood and the magnitude of the local isotopic gradients does not typically exceed $\sim 3\text{-}4\text{‰}$ (Wood et al., 2015). Thus, these gradients are significantly smaller in magnitude than the $> 10\text{‰}$ differences in $\delta^{13}\text{C}$ values of individual lipids and bulk OM between drill-core locations. Local and regional dissolved carbon isotope gradients do not explain the full $\sim 10\text{‰}$ enrichment for the Kotlin Regional Horizon in bulk TOC and individual lipids in Utkina Zavod drill core versus Ediacaran seawater-sourced sedimentary OM.

The anomalous and consistently ^{13}C -enriched signature of the Kotlin Regional Horizon succession in Utkina Zavod drill-core and the absence of marine gradients in productivity, nutrients, or $\delta^{13}\text{C}_{\text{DIC}}$ collectively suggest fundamentally different depositional environments for the drill-core locations. We suggest the Utkina Zavod section was deposited in a brackish epicontinental setting. This is supported by elevated $\text{C}_{26}/\text{C}_{25}$ TT values from 1.6 to 2.8 (Fig. 3.5, Table 3.1) that are consistent with low (fresh

to brackish) coastal salinity. Elevated 2-methylhopane index values of 5.1 to 9.9% for samples from Utkina Zavod drill core (Pehr et al., 2018) are also consistent with a low-salinity, coastal setting, and may signify cyanobacterial and/or proteobacterial sources for the hopanes and 2-methylhopanes (Naafs et al., 2022), along with bacterial heterotrophs, in these samples. Geochemical evidence suggests the brackish coastal waters transitioned into normal-marine salinity conditions further offshore at the Lugovoe drill-core location. Such environmental differences may ultimately be tied to global eustatic sea level, climatic, and ocean-atmosphere redox changes, which occurred during the late Ediacaran (Li et al., 2019) and likely shaped local salinity conditions in marginal marine settings.

4.3. Investigating Evidence for Inverse Isotopic Ordering

Samples from the Lugovoe, 4592, and 3628 drill cores all display an unusual isotopic enrichment of the *n*-alkanes relative to bulk TOC, a characteristic which has been described previously as an “inverse carbon isotopic ordering” because lipids are depleted in ^{13}C relative to biomass for most modern organisms (Hayes 2001) (Fig. 3.4). Among these samples, those from the Redkino Regional Horizon in the Lugovoe drill core also show a strong positive enrichment between $n\text{C}_{17}$ and $n\text{C}_{18}$ alkanes vs. pristane and phytane (Table 3.4). Similar trends are reported for other Neoproterozoic samples (Logan et al., 1995, 1997) and are considered a common characteristic in late Precambrian marine basins. Sample Lugovoe #13 (collected at 71 m depth), has a $\delta^{13}\text{C}_{n\text{C}_{17}\text{-Pr}}$ value of +4.92‰ and a $\delta^{13}\text{C}_{n\text{C}_{18}\text{-Ph}}$ value of +4.52‰, which are suggestive of this inverse carbon isotopic ordering. The remaining samples from the Utkina Zavod and Lugovoe drill cores

for which phytane isotopic compositions were measurable, feature much less positive $\delta^{13}\text{C}_{\text{nC18-Ph}}$ values, which ranged from -2.89 to +0.64‰ and which are closer to more typical Phanerozoic carbon isotope ordering.

Previous explanations for isotopic enrichment in *n*-alkanes included: (1) intense heterotrophic reworking of slowly sinking OM (in the absence of animals that repackage OM to fecal pellets) in a redox-stratified ocean (Logan et al., 1995, 1997), or (2) a significant difference in carbon isotope fractionation between bacterial and eukaryotic primary producers (Close et al., 2011). Both arguments assume preferential preservation of certain compounds within kerogen, which generally accounts for most of the bulk TOC in ancient rocks.

For the Redkino Regional Horizon samples from Lugovoe drill core in our dataset, there is a third potential explanation. Pristane and phytane are commonly derived from the phytol side chain of certain chlorophylls made by photosynthetic organisms, particularly cyanobacteria and algae (Rontani and Volkman, 2005). However, Lugovoe #13 sample (collected at 71 m depth) has a $\delta^{13}\text{C}_{\text{phytane}}$ value of -37.7‰ and a $\delta^{13}\text{C}_{\text{pristane}}$ value of -38.6‰, well below values typical for RuBisCO-CBB-utilizing phototrophs. Such low values (ca. -39‰) indicate the acyclic isoprenoids derived in part from microorganisms involved in methane cycling (Freeman et al., 1990) mixed with input from chlorophylls with a phytol side chain. Additionally, methanogenic and methanotrophic archaea synthesizing archaeol/hydroxy-archaeols have been proposed as a possible source for

phytane (Koga et al., 1993; Koga et al., 1998; Wakeham et al., 2003), and could have feasibly contributed to pristane from diagenetic modification of phytane.

Thus, the >4‰ offset for $\Delta\delta^{13}\text{C}_{n\text{C}18\text{-Ph}}$ could reasonably be explained by unusually ^{13}C -depleted phytane from an appreciable archaeal source, rather than ^{13}C -enrichment of *n*-alkanes due to intense heterotrophy. Archaeal lipid inputs is supported by CSIA data reported for pristane and phytane in Ediacaran-Cambrian oils from Siberia. These oils yielded similar $\delta^{13}\text{C}_{\text{pristane}}$ and $\delta^{13}\text{C}_{\text{phytane}}$ values that were as low as ca. -44‰ and about half of the samples had ^{13}C -depletion of $\delta^{13}\text{C}_{\text{pristane}}$ and $\delta^{13}\text{C}_{\text{phytane}}$ of -1 to -8‰ compared with *n*C17 and *n*C18 alkanes. (Kelly et al., 2011). The interiors of the deep oceans were likely not fully oxygenated through most of the Paleozoic Era (Stolper and Bucholz, 2019), which would have favored methanogenesis and sustained a vigorous methane cycle in the water column and in shallow sediments in the Precambrian and Early Paleozoic oceans (Rohrssen et al., 2013).

Our CSIA measurements were not limited to *n*-alkane and acyclic isoprenoid carbon isotopes. With the enhanced sensitivity of pico-CSIA, we were able to measure $\delta^{13}\text{C}$ signatures for the C₂₇-C₃₂ hopanes and the most abundant C₂₉ sterane ($\alpha\alpha\alpha\text{R}$). This allowed us to investigate the possible origins of these important and diagnostic markers of biological sources.

Hop/Ster ratios can be used as convenient estimates of bacterial versus eukaryotic source contributions to preserved sedimentary OM. Environments with high rates of heterotrophy may preserve elevated Hop/Ster ratios due to an abundance of hopanoid-producing heterotrophic bacteria. While the Lugovoe, 4592, and 3628 drill cores have high Hop/Ster ratios (>1), spanning from 2 to 119, there is no corresponding significant change in $\Delta\delta^{13}\text{C}_{n\text{-alkane} - \text{TOC}}$. Biomass from heterotrophic bacteria is also typically enriched in ^{13}C relative to their food source by $\sim 1\%$ (DeNiro and Epstein, 1978; Hullar et al., 1996). Previous models of inverse carbon isotopic ordering have assumed a significant difference in carbon isotope composition between photosynthetic bacteria and eukaryotic biomass of, at a minimum, 4% (Close et al., 2011). For the one Lugovoe drill-core sample (collected at 47 m depth) with a measurable $\delta^{13}\text{C}_{\text{C}_{29}\text{sterane}}$ value, the average $\delta^{13}\text{C}_{\text{hopane}}$ value is only $\sim 0.6\%$ more positive relative to $\delta^{13}\text{C}_{\text{C}_{29}\text{sterane}}$. This is much less than the 4% biogenic offset thought to be needed to produce a ^{13}C -enrichment in the n-alkanes. This is also in line with our other sterane measurements for the Utkina Zavod drill-core samples, which yield a mean and maximum $\Delta\delta^{13}\text{C}_{\text{hopane} - \text{C}_{29}\text{sterane}}$ of 0.8% and 2.7% , respectively.

Overall, this evidence suggests the late Ediacaran rocks reported here do not simply conform to the typically prescribed Precambrian inverse carbon isotopic ordering of linear alkanes versus acyclic isoprenoids. Further, we found no significant difference in the average carbon isotope abundances measured for polycyclic triterpanes from bacterial producers and consumers versus the main eukaryotic (green algal) primary producers in

the rock sample with measurable $\delta^{13}\text{C}_{\text{C}_{29}\text{sterane}}$ and $\delta^{13}\text{C}_{\text{hopanes}}$ (mean = 0.6‰). The combined evidence points to the abundant bacterial signal being at least partially sourced from phototrophic bacteria, particularly RuBisCO-CBB-utilizing bacteria, alongside a significant contribution from heterotrophic bacteria.

Importantly, multiple source contributions to *n*-alkanes and to phytane (including from archaeal sources as well as from chlorophylls), complicate the carbon isotopic systematics. Such source variations were likely tied to changing paleoenvironmental redox that can mute or exaggerate $\delta^{13}\text{C}$ differences between compounds. Indeed, the magnitude of Ediacaran inverse/normal carbon isotopic ordering of branched versus linear alkanes, normally attributed to a preferential heterotrophic reworking of *n*-alkanes or a significant difference in $\delta^{13}\text{C}$ between algal and bacterial lipids, was likely influenced by multiple environmental and ecological factors. Future studies utilizing the improved pico-CSIA method on ancient sedimentary rocks and oils will help shed new light on the secular patterns and the carbon isotopic systematics for a suite of ancient lipid compounds.

5. CONCLUSIONS

During the late Ediacaran, Baltica was covered by shallow, epicontinental seas extending from the foreland basins developed along the southwestern, eastern, and northeastern margins. This contributed to oligotrophic conditions and a high regional heterogeneity in

marine environments, including brackish coastal waters. The lipid biomarker and stable carbon isotopic characteristics of the strata from the Kotlin Regional Horizon from the Utkina Zavod drill core suggest that these sediments were deposited in a fresh to brackish water-column coastal setting rather than in an open-marine environment. $\delta^{13}\text{C}$ values for bulk organics and individual compounds from the Utkina Zavod drill core are more positive than typical Ediacaran marine settings (range -26.0 to -23.0‰) and generally track each other, slightly offset by <2‰. The $\delta^{13}\text{C}_{\text{TOC}}$ values matched those for pristane, phytane, and C_{29} $\alpha\alpha\alpha\text{R}$ sterane, which are typically derived from photoautotrophs. The low salinity coastal waters that prevailed during deposition of the Kotlin Regional Horizon strata at the Utkina Zavod drill-core location may have sustained high pH and/or elevated alkalinity of carbonate and bicarbonate from riverine input. This could have resulted in localized dissolved $\text{CO}_{2(\text{aq})}$ limitation that promoted carbon-concentration mechanisms or active bicarbonate uptake by photoautotrophs, explaining the consistently ^{13}C -enriched signature found for lipids and bulk TOC in the Kotlin Regional Horizon sediments.

By contrast, the sedimentary OM in sediments from the Kotlin and Redkino Regional horizons from the Lugovoe drill core exhibit isotope signatures that are more typical of Ediacaran marine settings ($\delta^{13}\text{C}_{\text{TOC}}$ ranging from -33.9 to -30.0‰). Very high ratios of Hop/Ster in these sediments, combined with similar $\delta^{13}\text{C}$ values for C_{29} sterane and individual hopanes, strongly indicate that the major source biota were photoautotrophic bacteria utilizing RuBisCO-CBB and heterotrophic bacteria, with a lesser contribution

from green algae. The most depleted $\delta^{13}\text{C}$ signatures for lipids are found in a Lugovoe drill-core sample from the Redkino Regional Horizon. $\delta^{13}\text{C}$ values for pristane and phytane are significantly depleted to -39‰, suggesting a partial contribution of acyclic isoprenoids from archaea involved in methane cycling.

Acknowledgements: We dedicate this paper to the late Marilyn Fogel, who pioneered methods in stable isotope geochemistry and organic geochemistry. Marilyn's dedication to science and the mentorship of young scientists over many years was recognized and appreciated by many individuals within the geochemistry community. G.D.L. acknowledges a NASA Exobiology award (grant number 80NSSC18K1085) for funding this research. A.B. thanks Petroleum Foundation of the American Chemical Society (grant number 624840ND2). We also thank the two anonymous reviewers for their helpful comments.

REFERENCES

- Baczynski, A.A., Polissar, P.J., Juchelka, D., Schwieters, J., Hilkert, A., Summons, R.E., Freeman, K.H., 2018. Picomolar-scale compound-specific isotope analyses. *Rapid communications in mass spectrometry* : RCM 32, 730–738.
- Badger, M.R., Price, G.D., 2003. CO₂ concentrating mechanisms in cyanobacteria: molecular components, their diversity and evolution. *Journal of Experimental Botany* 54, 609–622.
- Bobrovskiy, I., Hope, J.M., Golubkova, E., Brocks, J.J., 2020. Food sources for the Ediacara biota communities. *Nature Communications* 11, 1261.
- Bojanowski, M.J., Goryl, M., Kremer, B., Marciniak-Maliszewska, B., Marynowski, L., Środoń, J., 2019. Pedogenic siderites fossilizing Ediacaran soil microorganisms on the Baltica paleocontinent. *Geology* 48, 62–66.
- Boschker, H.T.S., Kromkamp, J.C., Middelburg, J.J., 2005. Biomarker and carbon isotopic constraints on bacterial and algal community structure and functioning in a turbid, tidal estuary. *Limnology and Oceanography* 50, 70–80.
- Brocks, J.J., Jarrett, A.J.M., Sirantoine, E., Hallmann, C., Hoshino, Y., Liyanage, T., 2017. The rise of algae in Cryogenian oceans and the emergence of animals. *Nature* 548, 578–581.
- Canfield, D.E., Raiswell, R., Westrich, J.T., Reaves, C.M., Berner, R.A., 1986. The use of chromium reduction in the analysis of reduced inorganic sulfur in sediments and shales. *Chemical Geology* 54, 149–155.
- Canfield, D.E., Raiswell, R., Bottrell, S.H., 1992. The reactivity of sedimentary iron minerals toward sulfide. *American Journal of Science* 292, 659–683.
- Carvalho, M., Eyre, B., 2011. Carbon stable isotope discrimination during respiration in three seaweed species. *Marine Ecology Progress Series* 437, 41–49.
- Close, H.G., Bovee, R., Pearson, A., 2011. Inverse carbon isotope patterns of lipids and kerogen record heterogeneous primary biomass. *Geobiology* 9, 250–265.
- Coplen, T.B., Brand, W.A., Gehre, M., Gröning, M., Meijer, H.A.J., Toman, B., Verkouteren, R.M., 2006. New Guidelines for $\delta^{13}\text{C}$ Measurements. *Analytical Chemistry* 78, 2439–2441.

- Corso, J.D., Mietto, P., Newton, R.J., Pancost, R.D., Preto, N., Roghi, G., Wignall, P.B., 2012. Discovery of a major negative $\delta^{13}\text{C}$ spike in the Carnian (Late Triassic) linked to the eruption of Wrangellia flood basalts. *Geology* 40, 79–82.
- DeNiro, M.J., Epstein, S., 1978. Influence of diet on the distribution of carbon isotopes in animals. *Geochimica et Cosmochimica Acta* 42, 495–506.
- Ershova, V.B., Ivleva, A.S., Podkovyrov, V.N., Khudoley, A.K., Fedorov, P.V., Stockli, D., Anfindon, O., Maslov, A.V., Khubanov, V., 2019. Detrital zircon record of the Mesoproterozoic to Lower Cambrian sequences of NW Russia: implications for the paleogeography of the Baltic interior. *GFF* 141, 1–10.
- Fedorova, N.M., Levashova, N.M., Bazhenov, M.L., Meert, J.G., Sergeeva, N.D., Golovanova, I.V., Danukalov, K.N., Kuznetsov, N.B., Kadyrov, A.F., Khidiyatov, M.M., 2013. The East European Platform in the late Ediacaran: new paleomagnetic and geochronological data 54, 1392–1401.
- Fogel, M.L., Cifuentes, L.A., Velinsky, D.J., Sharp, J.H., 1992. Relationship of carbon availability in estuarine phytoplankton to isotopic composition. *JSTOR* 82, 291–300.
- Fox, C.P., Cui, X., Whiteside, J.H., Olsen, P.E., Summons, R.E., Grice, K., 2020. Molecular and isotopic evidence reveals the end-Triassic carbon isotope excursion is not from massive exogenous light carbon. *Proceedings of the National Academy of Sciences* 117, 30171–30178.
- Freeman, K.H., Hayes, J.M., Trendel, J.-M., Albrecht, P., 1990. Evidence from carbon isotope measurements for diverse origins of sedimentary hydrocarbons. *Nature* 343, 254–256.
- Freeman, K.H., 2001. Isotopic Biogeochemistry of Marine Organic Carbon. *Reviews in Mineralogy and Geochemistry* 43, 579–605.
- Goryl, M., Marynowski, L., Brocks, J.J., Bobrovskiy, I., Derkowski, A., 2018. Exceptional preservation of hopanoid and steroid biomarkers in Ediacaran sedimentary rocks of the East European Craton. *Precambrian Research* 316, 38–47.
- Grande, S.M.B.D., Neto, F.R.A., Mello, M.R., 1993. Extended tricyclic terpanes in sediments and petroleum. *Organic Geochemistry* 20, 1039–1047.
- Grantham, P.J., Wakefield, L.L., 1988. Variations in the sterane carbon number distributions of marine source rock derived crude oils through geological time. *Organic Geochemistry* 12, 61–73.

- Grazhdankin, D.V., Marusin, V.V., Meert, J., Krupenin, M.T., Maslov, A.V., 2011. Kotlin regional stage in the South Urals. *Doklady Earth Sciences* 440, 1222.
- Grosjean, E., Love, G.D., Stalvies, C., Fike, D.A., Summons, R.E., 2009. Origin of petroleum in the Neoproterozoic–Cambrian South Oman Salt Basin. *Organic Geochemistry* 40, 87–110.
- Hartnett, H.E., Keil, R.G., Hedges, J.I., Devol, A.H., 1998. Influence of oxygen exposure time on organic carbon preservation in continental margin sediments. *Nature* 391, 572–575.
- Hayes, J.M., Freeman, K.H., Popp, B.N., Hoham, C.H., 1990. Compound-specific isotopic analyses: A novel tool for reconstruction of ancient biogeochemical processes. *Organic Geochemistry* 16, 1115–1128.
- Hayes, J.M., 1993. Factors controlling ^{13}C contents of sedimentary organic compounds: Principles and evidence. *Marine Geology* 113, 111–125.
- Hayes, J.M., 2001. Fractionation of Carbon and Hydrogen Isotopes in Biosynthetic Processes. *Reviews in Mineralogy and Geochemistry* 43, 225–277.
- Holtvoeth, J., Whiteside, J.H., Engels, S., Freitas, F.S., Grice, K., Greenwood, P., Johnson, S., Kendall, I., Lengger, S.K., Lücke, A., Mayr, C., Naafs, B.D.A., Rohrsen, M., Sepúlveda, J., 2019. The paleolimnologist's guide to compound-specific stable isotope analysis – An introduction to principles and applications of CSIA for Quaternary lake sediments. *Quaternary Science Reviews* 207, 101–133.
- Hoshino, Y., Poshibaeva, A., Meredith, W., Snape, C., Poshibaev, V., Versteegh, G.J.M., Kuznetsov, N., Leider, A., Maldegem, L. van, Neumann, M., Naehar, S., Moczydłowska, M., Brocks, J.J., Jarrett, A.J.M., Tang, Q., Xiao, S., McKirdy, D., Das, S.K., Alvaro, J.J., Sansjofre, P., Hallmann, C., 2017. Cryogenian evolution of stigmasteroid biosynthesis. *Science advances* 3, e1700887.
- Hullar, M., Fry, B., Peterson, B.J., Wright, R.T., 1996. Microbial utilization of estuarine dissolved organic carbon: a stable isotope tracer approach tested by mass balance. *Applied and Environmental Microbiology* 62, 2489–2493.
- Ivleva, A.S., Podkovyrov, V.N., Ershova, V.B., Anfinson, O.A., Khudoley, A.K., Fedorov, P.V., Maslov, A.V., Zdobin, D.Yu., 2016. Results of U–Pb LA–ICP–MS dating of detrital zircons from Ediacaran–Early Cambrian deposits of the eastern part of the Baltic monocline. *Doklady Earth Sciences* 468, 593–597.
- Ivleva, A.S., Podkovyrov, V.N., Ershova, V.B., Khubanov, V.B., Khudoley, A.K., Sychev, S.N., Vdovina, N.I., Maslov, A.V., 2018. U–Pb LA–ICP–MS Age of Detrital

- Zircons from the Lower Riphean and Upper Vendian Deposits of the Luga–Ladoga Monocline. *Doklady Earth Sciences* 480, 695–699.
- Jaraula, C.M.B., Grice, K., Twitchett, R.J., Böttcher, M.E., LeMetayer, P., Dastidar, A.G., Opazo, L.F., 2013. Elevated pCO₂ leading to Late Triassic extinction, persistent photic zone euxinia, and rising sea levels. *Geology* 41, 955–958.
- Kanzaki, Y., Murakami, T., 2018. Effects of atmospheric composition on apparent activation energy of silicate weathering: II. Implications for evolution of atmospheric CO₂ in the Precambrian. *Geochimica et Cosmochimica Acta* 240, 314–330.
- Kelly, A.E., Love, G.D., Zumberge, J.E., Summons, R.E., 2011. Hydrocarbon biomarkers of Neoproterozoic to Lower Cambrian oils from eastern Siberia. *Organic Geochemistry* 42, 640–654.
- Kodner, R.B., Pearson, A., Summons, R.E., Knoll, A.H., 2008. Sterols in red and green algae: quantification, phylogeny, and relevance for the interpretation of geologic steranes. *Geobiology* 6, 411–420.
- Koga, Y., Nishihara, M., Morii, H., Akagawa-Matsushita, M., 1993. Ether polar lipids of methanogenic bacteria: structures, comparative aspects, and biosyntheses. *Microbiological reviews* 57, 164–82.
- Koga, Y., Morii, H., Akagawa-Matsushita, M., Ohga, M., 1998. Correlation of Polar Lipid Composition with 16S rRNA Phylogeny in Methanogens. Further Analysis of Lipid Component Parts. *Bioscience, biotechnology, and biochemistry* 62, 230–6.
- Korkmaz, S., Kara-Gülbay, R., Khoitiyn, T., Erdoğan, M.S., 2022. Biomarkers geochemistry of the Alpagut oil shale sequence: an evaluation of dispositional environments and source rock potential from Dodurga-Çorum basin (N-Turkey). *Journal of Petroleum Exploration and Production Technology* 12, 2173–2189.
- Krishna, M.S., Viswanadham, R., Prasad, M.H.K., Kumari, V.R., Sarma, V.V.S.S., 2018. Export fluxes of dissolved inorganic carbon to the northern Indian Ocean from the Indian monsoonal rivers. *Biogeosciences* 16, 505–519.
- Kump, L.R., Arthur, M.A., 1999. Interpreting carbon-isotope excursions: carbonates and organic matter. *Chemical Geology* 161, 181–198.
- Kump, L.R., Arthur, M.A., Patzkowsky, M.E., Gibbs, M.T., Pinkus, D.S., Sheehan, P.M., 1999. A weathering hypothesis for glaciation at high atmospheric pCO₂ during the Late Ordovician. *Palaeogeography, Palaeoclimatology, Palaeoecology* 152, 173–187.

- Lan, C., Hong, Z., Ruizhong, H., Jiafei, X., Loung-Yie, T.L., Tien-Shun, L.A., Yanrong, Z., 2012. Paleooceanographic Indicators for Early Cambrian Black Shales from the Yangtze Platform, South China: Evidence from Biomarkers and Carbon Isotopes. *Acta Geologica Sinica - English Edition* 86, 1143–1153.
- Lee, C., Fike, D.A., Love, G.D., Sessions, A.L., Grotzinger, J.P., Summons, R.E., Fischer, W.W., 2013. Carbon isotopes and lipid biomarkers from organic-rich facies of the Shuram Formation, Sultanate of Oman. *Geobiology* 11, 406–419.
- Lee, C., Love, G.D., Fischer, W.W., Grotzinger, J.P., Halverson, G.P., 2015. Marine organic matter cycling during the Ediacaran Shuram excursion. *Geology* 43, 1103–1106
- Li, W.-P., Zhao, Y.-Y., Zhao, M.-Y., Zha, X.-P., Zheng, Y.-F., 2019. Enhanced weathering as a trigger for the rise of atmospheric O₂ level from the late Ediacaran to the early Cambrian. *Scientific Reports* 9, 10630.
- Logan, G.A., Hayes, J.M., Hieshima, G.B., Summons, R.E., 1995. Terminal Proterozoic reorganization of biogeochemical cycles. *Nature* 376, 53–56.
- Logan, G.A., Summons, R.E., Hayes, J.M., 1997. An isotopic biogeochemical study of Neoproterozoic and Early Cambrian sediments from the Centralian Superbasin, Australia. *Geochimica et Cosmochimica Acta* 61, 5391–5409.
- Love, G.D., Grosjean, E., Stalvies, C., Fike, D.A., Grotzinger, J.P., Bradley, A.S., Kelly, A.E., Bhatia, M., Meredith, W., Snape, C.E., Bowring, S.A., Condon, D.J., Summons, R.E., 2009. Fossil steroids record the appearance of Demospongiae during the Cryogenian period. *Nature* 457, 718–721.
- Martin, M.W., Grazhdankin, D.V., Bowring, S.A., Evans, D.A.D., Fedonkin, M.A., Kirschvink, J.L., 2000. Age of Neoproterozoic Bilatarian Body and Trace Fossils, White Sea, Russia: Implications for Metazoan Evolution. *Science* 288, 841–845.
- Meidla, T., 2017. Ediacaran and Cambrian stratigraphy in Estonia: an updated review. *Estonian Journal of Earth Sciences* 66, 152.
- Mens K. and Pirrus E. 1997. Geology and Mineral Resources of Estonia: Vendian-Tremadocclastogenic sedimentation basins. *Estonian Acad. Publ*, 184-191.
- Mills, B.J.W., Krause, A.J., Scotese, C.R., Hill, D.J., Shields, G.A., Lenton, T.M., 2019. Modelling the long-term carbon cycle, atmospheric CO₂, and Earth surface temperature from late Neoproterozoic to present day. *Gondwana Research* 67, 172–186.

- Moldowan, J.M., Fago, F.J., Lee, C.Y., Jacobson, S.R., Watt, D.S., Slougui, N.-E., Jeganathan, A., Young, D.C., 1990. Sedimentary 12-n-Propylcholestanes, Molecular Fossils Diagnostic of Marine Algae. *Science* 247, 309–312.
- Naafs, B.D.A., Bianchini, G., Monteiro, F.M., Sánchez-Baracaldo, P., 2022. The occurrence of 2-methylhopanoids in modern bacteria and the geological record. *Geobiology* 20, 41–59.
- Pagani, M., Arthur, M.A., Freeman, K.H., 1999. Miocene evolution of atmospheric carbon dioxide. *Paleoceanography* 14, 273–292.
- Pagani, M., Zachos, J.C., Freeman, K.H., Tipple, B., Bohaty, S., 2005. Marked Decline in Atmospheric Carbon Dioxide Concentrations During the Paleogene. *Science* 309, 600–603.
- Pagès, A., Schmid, S., Edwards, D., Barnes, S., He, N., Grice, K., 2016. A molecular and isotopic study of palaeoenvironmental conditions through the middle Cambrian in the Georgina Basin, central Australia. *Earth and Planetary Science Letters* 447, 21–32.
- Pancost, R.D., Damsté, J.S.S., 2003. Carbon isotopic compositions of prokaryotic lipids as tracers of carbon cycling in diverse settings. *Chemical Geology* 195, 29–58.
- Pancost, R.D., Freeman, K.H., Herrmann, A.D., Patzkowsky, M.E., Ainsaar, L., Martma, T., 2013. Reconstructing Late Ordovician carbon cycle variations. *Geochimica et Cosmochimica Acta* 105, 433–454.
- Paszkowski, M., Budzyń, B., Mazur, S., Sláma, J., Środoń, J., Millar, I.L., Shumlyanskyy, L., Kędzior, A., Liivamägi, S., 2021. Detrital zircon U-Pb and Hf constraints on provenance and timing of deposition of the Mesoproterozoic to Cambrian sedimentary cover of the East European Craton, part II: Ukraine. *Precambrian Research* 362, 106282.
- Pearson, A., Page, S.R.F., Jorgenson, T.L., Fischer, W.W., Higgins, M.B., 2007. Novel hopanoid cyclases from the environment. *Environmental Microbiology* 9, 2175–2188.
- Pearson, A., 2010. *Handbook of Hydrocarbon and Lipid Microbiology* 143–156.
- Peñr, K., Love, G.D., Kuznetsov, A., Podkovyrov, V., Junium, C.K., Shumlyanskyy, L., Sokur, T., Bekker, A., 2018. Ediacara biota flourished in oligotrophic and bacterially dominated marine environments across Baltica. *Nature Communications* 9, 1807.
- Pirrus, E., 1992. Freshening of the Late Vendian Basin on the East European Craton. *Proceedings of the Estonian Academy of Sciences Geology* 41, 115–123.

- Popp, B.N., Laws, E.A., Bidigare, R.R., Dore, J.E., Hanson, K.L., Wakeham, S.G., 1998. Effect of Phytoplankton Cell Geometry on Carbon Isotopic Fractionation. *Geochimica et Cosmochimica Acta* 62, 69–77.
- Poulton, S.W., Fralick, P.W., Canfield, D.E., 2004. The transition to a sulphidic ocean ~ 1.84 billion years ago. *Nature* 431, 173–177.
- Poulton, S.W., Canfield, D.E., 2005. Development of a sequential extraction procedure for iron: implications for iron partitioning in continentally derived particulates. *Chemical Geology* 214, 209–221.
- Poulton, S.W., Canfield, D.E., 2011. Ferruginous Conditions: A Dominant Feature of the Ocean through Earth's History. *Elements* 7, 107–112.
- Poulton, S., 2021. *Elements in Geochemical Tracers in Earth System Science: The Iron Speciation Paleoredox Proxy*. Cambridge University Press, Cambridge.
- Raiswell, R., Canfield, D.E., 1998. Sources of iron for pyrite formation in marine sediments. *American Journal of Science* 298, 219–245.
- Raiswell, R., Newton, R., Wignall, P.B., 2001. An Indicator of Water-Column Anoxia: Resolution of Biofacies Variations in the Kimmeridge Clay (Upper Jurassic, U.K.). *Journal of Sedimentary Research* 71, 286–294.
- Reinfelder, J.R., 2011. Carbon Concentrating Mechanisms in Eukaryotic Marine Phytoplankton. *Annual Review of Marine Science* 3, 291–315.
- Roeske, C.A., O'Leary, M.H., 1984. Carbon isotope effects on enzyme-catalyzed carboxylation of ribulose biphosphate. *Biochemistry* 23, 6275–6284.
- Rohmer, M., Bouvier-Nave, P., Ourisson, G., 1984. Distribution of Hopanoid Triterpenes in Prokaryotes. *Microbiology* 130, 1137–1150.
- Rohrsen, M., Love, G.D., Fischer, W., Finnegan, S., Fike, D.A., 2013. Lipid biomarkers record fundamental changes in the microbial community structure of tropical seas during the Late Ordovician Hirnantian glaciation. *Geology* 41, 127–130.
- Rontani, J.-F., Volkman, J.K., 2005. Lipid characterization of coastal hypersaline cyanobacterial mats from the Camargue (France). *Organic Geochemistry* 36, 251–272.
- Roussel, A., Cui, X., Summons, R.E., 2020. Biomarker stratigraphy in the Athel Trough of the South Oman Salt Basin at the Ediacaran-Cambrian Boundary. *Geobiology* 00, 1–19

- Schwark, L., Empt, P., 2006. Sterane biomarkers as indicators of palaeozoic algal evolution and extinction events. *Palaeogeography, Palaeoclimatology, Palaeoecology* 240, 225–236.
- Scott, K.M., Schwedock, J., Schrag, D.P., Cavanaugh, C.M., 2004. Influence of form IA RubisCO and environmental dissolved inorganic carbon on the $\delta^{13}\text{C}$ of the clam-chemoautotroph symbiosis *Solemya velum*. *Environmental Microbiology* 6, 1210–1219.
- Sliaupa, S., Fokin, P., Lazauskiene, J., Stephenson, R.A., 2006. The Vendian-Early Palaeozoic sedimentary basins of the East European Craton 32, 449–462.
- Smith, K.S., Jakubzick, C., Whittam, T.S., Ferry, J.G., 1999. Carbonic anhydrase is an ancient enzyme widespread in prokaryotes. *Proceedings of the National Academy of Sciences* 96, 15184–15189.
- Soldatenko, Y., Albani, A.E., Ruzina, M., Fontaine, C., Nesterovsky, V., Paquette, J.L., Meunier, A., Ovtcharova, M., 2019. Precise U-Pb age constrains on the Ediacaran biota in Podolia, East European Platform, Ukraine. *Scientific Reports* 9, 1675.
- Stolper, D.A., Bucholz, C.E., 2019. Neoproterozoic to early Phanerozoic rise in island arc redox state due to deep ocean oxygenation and increased marine sulfate levels. *Proceedings of the National Academy of Sciences* 116, 8746–8755.
- Wakeham, S.G., Lewis, C.M., Hopmans, E.C., Schouten, S., Damsté, J.S.S., 2003. Archaea mediate anaerobic oxidation of methane in deep euxinic waters of the Black Sea. *Geochimica et Cosmochimica Acta* 67, 1359–1374.
- Wang, N., Li, M., Hong, H., Song, D., Tian, X., Liu, P., Fang, R., Chen, G., Wang, M., 2019. Biological sources of sedimentary organic matter in Neoproterozoic–Lower Cambrian shales in the Sichuan Basin (SW China): Evidence from biomarkers and microfossils. *Palaeogeography, Palaeoclimatology, Palaeoecology* 516, 342–353.
- Wood, R.A., Poulton, S.W., Prave, A.R., Hoffmann, K.-H., Clarkson, M.O., Guilbaud, R., Lyne, J.W., Tostevin, R., Bowyer, F., Penny, A.M., Curtis, A., Kasemann, S.A., 2015. Dynamic redox conditions control late Ediacaran metazoan ecosystems in the Nama Group, Namibia. *Precambrian Research* 261, 252–271.
- Zhang, J., Quay, P.D., Wilbur, D.O., 1995. Carbon isotope fractionation during gas-water exchange and dissolution of CO_2 . *Geochimica et Cosmochimica Acta* 59, 107–114.
- Zumberge, J.A., Rocher, D., Love, G.D., 2020. Free and kerogen-bound biomarkers from late Tonian sedimentary rocks record abundant eukaryotes in mid-Neoproterozoic marine communities. *Geobiology* 115, 246.

Zumberge, J.E., 1987. Prediction of source rock characteristics based on terpane biomarkers in crude oils: A multivariate statistical approach. *Geochimica et Cosmochimica Acta* 51, 1625–1637.

Table 3.1. Selected-biomarker abundance ratios, bulk organic carbon isotope values and iron speciation redox proxies that provide biological and depositional environmental constraints.

Drill Core	Depth (m)	Location	Stage	Horizon	TOC (wt %)	C ₂₆ /C ₂₅ TT	FeHR/ FeT	Fepy/ FeHR	Hop/ Ster ¹	δ ¹³ C _{TOC} (‰)
Utkina Zavod	64.15	Baltic Monocline	Late Ediacaran	Kotlin	0.42 ^a	2.32	0.28	0.06	3.4	-23.8 ^a
Utkina Zavod	71.67	Baltic Monocline	Late Ediacaran	Kotlin	0.34 ^a	2.15	0.30	0.07	1.6	-25.9 ^a
Utkina Zavod	87	Baltic Monocline	Late Ediacaran	Kotlin	0.27 ^a	1.9	0.27	0.00	3.9	-26.0 ^a
Utkina Zavod	111.6	Baltic Monocline	Late Ediacaran	Kotlin	0.67 ^a	2.78	0.47	0.01	3.2	-23.0 ^a
Utkina Zavod	119.9	Baltic Monocline	Late Ediacaran	Kotlin	0.40 ^a	1.79	0.17	0.00	7.7	-23.6 ^a
Utkina Zavod	124.6	Baltic Monocline	Late Ediacaran	Kotlin	0.52 ^a	2.28	0.24	0.02	3.6	-24.1 ^a
Utkina Zavod	127.8	Baltic Monocline	Late Ediacaran	Kotlin	0.76 ^a	1.91	n.d.	n.d.	7.5	-23.1 ^a
Utkina Zavod	152.8	Baltic Monocline	Late Ediacaran	Kotlin	0.31 ^a	1.56	0.20	0.02	4.8	-25.4 ^a
Utkina Zavod	153.5	Baltic Monocline	Late Ediacaran	Kotlin	0.27 ^a	1.71	0.65	0.00	5.0	-24.2 ^a
Utkina Zavod	162.1	Baltic Monocline	Late Ediacaran	Kotlin	0.44 ^a	1.63	0.15	0.09	5.0	-25.2 ^a
Utkina Zavod	171.4	Baltic Monocline	Late Ediacaran	Kotlin	0.21 ^a	2.10	0.24	0.02	4.0	-25.0 ^a
Lugovoe #13	41	Baltic Monocline	Late Ediacaran	Kotlin	0.48 ^a	1.24	0.92	0.53	7.2	-30.0 ^a
Lugovoe #13	44	Baltic Monocline	Late Ediacaran	Kotlin	0.44 ^a	1.09	0.64	0.17	8.3	-32.9 ^a
Lugovoe #13	47	Baltic Monocline	Late Ediacaran	Kotlin	0.51 ^a	1.46	0.55	0.19	2.0	-33.9 ^a
Lugovoe #13	71	Baltic Monocline	Late Ediacaran	Redkino	1.06 ^a	1.04	0.69	0.60	35.3	-33.1 ^a
Lugovoe #13	73	Baltic Monocline	Late Ediacaran	Redkino	0.85 ^a	0.97	0.78	0.55	73.4	-32.8 ^a
Lugovoe #13	75	Baltic Monocline	Late Ediacaran	Redkino	0.49 ^a	0.54	0.63	0.46	29.5	-29.6 ^a
Gavrilov Yam -1	1860	Moscow Syncline	Cambrian	Lontova	0.23 ^a	0.66	0.34	0.03	27.8	-31.2 ^a
Gavrilov Yam -1	2018	Moscow Syncline	Late Ediacaran	Kotlin	0.26 ^a	0.44	0.21	0.01	22.2	-25.2 ^a
4529	~195	Volyn basin	Late Ediacaran	Kotlin	0.12 ^a	1.03	0.60	0.01	22.8	-27.5 ^a
4529	~207	Volyn basin	Late Ediacaran	Kotlin	0.09 ^a	0.67	0.35	0.07	25.9	-27.0 ^a
4504	~200	Volyn basin	Late Ediacaran	Kotlin	0.13 ^a	0.61	0.32	0.03	22.5	-27.6 ^a
4592	~166	Volyn basin	Late Ediacaran	Redkino	0.47 ^a	1.44	0.63	0.25	119.2	-31.6 ^a
3628	226.5	Podillya basin	Late Ediacaran	Redkino	0.30 ^a	1.03	n.d.	n.d.	16.1	-29.0 ^b
16PL	outcrop #22	Podillya basin	Late Ediacaran	Redkino	0.43 ^a	1.11	0.34	0.01	8.1	-26.8 ^a
16PL	outcrop #18	Podillya basin	Late Ediacaran	Redkino	0.18 ^a	1.13	0.33	0.00	11.1	-27.0 ^a
16PL	outcrop #11	Podillya basin	Late Ediacaran	Redkino	0.50 ^a	0.75	0.58	0.00	11.5	-24.0 ^a

^aPreviously reported in Pehr et al. (2018); isotope analyses were performed at Syracuse University

^bIsotopes analyses were performed at UCR

¹Hop/Ster is the ratio of major C₂₇ - C₃₅ hopane isomers/ C₂₇ - C₃₀ diasteranes and regular steranes; as previously reported in Pehr et al. (2018).

Table 3.2. Mean carbon isotope compositions for individual extractable hopanes and hopenes measured by pico-CSIA (ratios measured in per mil versus VPDB), C₂₉He = 29-norneohop-13(18)-ene, C₃₀He = neohop-13(18)-ene, stdev = standard deviation, n = number of analyses.

Drill Core	Depth (m)	C ₂₇ Tm		C ₂₇ β		C ₂₉ He		C ₂₉ αβ		C ₂₉ βα						
		δ ¹³ C (‰) stdev	n	δ ¹³ C (‰) stdev	n	δ ¹³ C (‰) stdev	n	δ ¹³ C (‰) stdev	n	δ ¹³ C (‰) stdev	n					
Utkina Zavod	64.15	-22.73	0.19	2	-23.45	0.23	2	n.d.			-23.72	1				
Utkina Zavod	71.67	-24.16	0.42	3	-24.11	0.19	3	-25.38	1							
Utkina Zavod	87	-23.54	0.35	2	-22.76	0.03	2	-25.60	0.11	3						
Utkina Zavod	111.6	-23.03	0.48	2	-22.95	0.13	2									
Utkina Zavod	124.6	-23.44	0.27	3	-23.37	0.31	3	-24.59	0.28	2	-23.94	1	-23.59	0.14	3	
Utkina Zavod	153.5											-24.91	0.01	2		
Lugovoe #13	41	-28.78	0.47	2	-28.22	0.05	2					-28.51	0.56	2		
Lugovoe #13	47	-32.87	0.16	2	-32.20	0.19	2	-33.94	0.54	4	-32.61	0.43	3	-32.38	0.20	3
Lugovoe #13	71	-33.52	0.26	2	-32.99	0.15	2				-34.28	0.33	2	-34.12	0.37	2
Lugovoe #13	73	-32.75	0.63	2	-32.26	0.38	3				-33.8	0.33	2	-33.81	0.53	2
Gavrilov Yam -1	1860	-33.23	0.20	3	-32.32	0.21	3	-31.57	0.24	2	-34.02	0.65	2	-34.44		1
3628	226.5	-25.76	0.11	2	-23.97	0.18	2	-27.88	0.16	2	-26.34	0.07	2	-26.37	0.23	2
4592	~166	-30.19	0.30	2	-29.4	0.21	2				-30.78	0.65	2	-30.41	0.35	2

Drill Core	Depth (m)	C ₃₀ αβ		C ₃₀ He		C ₃₀ βα		C ₃₁ αβS		C ₃₁ αβR						
		δ ¹³ C (‰) stdev	n	δ ¹³ C (‰) stdev	n	δ ¹³ C (‰) stdev	n	δ ¹³ C (‰) stdev	n	δ ¹³ C (‰) stdev	n					
Utkina Zavod	64.15	-24.52	0.06	2	-23.50		1	-23.85	0.11	2	-24.64	0.07	2			
Utkina Zavod	71.67	-27.90	0.97	3	-28.25		1				-25.16	0.08	3			
Utkina Zavod	87	-24.11	0.18	3							-24.11	0.18	3			
Utkina Zavod	111.6	-24.79	0.27	2							-24.64	0.26	2			
Utkina Zavod	124.6	-24.74	0.05	2							-25.11	0.10	2			
Utkina Zavod	153.5	-26.87	0.41	3							-26.75	0.8	3			
Lugovoe #13	41	-29.05	0.35	2				-28.28	0.41	2	-30.14	0.83	2			
Lugovoe #13	47	-32.60	0.06	3				-32.35	0.32	4	-32.90	0.09	3			
Lugovoe #13	71	-34.29	0.29	3				-33.81	0.26	3	-35.34	0.24	2	-35.28	0.03	3
Lugovoe #13	73	-33.86	0.11	2				-33.65	0.33	2	-34.87	0.53	2	-34.64	0.19	3
Gavrilov Yam -1	1860	-32.98	0.01	2				-33.29	0.03	2			-33.68	0.27	2	
3628	226.5	-27.69	0.35	2				-26.79		1	-28.32		1	-27.74		1
4592	~166	-30.56	0.24	2				-30.55	0.36	2	-32.29		1	-31.37	0.27	2

Drill Core	Depth (m)	C ₃₁ β _a			C ₃₁ β _β			C ₃₂ αβ _R		
		δ ¹³ C (‰)	stdev	n	δ ¹³ C (‰)	stdev	n	δ ¹³ C (‰)	stdev	n
Utkina Zavod	64.15	-24.19	0.12	3	-23.47	0.13	2			
Utkina Zavod	71.67	-24.71	0.39	3	-23.77	0.38	3			
Utkina Zavod	87									
Utkina Zavod	111.6	-23.99		1						
Utkina Zavod	124.6	-24.41	0.20	3	-24.52		1			
Utkina Zavod	153.5									
Lugovoe #13	41	-28.82	0.05	2						
Lugovoe #13	47	-32.32	0.52	3						
Lugovoe #13	71	-34.78	0.11	3				-35.17	0.61	2
Lugovoe #13	73	-34.44	0.47	3				-34.66	0.04	2
Gavrilov Yam -1	1860	-34.62	0.35	2						
3628	226.5	-25.47	0.06	2						
4592	~166	-31.29	0.30	2						

Table 3.3. Mean carbon isotope ratios ($\delta^{13}\text{C}$) for individual extractable *n*-alkanes measured by pico-CSIA (ratios measured in per mil versus VPDB), stdev = standard deviation, n = number of analyses per sample.

Drill Core	Depth (m)	nC17		nC18		nC19		nC20		nC21					
		$\delta^{13}\text{C}$ (‰) stdev	n	$\delta^{13}\text{C}$ (‰) stdev	n	$\delta^{13}\text{C}$ (‰) stdev	n	$\delta^{13}\text{C}$ (‰) stdev	n	$\delta^{13}\text{C}$ (‰) stdev	n				
Utkina Zavod	64.15			-26.81	0.13	2	-26.49	0.11	2	-25.73	0.19	3	-25.6	0.12	2
Utkina Zavod	71.67			-28.39	0.69	3	-27.79	0.27	2	-27.3	0.03	2	-27.22	0.63	2
Utkina Zavod	87									-30.34	0.33	2	-29.42	0.18	2
Utkina Zavod	111.6									-25.54	0.58	2	-27	0.09	2
Utkina Zavod	124.6			-26.99	0.01	2	-26.03	0.41	2	-26.64	0.09	2	-26.66	0.15	3
Utkina Zavod	153.5														
Lugovoe #13	41						-30.23	0.41	2	-29.83	0.28	2	-29.84	0.2	2
Lugovoe #13	47			-33.07	0.14	3	-33.59	0.22	4	-33.68	0.21	4	-33.56	0.11	3
Lugovoe #13	71	-33.71	1	-33.15		1	-33.48	0.14	3	-34.10	0.24	3	-33.85	0.24	2
Lugovoe #13	73									-33.01	0.28	2	-32.68	0.67	2
Gavrilov Yam -1	1860			-30.4	0.27	2	-29.84	0.2	2	-30.13	0.16	2	-30.64	0.2	2
3628	226.5			-29.55	0.06	2	-28.9	0.05	2	-28.83	0.23	2	-28.76	0.05	2
4592	~166						-33.41	0.17	2	-32.31	0.13	3	-32.00	0.15	2

Drill Core	Depth (m)	nC22		nC23		nC24		nC25		nC26						
		$\delta^{13}\text{C}$ (‰) stdev	n	$\delta^{13}\text{C}$ (‰) stdev	n	$\delta^{13}\text{C}$ (‰) stdev	n	$\delta^{13}\text{C}$ (‰) stdev	n	$\delta^{13}\text{C}$ (‰) stdev	n					
Utkina Zavod	64.15	-26.13	0.28	2	-26.32	0.13	3	-26.79	0.05	2	-28.19	0.14	2	-23.63	0.21	2
Utkina Zavod	71.67	-27.79	0.03	2	-27.73	0.39	2	-27.6	0.14	2	-27.74	0.45	2	-25.22	0.31	2
Utkina Zavod	87	-30.78	0.55	2	-30.75	0.51	2	-31.79	0.18	2	-32.61	0.3	2	-29.25	0.27	2
Utkina Zavod	111.6	-28.06	0.66	2	-28.77	0.24	2	-26.54	0.17	2	-29.01	0.17	2	-23.36	0.16	2
Utkina Zavod	124.6	-27.07	0.1	2	-28.38	0.11	2	-28.36	0.17	2	-29.35	0.19	2	-26.27	0.4	2
Utkina Zavod	153.5															
Lugovoe #13	41	-30.24	0.11	2	-30.36	0.15	2	-31.08	0.01	2	-30.71	0.05	2	-30.65	0	2
Lugovoe #13	47	-33.36	0.11	3	-33.36	0.1	3	-33.01	0.04	3	-33.24	0.08	3	-33.12	0.2	4
Lugovoe #13	71	-33.21	0.43	2	-34.19	0.14	3	-32.07	0.73	2	-32.93	0.14	3	-31.92	0.40	3
Lugovoe #13	73	-32.6	0.16	2	-32.86	0.12	2	-30.56	0.01	2	-32.49	0.27	3	-31.07	0.11	3
Gavrilov Yam -1	1860	-31.19	0.19	2	-32.13	0.21	2	-32.74	0.21	2	-33.55	0.06	2	-33.08	0.14	2
3628	226.5	-28.85	0.12	2	-29.09	0.22	2	-29.1	0.03	2	-29.44	0.24	2	-27.76	0.11	2
4592	~166	-31.51	0.00	2	-31.58	0.17	3	-31.20	0.60	2	-30.91	0.27	2	-30.24	0.41	2

Drill Core	Depth (m)	nC27			nC28			nC29		
		$\delta^{13}\text{C}$ (‰)	stdev	n	$\delta^{13}\text{C}$ (‰)	stdev	n	$\delta^{13}\text{C}$ (‰)	stdev	n
Utkina Zavod	64.15	-24.64	0	2	-21.93	0.27	2			
Utkina Zavod	71.67	-26.94	0.61	2	-24.15	0.4	2			
Utkina Zavod	87	-29.35	0.31	2	-23.84	0.26	2	-23.75	0.11	2
Utkina Zavod	111.6	-24.9	0.12	2	-22.27	0.47	2			
Utkina Zavod	124.6	-26.65	0.03	2	-22.64	0.46	2	-23.95	0.33	3
Utkina Zavod	153.5									
Lugovoe #13	41	-29.97	0.43	2	-29.52	0.09	2	-29.1	0.36	2
Lugovoe #13	47	-32.99	0.1	3	-32.79	0.19	4			
Lugovoe #13	71	-32.56	0.25	3	-33.22	0.36	2			
Lugovoe #13	73	-31.51	0.31	3	-31.37	0.27	3			
Gavrilov Yam -1	1860	-31.73	0.21	2	-30.83	0.07	2	-31.48	0.09	2
3628	226.5	-27.35	0.01	2	-25.3	0.47	2	-27.33	0.12	2
4592	~166	-29.75	0.07	2	-29.92	0.38	2			

Table 3.4. Mean carbon isotope compositions for extracted pristane (Pr), phytane (Ph), and C₂₉ *aaaR* sterane, measured by pico-CSIA (ratios measured in per mil versus VPDB) and carbon isotope difference between *n*-alkanes and acyclic isoprenoids from the same samples, including pristane (Pr), phytane (Ph), *n*C₁₇ and *n*C₁₈; stdev = standard deviation, n = number of repeat CSIA analyses per sample.

Drill Core	Depth (m)	Pr			Ph			C ₂₉ Ster <i>aaaR</i>			$\delta^{13}\text{C}_{n\text{C}17\text{-Pr}}$	$\delta^{13}\text{C}_{n\text{C}18\text{-Ph}}$
		$\delta^{13}\text{C}$ (‰)	stdev	n	$\delta^{13}\text{C}$ (‰)	stdev	n	$\delta^{13}\text{C}$ (‰)	stdev	n	(‰)	(‰)
Utkina Zavod	64.15				-25.14	0.13	2	-24.48		1		-1.67
Utkina Zavod	71.67				-27.7	0.31	3	-25.86	1.36	2		-0.69
Utkina Zavod	87											
Utkina Zavod	111.6							-23.22	0.26	2		
Utkina Zavod	124.6				-24.1	0.08	3	-23.51	0.16	2		-2.89
Utkina Zavod	153.5							-24.22	0.24	2		
Lugovoe #13	41											
Lugovoe #13	47				-33.71	0.18	2	-33.29	0.17	3		0.64
Lugovoe #13	71	-38.63		1	-37.67		1				4.92	4.52
Lugovoe #13	73											
Gavrilov Yam -1	1860				-29.84	0.29	2					-0.56
3628	226.5				-29.55	0.16	2					0.00
4592	~166											

CHAPTER 4

U–Pb geochronology of detrital zircon from the Ediacaran and Cambrian sedimentary successions of NE Estonia and Volyn region of Ukraine: implications for the provenance and comparison with other areas within Baltica

Ion Francovschi^{a,b}, Leonid Shumlyanskyy^{c,d}, Alvar Soesoo^e, Iryna Tarasko^f, Viktor Melnychuk^g, Adam Hoffmann^h, Alex Kovalick^h, Gordon Love^h, Andrey Bekker^{h,i}

^a University of Bucharest, Faculty of Geology and Geophysics, Bucharest, Romania

^b Institute of Geology and Seismology, Chişinău, Republic of Moldova

^c Institute of Geological Sciences, Polish Academy of Sciences (ING PAN), Research Centre in Kraków, Senacka 1, PL–31002 Kraków, Poland

^d School of Earth and Planetary Sciences, Curtin University, Australia

^e Institute of Geology, Tallinn University of Technology, Tallinn, Estonia

^f Rivne Complex Geological Enterprise of the State Ukrainian Geological Survey, Rivne, Ukraine

^g National University of Water and Environmental Engineering, Rivne, Ukraine

^h Department of Earth & Planetary Sciences, University of California, Riverside, CA 92521, USA

ⁱ Department of Geology, University of Johannesburg, Auckland Park 2006, South Africa

Abstract

Trends in detrital zircon age distribution patterns are used to constrain the paleotectonic and paleogeographic conditions during deposition of the late Ediacaran - Early Cambrian sedimentary successions in central, western, and southwestern Baltica. Detrital zircons from three sandstone samples collected from a drill-core drilled in northeastern Estonia and four sandstone samples collected from three drill-cores located in the Volyn Region of Ukraine were dated using the U-Pb LA-ICP-MS isotope technique. The obtained data are compared with the published data for southwestern Ukraine and Moldova, eastern Poland, Belarus, and northwestern Russia to constrain the late Ediacaran - Early Cambrian evolution of the sedimentary basins developed on Baltica. All sedimentary basins from these areas of Baltica show a transition during that time from passive continental margin to collisional settings, which has been triggered by the pre-Schythides and Santacrusades orogenies along the south-southwest and, to a lesser extent, by the Timanian Orogeny along the north-northeast margins of Baltica.

1. INTRODUCTION

Late Ediacaran - Early Cambrian intracratonic sedimentary basins extensively developed in Baltica and extended to the margins of the craton (e.g., Sliupa et al., 2006; Bush, 2014; Kheraskova et al., 2015). The development of these basins has been linked to the rifting and break-up of Rodinia, with passive continental margins formed around the

craton, followed by the transition to active continental margins and foreland basins, when Baltica collided with other cratons and island arcs during the late Ediacaran to Early Cambrian Baikalian (=Cadomian=Pan-African) orogenic cycle (Schatsky, 1935; Roberts and Siedlecka, 2002; Sliupa et al., 2006). In general, it is considered that there were at least three significant, geographically distant orogenic events during that period in Baltica: the Timanian along the northeastern margin (e.g., Roberts and Siedlecka, 2002), the pre-Uralian along the eastern margin (e.g., Bekker, 1988; Puchkov, 2010), and pre-Schythides or Santacrusades along the southwestern and western margins, respectively (e.g., Kheraskova et al., 2015; Żelaźniewicz et al., 2009, 2020; Buła and Habryn, 2011) orogenies. Lateral movement of terranes along the northern (in the present orientation) margin of Baltica likely led to episodic extensional and compressional events during that time (e.g., Kirkland et al., 2011).

Understanding the evolution of Baltica sedimentary basins in the tectonic and paleogeographic framework during the Ediacaran - Cambrian transition is critical as these basins host a rich record of the Ediacaran fauna and exquisitely well-preserved organic biomarkers (e.g., Grazhdankin, 2014; Pehr et al., 2018). Further, the sedimentary record provides an effective means to track the tectonic history. Although cratons have evolved through geological time with accretion, collision, and rifting/breakup, their lost components can be constrained with the detrital zircon records preserved in ancient sedimentary basins. Zircon, a key mineral for U–Pb geochronology, is a common accessory mineral in siliciclastic sediments and faithfully retains its U–Pb isotope

systematics during weathering, erosion, deposition, and metamorphism (Fedó et al., 2003; Gehrels, 2014; Guo et al., 2017). Consequently, detrital zircon U–Pb geochronology can be used to determine the age of magmatic activity and metamorphism in the source region and to establish provenance and contribution of different sources to sediments within sedimentary basins. Additionally, zircon dating is also useful in tracking tectonic events and is widely used to constrain tectonic evolution (e.g., Gehrels, 2014; Guo et al., 2017; Barham et al., 2018).

During recent years, a number of datasets were published with detrital zircon U–Pb geochronological data for the Ediacaran to Cambrian siliciclastic rocks throughout Baltica (e.g., Valverde-Vaquero et al., 2000; Andersen et al., 2007; Kirkland et al., 2011; Miller et al., 2011; Kuznetsov et al., 2011, 2014a, 2014b; Orlov et al., 2011; Isozaki et al., 2014; Põldvere et al., 2014; Sláma and Pedersen, 2015; Ivleva et al., 2016; Lorentzen et al., 2018; Ershova et al., 2019; Paszkowski et al., 2019, 2021; Roban et al., 2020; Żelaźniewicz et al., 2020; Francovschi et al., 2021; Kuznetsov and Romanyuk, 2021).

These datasets have been successfully used to establish sediment sources, estimate maximum depositional ages for sedimentary successions, and define the timing of tectonic, magmatic, and metamorphic events. However, the craton-scale synthesis of these data with a coherent perspective so far has not been presented.

The objective of this study is to provide a better understanding of the paleotectonic and paleogeographic conditions that accompanied deposition of the late Ediacaran - Early

Cambrian sedimentary successions in the southern, southwestern, and central Baltica with an emphasis on their provenance. Furthermore, the aim is to develop a detailed model for the late Ediacaran - Early Cambrian evolution of the area corresponding to present-day Estonia and for the late Ediacaran evolution of the area corresponding to the present-day Volyn region of western Ukraine with a broader perspective, based on published data, on the southwestern and central parts of Baltica (southwestern Ukraine and Moldova, eastern Poland, Belarus, and northwestern Russia), by identifying differences and similarities in the provenance and clastic sediment routing.

2. GEOLOGICAL SETTING AND STRATIGRAPHIC DATA

2.1 Geology of Estonia

In terms of the structural framework, Estonia is situated in the central part of Baltica (Fig. 4.1) and consists of two major crustal components, the crystalline basement and the sedimentary cover. The Precambrian basement of Estonia is a southern continuation of the Fennoscandian Shield. Based on geophysical and petrological studies, Precambrian complexes of Estonia can be divided into two major geological terranes – the North Estonian amphibolite facies and South Estonian granulite facies belts (Puura et al., 1983; Soesoo et al., 2004, 2006, 2020, 2021), which are separated by a tectonic boundary, the Paldiski-Pskov shear zone (Bodganova et al., 2015). The metamorphic rocks are cut by the Subjotnian (late Paleoproterozoic to early Mesoproterozoic) rapakivi granites. Overlying the Estonian Precambrian basement is an ancient, dominantly kaolinitic

(together with montmorillonite and illite) weathering crust with thickness ranging from a few meters to several tens of meters (Liivamagi et al., 2014; 2015). Due to intense denudation during the Neoproterozoic, the basement has been leveled forming a peneplain, which gently dips on average 0.1–0.2° southward (SSE–SSW; 150–200°; Puura et al., 1983; Soesoo et al., 2020).

There are three main age groups for the Estonian Precambrian basement rocks. The oldest group, similar in age to the Fennoscandian basement of southern Finland and southern and eastern Sweden, yielded dates between 1918 Ma and 1802 Ma. The U-Pb zircon age of amphibolite-facies metavolcanic rocks from North Estonia is 1918 ± 10 Ma (Petersell and Levchenkov, 1994; Soesoo et al., 2004; Kirs et al., 2009).

Granulitic metavolcanic rocks of southern Estonia yielded ages of 1832 ± 22 and 1827 ± 7 Ma (Petersell and Levchenkov, 1994; Soesoo et al., 2004). Zircons from tonalites of the Tapa area were dated at 1824 ± 26 Ma (Soesoo et al., 2006). Magnetite-rich gneisses of the Jõhvi area (northeastern Estonia) show three groups of ages: a small population of zircons with 1874 ± 18 Ma age, the most abundant group with 1826 ± 10 Ma age, and the youngest population represents the second largest abundance age group clustered at 1789 ± 19 Ma (Soesoo et al., 2020). Tonalites from southern Estonia yielded similar age, 1788 ± 16 Ma, while charnockites from the Tapa area (north-central Estonia) have an age of 1761 ± 11 Ma (Soesoo et al., 2006). Monazites from the South Estonia orthopyroxene-garnet gneisses yielded an age of 1778 ± 2 Ma (Puura et al., 2004), which is similar to

that of the gabbro-norite dyke, which cuts granulites in this area, 1774 ± 20 Ma (Soesoo et al., 2006).

The third age group (1635 to 1576 Ma) comprises plutons of rapakivi granites and associated rocks. These include the mafic Abja pluton with an age of 1635 ± 7 Ma, and cross-cutting dykes dated at 1622 ± 7 Ma (Kirs and Petersell, 1994). The Virtsu granitoid pluton yielded an age of 1606 ± 17 Ma (Soesoo and Hade, 2012). The large Riga rapakivi pluton has a 1584 ± 7 Ma age for the felsic part, while associated gabbro yielded an age of 1576 ± 2 Ma (Rämö et al., 1996). The small, rapakivi-type Märjamaa granodiorite pluton intruded at 1629 ± 7 Ma (Rämö et al., 1996).

The boundary between the Neoproterozoic to Paleozoic sedimentary cover of Baltica and the Precambrian basement extends along the shoreline of the Gulf of Finland, Baltic Sea, in northern Estonia. The sedimentary sequence consists of the late Ediacaran to Early Ordovician siliciclastic units, Early Ordovician to Late Silurian carbonate units, and Devonian siliciclastic units (Mens and Pirrus, 1997a, b; Fig. 4.2A).

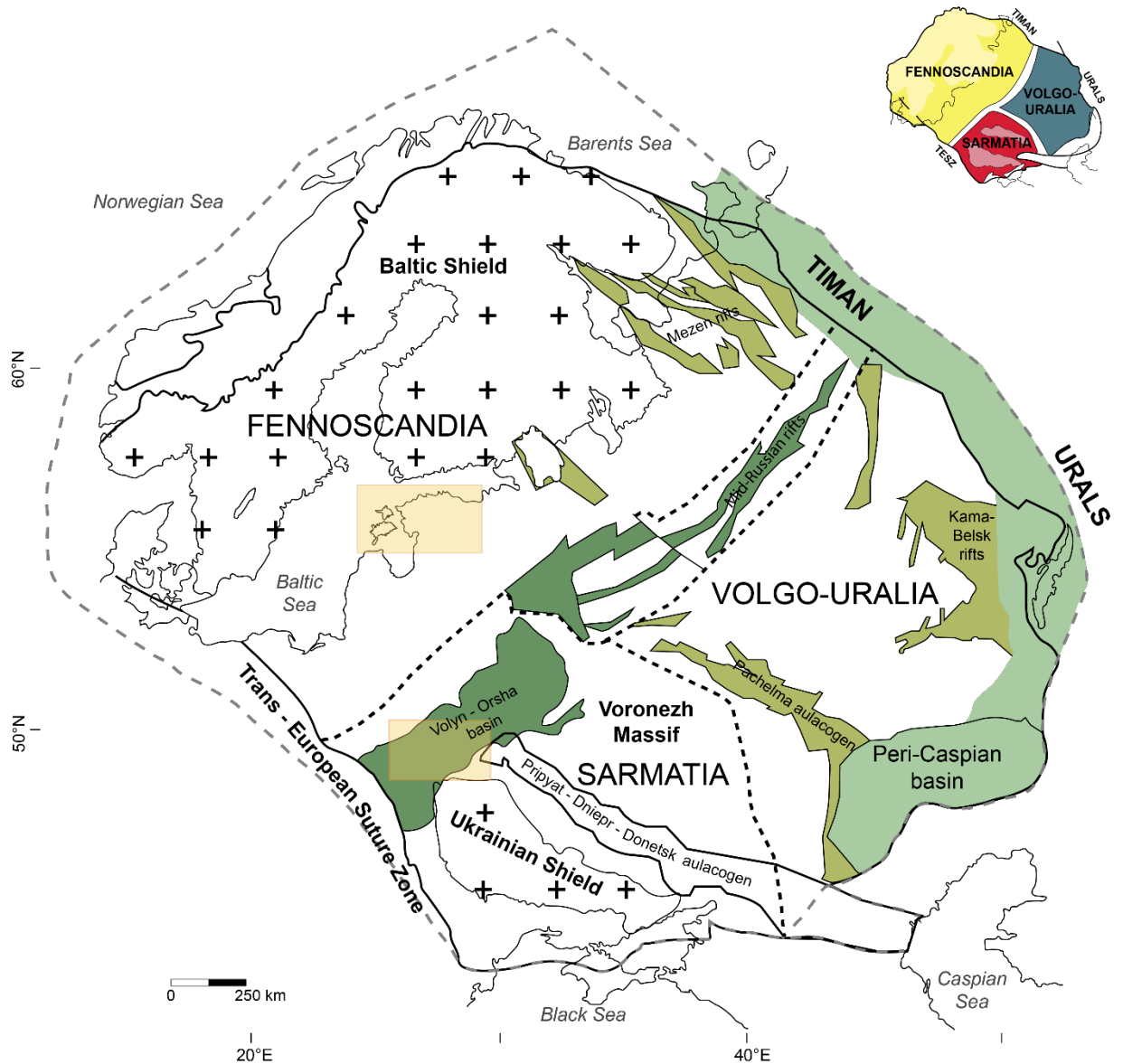


Figure 4.1. Schematic tectonic map of Baltica (modified after Bogdanova et al., 2016). The failed rifts/aulacogens, which were initiated before ca. 1.4 Ga, are marked with olive-green, while those younger than 1.0 Ga are colored dark-green. The passive margin shown in light-green was developed along the eastern margin of the craton at ca. 0.9–0.7 Ga. Yellow boxes highlight the study areas.

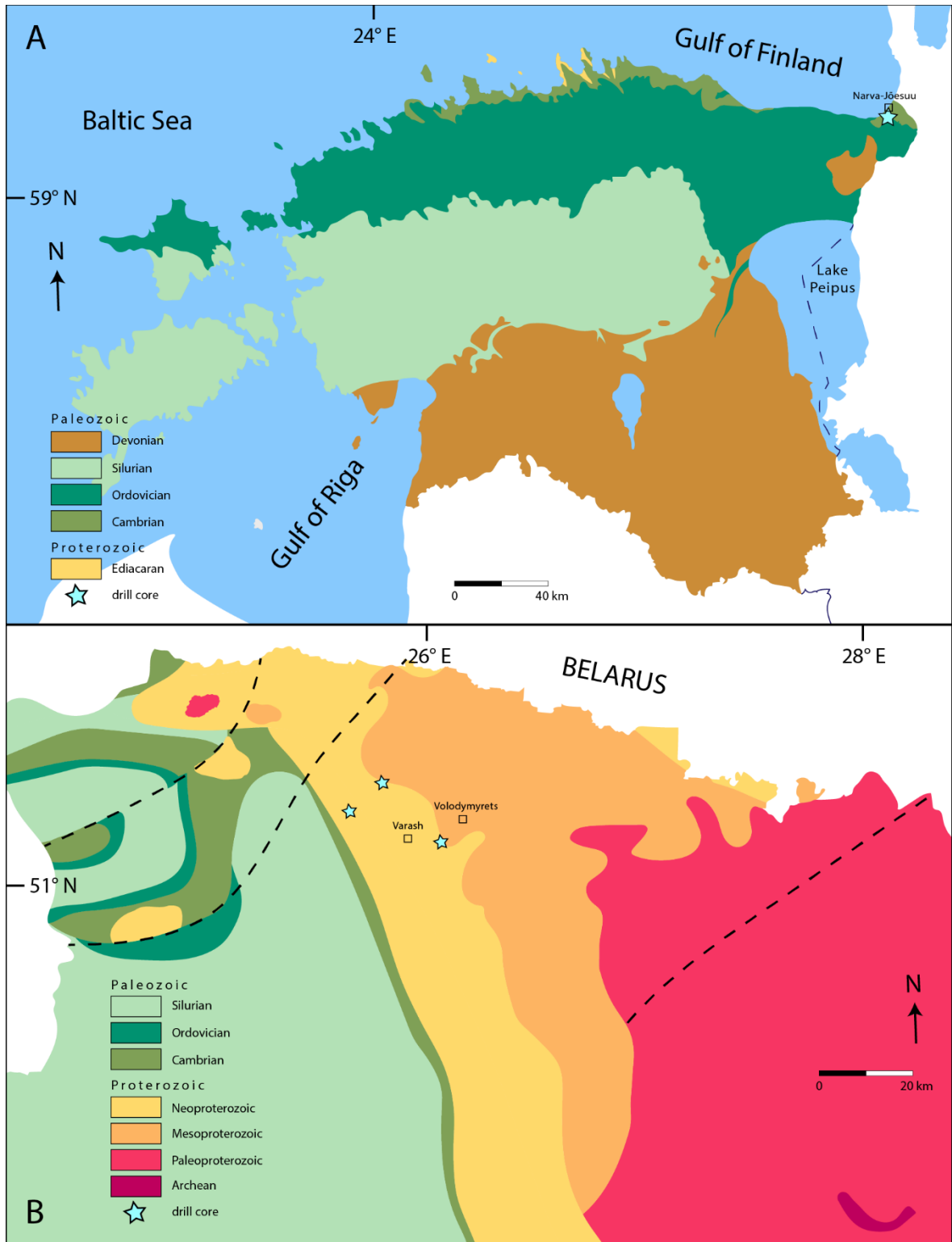
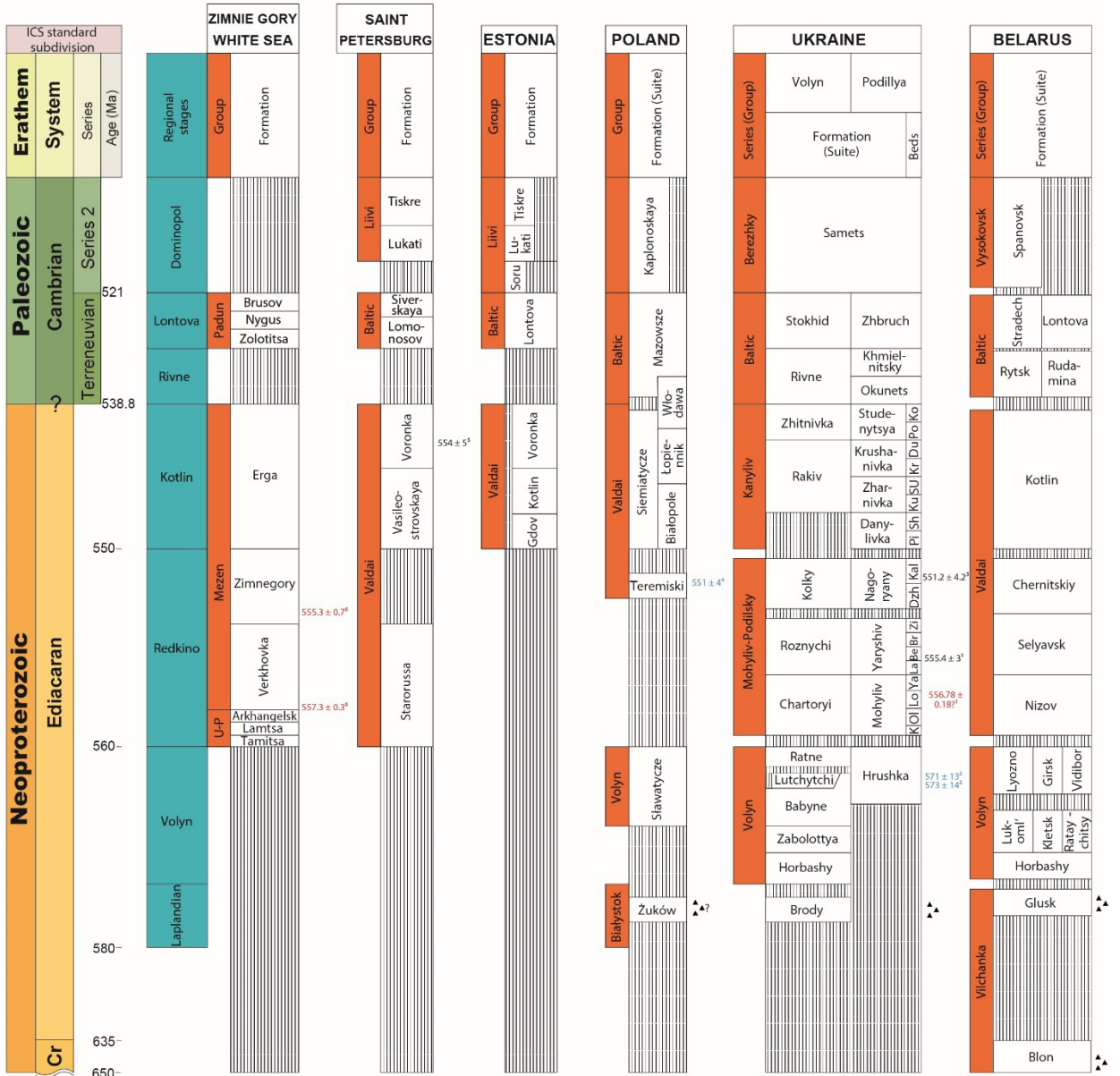


Figure 4.2. (A) Generalized geological map showing distribution of the Ediacaran - Lower Paleozoic sedimentary cover in Estonia as well as the position of the studied drill-core (modified after Puura and Vaher, 1997); (B) Generalized geological map with the Devonian and younger units removed showing distribution of the Ediacaran - Lower Paleozoic sedimentary cover of Volyn Region (western Ukraine) as well as the position of the studied drill-cores (modified after Hozhyk et al., 2013).

Due to the position on the structural high bounded with the sedimentary basins to the southeast (the Moscow basin) and to the west (the Baltic basin), and between the Fennoscandian Shield to the north and the Latvian Uplift to the south, Estonia had a transitional to nearshore, marine style of deposition during the Neoproterozoic to Paleozoic.

The oldest sedimentary rocks in Estonia, the Valdai Group (Fig. 4.3), are of late Ediacaran age and belong to the Kotlin Regional Stage (Mens and Pirrus, 1997a). Ediacaran sediments (previously called the Vendian Complex of the Vendian System) are located in northern, northeastern, and eastern Estonia (Meidla, 2017). The sediments were deposited on the weathering crust developed on the crystalline basement. The lowermost part of the Ediacaran sedimentary succession was largely derived from the weathering crust and redeposited in a nearshore environment. The maximum thickness of the Ediacaran Valdai Group is about 123 m in the extreme northeastern part of its distribution area in Estonia (Mens and Pirrus, 1997a). The strata have been described only from drill-cores as no natural outcrops exist in Estonia. The closest Ediacaran outcrops are in the westernmost Leningrad Region and on Kotlin Island, Russia. The Ediacaran sediments were deposited when the Baltica craton was at intermediate latitudes in the southern hemisphere (Cocks and Torsvik 2005; Merdith et al., 2017). There are no carbonate sediments in the Ediacaran succession of Estonia and neighboring areas.



Ko - Komariv
 Po - Polyvaniv
 Du - Dumnyakivka
 Kr - Kryvchany
 Ku - Kuleshivka
 SU - Stara Ushytsya
 Sh - Shebutyntsi
 Pi - Pylypy
 Kal - Kalyus
 Dzh - Dzhurzhyvka
 Zi - Zinkiv
 Br - Bronnytsya
 Be - Bernashivka
 La - Lyadova
 Ya - Yampil
 Lo - Lomoziv
 Ol - Olchedaiv
 K - Khrustovaya
 Cr - Cryogenian
 ▲▲ - glacially influenced units
 U-P - Ust'-Penega Group

Figure 4.3. Ediacaran – Lower Cambrian stratigraphic columns for the central, western, and southwestern parts of Baltica (modified from Areń, 1968; Makhnach et al., 2001, 2005; Paczeńna, 2014; Ivantsov et al., 2015; Meidla, 2017; Ershova et al., 2019). Ages in red represent TIMS analyses of volcanic zircons, ages in blue represent SHRIMP dates of volcanic zircons, and ages in black represent LA-ICP-MS analyses of detrital zircons, constraining the MDA (data from ¹ - Soldatenko et al., 2019; ² - Shumlyanskyy et al., 2016b; ³ - Francovschi et al., 2021; ⁴ - Compston et al., 1995; ⁵ - Ershova et al., 2019; ⁶ - Yang et al., 2021). Vertical lines correspond to hiatus in deposition. Note that the older Neoproterozoic glacial deposits in Belarus (Blon Formation) are considered to be time equivalent to the Cryogenian Marinoan glaciation (cf. Chumakov, 2015). A recent study, based on microfossils, suggested that the upper part of the Vasileostrovskaya Formation belongs to the Early Cambrian Lontova Regional Stage (Kushim et al., 2016).

On the basis of a very sparse record of acritarchs and algae *Vendotaenia antiqua Gnil.* and *Aataenia reticularis Gnil.* (Gnilovskaya et al., 1979; Gnilovskaya, 1988), the Ediacaran succession in Estonia is considered to belong to the Kotlin Regional Stage (Mens and Pirrus, 1997a). No radiometric dates are available for the Ediacaran in Estonia. However, its age can be tentatively constrained based on the available data for correlative units in Baltica. Sokolov (2011) estimated the age of the lower boundary of the Kotlin Regional Stage to be 580–570 Ma, while Grazhdankin et al. (2011) suggested, based on the correlation with the Ediacaran sedimentary successions of the Lublin slope of Baltica, an age of less than ca. 551 ± 4 Ma (Compston et al., 1995) for this boundary. The Kotlin Formation of the Valdai Group is now thought to have been deposited during the terminal ~10 myr of the Ediacaran Period, based on correlations with strata of the Lublin slope (Poland), Moldova, Podillya of Ukraine, and Urals and White Sea area of Russia, where U-Pb zircon dates for volcanic tuff horizons have yielded < ca. 551 Ma ages for the lower boundary (Moczydlowska, 1991; Compston et al., 1995; Grazhdankin et al., 2011; Meidla, 2017; Soldatenko et al., 2019; Francovschi et al., 2021). However, Early Cambrian age has recently been suggested for the Kotlin Regional Stage based on detrital zircon dates for sandstones from the Kanyliv Series in the Podillya basin in Ukraine (Paszkowski et al., 2021). The Early Cambrian detrital zircon age data were produced with the LA-ICP-MS method and should be further verified with the CA-ID-TIMS method to check for potential Pb loss responsible for younger dates (see further discussion in the Discussion section). We therefore follow the conventional late Ediacaran age for the Kotlin Regional Horizon in this study. Considering these age

estimates, the Estonian Ediacaran succession represents a relatively short (7-10 myr), late age interval of the late Ediacaran.

The Kotlin Regional Stage deposits are widespread in the northeastern subsurface of mainland Estonia (Meidla, 2017). The horizon is represented by siliciclastic rocks, accumulated under brackish, warm, and humid conditions (Pirrus, 1992). It includes in ascending order the Gdov, Kotlin, and Voronka formations (Fig. 4.3). The lowermost unit of the Kotlin Regional Horizon (Gdov Formation including the Oru, Moldova, and Uusküla members) consists of immature and poorly sorted arkosic sandstones. In Estonia, the Gdov Formation rests immediately upon the Paleoproterozoic crystalline basement and ranges in thickness from 0.2 to 58.3 m. It is overlain by the Kotlin Formation (including the Jaama, Meriküla, and Laagna members), a succession of laminated, greenish-gray mudstones intercalated with light-colored, fine-grained sandstones and siltstones with high contents of quartz and potassium feldspar. The lower boundary of the formation is placed at the level where the variegated deposits change color to gray. At the base of the formation, conglomerates and coarse-grained sandstones locally occur. The unit is locally rich in dark-brown films of organic matter; mica content (biotite and muscovite) is also generally high. The deposits often contain diagenetic siderite and lack pyrite and glauconite (Mens and Pirrus, 1971; Pirrus, 1992), suggesting brackish conditions in the basin. The clay fraction consists of illite (dominant clay mineral), kaolinite (15 to 40% of clay minerals), and, to a lesser degree, mixed layer illite-smectite and chlorite. Additionally, it is depleted in boron (Pirrus, 1992; Mens and Pirrus, 1997a),

consistent again with brackish conditions in the basin. Chlorite content is high in the middle part of the formation with its average content reaching 15–20% (Pirrus, 1992).

The Kotlin Formation ends with the reappearance of highly mature, variegated sediments of the Voronka Formation (including the Sirgala and Kaanuka members), which is 10 to 40 m thick, increasing in thickness to the north, and sits on the paleosols developed on the Kotlin Formation (Mens and Pirrus, 1997a). The Voronka Formation consists of siliciclastic rocks arranged into an upward-coarsening cycle from argillites to well-sorted sandstones. The lower boundary of the formation is drawn on the basis of color change to variegated sediments.

The Cambrian deposits, up to about 150 m thick in the western part of Estonia, are the oldest sediments that crop out in Estonia. These rocks, mostly sandstones, are exposed along the North Estonian Klint (escarpment of cuesta facing Baltic Sea), while mudstones crop out in abandoned and active clay quarries at the northern coast. The Cambrian lies unconformably over the Ediacaran with the Rivne Regional Horizon missing (Mens and Pirrus, 1997b; Meidla, 2017). The Cambrian succession begins with the “Blue Clay” (Lontova Formation of the Lontova Regional Stage), an extensive unit of silty, illitic, greenish-gray and variegated mudstones in eastern and central Estonia, laterally grading into a unit of interbedded mudstones and coarse- to fine-grained sandstones on the western islands of Estonia. Mudstone also grades upwards into siltstones and coarse- to fine-grained sandstones which are the dominant Cambrian rocks of Estonia (Meidla,

2017). The sandstones are poorly fossiliferous (contain trace fossils, *Sabellidites cambriensis* Jan. and *Platysolenites antiquissimus* Eichw.), but based on the correlation with the sedimentary succession in Latvia, which is characterized better paleontologically, the presence of both the Series 3 and the Furongian Series has been established in Estonia (Mens and Pirrus 1997b; Meidla, 2017). The formation is subdivided into the Sämi, Mahu, Kestla, and Tammneeme members (Mens and Pirrus, 1997b). The Lontova Formation thickness varies over a wide range, reaching up to about 90 m in northeastern Estonia.

The Sämi Member contains the pre-trilobite acritarch assemblage of *Asteridium tornatum* - *Comasphaeridium velvetum* that likely indicates the early to middle intervals of the Cambrian Stage 2 (ca. 529 - 526 Ma; Mens et al., 1993; Bagnoli and Stouge, 2014). The Sämi Member also contains trace fossils typical of the Early Cambrian, as well as the earliest agglutinated foraminifera, *Platysolenites antiquissimus* (cf. McIlroy et al., 2001).

In the studied drill-core F-169 all members of the Lontova Formation with the exception of the Tammneeme Member are present (Fig. 4.4).

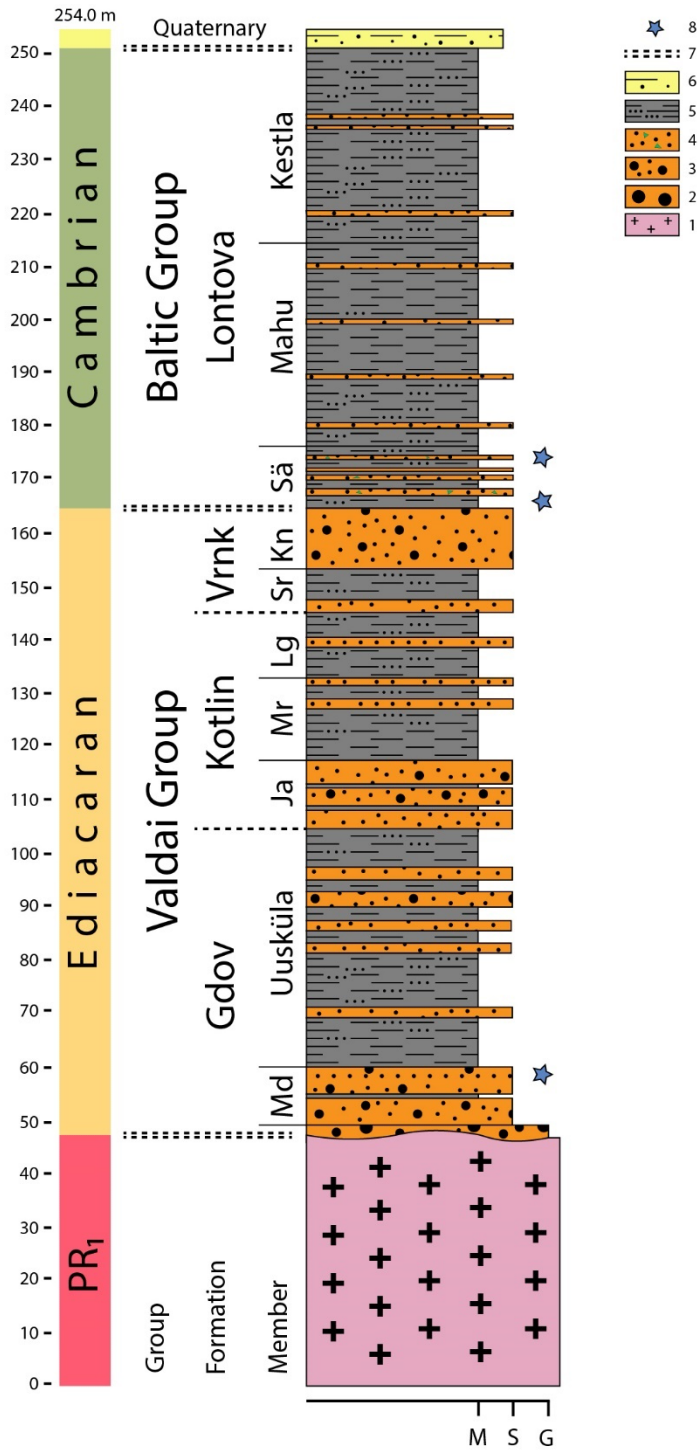


Figure 4.4. Ediacaran - Cambrian lithostratigraphic column of the F-169 drill-core in Estonia, showing the stratigraphic position of the analyzed sandstones from the Moldova and Sämi members within the sedimentary succession. 1 – crystalline basement; 2 – coarse-grained sandstones and conglomerates; 3 – fine- to coarse-grained sandstones; 4 – fine-grained sandstones with glauconite grains; 5 – mudstones; 6 – alluvial deposits; 7 – unconformity; 8 – position of the analyzed samples; MD - Moldova Member; Ja - Jaama Member; Mr - Meriküla Member; Lg - Laagna Member; Vrnk - Voronka Formation; Sr - Sirgala Member; Kn - Kaanuka Member; Sä - Sämi Member.

2.2 Geology of the Volyn Region

The Volyn Region in the northwestern part of Ukraine borders Belarus to the north, Poland to the west, and other parts of Ukraine, such as Podillya and Halychyna (Galicia), to the south. The eastern part of the Volyn Region is on the northwestern Ukrainian Shield, while the western part is on the northwestern slope of the Ukrainian Shield, which hosts the Mesoproterozoic Volyn-Orsha aulacogen and the Late Paleozoic Prypyat horst.

The basement in the Volyn Region broadly belongs to the junction zone between Sarmatia and Fennoscandia that are two main building blocks of Baltica. The basement comprises several SW-NE striking belts, extending parallel to the inferred suture between Sarmatia and Fennoscandia. The basement of the northwestern part of the Ukrainian Shield belongs to two main tectonic structures: the Teteriv Orogenic Belt and Osnitsk-Mikashevychi Igneous Belt. The Teteriv Orogenic Belt includes amphibolite-facies metamorphic rocks of the Teteriv Series and granitoids of the Zhytomyr and Sheremetiv complexes (Yesypchuk et al., 2004). The supracrustal rocks of the Teteriv Series were deposited between ca. 2150 and 2100 Ma (Shumlyanskyy et al., 2015b), whereas granitoids were emplaced between ca. 2150 and 2040 Ma (Shumlyanskyy et al., 2018; Vysotsky et al., 2021). The Osnitsk-Mikashevychi Igneous Belt developed between ca. 2030 and 1980 Ma on the predominantly juvenile basement of the Teteriv orogenic belt in an active continental margin setting (Claesson et al., 2001; Shumlyanskyy, 2014;

Bogdanova et al., 2016). Both belts developed due to subduction of the oceanic crust between Fennoscandia and Sarmatia under Sarmatia and their ultimate collision.

Further to the west, the Volyn Region basement is buried under the Stenian-Tonian, Ediacaran, and Phanerozoic supracrustal units. The thickness of the sedimentary cover gradually increases westward towards the margin of Baltica. To the northwest, the Osnitsk-Mikashevychi Igneous Belt is in contact with the tectonic unit extending along the suture between Sarmatia and Fennoscandia, the Central Belarusian Suture Zone. In the Volyn Region, this zone is composed of Paleoproterozoic (ca. 1880-1950 Ma) gneisses, amphibolites, gabbros, and granitoids (Melnychuk, 2013; Shumlyanskyy et al., 2021b).

The oldest sequence of the sedimentary cover is represented by the Stenian-Tonian (Riphean) sediments that fill the Volyn-Orsha aulacogen. In Ukraine, these sediments belong to the Polissya Series, which is a >800 m thick continental red-bed siltstone-sandstone succession (Vlasov et al., 1972), deposited in an epicontinental sea setting (Gojzhevsky et al., 1984). The maximum age of deposition as defined by detrital zircons is ca. 1050-950 Ma (Shumlyanskyy et al., 2015a; Paszkowski et al., 2019).

The erosional upper boundary of the Polissya Series is unconformably overlain by terrigenous sediments of the Ediacaran Brody Formation. In the northern part of the Volyn Region, the Brody Formation is composed of micaceous siltstones and mudstones

with rare pebble- and sand-sized detritus. Sandstones also locally occur. In the southern part of the Volyn Region, the Brody Formation is represented by red-colored sandstones and siltstones with fragments of the crystalline basement and conglomerates that were interpreted as tillites (Kotyk et al., 1976; Hozhyk et al., 2013). The thickness of the formation increases from the north (20-30 m) to the south (over 60 m). The Brody Formation has been correlated with the glacial deposits of the Vilchanka Series in Belarus (Veretennikov et al., 1972; Kotyk et al., 1976; Makhnach et al., 2001).

The Volyn Series is more widely developed. In the Volyn Region, it is represented by a thick (up to 500 m), predominantly volcanogenic sequence (Shumlyansky et al., 2007; Kuzmenkova et al., 2010). The age of the upper part of the Volyn Series has been defined as 573 ± 14 Ma based on U-Pb analyses of magmatic zircons (Shumlyansky et al., 2016b). In Ukraine, the Volyn Series comprises, from the bottom to the top, the Horbashi, Zabolotyya, Babyne, Luchychi, and Ratne formations. All of these formations contain mafic volcanic rocks with variable thicknesses and different lithologies (Shumlyansky et al., 2012).

The Horbashi Formation is widely distributed and is composed of variable grain-size, poorly sorted arkosic sandstones and conglomerates with layers of siltstones. Siltstones contain pebbles and poorly rounded clasts of quartz, quartzites, and granites. Tuffaceous sandstones and picrites that represent initial stages in the development of the Volyn flood basalt province also occur locally (Shumlyansky et al., 2018). The thickness of the

Horbashi Formation varies from 0.4 to 65.6 m. Sandstones contain *Leiosphaeridia crassa* (Naumova) Jankauskas and *L. obsuleta* (Naumova) Jankauskas microfossils (Ivanchenko et al., 2004).

The Zabolotta Formation comprises five to seven flows of olivine-bearing basalts that are interlayered with tuffs. The total thickness of the formation is up to 230 m. The 80 to 230 m thick Babyne Formation is widely distributed and is composed of layered, coarse-grained basaltic tuffs. In the middle part, it hosts one to two basaltic flows. The Luchychi Formation is also widely distributed and is composed of up to five basalt flows interlayered with volcanic breccia and conglomerates. The upper boundary of the formation is erosional, resulting in a highly variable unit thickness from 0 to 117 m. The Ratne Formation represents the uppermost unit of the Volyn Series and correlates with the Hrushka Formation of the Podillya Region. It includes the lower Zoryane beds and the upper Yakushiv beds. The Zoryane beds include sedimentary and tuffaceous rocks such as red-colored siltstones, mudstones (bentonites), brown-green sandstones, and variegated conglomerates. The latter contains pebbles of trachyte, granite, and felsic volcanic rocks. The thickness of the Zoryane beds varies from 0.6 to 63 m. Fragments of Ediacaran filamentous algae *Leiosphaeridia sp.* and *Spumosina rubiginosa* (Andreeva) Jankauskas et Medvedeva occur in siltstones and sandstones (Ivanchenko et al., 2004). The Yakushiv beds are composed of up to seven flows of high-Ti basalts, locally interlayered with basaltic tuffs. The thickness of the beds reaches 135 m (Hozhyk et al., 2013).

The Volyn Series is overlain by the Mohyliv-Podilsky and Kanyliv series that belong to the Novodnistrovsk and Ushytsya Regional horizons, respectively. The Mohyliv-Podilsky Series includes Chartoryi, Roznychi, and Kolky formations. The boundary between the Mohyliv-Podilsky and Volyn series is sharp with a conglomerate at the base of the Mohyliv-Podilsky Series. Basalts show evidence of surface weathering.

The Chartoryi Formation comprises two parts. The lower part includes siltstones, mudstones, sandstones, and conglomerates that contain an admixture of volcanoclastic sediments. The thickness of the lower part is about 39.5 m. The upper part of the formation comprises interlayered dark-grey and grey micaceous siltstones, mudstones, and sandstones having a combined thickness of up to 47 m. According to the microfossils found in the Chartoryi Formation, it is correlative with the Lyadova and Yampil beds of the Mohyliv-Podilsky Series in the Podillya Region (Ivanchenko et al., 2004). The Roznychi Formation is composed of interlayered brown-red conglomerates, sandstones, and siltstones. The thickness of the formation varies from 28 to 43 m, and it correlates with the Yaryshiv Formation in the Podillya Region (Ivanchenko, 2007).

The Kolky Formation consist of two parts. The lower part comprises pink and light-grey arkosic sandstone of variable grain size with pebbles at the bottom, or an interlayering of mudstones, siltstones, and sandstones. The thickness of the lower part varies from 14 to 36 m. The upper part is composed of variegated mudstones and siltstones with rare

sandstone beds. The thickness of the upper part varies from 16 to 34 m. The Kolky Formation contains microfossils that occur in the Kalyus beds in the Podillya Region (Ivanchenko, 2007).

The Kanyliv Series in the Volyn Region belongs to the Ushytsya Regional Horizon and completes the succession of the Ediacaran deposits in the area. It is composed of the Rakiv and Zhytnivka formations. The Rakiv Formation transgressively overlies the Mohyliv-Podislky Series. The boundary is marked by the unconformity, hiatus, and weathering horizon. The Rakiv Formation contains light-grey arkose sandstones and siltstones that vary in thickness from 12 to 35 m. The Zhytnivka Formation is a thick (up to 135 m) sequence of greenish-grey siltstones and sandstones. The Rakiv and Zhytnivka formations correlate with the Zharnivka and Krushanivka formations and the Studenytsya Formation in the Podillya Region, respectively (Ivanchenko et al., 2004).

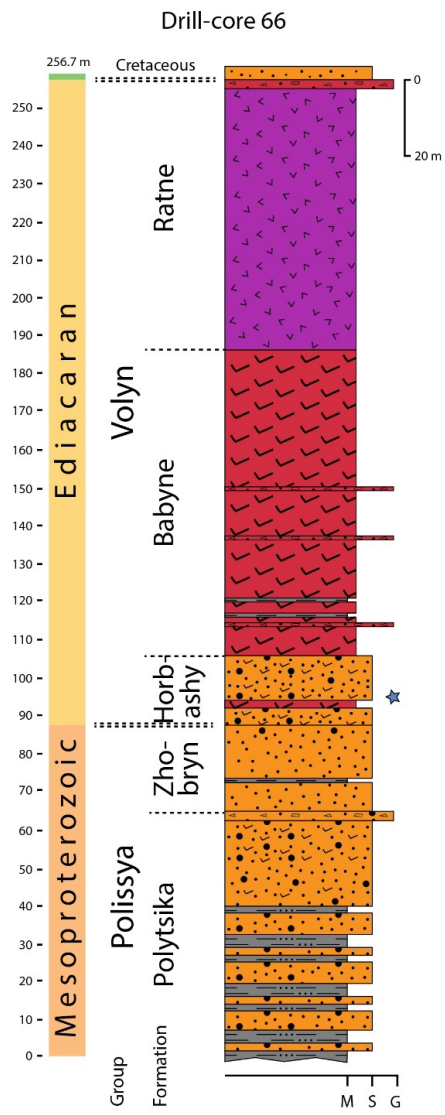
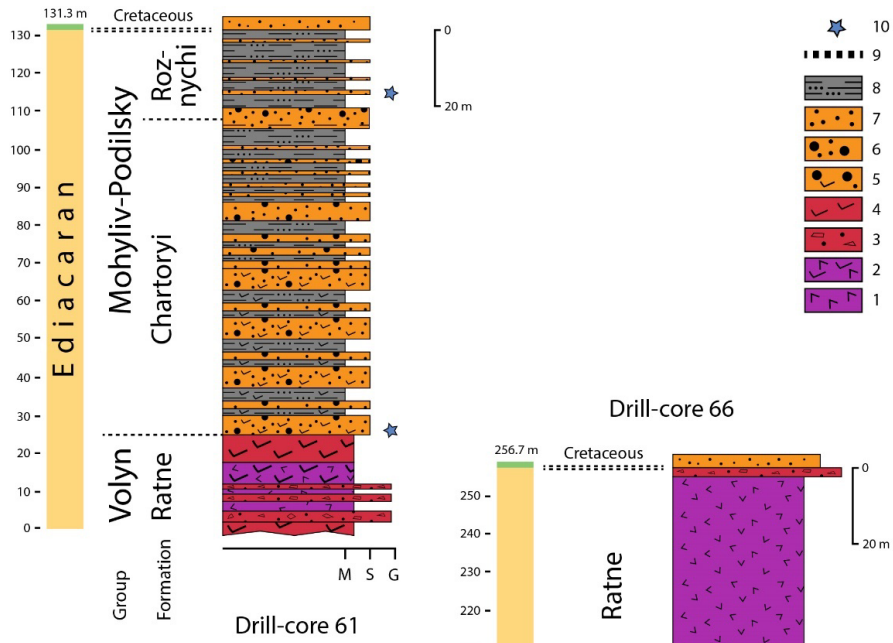


Figure 4.5. Lithostratigraphic column of the N61 and N66 drill-cores (Ukraine), showing the stratigraphic position of the studied Ediacaran sandstones of the Chartoryi and Roznychi formations, and of the Horbashy Formation, respectively, within the sedimentary succession. 1 – basalts; 2 – basaltic tuffs; 3 – tuff breccias; 4 – tuffs; 5 – tuffitic sandstones; 6 – medium- to coarse-grained sandstones; 7 – fine-grained sandstones; 8 – mudstones; 9 – unconformity; 10 – position of the studied samples.

3. SAMPLING AND METHODOLOGY

In this study, we report the results of U–Pb detrital zircon analysis of three sandstone samples collected from F-169 drill-core located in northeastern Estonia (Fig. 4.2A) and four sandstone samples from 61, 66, and 4374 drill-cores located in the Volyn Region of Ukraine (Fig. 4.2B).

In Estonia, sample K194 was collected from the basal part of the Moldova Member of the Ediacaran Gdov Formation, at a depth of 194.1 m, whereas samples L80 and L88 are from the Sämi Member of the Lower Cambrian Lontova Formation from 80.5 and 88.0 m depth, respectively (Fig. 4.4).

The sampled sandstones from the Moldova Member of the Gdov Formation are brown, medium-grained, weakly cemented, and well-sorted; quartz and feldspar grains are rounded to well rounded. The sampled sandstone beds from the Sämi Member of the Lontova Formation contain glauconite grains and, occasionally, flattened phosphatized pebbles.

In the Volyn Region (Fig. 4.5), sample 61/126 was collected from the upper part of the Roznychi Formation of the Ediacaran Mohyliv-Podilsky Group, at a depth of 126.0 m, whereas sample 61/212 was collected at a 212.0 m depth from the Chartoryi Formation of the same Mohyliv-Podilsky Group. Sample 66/221 was collected at a depth of 221.5 m

from the basal part of the Horbashy Formation of the Ediacaran Volyn Group. Sample 4374/102 was collected at a depth of 102.0 m from the Ediacaran Brody Formation.

The sampled coarse-grained sandstone to conglomerate from the Roznychi Formation contains quartz pebbles and heavily altered clasts of K-feldspar and volcanic rocks. Conglomerate forms thin (few centimetre-thick) beds in medium-grained sandstones, siltstones, and tuffaceous siltstones. Conglomerates developed at the base of the Chartoryi Formation contain small basalt pebbles derived from the Volyn Series and are overlain by the 40 meters thick tuffaceous sandstones and siltstones. The sampled sandstone to conglomerate from the Horbashy Formation is light-gray to light-green, fine- to coarse-grained, weakly cemented, and quartzitic to arkosic in composition. It contains clasts of quartz and K-feldspar and forms up to 20 cm thick beds in tuffaceous sandstones and tuffs. The studied sandstones from the Brody Formation are red-colored and contain small pebbles.

U–Pb zircon geochronology was performed at the University of California, Santa Barbara, using a Nu Plasma HR MC-ICP-MS and a Photon Machines Analyte Excite 193 nm excimer ArF laser-ablation system equipped with a HelEx sample cell. Spots were ablated during a 15-second analysis, run at 4 Hz and $\sim 1 \text{ J/cm}^2$, yielding pit depth of $\sim 5 \text{ }\mu\text{m}$. Analyses were preceded by a 15-second baseline measurements and analyses of unknowns were calibrated using the 91500 reference material ($1062.4 \pm 0.4 \text{ Ma}$; Wiedenbeck et al., 1995), which was analyzed after approximately every 10 analyses. For

quality control, secondary reference materials, including GJ-1 (601.7 ± 1.3 Ma; Jackson et al., 2004; Kylander-Clark et al., 2013) and Plešovice (337.13 ± 0.37 Ma; Sláma et al., 2008), were analyzed and yielded dates within 2% of the accepted $^{206}\text{Pb}/^{238}\text{U}$ ages. All errors are reported within 2σ .

The kernel density estimation (KDE) plots were generated by using the Python `pandas.DataFrame.plot.kde` library. The selected estimator bandwidth was the ‘scott’ method, which was set to a value of 0.05.

4. RESULTS

The results of LA-ICP-MS U–Pb zircon dating of sandstone samples from Estonia and the Volyn Region are provided in the Supplementary Information. A total of 228 and 535 analyses were performed, respectively. Six hundred ninety analyses (~90 %) yielded <5 % discordant data. Most of the age clusters defined in this work, except one, are dominated by concordant dates.

4.1. Estonia

Sample K194 (from the Moldova Member of the Gdov Formation; Ediacaran Kotlin Regional Stage) yielded four detrital zircon age populations. The oldest detrital zircon age cluster is represented by relatively few concordant dates between ca. 2065 and 1880 Ma. The two-mode distribution of $^{207}\text{Pb}/^{206}\text{Pb}$ dates within this peak indicates two

separate zircon populations. The oldest population has a $^{207}\text{Pb}/^{206}\text{Pb}$ weighted average age of 2083 ± 55 Ma, whereas the second population has a $^{207}\text{Pb}/^{206}\text{Pb}$ weighted average age of 1929 ± 21 Ma.

The second cluster of detrital zircon dates for the sample comprises a group with concordant results. Their significant spread along the concordia does not allow calculation of concordia or precise upper intercept date. Their $^{207}\text{Pb}/^{206}\text{Pb}$ weighted average date is 1803 ± 18 Ma. The third cluster of detrital zircon dates form a tight concordant group with the concordia age of 1641 ± 11 Ma.

Sample L88 (Sämi Member of the Cambrian Lontova Formation) includes zircons that form four clusters of dates. The oldest cluster is poorly defined and represented by a group of zircons that yielded concordant dates ranging from 1896 to 1692 Ma; the weighted average age is 1790 ± 40 Ma. Considering the large MSWD value of 200, these zircons likely belong to several age groups. The remaining three clusters are formed by concordant zircon dates with the following concordia ages: 1577 ± 10 , 1485 ± 11 , and 1246 ± 30 Ma.

The last sample, L80 (Sämi Member of the Cambrian Lontova Formation), has five well-defined date clusters and three grains that do not belong to any of these five clusters. The oldest three clusters are formed by concordant to nearly concordant zircon dates with a rather wide spread along the concordia that makes it impossible to calculate neither the

concordia nor reasonable upper intercept dates. Instead, we calculated $^{207}\text{Pb}/^{206}\text{Pb}$ weighted average dates for these clusters. These dates are 1828 ± 25 Ma (MSWD = 18), 1682 ± 21 Ma (MSWD = 50), and 1576 ± 4 Ma (MSWD = 18). The last two clusters are comprised of concordant dates with concordia ages of 1483 ± 7 and 1213 ± 20 Ma. There are also three single grains with $^{207}\text{Pb}/^{206}\text{Pb}$ dates of 2452 ± 18 , 1977 ± 5 , and 960 ± 12 Ma.

The Ediacaran sample differs from the two Cambrian samples by the oldest populations (2083 ± 55 and 1929 ± 21 Ma), and the absence of zircons younger than ca. 1600 Ma. Zircons with an age of ca. 1800 Ma are present in all three samples. The next, younger clusters have dates of 1641 ± 11 Ma (sample K194) and 1682 ± 21 Ma (sample L80). The ages of these clusters are significantly different, and they may have been derived from different sources. The next three clusters are only shown by the Cambrian samples. Two clusters have overlapping, well-defined ages (1576 ± 4 Ma and 1577 ± 10 Ma, and 1483 ± 7 Ma and 1485 ± 11 Ma for samples L80 and L88, respectively). The youngest clusters for both Cambrian samples have ages of 1213 ± 20 and 1246 ± 30 Ma, again overlapping within an error.

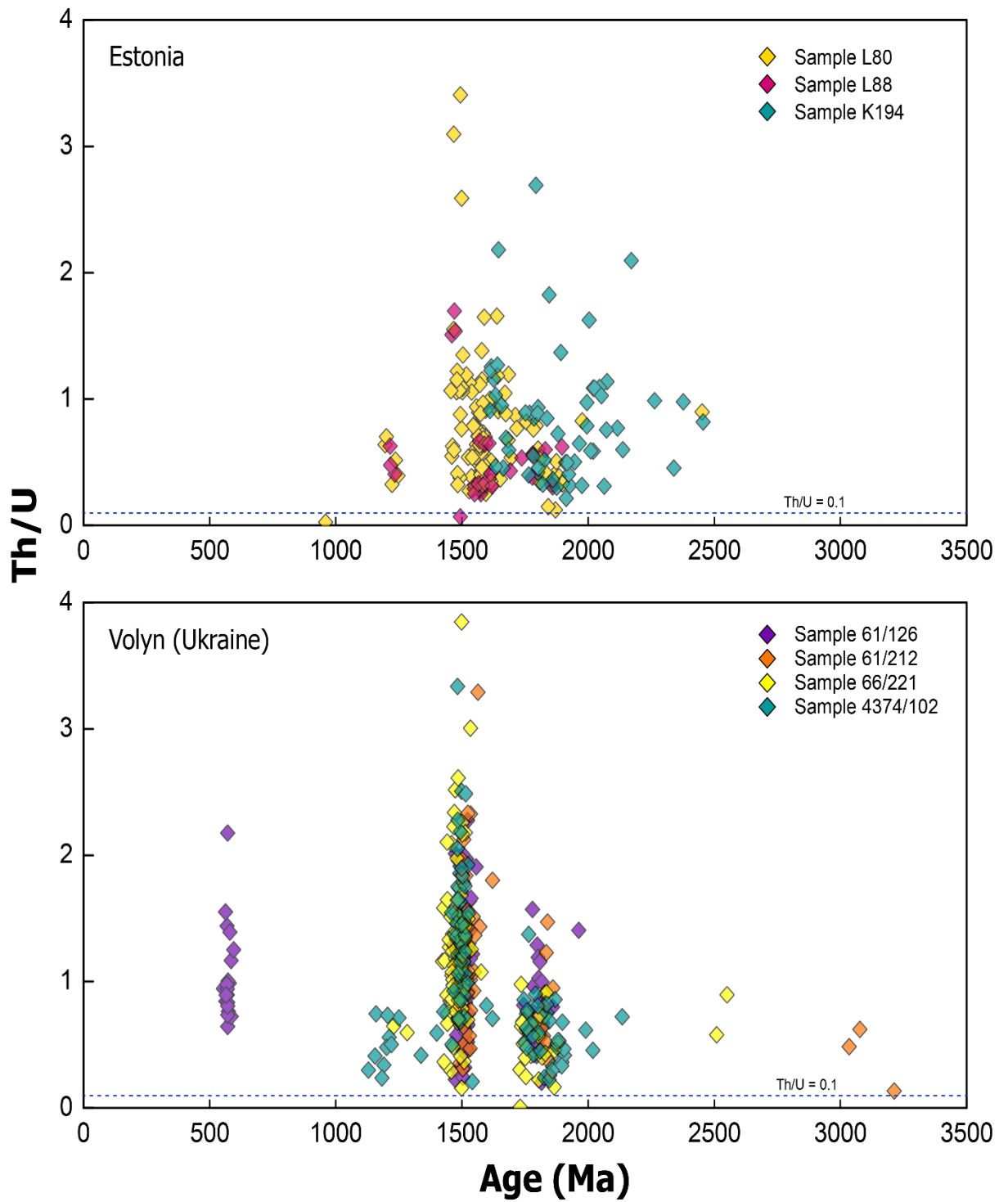


Figure 4.6. Plot of Th/U ratio versus age for zircons from Estonia and the Volyn Region of Ukraine, respectively. Most of the Th/U ratios indicate magmatic origin for zircons.

likely reflecting their metamorphic or hydrothermal origin. There is no correlation between Th/U ratios and age (see Fig. 4.6).

4.2 Volyn Region of Ukraine

The youngest studied sample (61/126), from the Roznychi Formation of the upper Mohyliv-Podilsky Group, contains three well-defined zircon populations. The youngest one yielded a tight concordia age of 573 ± 3 Ma. Other two populations yielded upper intercept ages of 1792 ± 5 and 1502 ± 3 Ma.

The next sample (61/212) is from the Chartoryi Formation of the lower Mohyliv-Podilsky Group. It contains two well-defined zircon populations, having the concordia age of 1506 ± 5 Ma and the upper intercept age of 1834 ± 6 Ma. Three zircon grains have dates older than 3000 Ma.

Zircons from sample 66/221 of the Horbashy Formation, the lowermost Volyn Group, define two major and two minor populations. The youngest one is represented by two grains with a concordia age of 1253 ± 16 Ma. The next population contains numerous (67) zircon grains with a very tight upper intercept age of 1505 ± 10 Ma. In contrast, the next population is widespread along the concordia, with $^{207}\text{Pb}/^{206}\text{Pb}$ ages varying between 1881 ± 28 and 1729 ± 30 Ma. The $^{207}\text{Pb}/^{206}\text{Pb}$ weighted average age for this population is

1778 ± 19 Ma. However, several peaks at ca. 1880, 1820, and 1740 Ma can be identified within this population. Lastly, two zircon grains in this sample yielded concordia age of 2567 ± 17 Ma.

Zircons of the oldest sample (4374/102; Brody Formation) form four populations. The youngest one yielded an upper intercept age of 1204 ± 26 Ma. The next population, most abundant in this sample, yielded a very tight upper intercept age of 1481 ± 15 Ma. The last two populations have close, but distinguishable, ages of 1783 ± 12 Ma (concordia age) and 1818 ± 37 Ma (upper intercept age).

The important feature of detrital zircon age distribution for the studied units is the rarity of Archean ages: only five grains yielded Neoproterozoic (2 grains) and Mesoproterozoic (3 grains) dates. The ca. 1830-1820 Ma detrital zircon age population was found in three of the four samples, except for the uppermost Roznychi Formation. The ca. 1790-1780 Ma detrital zircon age population was also observed in three samples, but not in the conglomerate of the Chartoryi Formation. The most prominent age population in all the studied samples is at ca. 1500 Ma; its abundance varies from 58% in the Brody Formation to 81% in the Chartoryi Formation. The next population having an age of ca. 1250-1200 Ma is shown by the two stratigraphically lowermost samples representing the Brody and Horbashy formations, but it is entirely lacking up section. The youngest population (573 ± 3 Ma) has been found in a single sample representing the uppermost Roznychi Formation.

The high Th/U ratios (mostly between 0.2 and 4) of zircons in the studied samples are consistent with their magmatic origin. Only one zircon is characterized by a low Th/U ratio (<0.1), likely reflecting its metamorphic or hydrothermal origin. There is no observable correlation between zircon Th/U ratios and the age (Fig. 4.6).

5. DISCUSSION

5.1 Possible sources for detrital zircons

5.1.1 Estonia

As summarized above, detrital zircon U–Pb ages for the K194, L88, and L80 samples define several major clusters of the Paleoproterozoic and Mesoproterozoic dates.

There are several potential source areas within Fennoscandia that correspond to the obtained clusters (Figs. 4.7A and B). These include the Archean Kola-Karelia craton, numerous massifs of A-type rapakivi granites, and lithotectonic units belonging to the Svecofennian and Sveconorwegian orogens (Kozlovskaya et al., 2008; Bogdanova et al., 2015; Hölttä et al., 2020). On the Fennoscandian Shield, the widespread Archean crust yields U–Pb zircon ages ranging between 3100–2900 Ma and 2800–2600 Ma (Kozlovskaya et al., 2008; Hölttä et al., 2020). The Paleoproterozoic lithotectonic units include igneous and metamorphic rocks associated with the ca. 1950–1850 Ma

Svecofennian Orogen and ca. 1850–1650 Ma granites and volcanic rocks of the Transscandinavian Igneous Belt (TIB) (Bogdanova et al., 2001, 2008; Söderlund et al., 2005; Lahtinen et al., 2005; Nironen 1997; Korja et al. 2006; Larson and Berglund, 1992; Andersson et al., 2004; Gorbatshev, 2004). The Mesoproterozoic units of Fennoscandia that could have been potential sediment sources include granitoids and volcanics formed at ca. 1500–1400 Ma and the granite-syenite complex intruded at ca. 1220–1200 Ma (Bingen and Viola, 2018). The westernmost Telemark lithotectonic unit records magmatism at ca. 1520–1480 Ma and bimodal volcanism between ca. 1280 and 1145 Ma (Bingen et al., 2008; Bogdanova et al., 2008; Johansson et al., 2016; Bingen and Viola, 2018). The Sveconorwegian Orogen, which is an extension of the Grenvillian orogenic belt, yields U–Pb zircon ages varying from 1200 to 900 Ma (e.g., Gaal and Gorbatshev, 1987; Söderlund et al., 2005; Bogdanova et al., 2008; 2016; Bingen et al., 2008; Möller et al. 2015; Lundmark and Lamminen, 2016). The massif-type anorthositic rocks and related A-type rapakivi granites of the anorthosite–mangerite–charnockite–granite (AMCG) intrusive suites widely developed on Fennoscandia were intruded at ca. 1650–1500 Ma (e.g., Amelin et al. 1997; Rämö et al. 2014; Wiszniewska et al., 2007; Skridlaite et al., 2008; Heinonen et al., 2010; 2015; Soesoo et al., 2020).

Although the Archean rocks are common in Baltica and should have been a significant source of detrital zircons to Baltica’s sedimentary basins (e.g., Valverde-Vaquero et al., 2000; Isozaki et al., 2014; Paszkowski et al., 2019), no zircons having ages ca. 3500–2500 Ma have been identified in our samples. Zircons with the late Paleoproterozoic ages

(ca. 1930 and 1800 Ma) were likely derived from the Svecofennian Orogen, while zircons with ca. 1682, 1641, 1576, and 1485 Ma ages were probably sourced from the felsic intrusive rocks associated with the AMCG complexes. The youngest, ca. 1220 Ma peak could have been derived either from the ca. 1220–1200 Ma granite-syenite complex or bimodal igneous rocks of the ca. 1280–1145 Ma Telemark terrane.

Fig. 4.8C summarizes the detrital zircon age populations from the Ediacaran and Cambrian sandstone samples K194, L88, and L80 and also displays at the same scale the results from Estonia published by Isozaki et al. (2014) and Põldvere et al. (2014). Data are plotted as Kernel Density Estimation diagrams. All figures use only zircons with concordant dates. All samples share an almost identical detrital zircon age spectrum, which is characterized by two distinct age populations in all three samples: Paleoproterozoic (2000–1700 Ma) and predominantly Mesoproterozoic (1680–1220 Ma). Comparison of the composite detrital zircon age distribution from our study with those from Isozaki et al. (2014) and Põldvere et al. (2014) for sandstone samples from the Kotlin and Lontova formations, especially samples VKT and VLN, shows that the spectra contain the same overall age range.

The cumulative detrital zircon age distribution diagram (Fig. 4.8C) suggests that detrital zircon modes from the studied sedimentary units could be fully accounted for with Baltica provenance and are thus not useful for testing Baltica-centered plate reconstructions. All three samples show detrital zircon dates that are much older than the

time of deposition. Consequently, the detrital zircon age spectra for the Moldova and Sămi member sandstones (Gdov and Lontova formations) reflect the age of the crystalline basement and lack contribution from syn-depositional volcanic activity.

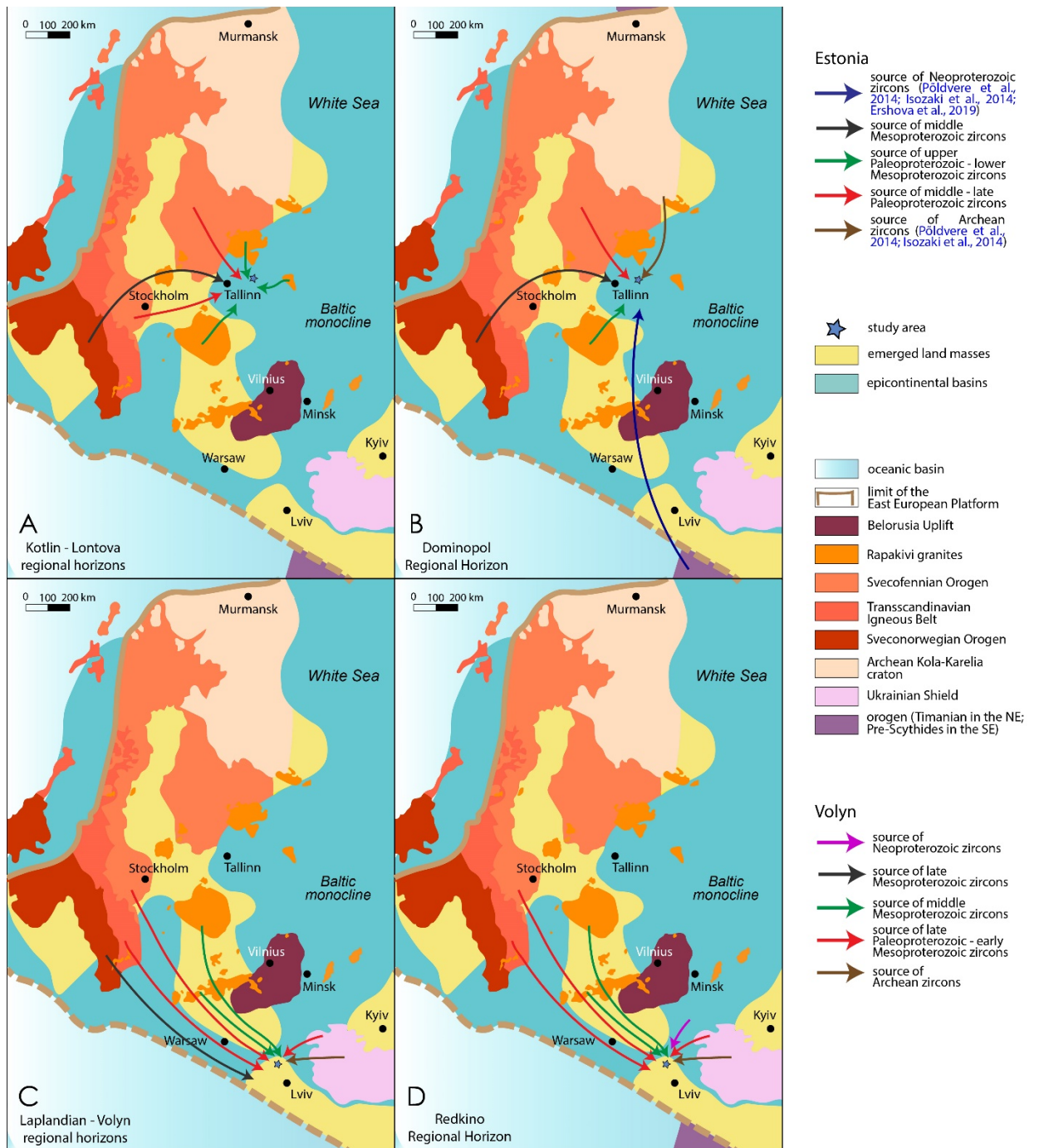


Figure 4.7. Paleogeographic map of western Baltica during (A) the late Ediacaran – Early Cambrian (Kotlin – Lontova regional stages) time and (B) Early Cambrian (Dominopol Regional Stage) time, showing possible provenance for detrital zircons in the Estonian samples; and (C) Laplandian – Volyn regional stages and (D) Redkino Regional Stage, both of the Late Ediacaran age, showing possible provenance for detrital zircons in the Volyn Region samples (modified from Nikishin et al., 1996; Poldvere et al., 2014). The late Ediacaran to Early Cambrian Timanian Orogen (cf. Gee et al., 2000; Pease et al., 2004; Kuznetsov et al., 2007), shown to the north of Murmansk, bordered Baltica to the northeast, whereas the inferred pre-Scythian and Santacrusades orogens with the broadly similar age (cf. Kheraskova et al., 2015; Żelaźniewicz et al., 2020), shown to the southeast of Lviv, sutured Baltica along its southwestern-western margin. B shows docking of Timan to Baltica between late Early and early Middle Cambrian, based on recent age constraints (Kuznetsov et al., 2014a, 2014b).

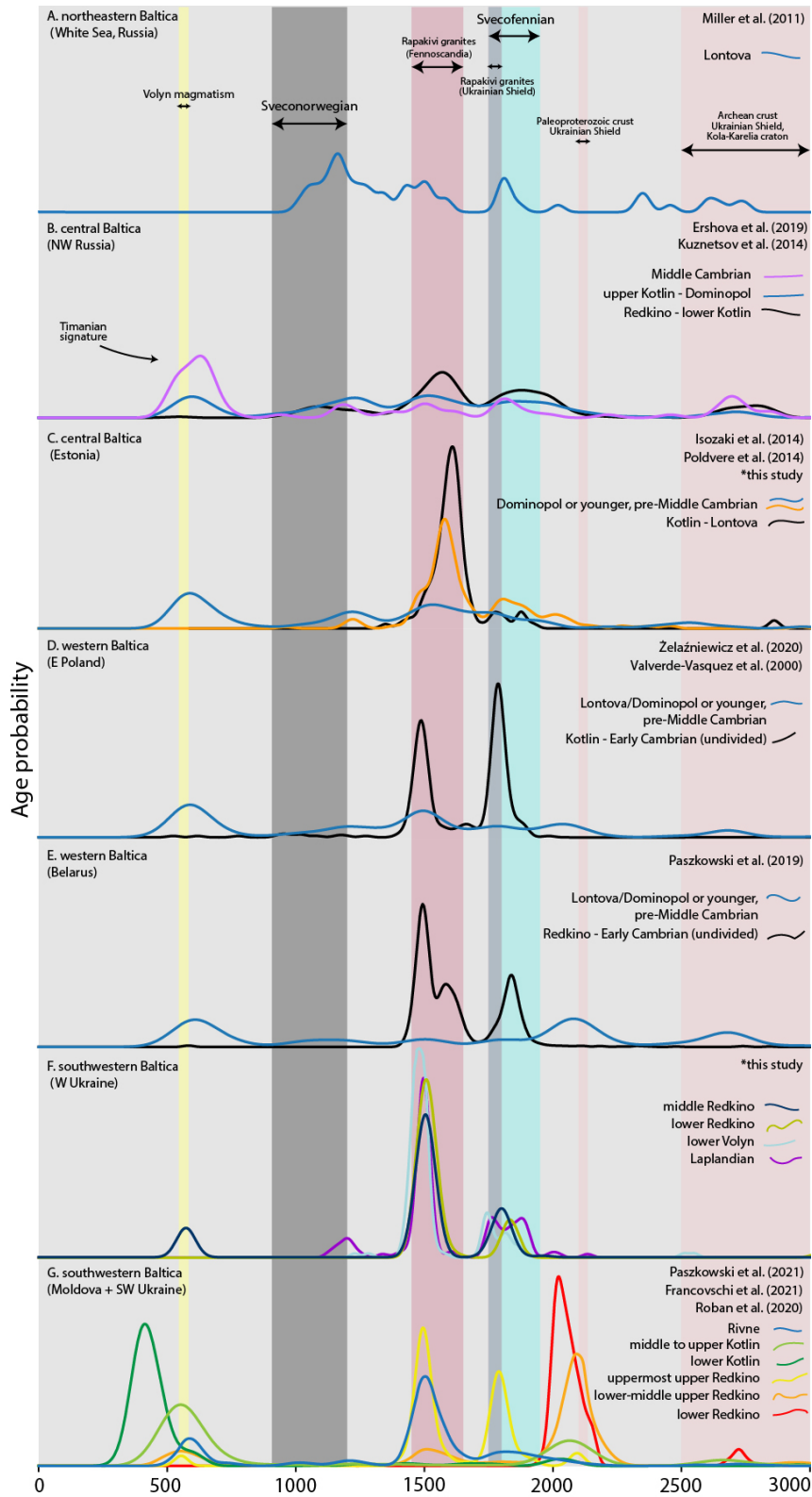


Figure 4.8. Comparison of detrital zircon age spectra (KDE plots) of the late Ediacaran - Early Cambrian sedimentary rocks from A. northeastern Baltica (White Sea area, Russia) B. central Baltica (northwestern Russia); C. central Baltica (Estonia); D. western Baltica (Eastern Poland); E. western Baltica (Belarus); F. southwestern Baltica (western Ukraine); G. southwestern Baltica (Moldova and southwestern Ukraine). A significant change in the detrital zircon age patterns is expressed in all regions during the Kotlin Regional Stage or later.

5.1.2 Volyn Region

Detrital zircon U–Pb dates obtained for the 61/126, 61/212, 66/221, and 4374/102 samples define several major clusters with the Paleoproterozoic, Mesoproterozoic, and Neoproterozoic ages. There are several potential source areas within Baltica that correspond to the obtained clusters (Figs. 4.7C and D).

Rare Archean zircon grains are present in the Horbashy and Chartoryi formations. Their content is surprisingly low, considering the widespread distribution of the Archean units on the Ukrainian Shield (e.g., Shcherbak et al., 2005; Claesson et al., 2015, 2019).

Further, while the Volyn Region is underlain by the ca. 2100–1950 Ma Paleoproterozoic basement, which also crops out nearby in the northwestern part of the Ukrainian Shield (e.g., Bogdanova et al., 2001; 2016; Claesson et al., 2001; Melnychuk, 2013; Shumlyanskyy, 2014; Shumlyanskyy et al., 2018; 2021a; Stepanyuk et al., 2017; Ponomarenko et al., 2014), detrital zircons of this age are completely absent in the studied Ediacaran rocks from the Volyn Region.

The oldest zircon population has an age of 1830–1820 Ma. It is significantly younger than the Paleoproterozoic granitoids widely distributed in the area. In contrast, igneous and metamorphic rocks associated with the ca. 1950–1850 Ma Svecofennian Orogen (Bogdanova et al., 2001, 2008; Lahtinen et al., 2005; Nironen 1997; Korja et al. 2006) are a possible source of detrital zircons for this population. The ca. 1850–1650 Ma granites and volcanic rocks of the Transscandinavian Igneous Belt (TIB; Bogdanova et al., 2001,

2008; Söderlund et al., 2005; Lahtinen et al., 2005; Nironen 1997; Korja et al. 2006; Larson and Berglund, 1992; Andersson et al., 2004; Gorbatshev, 2004) and ca. 1860-1760 Ma igneous rocks of the Mid-Baltic Belt in Lithuania (Skridlaite et al., 2021) could have also provided detrital zircons to the sedimentary basin.

The next population of zircons has an age of ca. 1790-1780 Ma. This age exactly corresponds to the time of emplacement of the Korosten AMCG complex in the northwestern part of the Ukrainian Shield, which is proximal to the Volyn basin (Shumlyanskyy et al., 2017; 2021c) and to the time of formation of the Prutivka-Novogol Large Igneous Province (Shumlyanskyy et al., 2012, 2016b, 2021a; Duchesne et al., 2017).

The most abundant population of zircons has 1500-1480 Ma age. The Ukrainian Shield does not host any known igneous rocks younger than ca. 1720 Ma and, therefore, cannot be considered as a source for this zircon population. The large Mazury AMCG Complex in northeastern Poland formed at 1548–1499 Ma (Wiszniewska et al., 2007; Wiszniewska and Krzeminska, 2021; Skridlaite et al., 2008) might be a possible source for zircons of this age range found in the Ediacaran samples from the Volyn Region. Similarly, some igneous rocks in southern and western Norway and Sweden crystallized at ca. 1500 Ma (Andersen et al., 2002, 2009) and might also be a possible source of detrital sediments for the analyzed samples.

The next population of zircons crystallized at ca. 1250-1200 Ma and is unique to the samples of the Horbashy and Brody formations. This detrital zircon population could have been derived either from the ca. 1220–1200 Ma granite-syenite complex of Fennoscandia (Bingen and Viola, 2018) or bimodal igneous rocks of the ca. 1280–1145 Ma Telemark terrane (Bingen et al., 2008; Bogdanova et al., 2008; Johansson et al., 2016; Bingen and Viola, 2018).

The youngest detrital zircon population yielded an age of 573 ± 3 Ma and is confined to the sample from the Roznychi Formation. This population was most likely been derived from the magmatic rocks of the Volyn flood basalt province (Shumlyanskyy et al., 2016b; Poprawa et al., 2020). While both the Roznychi and Chartoryi formations of the Mohyliv-Podilsky Group are younger than the Volyn flood basalt province, there are no zircons of this age in the Chartoryi Formation. The distribution plots for the Roznychi and Chartoryi formations are similar, with the ca. 573 Ma detrital zircon population being the only difference. A similar detrital zircon age cluster with a range between ca. 579 and 545 Ma has been found in the sedimentary rocks of the Volyn Group in Belarus (Paszkowski et al., 2019). The latter authors also inferred derivation of detrital zircons from the Volyn flood basalt province. The formations in Belarus that are stratigraphically equivalent to the Roznychi Formation in the Volyn Region (Nizov and Selsk formations) did not yield zircons with a similar age cluster.

5.2 Comparison with other areas within Baltica

Previous studies of detrital zircons from the Ediacaran and Cambrian rocks of Baltica have been focused on the western (Poland and Belarus), southwestern (Podillya Region of Ukraine and Moldova) and central (northwestern Russia) parts of the craton. By combining our own and previously published detrital zircon age data and within the framework of the tectonic history of Baltica, we propose a comprehensive scenario for the late Ediacaran to Early Cambrian paleogeographic evolution of southwestern, central, and western Baltica (Fig. 4.9).

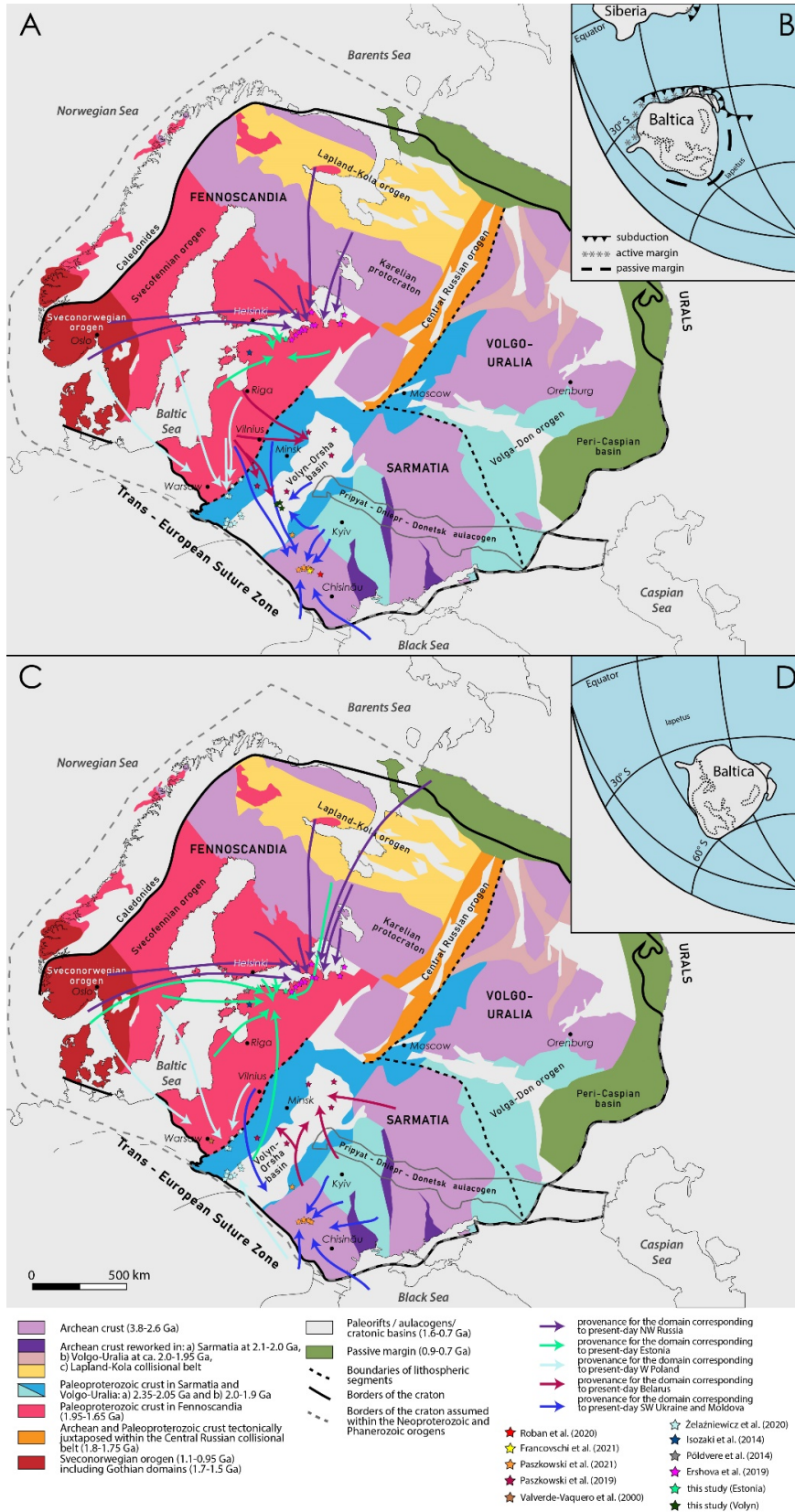


Figure 4.9. (A) Location of the studied Ediacaran samples from the Ediacaran - Early Paleozoic basins of Baltica and directions of the detrital sediment transport; (B) Schematic map showing the late Ediacaran position of Baltica (modified after Merdith et al., 2017). (C) Location of the studied Cambrian samples from the Ediacaran - Early Paleozoic basins of Baltica and directions of the detrital sediment transport; (D) Schematic map showing the Early Cambrian position of Baltica (modified after Merdith et al., 2017). (A) and (B) are modified from the schematic tectonic map of Baltica (Bogdanova et al., 2016).

The Ediacaran and Cambrian units from the western margin of Baltica, specifically from eastern Poland (Valverde-Vaquero et al. 2000; Żelaźniewicz et al., 2020) and Belarus (Paszkowski et al., 2019), show several prominent peaks in detrital zircon age distribution. The Ediacaran and Early Cambrian units have yielded detrital zircon modes at 1900 to 1800 Ma, 1700 to 1500 Ma, and 579 to 545 Ma. The latter cluster is considered to be derived from the Ediacaran Volyn flood basalts (cf. Paszkowski et al., 2019). The Mesoproterozoic (ca. 1700–1500 Ma) zircons are similar in age to granites and gneisses from the island of Bornholm (Johansson et al., 2016) and rapakivi granites of southwestern Fennoscandia (Heinonen et al., 2010, 2015). The exposed topographic highs of the Svecofennian basement (Żelaźniewicz et al., 2020) could have been the source for the 1900–1800 Ma zircons. The Early Cambrian units show a slightly different provenance from that of the Ediacaran units. Their detrital zircon distribution pattern is dominated by ca. 1500 Ma dates, while ca. 1850–1700 Ma and ca. 1100 Ma zircons are less abundant, and the Ediacaran ones are absent. The Middle Cambrian units indicate a significant change in provenance in western Baltica before their deposition during the Dominopol Regional Stage. The Middle Cambrian detrital zircon distribution pattern is dominated by ca. 670–540 Ma dates, accompanied by a minor ca. 1500 Ma peak, and prominent ca. 2100–2000 Ma and ca. 2700–2500 Ma peaks. This age spectrum, being consistent with the continued supply from the Sveconorwegian and Svecofennian orogens, and Karelia-Kola craton (or Ukrainian Shield), also indicates a significant delivery of detrital materials from the Ediacaran sources. Żelaźniewicz et al. (2020) and Valverde-Vaquero et al. (2000) considered that the Neoproterozoic cluster indicates the

development of a Neoproterozoic orogenic belt at the southwestern margin of Baltica at the end of the Ediacaran - beginning of the Cambrian.

For the southwestern margin of Baltica, which includes the territory of Moldova and the Podillya Region of Ukraine, the Ediacaran units reveal multiple detrital zircon age peaks (Roban et al., 2020; Francovschi et al., 2021; Paszkowski et al., 2021). Archean zircons, ranging in age from 2900 to 2600 Ma, were likely derived from the Archean domains of Sarmatia, presently exposed on the Ukrainian Shield. Zircons dated between 2200 and 1900 Ma were likely derived from the Paleoproterozoic belts of Sarmatia (Claesson et al., 2015, 2019; Stepanyuk et al., 2017; Shumlyanskyy et al., 2018, 2021a). The Belarusian crystalline basement (Paszkowski et al., 2019) and the Ukrainian Shield (Ponomarenko et al., 2014; Shumlyanskyy, 2014) could have supplied the ca. 1945 Ma zircons. The most abundant ca. 1780 Ma mode corresponds to the age of the Korosten AMCG complex (Shumlyanskyy et al., 2017; 2021c) and Prutivka-Novogol Large Igneous Province (Shumlyanskyy et al., 2012, 2016b, 2021b; Duchesne et al., 2017). The numerous Fennoscandian AMCG suites formed at ca. 1660–1450 Ma are also potential sources of terrigenous sediments for the Moldova-Podillya basin (Paszkowski et al., 2021). The source of the youngest detrital zircon mode at ca. 620–535 Ma might be linked to the Volyn flood basalt province (Kuzmenkova et al., 2010; Shumlyanskyy et al., 2016b), felsic volcanic activity on the adjacent continents, such as Laurentia and Amazonia that were proximal at that time to Baltica (Weber et al., 2020; Youbi et al., 2020), or the arc magmatic activity on terranes subsequently incorporated into the pre-Scythides and

Santacrusades orogens located along the southwestern and western margins of Baltica (Żelaźniewicz et al., 2009, 2020; Buła and Habryn, 2011; Paszkowski et al., 2021; Collett et al., 2022).

Lastly, the Ediacaran - Cambrian units from the central part of Baltica (northwestern Russia) have been studied by Ershova et al. (2019). The late Ediacaran samples yielded major zircon peaks at ca. 2000 to 1850 Ma and ca. 1600 to 1550 Ma. Middle Paleoproterozoic dates (ca. 1950–1850 Ma) correspond to the age of the Svecofennian Orogeny. The other prominent zircon peak, which ranges in age between ca. 1600 and 1550 Ma, corresponds to the Fennoscandian rapakivi granite complexes. Archean zircons are rare, with peaks at ca. 2800 and 2670 Ma, corresponding in age to the accretionary events, which led to the formation of the Karelia-Kola craton (Bogdanova et al., 2008). The uppermost upper Ediacaran to lowermost Lower Cambrian stratigraphic interval is characterized by a wide range of dates from ca. 2800 to 530 Ma. Neoproterozoic dates (ca. 2700–2500 Ma) correspond to the known accretionary events in Fennoscandia. Zircon dates of ca. 1950–1800 Ma could represent magmatic events in the Svecofennian Orogen. Most of the zircons falling in the ca. 1800–1600 Ma age range might be derived from the Transscandinavian Igneous Belt. Detrital zircon clusters with the ca. 1600–1500, 1300–1200, and 1100–950 Ma ages closely correspond to the magmatic events in the Sveconorwegian Orogen. Ershova et al. (2019) suggested that the source of ca. 554 Ma detrital zircons for the units corresponding to the uppermost upper Kotlin Regional Stage was from the Timanian Orogen. However, a recent study, based on microfossils,

suggested that the units of the uppermost upper Kotlin Regional Stage in the Saint Petersburg area (the upper part of the Vasileostrovskaya Formation) likely belong to the Early Cambrian Lontova Regional Stage (Kushim et al., 2016). Thus, the sediment supply from the Ediacaran provenance started during the Early Cambrian Lontova Regional Stage in the Saint Petersburg area.

5.3 General patterns in the Ediacaran - Cambrian evolution of Baltica sedimentary basins

Detrital zircons data from several regional studies indicate complex evolution of the sedimentary basins of Baltica during the late Ediacaran to the Early to Middle Cambrian time interval. In the case of Estonia, despite sampling at different stratigraphic positions, detrital zircon age peaks are broadly similar, suggesting only minor changes in the provenance during deposition in the Baltic basin. Comparison with detrital zircon age distribution trends for the Ediacaran (Kotlin Regional Stage) and Early Cambrian (Lontova Regional Stage) (Isozaki et al., 2014) demonstrates the same age peaks as those identified in our study, consistent with an invariable provenance during deposition of the late Ediacaran to Early Cambrian units in Estonia (Fig. 4.8C). Nielsen and Schovsbo (2011) suggested that the Early Cambrian transgression was largely controlled by the development of a successor, extensive sag ('steer-horn') basin after the inversion of the late Neoproterozoic Volyn-Orsha Rift in Belarus and Ukraine. For the central part of Baltica with an east-facing slope (e.g., Baltic basin in Estonia), terrigenous sediments were delivered mostly from the areas to the north and west of the basin, i.e., from the central and western parts of the Fennoscandian Shield. In particular, the prominent age

peak at ca. 1650 to 1500 Ma in all samples is noteworthy since it suggests derivation from the rapakivi granitic suites of the Fennoscandian Shield during the late Ediacaran to Early Cambrian (throughout the Lontova Regional Stage; Fig. 4.7A). In contrast, new detrital zircon age peaks appear during deposition of the Early Cambrian Dominopol Regional Horizon (Isozaki et al., 2014; Põldvere et al., 2014), suggesting a major change in the provenance (Fig. 4.7B). Specifically, the overall input from the ca. 1650–1500 Ma rapakivi granites significantly decreased with an associated increase in the input of zircons clustering in three age groups: Archean, Stenian-Tonian (ca. 1300–900 Ma), and Neoproterozoic-Early Cambrian. Appearance and persistent presence of ca. 1300–900 Ma detrital zircons during deposition of the Dominopol Regional Horizon indicates terrigenous flux from the Sveconorwegian basement in western Baltica. Decrease in the Mesoproterozoic rapakivi granite-derived sediments and an increase in the abundance of the Neoproterozoic-Early Cambrian zircons suggest tectonically induced change in the provenance before deposition of the Early Cambrian Dominopol Regional Horizon started. Furthermore, the detrital zircon age distribution of the Dominopol Regional Horizon is similar to that of the Devonian units (Põldvere et al., 2014), suggesting that the provenance of the Baltic basin did not change until sometime after deposition of the Devonian succession. The Dominopol Regional Horizon in Estonia is characterized by detrital zircons with ages that are close to the depositional age (e.g., the difference between zircon crystallization age and sediment depositional age is <100 Ma for >25% of the zircon population in both samples), indicating either a convergent or collisional basinal setting (Cawood et al., 2012). Therefore, at the onset of the Dominopol Regional

Stage, during a relatively short time interval (5 to 10 m.y.), the provenance for sedimentary successions deposited in Estonia (Fig. 4.10) changed. Possibly, more than one source of Neoproterozoic zircons existed at that time at Baltica's exterior, one of which could have been the Timanian Orogen (Isozaki et al., 2014; Sláma and Pedersen, 2015; Ivleva et al., 2016, 2018; Sláma, 2016; Ershova et al., 2019). Another possible source might have been located at the southwestern to western margin of Baltica, where Neoproterozoic terranes (e.g., pre-Scythia and Brunovistulia), which broke away from cratons that later formed Gondwana (e.g., São Francisco or Congo), collided with Baltica, giving the rise to the pre-Scythides and Santacrusades orogens (Żelaźniewicz et al., 2009, 2020; Buła and Habryn, 2011; Kheraskova et al., 2015; Kuznetsov and Romanyuk, 2021; Collett et al., 2022). The latter sources, although plausible, are poorly constrained and were likely located far from Estonia.

In comparison to other Ediacaran to Early Cambrian basins of Baltica, the Moldova-Podillya-Volyn basin might have experienced more complex evolution during the late Ediacaran - Early Cambrian (Fig. 4.10). This might be related to its collision with the Neoproterozoic terranes (e.g., pre-Scythia and Brunovistulia) potentially separated from Amazonia (cf. Żelaźniewicz et al., 2020; Collett et al., 2022). The earliest change in the provenance happened after deposition of the lower to middle parts of the upper Redkino Regional Horizon in the Moldova-Podillya-Volyn basin (Figs. 4.8F and G). At that time, sediment supply from the Fennoscandian Shield, in contrast to the Volyn and Redkino Regional horizons of Belarus, contributed only a minor cluster of detrital zircons

characteristic of the Fennoscandian AMCG plutons (Paszkowski et al., 2019). During this period, sediments to the Moldova-Podillya-Volyn basin were predominantly supplied from the adjacent Paleoproterozoic belts of Sarmatia, with only a weak, if any, contribution from Fennoscandia. There was a progressive change in the provenance from Sarmatia back to Fennoscandia during deposition of the upper part of the Redkino Regional Horizon in Moldova and southwestern – western Ukraine (Paszkowski et al., 2021). Considerable changes in the tectonic setting and sea level took place after deposition of the Redkino Regional Horizon: the sedimentary basin became smaller (Bukatchuk, 1973; Bukatchuk et al., 1988), which led to a major hiatus followed again by a change in the provenance. The lowermost Kotlin Regional Horizon of the Moldova-Podillya-Volyn basin predominantly contains Ediacaran detrital zircons with only a minor component of older detrital zircons, implying derivation from an adjacent volcanic arc (Paszkowski et al., 2021) within a foreland basin setting (cf. Cawood et al., 2012), developed on the SW margin of Baltica (Kheraskova et al., 2015; Żelaźniewicz et al., 2020). During deposition of the middle to upper parts of the Kotlin Regional Horizon, the volcanic arc/orogenic source remained important (Paszkowski et al., 2021), but there was also a renewed supply of terrigenous sediments from the Archean and Paleoproterozoic units of the Ukrainian Shield. The Early Cambrian Rivne Regional Horizon in the Moldova-Podillya-Volyn basin (Paszkowski et al., 2021), Belarus (Paszkowski et al., 2019), Estonia (Isozaki et al., 2014; Põldvere et al., 2014), Russian part of the Baltic Monocline (Kuznetsov et al., 2011; Ivleva et al., 2016; Ershova et al., 2019), and Scandinavia (Lorentzen et al., 2018) have similar detrital zircon age patterns with the age

spectrum dominated by the sediments derived from Fennoscandia and late Neoproterozoic volcanic arcs. We thus consider that the Moldova-Podillya-Volyn basin represents a distal part of the foreland basin to the pre-Scythian and Santacrusades orogenic belts, which formed at the southwestern and western margins of Baltica during deposition of the Redkino to Kotlin Regional horizons. Thereafter, the eroded and weathered sediments were distributed to the north-northeast into other sedimentary basins of Baltica and affected the overall detrital zircon age populations as the fold-and-thrust belt and foreland basin propagated to the north-northeast.

These detrital zircon age trends observed in a number of the Ediacaran to Early Cambrian sedimentary basins of Baltica are indicative of regional changes related to the propagation of the Timanian and pre-Uralian foreland basins to the west-southwest and the pre-Scythian and Santacrusades foreland basins to the north-northeast. The high proportion of detrital zircons with ages close to the depositional age of sediments in these basins (Fig. 4.8) is indicative of arc magmatism at the southwestern and northeastern convergent plate margins of Baltica in the late Ediacaran – Early Cambrian.

5.4 Inconsistencies in the late Ediacaran – Early Cambrian detrital zircon age distribution patterns for the sedimentary basins of Baltica

The youngest detrital zircons clusters for the late Ediacaran, Kotlin Regional Stage samples presented in Ershova et al. (2019) and Paszkowski et al. (2021) are inconsistent

with the previously discussed stratigraphic detrital zircon age distribution patterns, potential sediment sources, and the general tectonic history of Baltica, based on the Middle Cambrian age for the Timanian Orogeny (Kuznetsov et al., 2007, 2011, 2014a, 2014b, 2015). In the Saint Petersburg area, Ershova et al. (2019) suggested that the source of the ca. 706-552 Ma concordant detrital zircons of the Voronka Formation (upper Kotlin Regional Horizon; west of Saint Petersburg), with the weighted average age of the three youngest grains of 554 ± 5 Ma, reflects magmatic and metamorphic events related to the west-directed subduction under Baltica, leading to and during the Timanian Orogeny. However, U-Pb detrital zircon dates for the lower Redkino Regional Horizon Tamitsa and upper Lontova Regional Horizon Brusov formations from the White Sea area (Kuznetsov, 2014a, 2014b), more proximal to the Timanian Orogen, do not fall within the ca. 750-500 Ma time interval, corresponding to the Timanian Orogen signature. This seems to indicate that during the upper Lontova Regional Stage, the Timanian Orogen did not yet provide sediments to the eastern part of Baltica, whereas by the Middle Cambrian, sediments were already supplied from this orogen (cf. Kuznetsov et al., 2007, 2011, 2014a, 2014b, 2015). However, a recent study, based on microfossils, suggested that the upper part of the Vasileostrovskaya Formation, conformably underlying the Voronka Formation to the west of Saint Petersburg belongs to the Early Cambrian Lontova Regional Stage (Kushim et al., 2016). Even if the Voronka Formation was deposited during the Lontova Regional Stage, it seems to still precede in its depositional age the inferred time of delivery of sediments derived from the Timanian Orogen to the eastern part of Baltica.

Potentially relevant to this discrepancy between the time when the Timanian Orogen supposedly started to supply sediments and the depositional age of the Voronka Formation hosting detrital zircons with dates characteristic of the Timanian Orogen is the detrital zircon U-Pb study of the Ediacaran to Early Cambrian Dividal Group in Finnmark, Norway (Andresen et al., 2014). There, the Timanian Orogen detrital zircon signature has been recognized in the Early Cambrian (Terreneuvian – Series 2; Slama and Pedersen, 2015) sandstones deposited in the distal part of the foreland basin of the Timanian Orogen. In contrast, our study combined with the literature data (Isozaki et al., 2014; Poldvere et al., 2014) suggests that the Timanian Orogen-derived sediments did not arrive to Eastern Estonia until the beginning of the Cambrian Stage 3. We thus infer that the collision and unroofing of the Timanian Orogen was already underway by the Early Cambrian and that sediment routing with fluvial systems and topography largely controlled when sediments from the Timanian Orogen were first delivered to the sedimentary basins of Baltica.

In the Moldova-Podillya basin, Paszkowski et al. (2021) reported the detrital zircon age clusters from the units of the Kotlin Regional Stage with maximum depositional ages ranging from 547 to 523 Ma, implying a depositional age equivalent to that of the upper part of the Cambrian Stage 2. Furthermore, Paszkowski et al. (2019) inferred, based on detrital zircon ages of the siliciclastic units overlying and interbedded with the Volyn LIP that it lasted from ca. 579 to 545 Ma. These data are inconsistent with our own and

literature detrital zircon data for the Redkino and Kotlin Regional horizons presented and discussed above as well as their paleontological records. *Harlaniella podolica* Sokolov, which is found in the Kanyliv Group in the Volyn-Podillya basin of Ukraine, is not known in units of the Cambrian age (e.g., Velikanov et al., 1983; Narbonne et al., 1987; Jensen, 2003; Högström et al., 2013; Ivantsov et al., 2015; McIlroy and Brasier, 2017; Jensen et al., 2018). Previous studies of the Ukrainian and Moldavian successions have shown that there are no Cambrian acritarchs in the Kanyliv Group (e.g., Aseeva, 1976, 1988; Velikanov et al., 1983), whereas *Vendotaenia antiqua* that is found in this unit is not known in the Cambrian rocks (Velikanov et al., 1983; Gnilovskaya et al., 1988; Gnilovskaya, 1990; Cohen et al., 2009). Furthermore, the Precambrian-Cambrian boundary has been defined to be at about 6.5 meters from the base of the Baltic Series in the Khmielnitsky Formation based on the disappearance of *Harlaniella podolica* Sokolov and the first appearance of *Phycodes (Treptichnus) pedum* and *Planolites* trace fossils (Gureev, 1988; Ivantsov et al., 2015). If the Danylivka Formation of the Kanyliv Group indeed has an Early Cambrian age (ca. 523 Ma), this formation and the overlying units should show a higher diversity of trace and body fossils, unless they were of non-marine origin. Nesterovsky et al. (2019) reported *Dickinsonia costata* Sprigg and *Swarpuntia* from the lower part of the Kanyliv Group (Pylypy Beds) of the Kotlin Regional Horizon. The low diversity of Ediacaran fossils from the Kotlin Regional Horizon is more consistent with their late Ediacaran rather than Early Cambrian age (e.g., Muscente et al., 2018). Finally, throughout Baltica, the Kotlin Regional Horizon sedimentary successions do not contain detrital zircons with the Early Cambrian age (see discussion above).

Hence, until the Early Cambrian detrital zircon ages are confirmed with CA-TIMS analysis, data presented by Paszkowski et al. (2021) should not be relied upon to constrain the MDA of the Kotlin Regional Stage. Similarly, the youngest tight concordia age of 573 ± 3 Ma for detrital zircons from the Roznychi Formation of the upper Mohyliv-Podilsky Group, overlying the Volyn LIP, provides the best age constraint for this LIP, arguing against its long duration until ca. 545 Ma as inferred by Paszkowski et al. (2019) and Poprawa et al. (2020). Although island arcs proximal to Baltica sourced volcanic tuffs with ca. 557-551 Ma ages (see Fig. 4.3) and foreland basins started to develop around Baltica in the late Ediacaran (e.g., South Urals: Bekker, 1988; Puchkov, 2010; Poland and Romania: Żelaźniewicz et al., 2009, 2020; Buła and Habryn, 2011), orogenic mountains did not supply sediments at that time to the interior of Baltica.

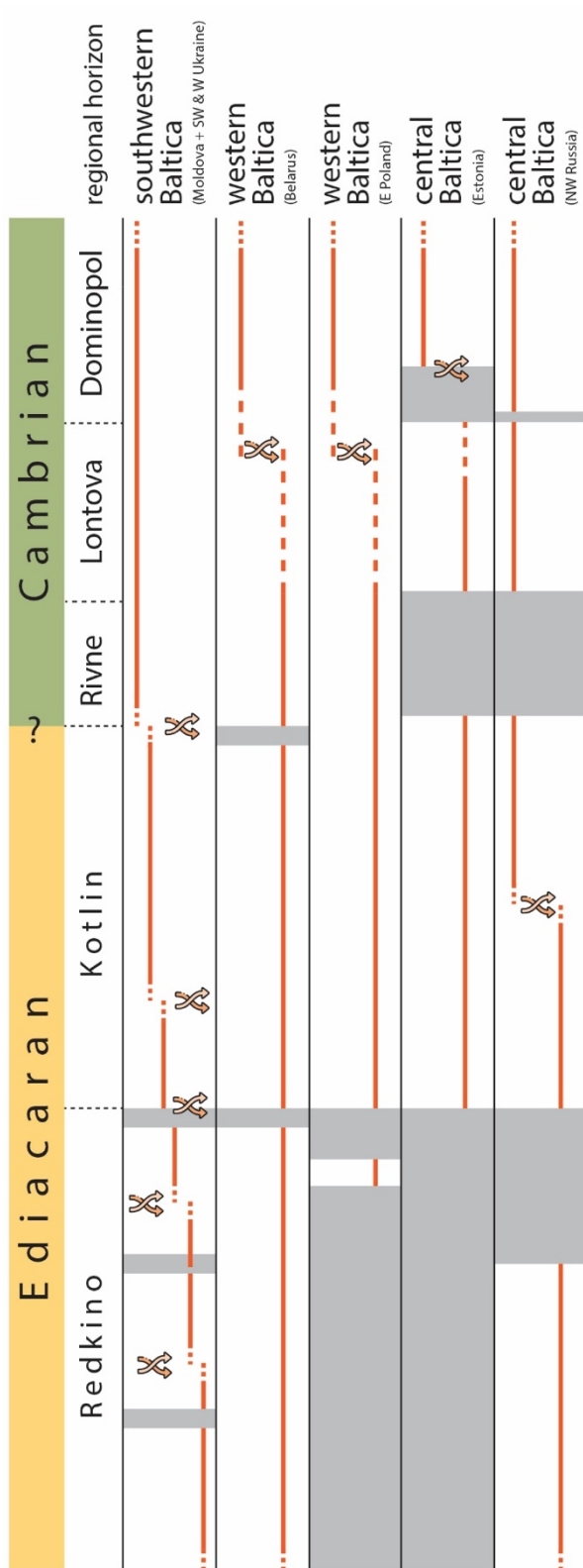


Figure 10. Schematic diagram highlighting timing of changes in the provenance in the western, southwestern, and central parts of Baltica. Gray boxes represent hiatuses. Crossed arrows indicate change in the provenance. Hiatuses in deposition are shown after Bukatchuk et al. (1988), Meidla (2017), Ershova et al. (2019), Paszkowski et al. (2019), and Żelaźniewicz et al. (2020).

6. CONCLUSIONS

Synthesis of the currently available data on the ages of detrital zircons from the late Ediacaran to Early Cambrian sedimentary basins of the central, western, and southwestern Baltica allows to constrain their evolution and sedimentary provenance. The following conclusions can be drawn in this respect.

The Moldova-Podillya-Volyn basin in southwestern Baltica developed during the early Redkino Regional Stage on the peneplaned Precambrian basement and pre-Ediacaran supracrustal successions in the distal part of the foreland basin, behind the forebulge, with a steady and monotonous supply of terrigenous sediments from the adjacent Ukrainian Shield. Tectonic conditions changed during deposition of the lower to middle parts of the upper Redkino Regional Horizon and led to a decreasing, but still persistent, input from the same provenance on the Ukrainian Shield, and delivery of tuffs derived from the late Ediacaran volcanic arcs proximal to, but separate from Baltica. The Moldova-Podillya-Volyn basin experienced emergence as the forebulge passed across it during the late Redkino Regional Stage and submerged again into a foredeep of the foreland basin during the Kotlin Regional Stage. The upper Redkino Regional Horizon records an increase in supply of terrigenous sediments from Fennoscandia to Sarmatia as the basin enlarged. Provenance for the lowermost Kotlin Regional Horizon changed again with an increased supply from the Ukrainian Shield. The latter source also contributed detrital sediments to other Baltica sedimentary basins to the north and west. During

deposition of the Rivne Regional Horizon, the Fennoscandian Shield became a secondary source of sediments.

The central part of Baltica (northwestern Russia) received terrigenous input from the northwestern part of Baltica (Fennoscandia) during deposition of the Redkino Regional Horizon. Starting with deposition of the Dominopol Regional Horizon, the Timanian Orogen contributed sediments to the Saint Petersburg region of Russia, White Sea area, and Estonia.

The late Ediacaran to Early Cambrian sedimentary deposits from the western part of Baltica (eastern Poland and Belarus) show a common, bimodal distribution pattern of detrital zircon ages during deposition of the Redkino Regional Horizon to the Early Cambrian with the detrital sediments supplied from the Precambrian basement of Baltica. The limited range of detrital zircon age spectra suggests a short-distance transport. The change from bimodal to polymodal distribution pattern occurred during the Dominopol Regional Stage and was associated with major tectonic changes that led to the reorganization of the drainage system.

The central part of Baltica (Estonia) in comparison with the previously discussed regions shows the most invariable tectonic and palaeogeographic conditions during the long period when the late Ediacaran Kotlin to Early Cambrian Lontova Regional horizons were deposited. During that time, the Ediacaran to Early Cambrian intracratonic

sedimentary basin of central Baltica had a provenance that was essentially confined to the Precambrian basement rocks of Baltica. The predominant supply of terrigenous sediments were from the Svecofennian (ca. 1900–1800 Ma) Orogen and ca. 1700–1500 Ma plutonic rocks of the rapakivi affinity from southwestern Fennoscandia. The provenance did not change for nearly 50 m.y., until deposition of the upper part of the Dominopol Regional Horizon, when input from the earlier sources slightly decreased while new, dominant provenances of magmatic arcs hosted in orogens developed along the northeastern and southwestern/western margins of Baltica appeared.

Acknowledgements

We dedicate this contribution to Kaisa A. Mens and Enn A. Pirrus, pioneers in the study of the Ediacaran of Estonia, and to the heroic efforts of the Armed Forces of Ukraine and the resilience and courage of Ukrainian people. LS acknowledges the Curtin Research Office for providing support. Participation by IF was supported by the Project PN-III-P1-1.1-PD-2021-0400, No. 60/2022 of the Romanian Executive Agency for Higher Education, Research, Development and Innovation, UEFISCDI. Participation by AB was supported by ACS PRF grant (624840ND2). John Cottle and Andrew Kylander-Clark at UCSB helped to generate LA-ICP-MS detrital zircon U-Pb data. This paper has benefitted from constructive comments of two anonymous reviewers.

REFERENCES

- Amelin, Y.A., Larin, A.M., Tucker, R.D., 1997. Chronology of multiphase emplacement of the Salmi Rapakivi granite anorthosite complex, Baltic Shield: implications for magmatic evolution. *Contr. Mineral. Petrol.* 127, 353–368. <http://10.1007/s004100050285>
- Andersen, T., Andresen, A., Sylvester, A.G., 2002. Timing of late- to post-tectonic Sveconorwegian granitic magmatism in South Norway. *NGU Bulletin* 440, 5–18.
- Andersen, T., Griffin, W.L., Sylvester, A.G., 2007. Sveconorwegian crustal underplating in southwestern Fennoscandia: LAM-ICPMS U–Pb and Lu–Hf isotope evidence from granites and gneisses in Telemark, southern Norway. *LITHOS* 93, 273–187. <https://doi.org/10.1016/j.lithos.2006.03.068>
- Andersen, T., Graham, S. and Sylvester, A.G., 2009. The geochemistry, Lu-Hf isotope systematics, and petrogenesis of Late Mesoproterozoic A-type granites in southwestern Fennoscandia. *Can. Mineral.*, 47, 1399–1422. <https://doi.org/10.3749/canmin.47.6.1399>
- Andersson, U.B., Sjöström, H., Högdahl, K.H.O., Eklund, O., 2004. The Transscandinavian Igneous Belt, evolutionary models. In: *The Transscandinavian Igneous Belt (TIB) in Sweden: A Review of its Character and Evolution* (Högdahl K., Andersson U. B. (eds)). Geol. Survey Finland, Spec. Paper 37, Espoo, 104–112.
- Andresen, A., Agyei-Dwarko, N.Y., Kristoffersen, M., Hanken, N.-M., 2014. A Timanian foreland basin setting for the late Neoproterozoic – Early Paleozoic cover sequences (Dividal Group) of northeastern Baltica. *Geol. Soc. Spec. Publ.* 390, 157–175. <https://doi.org/10.1144/SP390.29>
- Areń, B., 1968. Tillites of Eastern Poland. *Inst. Geolog.*, 221–226.
- Aseeva, E.A., 1976. Microphytofossils and algae from the upper Precambrian deposits of Volyn-Podillya. In: *Paleontology and stratigraphy of the upper Precambrian and lower Cambrian from the southwestern part of the East European Platform*. Kyiv, Naukova Dumka, 40–63 (in Russian).
- Aseeva, E.A., 1988. Microfossils in Upper Precambrian. *Biostratigraphy and Paleogeographic Reconstructions of the Precambrian of Ukraine*. Kyiv, Naukova Dumka, 81–92 (in Russian).
- Bagnoli, G., Stouge, S. 2014. Upper Furongian (Cambrian) conodonts from the Degerhamn quarry road section, southern Öland, Sweden. *GFF* 136, 436–458. <https://doi.org/10.1080/11035897.2013.858768>

- Barham, M., Reynolds, S., Kirkland, C.L., O’Leary, M.J., Evans, N.J., Allen, H.J., Haines, P.W., Hocking, R.M., McDonald, B.J., 2018. Sediment routing and basin evolution in Proterozoic to Mesozoic east Gondwana: a case study from southern Australia. *Gondwana Res.* 58, 122–140. <https://doi.org/10.1016/j.gr.2018.03.006>
- Bekker, Yu.R., 1988. Precambrian molasse. Nedra Leningrad, 1–288 (in Russian).
- Belousova, E., Griffin, W., O’Reilly, S.Y., Fisher, N., 2002. Igneous zircon: trace element composition as an indicator of source rock type. *Contr. Mineral. Petrol.* 143, 602–622. <https://doi.org/10.1007/s00410-002-0364-7>
- Bingen, B., Nordgulden, Ø., Viola, G., 2008. A four-phase model for the Sveconorwegian orogeny, SW Scandinavia. *Norw. J. Geol.* 88, 43–72.
- Bingen, B., Viola, G., 2018. The early-Sveconorwegian orogeny in southern Norway: tectonic model involving delamination of the sub-continental lithospheric mantle. *Precam. Res.* 313, 170–204. <https://doi.org/10.1016/j.precamres.2018.05.025>
- Bogdanova, S.V., Page, L.M., Skridlaite, G., Taran, L.N., 2001. Proterozoic tectonothermal history in the western part of the East European Craton: 40Ar/39Ar geochronological constraints. *Tectonophys.* 339, 39–66. [https://doi.org/10.1016/S0040-1951\(01\)00033-6](https://doi.org/10.1016/S0040-1951(01)00033-6)
- Bogdanova, S.V., Bingen, B., Gorbatshev, R., Kheraskova, T.N., Kozlov, V.I., Puchkov, V.N., Volozh, Yu.A., 2008. The East European Craton (Baltica) before and during the assembly of Rodinia. *Precam. Res.* 160, 23–45. <https://doi.org/10.1016/j.precamres.2007.04.024>
- Bogdanova, S., Gorbatshev, R., Skridlaite, G., Soesoo, A., Taran, L., Kurlovich, D., 2015. Trans-Baltic Palaeoproterozoic correlations towards the reconstruction of supercontinent Columbia/Nuna. *Precam. Res.* 259, 5–33. <https://doi.org/10.1016/j.precamres.2014.11.023>
- Bogdanova, S.V., Gorbatshev, R., Garetsky, R.G., 2016. Europe/East European Craton. Reference Module in Earth Systems and Environmental Sciences, Elsevier, 1–18.
- Buła, Z., Habryn, R., 2011. Precambrian and Paleozoic basement of the Carpathian Foredeep and the adjacent Outer Carpathians (SE Poland and western Ukraine). *Ann. Soc. Geo. Polon.* 81, 221–239.
- Bukatchuk, P.D., 1973. Upper Precambrian deposits from the southwestern part of the East-European Platform, Stratigraphy and Paleogeography (Ph.D. Thesis). Moldovageology (in Russian), Chişinău, 1–272.

- Bukatchuk, P.D., Bliuk, I.B., Pokatilov, V.P., 1988. Geological map of the Moldavian Soviet Socialist Republic, scale 1:200 000. Explanatory notes. *Moldovageology*, Chişinău, 1–273 (in Russian).
- Bush, V.A., 2014. The deep structure of the Scythian Plate basement. *Geotectonics* 48/6, 413–426. <https://doi.org/10.1134/S0016852114060028>
- Cawood, P.A., Hawkesworth, C.J., Dhuime, B., 2012. Detrital zircon record and tectonic setting. *Geology* 40, 875–878. <https://doi.org/10.1130/G32945.1>
- Chumakov, N.M., 2015. Glaciations of the Earth. History, stratigraphic and biospheric significance. *Trans. Geol. Inst.* 611, 1–160 (in Russian).
- Claesson, S., Bogdanova, S.V., Bibikova, E.V., Gorbatshev, R., 2001. Isotopic evidence for Palaeoproterozoic accretion in the basement of the East European Craton. *Tectonophysics* 339, 1–18. [https://doi.org/10.1016/S0040-1951\(01\)00031-2](https://doi.org/10.1016/S0040-1951(01)00031-2)
- Claesson, S., Bibikova, E., Shumlyansky, L.V., Dhuime, B., Hawkesworth, C.J., 2015. The oldest crust in the Ukrainian Shield – Eoarchean U–Pb ages and Hf–Nd constraints from enderbites and metasediments. In: Roberts, N.M.W., Van Kranendonk, M., Parman, M., Shirey, S., Clift, P.D. (Eds.) *Continental Formation Through Time*. Geol. Soc., London, Spec. Publ. 227–259. <https://doi.org/10.1144/SP389.9>
- Claesson, S., Artemenko, G., Bogdanova, S., Shumlyansky, L., 2019. Archean crustal evolution in the Ukrainian shield. In: Martin J. Van Kranendonk, Vickie Bennett, Elis Hoffmann (Eds.), *Earth's oldest rocks*, second edition, 837–854. <https://doi.org/10.1016/B978-0-444-63901-1.00033-2>
- Cocks, L. R. M., Torsvik, T. H., 2005. Baltica from the late Precambrian to mid-Palaeozoic times: the gain and loss of a terrane's identity. *Earth-Sci. Rev.* 72, 39–66. <https://doi.org/10.1016/j.earscirev.2005.04.001>
- Cohen, P.A., Knoll, A.H., Kodner, R.B., 2009. Large spinose microfossils in Ediacaran rocks as resting stages of early animals. *Proc. Natl. Acad. Sci.* 106, 6519–6524. <https://dx.doi.org/10.1073/pnas.0902322106>
- Compston, W., Sambridge, M.S., Reinfrank, R.F., Moczyłowska, M., Vidal, G., Claesson, S., 1995. Numerical ages of volcanics and the earliest faunal zone within the Late Precambrian of East Poland. *J. Geol. Soc. London* 152, 599–611. <https://doi.org/10.1144/gsjgs.152.4.0599>

- Duchesne, J.-C., Shumlyansky, L., Mytrokhyn, O.V., 2017. The jotunite of the Korosten plutonic complex (Ukrainian shield): crust- or mantle-derived? *Precam. Res.* 299, 58–74. <http://doi.org/10.1016/j.precamres.2017.07.018>
- Ershova, V.B., Ivleva, A.S., Podkovyrov, V.N., Khudoley, A.K., Fedorov, P.V., Stockli, D., Anfinson, O., Maslov, A.V., Khubanov, V., 2019. Detrital zircon record of the Mesoproterozoic to 1282 Lower Cambrian sequences of NW Russia: implications for the paleogeography of the Baltic 1283 interior. *GFF* 141, 1–10. <http://doi.org/10.1080/11035897.2019.1625073>
- Fedo, C.M., Sircombe, K.N., Rainbird, R.H., 2003. Detrital zircon analysis of the sedimentary record. *Rev. Miner. Geochem.* 53, 277–303. <https://doi.org/10.2113/0530277>
- Francovschi, I., Grădinaru, E., Li, H., Shumlyansky, L., Ciobotaru V., 2021. U–Pb geochronology and Hf isotope systematics of detrital zircon from the late Ediacaran Kalyus Beds (East European Platform): paleogeographic evolution of southwestern Baltica and constraints on the Ediacaran biota. *Precam. Res.* 355, 106062. <https://doi.org/10.1016/j.precamres.2020.106062>
- Gaal, G., Gorbatshev, R., 1987. An outline of the Precambrian evolution of the Baltic Shield, *Precam. Res.* 35, 15–52.
- Gee, D.G., Beliakova, L., Pease, V., Larionov, A., Dovshikova, L., 2000. New, single zircon (Pb-evaporation) ages from Vendian intrusions in the basement beneath the Pechora Basin, northeastern Baltica. *Polarforschung, Bremerhaven, Alfred Wegener Institute for Polar and Marine Research & German Society of Polar Research* 68, 161–170.
- Gehrels, G. 2014. Detrital Zircon U–Pb Geochronology applied to tectonics. *Ann. Rev. Earth Planet. Sci.* 42, 127–149. <http://doi.org/doi.org/10.1146/annurev-earth-050212-124012>
- Gnilovskaya, M.B., 1979. Vendotaenids. *Paleontology of upper Precambrian and Cambrian deposits of the East European Platform.* 39–48 (in Russian).
- Gnilovskaya, M.B., Istchenko, A.A., Kolesnikov, C.M., Korenchuk, L.V., Udaltsov, A.P., 1988. Vendotaenids of the East European Platform. *Nauka, Leningrad*, 1–143 (in Russian).
- Gnilovskaya, M.B., 1990. Vendotaenids – Vendian Metaphyta. in *Vendian System*, Nauka, Moscow, Vol. 1, 117–125 (in Russian).

- Gojzhevsky, A.A., Skarzhynsky, V.I., Shumlyansky, V.A., 1984. Metallogeny of the Phanerozoic of the platformal part of Ukraine. Naukova Dumka publisher, 1–204 (in Russian).
- Gorbatshev, R., 2004. The Transscandinavian Igneous Belt – introduction and background. In: *The Transscandinavian Igneous Belt (TIB) in Sweden: A Review of its Character and Evolution* (Högdahl K., Andersson U. B. (eds)). Geol. Survey Finland, Spec. Paper 37, Espoo, 9–15.
- Grazhdankin, D., 2004. Late Neoproterozoic sedimentation in the Timan foreland. *Geological Society, London, Memoirs* 30, 37–46. <https://doi.org/10.1144/GSL.MEM.2004.030.01.04>
- Grazhdankin, D.V., Marusin, V.V., Meert, J., Krupenin, M.T., Maslov, A.V., 2011. Kotlin Regional Stage in the South Urals. *Doklady Earth Sci.* 440, 1222–1226. <https://doi.org/10.1134/S1028334X11090170>
- Gureev, Yu.A., 1988. Vendian Non-Skeletal Fauna. Biostratigraphy and Paleogeographic Reconstructions of the Precambrian of the Ukraine. Kyiv, Naukova Dumka, 65–80 (in Russian).
- Heinonen, A.P., Andersen, T., Rämö, O.T., 2010. Re-evaluation of rapakivi petrogenesis: source constraints from the Hf isotope composition of zircon in the rapakivi granites and associated mafic rocks of southern Finland. *J. Petrol.* 51, 1687–1709. <https://doi.org/10.1093/petrology/egq035>
- Heinonen, A., Andersen, T., Rämö, O.T., Whitehouse, M., 2015. The source of Proterozoic anorthosite and rapakivi granite magmatism: evidence from combined in situ Hf–O isotopes of zircon in the Ahvenisto complex, southeastern Finland. *J. Geol. Soc.* 172 (1), 103–112. <https://doi.org/10.1144/jgs2014-013>
- Högström, A.E.S., Jensen, S., Palacios, T., Ebbestad, J.O.R., 2013. New information on the Ediacaran–Cambrian transition in the Vestertana Group, Finnmark, northern Norway, from trace fossils and organic-walled microfossils. *Norwegian Journal of Geology* 93, 95–106.
- Hölttä, P., Kivisaari, T., Huhma, H., Rollinson, G., Kurhila, M., Butcher, A.R., 2020. Paleoproterozoic Metamorphism of the Archean Tuntsa Suite, Northern Fennoscandian Shield. *Minerals* 10/11, 1034. <https://doi.org/10.3390/min10111034>
- Hoskin, P.W.O., Schaltegger, U., 2003. The Composition of Zircon and Igneous and Metamorphic Petrogenesis. In: *Reviews in Mineralogy and Geochemistry*, 53/1, 27–62. <https://doi.org/10.2113/0530027>

- Hozhyk P.F., Semenenko V.M., Maslun N.V., Poletaev V.I., Ivanik M.M., Mikhnitska T.P., Velikanov V.Y., Melnychuk V.G., Konstantynenko L.I., Kyryanov V.V., Tsehelnjuk P.D., Kotlyar O.Y., Berchenko O.I., Vdovenko M.V., Shulha V.F., Nemyrovska T.I., Shchoholev O.K., Boyarina N.I., Efimenko V.I., Pyatkova D.M., Plotnikova L.F., Leshchukh P.Y., Zhabina N.M., Shevchuk O.A., Yakushyn L.M., Anikeeva O.V., Veklych O.D., Prykhodko M.G., Tuzyak Y.M., Matlai L.M., Dorotyak Y.B., Shainoha I.V., Klymenko Y.V., Hotsanyuk H.I., 2013. Stratigraphy of the upper Proterozoic and Phanerozoic of Ukraine. V. 1. Stratigraphy of the upper Proterozoic, Paleozoic and Mesozoic of Ukraine. Kyiv, Logos publisher, 1–637 (in Ukrainian).
- Isozaki, Y., Pöldvere, A., Bauert, H., Nakahata, H., Aoki, K., Sakata, S., Hirata, T., 2014. Provenance shift in Cambrian mid-Baltica: detrital zircon chronology of Ediacaran-Cambrian sandstones in Estonia. *Estonian J. Earth Sci.* 63 (4), 251–256. <http://doi.org/10.3176/earth.2014.27>
- Ivanchenko, K.V., Mikhnitska, T.P., Mateyuk, V.V., Melnychuk, V.G., Kosovskiy, Y.O., Hrechko, F.O., 2004. Vendian microfossils of the Volyn region and their stratigraphic significance. *Heologichnyi Zhurnal*, 4, 44–52 (in Ukrainian).
- Ivanchenko K.V., 2007. Microfossils of the Vendian of Volyn and their stratigraphic significance. Resume of the Ph.D. thesis, Kyiv, 1–32 (in Ukrainian).
- Ivantsov A.Yu., Gritsenko V.P., Paliy V.M., Velikanov V.A., Konstantinenko L.I., Menasova A.Sh., Fedonkin M.A., Zakrevskaya M.A., Serezhnikova E.A., 2015. Upper Vendian macrofossils of Eastern Europe. Middle Dniester area and Volhynia. Moscow, PIN RAS. 1–144.
- Ivleva, A.S., Podkovyrov, V.N., Ershova, V.B., Anfinson, O.A., Khudoley, A.K., Fedorov, P.V., Maslov, A.V., Zdobin, D.Yu., 2016. Results of U–Pb LA–ICP–MS dating of detrital zircons from Ediacaran-Early Cambrian deposits of the Eastern part of the Baltic Monocline. *Dokl. Earth Sci.* 1374 468, 593–597. <https://doi.org/10.1134/S1028334X16060064>
- Ivleva, A.S., Podkovyrov, V.N., Ershova, V.B., Khubanov, V.B., Khudoley, A.K., Sychev, S.N., Vdovina, N.I., Maslov, A.V., 2018. U–pb LA–ICP–MS age of detrital zircons from the Lower Riphean and Upper Vendian deposits of the Luga–ladoga Monocline. *Doklady Earth Sci.* 480/2, 695–699. <https://doi.org/10.1134/S1028334X1806003X>
- Jackson, S.E., Pearson, N.J., Griffin, W.L., Belousova, E.A., 2004. The application of laser ablation-inductively coupled plasma-mass spectrometry to in situ U–Pb zircon

geochronology. Chem. Geol. 211, 47–69.
<https://doi.org/10.1016/j.chemgeo.2004.06.017>

Jensen, S., 2003. The proterozoic and earliest cambrian trace fossil record; patterns, problems and perspectives. *Integrative and Comparative Biology* 43/1, 219–228.
<https://doi.org/10.1093/icb/43.1.219>

Jensen, S., Högström, E.E., Hoyberget, M., Meinhold, G., McIlroy, D., Ebbestad, J.O.R., Agic, H., Palacios, T., 2018. New occurrences of *Palaeopascichnus* from the Ståhpogieddi Formation, Arctic Norway, and their bearing on the age of the Varanger Ice Age. *Canadian J. Earth Sci.* 55/11, 1253–1261.
<https://doi.org/10.1139/cjes-2018-0035>

Johansson, Å., Waight, T., Andersen, T., Simonsen, S.L., 2016. Geochemistry and petrogenesis of Mesoproterozoic A-type granitoids from the Danish island of Bornholm, southern Fennoscandia. *Lithos* 244, 94–108.
<https://doi.org/10.1016/j.lithos.2015.11.031>

Kheraskova, T.N., Volozh, Yu.A., Antipov, M.P., Bykadorov, V.A., Sapozhnikov, R.B., 2015. Correlation of Late Precambrian and Paleozoic events in the East European Platform and the adjacent paleoceanic domains. *Geotectonics* 49, 27–52.
<http://doi.org/10.1134/S0016852115010021>

Kirkland, C., Bingen, B., Whitehouse, M., Beyer, E., Griffin, W. L. 2011. Neoproterozoic Palaeogeography in the North Atlantic Region: inferences from the Akkajaure and Seve Nappes of the Scandinavian Caledonides. *Precambrian Research*, 186, 127–146. <https://doi.org/10.1016/j.precamres.2011.01.010>

Kirs, J., Puura, V., Soesoo, A., Klein, V., Konsa, M., Koppelmaa, H., Niin, M., Urtson, K., 2009. The crystalline basement of Estonia: rock complexes of the Paleoproterozoic Orosirian and Statherian and Mesoproterozoic Calymmian Periods, and regional correlations. *Estonian Journal of Earth Sciences*, 58, 219–228.

Kirs, J., Petersell, V., 1994. Age and geochemical character of plagiomicrocline granite veins in the Abja gabbro-dioritic massif. In: A. Loog, J. Kirs and L. Ainsaar (Editors), *Eesti alusp Shja geokeemia ja mineraloogia küsimusi--T/Sid geoloogia alalt XIV*. *Acta et Commentationes Universitatis Tartuensis*, 972. 3–15.

Korja, A., Lahtinen, R., Nironen, M., 2006. The Svecofennian orogen: A collage of microcontinents and island arcs. *Geol. Soc. Mem.* 32, 561–578.
<http://doi:10.1144/GSL.MEM.2006.032.01.34>

- Kotyk, V.A., Markovskiy, V.M., Makovskaya, I.A., 1976. Upper Proterozoic deposits from western Ukraine, based on borehole data. *Tectonics and Stratigraphy*, 61–74 (in Russian).
- Kozlovskaya, E., Kosarev, G., Aleshin, I., Riznichenko, O., Sanina, I., 2008. Structure and composition of the crust and upper mantle of the Archean-Proterozoic boundary in the Fennoscandian shield obtained by joint inversion of receiver function and surface wave phase velocity of recording of the SVEKALAPKO array. *Geophysical Journal International* 175, 135–152. <https://doi.org/10.1111/j.1365-246X.2008.03876.x>
- Kushim, E.A., Golubkova, E.Y., Plotkina, Y.V., Biostratigraphic characteristics of the Vendian – Cambrian deposits of the South Ladoga. *Vestnik VGU Geo.* 4, 18–22 (in Russian).
- Kuzmenkova, O.F., Nosova, A.A., Shumlyansky, L.V., 2010. A comparison of the Neoproterozoic Volyn-Brest magmatic province with large continental flood basalt provinces of the world, the nature of low-Ti and high-Ti basic magmatism. *Litosfera*, 33, 3–16 (in Russian).
- Kuznetsov, N.B., Soboleva, A.A., Udoratina, O.V., Hertseva, M.V., Andreichev, V., 2007: Pre-Ordovician tectonic evolution and volcano–plutonic associations of the Timanides and northern Pre-Uralides, northeast part of the East European Craton. *Gondwana Res.* 12, 305–323. <https://doi.org/10.1016/j.gr.2006.10.021>
- Kuznetsov, N.B., Orlov, S.Y., Miller, E.L., Shazillo, A.V., Dronov, A.V., Soboleva, A.A., Udoratina, O.V., Gehrels, G., 2011. First results of U/Pb dating of detrital zircons from Early Paleozoic and Devonian sandstones of the Baltic-Ladoga Region (south Ladoga area). *Doklady Earth Sci.* 438/2, 759–765. <https://doi.org/10.1134/S1028334X11060316>
- Kuznetsov, N.B., Alekseev, A.S., Belousova, E.A., Romanyuk, T.V., Reimers, A.N., Tselmovich, V.A., 2014a. Testing the models of late Vendian evolution of the northeastern periphery of the East European Craton based on the first U/Pb dating of detrital zircons from upper Vendian sandstones of southeastern White Sea Region. *Doklady Earth Sci.* 458/1, 1073–1076. <https://doi.org/10.1134/S1028334X14090311>
- Kuznetsov, N.B., Belousova, E.A., Alekseev, A.S., Romanyuk, T.V., 2014b. New data on detrital zircons from the sandstones of the lower Cambrian Brusov Formation (White Sea region, East-European Craton): unravelling the timing of the onset of the Arctida–Baltica collision. *Int. Geol. Rev.* 56/16, 1945–1963. <https://doi.org/10.1080/00206814.2014.977968>

- Kuznetsov, N.B., Romanyuk, T.V., 2021. Peri-Gondwanan blocks in the structure of the southern and southeastern framing of the East European Platform. *Geotectonics* 55/4, 439-472 (in Russian). <https://doi.org/10.31857/S0016853X2104010X>
- Lahtinen, R., Korja, A., Nironen, M., 2005. Paleoproterozoic tectonic evolution. In: M. Lehtinen, P.A. Nurmi, & O.T. Rämö (eds.): *Precambrian geology of Finland—key to the evolution of the Fennoscandian Shield*, 481–532. Elsevier, Amsterdam.
- Larson, S.Å., Berglund, J., 1992. A chronological subdivision of the Transscandinavian Igneous Belt – three magmatic episodes? *GFF* 115, 459–461. <https://doi.org/10.1080/11035899209453912>
- Liivamägi, S., Somelar, P., Mahaney, W.C., Kirs, J., Vircava, I., Kirsimäe, K., 2014. Late Neoproterozoic Baltic paleosol: Intense weathering at high latitude? *Geology* 42(4), 323–326. <https://doi.org/10.1130/G35209.1>
- Liivamägi, S., Somelar, P., Vircava, I., Mahaney, W.C., Kirs, J., Kirsimäe, K., 2015. Petrology, mineralogy and geochemical climofunctions of the Neoproterozoic Baltic paleosol. *Precam. Res.* 256, 170–188. <https://doi.org/10.1016/j.precamres.2014.11.008>
- Lorentzen, S., Augustsson, C., Nystuen, J.P., Berndt, J., Jahren, J., Schovsbo, N.H., 2018. Provenance and sedimentary processes controlling the formation of lower Cambrian quartzarenite along the southwestern margin of Baltica. *Sed. Geol.* 375, 203–217. <https://doi.org/10.1016/j.sedgeo.2017.08.008>
- Lundmark, A.M., Lamminen, J., 2016. The provenance and setting of the Mesoproterozoic Dala Sandstone, western Sweden, and paleogeographic implications for southwestern Fennoscandia. *Precam. Res.* 275, 197–208. <https://doi.org/10.1016/j.precamres.2016.01.003>
- Makhnach, A.S., Garetskiy, R.G., Matveev, A.V., Aposhko, Y. I., Ilikevich, G.I., Kopsishev, V.S., Kruchek, S.A., Makhnach, A.A., Naydenkov, I.V., Pashkevich, V.I., 2001. *Geology of Belarus*. Institute of Geological Sciences. Minsk, Belarus, 1–815 (in Russian).
- Makhnach, A.S., Veretennikov, N.V., Shkuratov, V.I., Laptsevich, A.G., Piskun, L.V., 2005. Stratigraphic chart of Vendian deposits of Belarus. *Litasfera* 22, 36–44 (in Russian).

- McIlroy, D., Green, O.R., Brasier, M.D., 2001. Palaeobiology and evolution of the earliest agglutinated Foraminifera: Platysolenites, Spirosolenites and related forms. *Lethaia* 34, 13–29.
- McIlroy, D., Brasier, M.D., 2017. Ichnological evidence for the Cambrian explosion in the Ediacaran to Cambrian succession of Tanafjord, Finnmark, northern Norway. *Geol. Soc. Spec. Publ.* 448/1, 351–368. <https://doi.org/10.1144/SP448.7>
- Meidla, T., 2017. Ediacaran and Cambrian stratigraphy in Estonia: an updated review. *Estonian J. Earth Sci.* 66/3, 152–160.
- Melnychuk, G.V., 2013. The Paleoproterozoic crystalline basement of the Volyn Paleozoic uplift. Peculiarities of the construction and geological history. *Geol. Zhurnal* 4, 24–32 (in Ukrainian).
- Mens, K., Pirrus, E., 1971. On stratigraphy of the boundary layers between the Vendian and Cambrian on the northwest of the Russian platform. *Izvestiya Akademii Nauk SSSR, Seriya Geologicheskaya* 11, 93-103 (in Russian).
- Mens, K., Viira, V., Paalits, I., Puura, I., 1993. Upper Cambrian biostratigraphy of Estonia. *Proceed. Estonian Acad. Sci. Geology* 42, 148–159.
- Mens, K., Pirrus, E., 1997a. Vendian. In *Geology and Mineral Resources of Estonia* (Raukas, A., Teedumäe, A., eds). Estonian Academy Publishers, Tallinn. 35–38.
- Mens, K., Pirrus, E., 1997b. Cambrian. In *Geology and Mineral Resources of Estonia* (Raukas, A., Teedumäe, A., eds). Estonian Academy Publishers, Tallinn, 39–51.
- Merdith, A.S., Collins, A.S., Williams, S.E., Pisarevsky, S., Foden, J.D., Archibald, D.B., Blades, M.L., Alessio, B.L., Armistead, S., Plavsa, D., Clark, C., Dietmar Muller, R., 2017. A full-plate global reconstruction of the Neoproterozoic. *Gondwana Res.* 50, 84–134. <http://dx.doi.org/10.1016/j.gr.2017.04.001>
- Miller, E.L., Kuznetsov, N., Soboleva, A., Udoratina, O., Grove, M.J., Gehrels, G., 2011. Baltica in the Cordillera? *Geology* 39/8, 791–794. <https://doi.org/10.1130/G31910.1>
- Moczydlowska, M., 1991. Acritarch biostratigraphy of the Lower Cambrian and the Precambrian-Cambrian boundary in southeastern Poland. *Fossils and Strata* 29, 1–127.
- Möller, C., Andersson, J., Dyck, B., Lundin, I., 2015. Exhumation of an eclogite terrane as a hot migmatitic nappe, Sveconorwegian orogeny. *Lithos* 226, 147–168. <https://doi.org/10.1016/j.lithos.2014.12.013>

- Muscente, A. D., Boag, T. H., Bykova, N., Schiffbauer, J. D., 2018. Environmental disturbance, resource availability, and biologic turnover at the dawn of animal life. *Earth Sci. Rev.* 177, 248–264. <https://doi.org/10.1016/j.earscirev.2017.11.019>
- Narbonne, G.M., Myrow, P.M., Landing, E., and Anderson, M.M., 1987, A candidate stratotype for the Precambrian-Cambrian boundary, Fortune Head, Burin Peninsula, southeastern New- foundland: *Canadian J. of Earth Sci.* 24, 1277–1293.
- Nesterovsky, V.A., Martyshyn, A.I., Chupryna, A.M., 2018. New biocenosis model of Vendian (Ediacaran) sedimentation basin of Podilia (Ukraine). *J. Geol., Geogr. Geocol.* 27/1, 95–107.
- Nielsen, A.T., Schovsbo, N.H., 2011. The Lower Cambrian of Scandinavia: depositional environment, sequence stratigraphy and palaeogeography. *Earth-Sci. Rev.*, 107, 207–310. <https://doi.org/10.1016/j.earscirev.2010.12.004>
- Nikishin, A.M., Ziegler, P.A., Stephenson, R.A., Cloetingh, S.A.P.L., Furne, A.V., Fokin, P.A., Eshov, A.V., Bolotov, S.N., Korotaev, M.V., Alekseev, A.S., Gorbachev, V.I., Shipilov, E.V., Lankreijer, A., Bembinova, E.Y., Shalimov, I.V., 1996. Late Precambrian to Triassic history of the East European Craton: dynamics of sedimentary basin evolution. *Tectonophysics* 268, 23–63. [https://doi.org/10.1016/S0040-1951\(96\)00228-4](https://doi.org/10.1016/S0040-1951(96)00228-4)
- Nironen, M., 1997: The Svecofennian orogen: a tectonic model. *Precam. Res.* 86, 21–44. [https://doi.org/10.1016/S0301-9268\(97\)00039-9](https://doi.org/10.1016/S0301-9268(97)00039-9)
- Orlov, S.Yu., Kuznetsov, N.B., Miller, E.D., Soboleva, A.A., Udoratina, O.V., 2011. Age constraints for the Pre-Uralide-Timanide Orogenic event inferred from the study of detrital zircons. *Doklady Earth Sci.* 440/1, 1216–1221. <https://doi.org/10.1134/S1028334X11090078>
- Paczeńska, J., 2014. Lithostratigraphy of the Ediacaran deposits in the Lublin-Podlasie sedimentary basin (eastern and south-eastern Poland). *Biul. Panzst. Inst. Geol.* 460, 1–24.
- Paszkowski, M., Budzyn, B., Mazur, S., Slama, J., Shumlyanskyy, L., Środoń, J., Dhuime, B., Kedzior, A., Liivamagi, S., Piszczowska, A., 2019. Detrital zircon U–Pb and Hf constraints on provenance and timing of deposition of the Mesoproterozoic to Cambrian sedimentary cover of the East European Craton, Belarus. *Precambr. Res.* 331, 1–19. <http://doi.org/10.1016/j.precamres.2019.105352>
- Paszkowski, M., Budzyn, B., Mazur, S., Slama, J., Środoń, J., Millar, I.L., Shumlyanskyy, L., Kędzior, A., Liivamägi, S., 2021. Detrital zircon U-Pb and Hf constraints on

- provenance and timing of deposition of the Mesoproterozoic to Cambrian sedimentary cover of the East European Craton, part II: Ukraine. *Precam. Res.* 362, 106282. <https://doi.org/10.1016/j.precamres.2021.106282>
- Pease, V., Dovzghikova, E., Beliakova, L., Gee, D.G., 2004. Late Neoproterozoic granitoid magmatism in the basement to the Pechora Basin, NW Russia: geochemical constraints indicate westward subduction beneath NE Baltica. In D.G. Gee & V. Pease (eds.): *The Neoproterozoic Timanide Orogen of Eastern Baltica*. *Geol. Soc., London Memoirs* 30, 75–85.
- Pehr, K., Love, G.D., Kuznetsov, A., Podkovyrov, V., Junium, C.K., Shumlyanskyy, L., Sokur, T., Bekker, A., 2018. Ediacara biota flourished in oligotrophic and bacterially dominated marine environments across Baltica. *Nature Communications* 9, 1–10. <https://doi.org/10.1038/s41467-018-04195-8>
- Petersell, V., Levchenkov, O., 1994. On the geological structure of the crystalline basement of the southern slope of the Baltic Shield. *Acta Comment. Univ. Tartuensis* 972, 3–15
- Pirrus, E., 1992. Freshening of the late Vendian basin on the East European Craton. *Proceedings of the Estonian Academy of Sciences. Geology* 41, 115–123.
- Pöldvere, A., Isozaki, Y., Bauert, H., Aoki, K., Sakata, S., Hirata, T., 2014. Detrital zircon ages of Cambrian and Devonian sandstones from Estonia, central Baltica: a possible link to Avalonia during the Late Neoproterozoic. *GFF* 136, 214–217. <https://doi.org/10.1080/11035897.2013.873986>
- Ponomarenko, A.N., Stepanyuk, L.M., Shumlyanskyy, L.V., 2014. Geochronology and geodynamics of Paleoproterozoic of the Ukrainian Shield. *Min. J. (Ukraine)* 36 (2), 48–60 (in Russian).
- Poprawa, P., Krzeminska, E., Paczesna, J., Armstrong, R., 2020. Geochronology of the Volyn volcanic complex at the western slope of the East European Craton – relevance to the Neoproterozoic rifting and the break-up of Rodinia/Pannotia. *Precamb. Res.* 346, 105817. <https://doi.org/10.1016/j.precamres.2020.105817>
- Puchkov, V.N., 2010. *Geology of the Urals and Cis-Urals (actual problems of stratigraphy, tectonics, geodynamics and metallogeny)*. Ufa, DesignPoligraphService, 1–280 (in Russian).
- Puura, V., Vaher, R., Klein, V., Koppelmaa, H., Niin, M., Vanamb, V., Kirs, J., 1983. *Crystalline basement of Estonia*. Moscow, Nauka Publ., 1–208 (in Russian).

- Puura, V., Vaher, R., 1997. Deep structure. In: Raukas, A. & Teedumäe, A. (eds). *Geology and mineral resources of Estonia*. Estonian Academy Publishers, Tallinn, 163.
- Rämö, O.T., Turkki, V., Mänttari, I., Heinonen, A., Larjamo, K.L., Ahaye, Y., 2014. Age and isotopic fingerprints of some plutonic rocks in the Wiborg rapakivi granite batholith with special reference to the dark wiborgite of the Ristisaari island. *Bull. Geol. Soc. Finland* 86, 71–91. <https://doi.org/10.17741/bgsf/86.2.002>
- Roban, R.D., Ducea, M.N., Maţenco, L., Panaiotu, G.C., Profeta, L., Krezsek, C., Melinte-Dobrinescu, M.C., Anastasiu, N., Dimofte, D., Apostrosoaei, V., Francovschi, I., 2020. Lower Cretaceous provenance and sedimentary deposition in the Eastern Carpathians: Inferences for the evolution of the subducted oceanic domain and its European passive continental margin. *Tectonics* 39/7. <https://doi.org/10.1029/2019TC005780>
- Roberts, D., Siedlecka, A., 2002. Timanian orogenic deformation along the northeastern margin of Baltica, Northwest Russia and Northeast Norway, and Avalonian–Cadomian connections. *Tectonophysics* 352, 169–184. [https://doi.org/10.1016/S0040-1951\(02\)00195-6](https://doi.org/10.1016/S0040-1951(02)00195-6)
- Rubatto, D., 2002. Zircon trace element geochemistry: partitioning with garnet and the link between U–Pb ages and metamorphism. *Chem. Geol.* 184, 123–138. [https://doi.org/10.1016/S0009-2541\(01\)00355-2](https://doi.org/10.1016/S0009-2541(01)00355-2)
- Rubatto, D., 2017. Zircon: The Metamorphic Mineral. *Reviews in Mineralogy and Geochemistry* 83/1, 261–295. <https://doi.org/10.2138/rmg.2017.83.9>
- Schatsky, N.S., 1935. On tectonics of the Arctic. *Geology and Economic Deposits in northern USSR*, vol. 1, 476–509 (in Russian).
- Shcherbak, N.P., Artemenko, G.V., Lesnaya, I.M., Ponomarenko, A.N., 2005. Geochronology of the early Precambrian of the Ukrainian Shield. *Archean*. Kyiv. Naukova dumka publisher, 1–1244 (in Russian).
- Shumlyanskyy, L.V., Andréasson, P.G., Buchan, K.L., Ernst, R.E., 2007. The Volynian Flood Basalt Province and coeval (Ediacaran) magmatism in Baltoscandia and Laurentia. *Mineral. J. (Ukr.)*, 29, 47–55.
- Shumlyanskyy, L., Billstrom, K., Hawkesworth, C., Elming, S.-Å., 2012. U–Pb age and Hf isotope compositions of zircons from the north-western region of the Ukrainian shield: mantle melting in response to post-collision extension. *Terra Nova* 24, 373–379. <http://doi.org/10.1111/j.1365-3121.2012.01075.x>

- Shumlyanskyy, L., 2014. Geochemistry of the Osnitsk-Mikashevichy volcanoplutonic complex of the Ukrainian Shield. *Geochem. Int.* 52, 912–924. <http://doi.org/10.1134/S0016702914110081>
- Shumlyanskyy, L., Hawkesworth, C., Dhuime, B., Billström, K., Claesson, S., Storey, C., 2015a. 207Pb/206Pb ages and Hf isotope composition of zircons from sedimentary rocks of the Ukrainian shield: crustal growth of the south-western part of East European craton from Archaean to Neoproterozoic. *Precam. Res.* 260, 39–54. <https://doi.org/10.1016/j.precamres.2015.01.007>
- Shumlyanskyy, L., Bekker, A., Claesson, S., 2015b. U-Pb zircon geochronology of rocks of the Teteriv Series, Northwestern region of the Ukrainian shield. *Actual problems in Earth sciences. Abstract volume. Brest, Belarus, 21-25 Sept. 2015*, 242–244.
- Shumlyanskyy, L., Ernst, R., Söderlund, U., Billström, K., Mitrokhin, O., Tsymbal, S., 2016a. New U–Pb ages for mafic dykes in the Northwestern region of the Ukrainian shield: coeval tholeiitic and jotunitic magmatism. *GFF* 138, 79–85. <http://doi.org/10.1080/11035897.2015.1116602>
- Shumlyanskyy, L., Nosova, A., Billström, K., Söderlund, U., Andréasson, P.-G., Kuzmenkova, O., 2016b. The U-Pb zircon and baddeleyite ages of the Neoproterozoic Volyn Large Igneous Province: Implication for the age of the magmatism and the nature of a crustal contaminant. *GFF* 138, 17–30. <https://doi.org/10.1080/11035897.2015.1123289>
- Shumlyanskyy, L., Krzemińska, E., Kuzmenkova, O., Nosova, A., 2018. Geochemistry of picrites of the Ediacaran Volyn continental flood basalt province. In: *Geology and mineral resources of Ukraine. Abstract volume of the conference dedicated to the 100th anniversary of the National Academy of Sciences of Ukraine, 2-4 October 2018, Kyiv*, 259–261.
- Shumlyanskyy, L., Hawkesworth, C., Billström, K., Bogdanova, S., Mytrokhyn, O., Romer, R., Dhuime, B., Claesson, S., Ernst, R., Whitehouse, M., Bilan, O., 2017. The origin of the Palaeoproterozoic AMCG complexes in the Ukrainian Shield: new U–Pb ages and Hf isotopes in zircon. *Precam. Res.* 292, 216–239. <http://doi.org/10.1016/j.precamres.2017.02.009>
- Shumlyanskyy, L.V., Stepanyuk, L.M., Claesson, S., Rudenko, K.V., Bekker, A.Y., 2018. The U–Pb zircon and monazite geochronology of granitoids of the Zhytomyr and Sheremetiv Complexes, the North-Western region of the Ukrainian Shield. *Mineral. J. (Ukraine)* 40(2), 63–85 (in Ukrainian).
- Shumlyanskyy, L., Wilde, S.A., Nemchin, A.A., Claesson, S., Billström, K., Bagiński, B., 2021a. Eoarchean rock association in the Dniester-Bouh Domain of the Ukrainian

- shield: a suite of LILE-depleted enderbites and mafic granulites. *Precam. Res.*, 352, 106001. <https://doi.org/10.1016/j.precamres.2020.106001>
- Shumlyanskyy, L., Ernst, R.E., Albekov, A., Söderlund, U., Wilde, S.A., Bekker A., 2021b. The early Statherian (ca. 1800-1750 Ma) Prutivka-Novogol large igneous province of Sarmatia: geochronology and implication for the Nuna/Columbia supercontinent reconstruction. *Precam. Res.* 106185. <https://doi.org/10.1016/j.precamres.2021.106185>
- Shumlyanskyy L., Franz G., Glynn S., Mytrokhyn O., Voznyak D., Bilan O., 2021c. Geochronology of granites of the western Korosten AMCG complex (Ukrainian Shield): implications for the emplacement history and origin of miarolitic pegmatites. *European J. Mineral.*, 33, 703–716. <https://doi.org/10.5194/ejm-33-703-2021>
- Skridlaite, G., Baginski, B., Whitehouse, M., 2008. Significance of ~1.5 Ga zircon and monazite ages from charnockites in southern Lithuania and NE Poland. *Gondwana Res.* 14, 663–674. <https://doi.org/10.1016/j.gr.2008.01.009>
- Sláma, J., Košler, J., Condon, D.J., Crowley, J.L., Gerdes, A., Hanchar, J.M., Horstwood, M.S., Morris, G.A., Nasdala, L., Norberg, N., 2008. Plešovice zircon – a new natural reference material for U–Pb and Hf isotopic microanalysis. *Chem. Geol.* 249, 1–35. <http://doi.org/10.1016/j.chemgeo.2007.11.005>
- Sláma, J., Pedersen, R.B., 2015. Zircon provenance of SW Caledonian phyllites reveals a distant Timanian sediment source. *J. Geol. Soc.* 172/4, 465–478. <https://doi.org/10.1144/jgs-143>
- Sláma, J., 2016. Rare late Neoproterozoic detritus in SW Scandinavia as a response to distant tectonic processes. *Terra Nova* 28/6, 394–401. <https://doi.org/10.1111/ter.2016.28.issue-6>
- Sliaupa, S., Fokin, P., Lazauskiene, J., Stephenson, A., 2006. The Vendian-Early Palaeozoic sedimentary basins of the East European Craton. *Geological Society London* 32, 449–462. <https://10.1144/GSL.MEM.2006.032.01.28>
- Sokolov, B.S., 2011. The chronostratigraphic space of the lithosphere and the Vendian as a geohistorical subdivision of the Neoproterozoic. *Geol. Geophys.* 52, 1334–1348 (in Russian, with English summary).
- Söderlund, U., Isachsen, C., Bylund, G., Heaman, L., Patchett, J., Vervoort, J., Andersson, U., 2005. U–Pb baddeleyite ages and Hf, Nd isotope chemistry constraining repeated mafic magmatism in the Fennoscandian Shield from 1.6 to 0.9 Ga.

- Contrib. Mineral Petrol. 150, 174–194. <https://doi.org/10.1007/s00410-005-0011-1>
- Soesoo, A., Puura, V., Kirs, J., Petersell, V., Niin, M., All, T., 2004. Outlines of the Precambrian basement of Estonia. *Proc. Est. Acad. Sci., Geology* 53, 149–164.
- Soesoo, A., Kosler, J., Kuldkepp, R., 2006. Age and geochemical constraints for partial melting of granulites in Estonia. *Miner. and Pet.* 86, 277–300. <http://doi.org/10.1007/s00710-005-0110-8>
- Soesoo, A., Hade, S., 2012. Geochemistry and age of some A-type granitoid rocks of Estonia. *LITHOSPHERE 2012 - Symposium (Nov. 6-8, 2012)*. Espoo, Finland 97–101.
- Soesoo, A., Nirgi, S., Plado, J., 2020. The evolution of the Estonian Precambrian basement: geological, geophysical and geochronological constraints. *Proceedings of the Karelian Research Centre of The Russian Academy of Sciences* 2, 18–33. <https://doi.org/10.17076/geo1185>
- Soesoo, A., Nirgi, S., Urtson, K. and Voolma, M., 2021. Geochemistry, mineral chemistry and pressure–temperature conditions of the Jõhvi magnetite quartzites and magnetite-rich gneisses, Estonia. *Est. J. Earth Sci.* 70, 71–93. <https://doi.org/10.3176/earth.2021.05>
- Soldatenko, Y., El Albani, A., Ruzina, M., Fontaine, C., Nesterovsky, V., Paquette, J.-L., Meunier, A., Ovtcharova, M., 2019. Precise U–Pb age constrains on the Ediacaran biota in Podolia, East European Platform, Ukraine. *Sci. Reports* 9, 1–13. <https://doi.org/10.1038/s41598-018-38448-9>
- Stepanyuk, L.M., Kurylo, S.I., Dovbush, T.I., Grinchenko, O.V., Syomka, V.O., Bondarenko, S.M., Shumlyansky, L.V., 2017. Geochronology of granitoids of the eastern part of the Inhul region (the Ukrainian Shield). *Geochem. Ore Form.* 38, 3–13. <https://doi.org/10.15407/gof.2017.38.003>
- Valverde-Vaquero, P., Dörr, W., Belka, Z., Franke, W., Wiszniewska, J., Schastok, J., 2000. U–Pb single-grain dating of detrital zircon in the Cambrian of central Poland: implications for Gondwana versus Baltica provenance studies. *Earth Planet. Sci. Lett.* 184, 225–240. [http://doi.org/10.1016/S0012-821X\(00\)00312-5](http://doi.org/10.1016/S0012-821X(00)00312-5)
- Velikanov, V.A., Aseeva, E.A., Fedonkin, M.A., 1983. Vendian of Ukraine. *Naukova Dumka*, Kiev, 1–161 (in Russian).
- Veretennikov, N.V., Vernikovskiy, V.N., Klevtsova, A.A., 1972. Tillites in the upper Precambrian of Belarus and northwestern Ukraine (Volyn) and their significance

for the stratigraphy of the transitional layers between the Riphean and Vendian. *Novye dannye po geol. i neftegaz. USSR* 7, 3–18 (in Russian).

- Vlasov, B.I., Volovnik, B.Ya., Gruzman, G.G., 1972. Peculiarities of the structure and the principle of the stratification of the Polissya Series in Volyn. *Geol. J.* 32/4, 56–67 (in Russian).
- Vysotsky, O.B., Stepanyuk, L.M., Shumlyansky, L.V., 2021. The U-Pb zircon age of the pre-Klesiv rock association in the Osnitsk block. *Geochem. Ore Formation*, 42, 80–88 (in Ukrainian). <https://doi.org/10.15407/gof.2021.42.080>
- Weber, B., Schmitt, A.K., Cisneros de León, A., Gonzalez-Guzman, R., Gerdes, A., 2020. Neoproterozoic extension and the Central Iapetus Magmatic Province in southern Mexico – New U–Pb ages, Hf–O isotopes and trace element data of zircon from the Chiapas Massif Complex. *Gondwana Res.* 88, 1–20. <https://doi.org/10.1016/j.gr.2020.06.022>
- Wiedenbeck, M., Alle, P., Corfu, F., Griffin, W.L., Meier, M., Oberli, F., von Quadt, A., Roddick, J.C., Spiegel, W., 1995. Three natural zircon standards for U-Th-Pb, Lu-Hf, trace-element and REE analyses. *Geostand. Newslett.* 19, 1–23. <http://doi.org/10.1111/j.1751-908X.1995.tb00147.x>
- Wiszniewska, J., Kusiak, M.A., Krzemińska, E., Dörr, W., Suzuki, K., 2007. Mesoproterozoic AMCG granitoids in the Mazury complex, NE Poland — a geochronological update. *Granitoids Poland AM Monograph* 1, 31–39.
- Wiszniewska, J., Krzemińska, E., 2021. Advances in geochronology in the Suwałki anorthosite massif and subsequent granite veins, northeastern Poland. *Precamb. Res.*, 361, 106265. <https://doi.org/10.1016/j.precamres.2021.106265>
- Yang, C., Rooney, A.D., Condon, D.J., Li, X.-H., Grazhdankin, D.V., Bowyer, F.T., Hu, C., Macdonald, F.A., Zhu, M., 2021. The tempo of Ediacaran evolution. *Sci. Adv.* 7, eabi9643. <https://doi.org/10.1126/sciadv.abi9643>
- Yesypchuk, K.Yu., Bobrov, O.B., Stepanyuk, L.M., Shcherbak, M.P., Glevaskiy, E.B., Skobelev, V.M., Drannik, V.S. and Geichenko, M.V. 2004. Correlated chronostratigraphic scheme of Early Precambrian of the Ukrainian Shield (scheme and explanatory note), NSC Ukraine, UkrDGRI, Kyiv, 1–30 (in Ukrainian).
- Youbi, N., Ernst, R.E., Soderlund, U., Boumehdi, M.A., Ait Lahna, A., Tassinari, C.C.G., El Moume, W., Bensalah, M.K., 2020. The Central Iapetus magmatic province: An updated review and link with the ca. 580 Ma Gaskiers glaciation. In: Adatte, T., Bond, D.P.G., and Keller, G., eds., *Mass Extinctions, Volcanism, and Impacts:*

New Developments. Geol. Soc. Am. Spec. Paper 544.
[https://doi.org/10.1130/2020.2544\(02\)](https://doi.org/10.1130/2020.2544(02))

Żelaźniewicz, A., Buła, Z., Fanning, M., Seghedi, A., Żaba, J., 2009. More evidence on Neoproterozoic terranes in Southern Poland and southeastern Romania. *Geological Quarterly*, 53/1, 93–124.

Żelaźniewicz, A., Oberc-Dziedzic, T., Slama, J., 2020. Baltica and the Cadomian orogen in the Ediacaran–Cambrian: a perspective from SE Poland. *Int. J. Earth Sci (Geol Rundsch)* 109, 1503–1528. <http://doi.org/10.1007/s00531-020-01858-0>

CHAPTER 5

Conclusions

This dissertation examines the impact of environmental salinity and redox heterogeneity on late Ediacaran marine communities across Baltica, focusing on the changes preceding the Cambrian Period. The research highlights that the significant decline in the diversity and abundance of the Ediacara biota, particularly at the boundary between the Redkino and Kotlin Regional Stages coincided with a shift to lower salinity and increased oxygen concentrations in near coastal settings. This is in contrast with the older, normal marine, ferruginous conditions that were present during the time of highest abundance and diversity of the Ediacara biota on Baltica during the Redkino. Through a combination of organic and stable isotope geochemistry, Fe-mineral speciation and P-phase partitioning and major and trace element analyses, detailed chemo-stratigraphic records were compiled from multiple drill cores and outcrop samples from Russia, Ukraine, and Estonia, suggesting that changes in salinity and redox played a crucial role in this ecological shifts. Moreover, the compound-specific carbon isotope analysis (CSIA) of lipid biomarkers from Ediacaran rocks provides additional context by revealing regional heterogeneity in the $\delta^{13}\text{C}$ values of biomarkers when compared to the isotopic composition of bulk organic matter. This heterogeneity reflects variations in local depositional environments, with some regions exhibiting enriched $\delta^{13}\text{C}$ values

indicative of brackish, high-pH settings influenced by deltaic inputs, while others display more typical marine ^{13}C -depleted signatures common of late Ediacaran.

In addition, the detrital zircon U-Pb geochronology study provides insights into the provenance and sedimentary evolution of the late Ediacaran to Early Cambrian sedimentary basins of Baltica. The Moldova-Podillya-Volyn basin, for example, evolved from a peneplained Precambrian basement to a foredeep receiving sediments from both the Ukrainian Shield and Fennoscandia, indicating significant tectonic changes and drainage system reorganization. The transition from a bimodal to polymodal distribution of detrital zircon ages further supports the notion of major tectonic changes during this period.